Fall 2012

Underground mine fire simulation using multiscale modeling approach

Xichen Zhang

Department: Mining Engineering

Recommended Citation

Zhang, Xichen, "Underground mine fire simulation using multiscale modeling approach" (2012). *Doctoral Dissertations*. 88.
https://scholarsmine.mst.edu/doctoral_dissertations/88

UNDERGROUND MINE FIRE SIMULATION USING MULTISCALE MODELING APPROACH

by

XICHEN ZHANG

A DISSERTATION

Presented to the Faculty of the Graduate School of the

MISSOURI UNIVERSITY OF SCIENCE AND TECHNOLOGY

In Partial Fulfillment of the Requirements for the Degree

DOCTOR OF PHILOSOPHY
in
MINING ENGINEERING

2012

Approved by

Jerry C. Tien, Advisor
Liming Yuan
Kelly O. Homan
Kwame Awuah-Offei
Maochen Ge

ABSTRACT

Underground mine fires have always been a major concern. Past events show that fire poses a severe safety hazard to mine workers, and causes tremendous economic loss to the mine and surrounding communities. A good understanding of the interaction between a mine fire and the mine ventilation network is crucial for effective fire emergency planning and hazard control. Unfortunately our understanding of a fire is still limited due to the complex nature of mine fires and a lack of adequate resource for studying them.

A new multiscale modeling approach coupling conventional 1D and 3D techniques has shown to be a useful tool to study a mine fire with the latter providing boundary conditions to the former and vice-versa. During simulation, the 1D and 3D models dynamically exchange information at the interfaces and operate in parallel. This method has the advantage of low computational complexity when compared to a full 3D model, but provides the same accuracy.

Two cases studies were used to demonstrate that the multiscale model was a valid technique for simulating a complex mine fire and the accompanying airflow behavior such as throttling and buoyancy effects during a fire emergency. In both cases, the multiscale model presented a result that was superior to both the full 1D model and the 3D model.

ACKNOWLEDGEMENTS

I would like to express my sincere thanks and gratitude to my advisor Dr. Jerry C. Tien for his continuous guidance, advice, and encouragement during my study and research at Missouri S&T. Without his kind help and support, I could have never gotten this far. I am also thankful to him for the financial assistance he has given me in the form of Research and Teaching Assistantships.

I would like to thank all the committee members, Dr. Liming Yuan, Dr. Kelly O. Homan, Dr. Kwame Awuah-Offei and Dr. Maochen Ge for their advice, constructive criticism, and for their time and efforts in examining the dissertation. Special thanks to Dr. Kwame Awuah-Offei for providing the fire test with the Experimental Mine survey data.

I would like to take this opportunity to thank Mr. Jimmie E. Taylor Sr., Mr. Curtis D. Phelps, Dr. Jason Baird, Mr. Phillip Mulligan for their support on the implement of the fire experiment. Thanks to Mr. Javanbakht Arash Habibi for his great help on preparing and conducting the experiment. Thanks to Mr. Casey Slaughter and his fellows from mine rescue team for their contributions on safety issue of the fire test. Thanks to Mr. Yutao Zhang, Mr. Chenxing Lou, and Mr. Liang Wang for their helps during the experiment. I also like to thank Dr. Magesh Thiruvengadam for his advice and generous help during the numerical simulation work.

I would like to acknowledge the National Institute for Occupational Safety and Health for supporting this research. I would also like to acknowledge the financial support received from the Department of Mining Engineering at Missouri S&T for Graduate Research Assistantship and Graduate Teaching Assistantship.

Finally, I would like to thank my parents. The feeling of missing you always encourages me to overcome any difficulties. I would also like to thank my family and friends in china for their support and encouragement.

TABLE OF CONTENTS

Page

LIST OF ILLUSTRATIONS

LIST OF TABLES

Table Page

1. INTRODUCTION

1.1. MINE FIRE ACCIDENTS

Mining has always been considered to be one of the most hazardous of all industrial activities. Mine safety has been a major concern for all miners, mine operators, health and safety personnel in the United States and the rest of the world. Over the years, mine disasters have resulted in thousands of miner deaths and most of these occurred in underground mines. From 1900 to 2008, 11,624 underground coal mine workers died in 515 U.S. underground coal mining accidents (Gates et al., 2007; Kowalski-Trakofler et al., 2009). Mine fires, the second most common safety harzard, accounts for 793 out of 11,624, or approximately 6.82% of the total number of deaths, and 18 out of 515 (or 3.50%) of the number of accidents between 1900 and 2008 in the United States. These fires are a result of both increased mechanization and the introduction of greater numbers of electrical machines. Table 1.1 lists all mine fire accidents (not including explosion death) since 1900 in United States.

Based on data from both of National Institute for Occupational Safety and Health (NIOSH) (Anon., 2008 and 2010a; McDonald and Pomroy, 1980; Pomroy and Carigiet, 1995; DeRosa, 2004; Trevits et al., 2008) and the Mine Safety and Health Administration (MSHA) (2009b), 256 reportable fires occurred in underground coal mines which caused 27 fatalities and 70 injuries between 1978 and 2001 in the United States. The number of underground coal mine fires, as well as associated fatalities and injuries for the 24 successive years (1978-2001), is illustrated in Figure 1.1.

Mine fires have also resulted in devastating accidents in underground metal/nonmetal mines. For example, a fire at the Sunshine Silver Mine in Idaho in 1972 resulted in 91 deaths (Trevits, 2008 and Table 1.1). The most recent fatal underground mine fire occurred on January 19, 2006, at the Aracoma Alma Mine No. 1 in Logan County, West Virginia, where a conveyor belt ignited and poured smoke through the gaps of stoppings into intake airways that killed two miners.

Table 1.1. Fires Accidents in U.S. Underground Mines, Since 1900

Date	Mine Name	City	State	Product	Fatal
11/06/1903	Koarsarge	Virginia City	MT	Gold	9
11/13/1909	Cherry	Cherry	IL	Coal	259
11/08/1901	Victor American 3	Delagua	CO	Coal	79
02/23/1911	Belmont	Tonopah	NV	Gold/Silver	17
05/05/1911	Hartford	Negaunee	MI	Iron	7
08/23/1911	Giroux	Ely	NV	Gold/Silver	7
02/14/1916	Pennsylvania	Butte	MT	Copper	21
06/08/1917	Granite Mountain	Butte	MT	Copper	164
08/27/1922	Argonaut	Jackson	CA	Gold	47
11/24/1927	Magma	Superior	AZ	Copper	7
07/16/1950	Lark, U.S. Smelting	Lark	UT	Lead, Zinc	5
03/08/1960	No. 22	Pine Creek	WV	Coal	18
03/05/1968	Belle Isle Mine	Franklin	LA	Salt	21
03/26/1971	Nemacolin	Nemacolin	Pa	Coal	3
05/02/1972	Sunshine Mining Company	Kellogg	ID	Silver	91
07/22/1972	Blacksville No. 1	Blacksville	WV	Coal	9
12/19/1984	Wilberg Mine	Orangeville	UT	Coal	27
01/19/2006	Aracoma Alma	Melville	WV	Coal	2

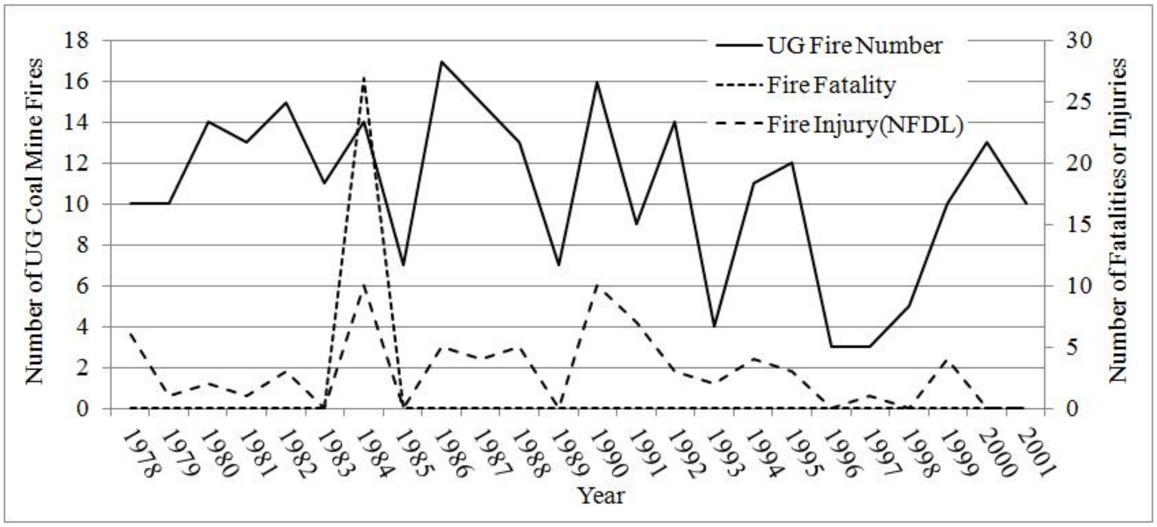

Figure 1.1. Number of Reported U. S. Underground Coal Mine Fires, Fatalities, and Injuries (1978-2001)

In addition to safety problems, mine fires can also cause significant production losses, placing huge financial burdens on mining companies. One example is the February 2005 fire in the Buchanan Mine of Consol Energy, Inc. in Virginia. The mine was idled for nearly 4 months and caused US$23.3 million in property damage alone (Zhou, 2009).

Mine fires are qualitatively different from well-known structural fires (Mitchell, 1996). Some of the major differences are listed below:

- Oftentimes mine workers must evacuate long distances (sometimes miles) in both smoke and a dark environment.
- Miners must crawl out to escape because sometimes the seam height maybe be from feets down to inches.
- Accesses to outside from underground workings are always limited to a few (sometimes only two) openings.
- A mine's roofs and ribs are impenetrable, often lying hundreds of feet below the Earth's surface.
- Underground workings, especially coal, provide an inexhaustible supply of fuel.
- Potentially explosive and lethal concentrations of gas may build quickly in a mine fire.
- No safe place to vent the fire products such as heat, CO and smoke.
- Firefighting logistics are difficult.
- There may be cases where fire source and trapped miners are difficult to even locate, making mine rescue and firefighting difficult, if not impossible.

Given these variables, anyone who delays too long before beginning an escape attempt, who cannot travel the necessary distance to fresh air, or who gets lost in the maze of dark, smoke-filled entries will likely die. Therefore, to best assist with the mine design, firefighting plan, fire-detection system, and evacuation route, fire behaviors, as well as the interaction between mine fires and ventilation must be thoroughly understood.

1.2. STATEMENT OF THE PROBLEMS

A mine fire typically occurs when airways are ventilated. Fire behavior, smoke dynamics, and ventilation flows are interrelated and must, therefore, be studied together. The resulting airflow within a mine is dependent on the combination of fire-induced flows, how a section is ventilated, the mine layout, as well as the atmospheric conditions on the surface. As a result, it is very difficult to characterize the interaction between the mine fire and ventilation. Depending on both the level of accuracy required and the amount of resources available, a rough characterization of the problem using a different approach may be possible.

Experimental simulation is a popular approach to study the interaction between mine fires and ventilation. Depending on the purpose, a fire test can be either a large-scale experiment or small-scale experiment. Large-scale tests, generally conducted within either experimental or idled mines, require large financial investments. Although it provides valuable information, due to the huge associated costs and resources not always available, only a limited number of tests were conducted. Small-scale tests are usually conducted in the lab with results that are less realistic.

Numerical modeling has been used to study mine ventilation systems with a fire. They are highly flexible and economical, allowing for both large parametric studies and sensitivity analysis. The accuracy of numerical models must always be addressed by comparing the results to experimental findings to assess the range of both applicability and limitations. Two models have been used to simulate mine fire behavior: 1D (a network model) and 3D (Computational Fluid Dynamic model) models.

The overall behavior of a ventilation system is approximated using an 1D fluid dynamic model. It is assumed that all the fluid dynamic quantities are uniform in each airway cross section and pressure gradients are only present in the longitudinal direction. An 1D model has low computational requirements and is especially attractive for parametric studies in which a large number of simulations must be conducted.

3D techniques are typically adopted in fire safety science when detailed flow field data is needed. Such techniques are able to provide detailed temperature and velocity fields, smoke movement and stratification, toxic species evolution, heat fluxes mapping, and other important variables. The 3D model can present visualized simulation results of the studied field. Additionally, a 3D model can improve the accuracy of the simulation by treating fire source more realistically.

Both of these two numerical methods, however, have their limitations. In an 1D model, the fire source must be simplified as a node with either fixed or varied heat emission rates. Fire gases are calculated from the released heat based on an empirical formula rather than chemical combustion reaction. Such treatment will likely yield less accurate simulation results. A 3D model requires significant computational resources. It is impossible to simulate the entire mine using a 3D model. Especially in the mining industry, the calculated domain, even in a small size mine, is huge.

1.3. OBJECTIVES AND RESEARCH PROCESS

The primary objective of this research was to develop a new technique capable of modeling a mine fire – a multiscale modeling protocol. This model was to couple conventional 1D and 3D modeling techniques interactively, with the latter providing the boundary condition to the former and vice-versa. In other words, the result of an initial 1D model will serve as the boundary condition for a subsequent 3D model, the results of which will then be used as boundary input for a second iteration in the 1D model for further refinemint. The process goes on until global convergence is achieved.

During the procedure, the 1D and 3D models would dynamically exchange information at the 1D-3D interfaces, operating in parallel. Simulation results were to be verified and validated with both existing programs (Ventsim Visual, VnetPC Pro, and Ventgraph) and experimental data from the field test. The resulting information is expected to improve the theories of interaction between mine fires and ventilation. Additionally, this technique could be used to assess the capabilities of a ventilation system to manage fire behavior, planning detection strageties, and plan evacuation strategies.

A detailed literature survey was conducted to identify both current problems and existing techniques used to characterize not only mine fire simulation but also experiments. The 3D fire simulation was one of the most important components of this research. Fire tests were conducted in the Wombat Mine, one part of Missouri University of Science and Technology's (Missouri S&T) Experimental Mine, to help build a reliable fire model. Test results were used to validate a numerical model with FLUENT. The sensitivity analysis of the numerical model was also performed for different test scenarios. Once the model was validated, it was used for the coupling process. An 1D ventilation survey was conducted at the Main Mine of Missouri S&T's Experimental Mine. The ventilation network model was built with Flowmaster and verified using both VentSim Visual and VnetPC Pro. Once the 1D model was complted, it was coupled with a 3D fire model resulting in a multiscale model. At the end of the research, several scenarios were designed for experimenting with the multiscale model. The main process of this research is illustrated in Figure 1.2.

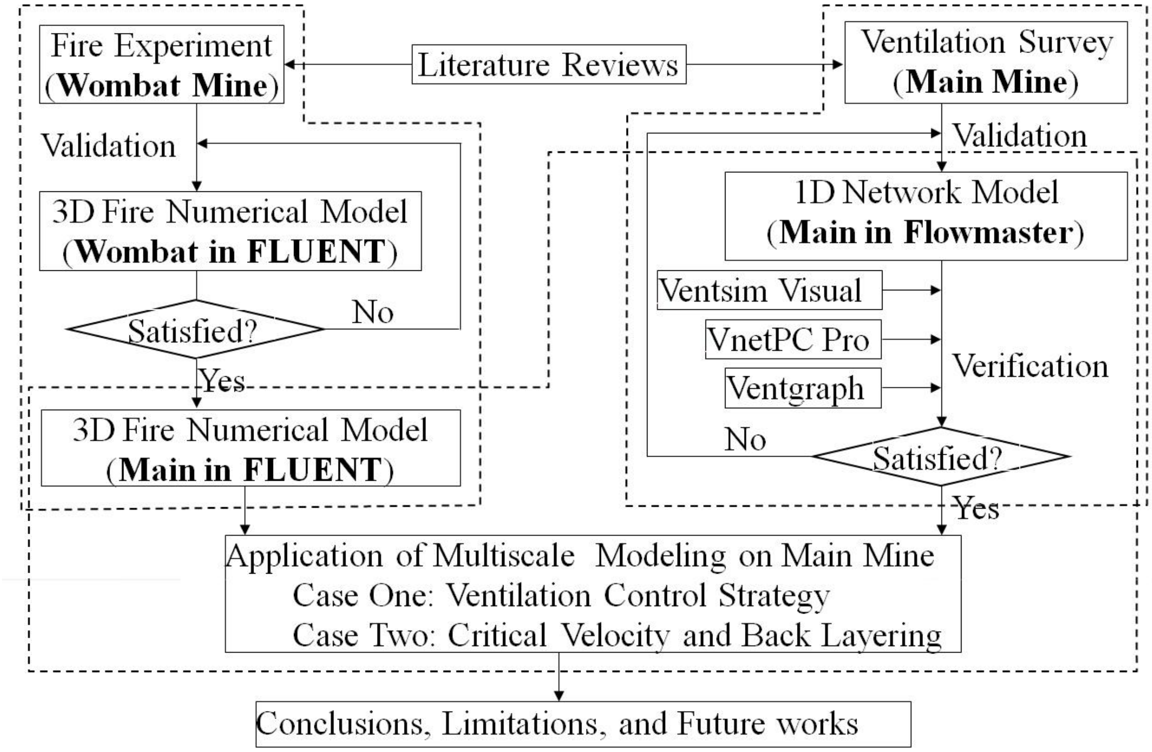

Figure 1.2. Schematic of Research Procedure

1.4. STRUCTURE OF THE DISSERTATION

This research has been organized into the following eight sections.

Section 1. Underground mine fire disasters have been studied since the 1950s. According to the specific characteristic of an underground mine, different research methods, such as experimental and numerical methods, are described for both fires and ventilation in a mine. The limitations of these approaches are discussed. In conclusion, the research objectives, together with a detailed research process, are described.

Section 2. This section includes a comprehensive review of relevant literature on four aspects: mine ventilation, mine fire, the interaction between a mine fire and ventilation, and related analysis of both methods and tools. Both the fundamental knowledge and calculation method for the underground mine ventilation network are reviewed first. As for the mine fire, the principle, the component, and the detection, as well as firefighting technologies, are reviewed. Both the throttling and the buoyancy effects, as two key phenomena of the interaction between an underground mine fire and ventilation, are reviewed theoretically. In the last part of this section, the analysis methods, including both an experimental and a numerical approach, are reviewed in detail.

Section 3. This section is used to develop a 3D fire model that is reliable in an underground mine environment. Both the experimental method and numerical method are adopted in this research. A series of in-site fire tests are conducted in the Wombat Mine. Test scenarios are designed by varying with fire intensity, fuel type, ventilation conditions, and fire source location. The test results are used to validate the numerical model. The entire Wombat Mine numerical model is built and analyzed with FLUENT. Basic partial equations, including the continuity equation, momentum equation, energy equation, and the modified k-ε turbulent model, as well as the P1 radiation model, are introduced in detail. The numerical model is validated before being applied to the 3D model of part of the Main Mine in the multiscale modeling process.

Section 4. This section introduces the multiscale model, including both the basic theory and the coupling technique. The direct coupling technique on transferring the fluid information at the interface between the 1D and 3D model is selected in this research. The corresponding coupling method is developed and described in detail. As a novel tool for solving the 1D model, Flowmaster is introduced in both theoretical fundamental and practical application. A co-simulation package, named as MpCCI is adopted to realize the coupling process. At the end, a simple example is calculated for showing the whole multiscale modeling process.

Section 5. A ventilation survey is conducted in the Main Mine, and survey data is used to construct a network model in Flowmaster. A detailed process on building the network model is described. Steady state ventilation calculation results are compared with results from Ventsim Visual and VnetPC Pro. Two cases of heat transient state simulation are designed in the Main Mine. The heat calculation results are verified by Ventsim Visual and Ventgraph.

Section 6. The validated numerical 3D model in Section 3 is applied in the Main Mine. Two 3D numerical models in the Main Mine are developed with FLUENT. The fire sources are located at the same position where heat sources in Section 4 are located. Great care is given to analyze the meshing requirements and the location of the boundaries.

Section 7. Multiscale modeling techniques are first applied to simulate transient fire simulation in the Main Mine. The 1D and 3D model prepared in Section 5 and Section 6, respectively, were coupled with each other for both Case One and Case Two. In this section, the multiscale models are calculated for both practical and theoretical purposes. Case One is designed to simulate the response of the ventilation devices during a fire emergency, while Case Two is simulated for studying the critical velocity and back layering effects under different ventilation conditions.

Section 8. At the end, conclusions from each section are summaried, including the calculation results, comparison results, and brief comments. The need for additional work that needs to be done in future is also mentioned.

2. LITERATURE REVIEW

2.1. RESEARCH METHODS FOR MINE VENTILATION AND FIRE

A mine fire typically occurs when airways are ventilated. Fire behavior, smoke dynamics, and ventilation flows are deeply interrelated. Thus, they must be studied together. The airflow within a mine is dependent on a combination of fire-induced flows, the ventilation status, the mine layout, and atmospheric conditions on the surface. It is not easy to characterize the airflow within a mine under fire emergency.

Although an overall analysis of mine ventilation flows and fires can be very complex, the resulting information is crucial for mine fire safety purposes. Studies conducted on both are indeed fundamental in assessing the capabilities of a ventilation system. These capabilities include managing smoke, designing ventilation and evacuation strategies, predicting loss of tenability in the environment, and minimizing damages to the mine. Depending on the accuracy required and the resources available, a solution to these studies can be reached using different ways.

2.1.1. Experimental Simulation. Depending on the test scale, a fire test can be divided into either a bench-scale or large-scale experiment. The former is usually conducted in the lab, resulting in data that lacks accuracy. A large-scale test is conducted in either an experimental mine or idled mine. This test can provide more valuable information than a bench-scale test though it requires large financial investments. The experimental data obtained from large-scale tests is widely used to derive constants in semi-empirical correlations to predict length of back layering, smoke front velocity, and temperature.

A series of bench-scale fire tests were used to study the flammability properties of conveyor belts. Nine different rubber conveyor belts were examined in both an inclined gallery and a horizontal gallery (Nakagawa et al., 1991). Nakagawa et al. (1991) concluded that both ignitability and flame-propagation depend on not only the specimen width, but also the ventilation flow conditions. Another conclusion they found is that the flame-propagation speed seems to be almost independent of whether the ventilation flow in the gallery is horizontal or upward. This finding is inconsistent with those recorded by

Hwang et al. (1985). One reason for this inconsistency could be that the belt surface-to-roof distance in the tests was small (85 mm), thus resulting in early flame deflection.

Yuan et al. (2007) studied conveyor belt flame spreads in a small-scale tunnel. The purpose of the study was to investigate the effects of belt type, varying ventilation velocity, belt surface-to-roof distance, and ignition source power on flame spread properties. A total of four belt types were tested. Yuan et al. (2007) found that a greater belt surface-to-roof distance will result in a decrease in the re-radiation of the belt. A greater ventilation velocity will result in a decrease in the fuel-rich environment (Yuan et al., 2007).

Svenska Gruvföreningen (1985) conducted a large-scale fire experiment with a mobile rescue chamber. The experimental fire was in a loader (CAT 960) containing 2200 kg rubber and 600 liters of oil. The experiment was videotaped for 5 hours (from ignition until the fire was almost completely extinguished). During the experiment, both the CO-level and the temperature, not only inside but also outside the rescue chamber, were continually measured. Both the smoke density at the rescue chamber and the airflow in the drift (unidirectional flow) were also measured. Svenska Gruvföreningen (1985) concluded that the critical velocity was between 1 and 2 m/s, depending on the heat release rate (HRR) of the fire.

A series of large-scale tests was conducted by MSHA to study the flammability of conveyor belts (Verakis H.C., 1985). Various types of mine conveyor belts were burned with airflows (between 0 to 6.1 m/s). Test results indicated that the highest flame spread rates occurred when the airflow was 1.5 m/s. These results were utilized to develop a new MSHA bench-scale test. This test evaluated the flame resistance of conveyor belts used in underground coal mines. The peak value (at an air speed of 1.5 m/s) was found to be valid for larger belt surface-to-roof distances only. Unfortunately, the influence of the belt surface-to-roof distance was not investigated.

Both fire development and spread along conveyor belts in ventilated ducts were investigated not only experimentally but also theoretically (Hwang et al., 1985). Various types of conveyor belts used in mining applications (fire resistant belts were among those tested) were ignited and burned under various flow conditions in a large-scale gallery. A theoretical model was developed to correlate the fire spread with both the material properties of the conveyor belts and the environment. Strong agreement was found between the experimental and theoretical results. The experimental results of flow-assisted flame spread along horizontal conveyor belts indicate that radiative heat transfer plays a major role in flame spread mechanism. A greater belt surface-to-roof distance will result in a decrease in the re-radiation to the belt. And a greater ventilation velocity will result in a decrease in the fuel-rich environment. These conclusions are in accordance with conclusions drawn by Yuan et al. (2007).

Fire tests were performed in a blasted rock tunnel measuring 3m wide, 3m high and 100m long (Ingason et al., 1997). The fire was located at two different locations in the tunnel. The tunnel was ventilated naturally through a 13m high chimney located at one end. Tests with different ventilation conditions and fuels were conducted. Both the effects of ventilation on the HRR as well as correlations between optical density and gas concentration at different locations were investigated. These tests indicated a slight difference between the degree of ventilation and HRR for pool fires. The difference for solid materials, however, was large.

A large-scale experiment on a conveyor belt 42m long and 0.5m wide was conducted (Wachowicz, 1997). A total of six different types of belts were burned during the experiments. Temperature, CO, CO_2, and O_2 were all measured. No innovative conclusions were found during these tests. Something from the article that could be used in the future work are the HRR curves of the conveyor belts. The HRR curves taken from this experiment could be used, however, when looking into different fire scenarios in different regions of the mine.

Lowndes et al. (2007) conducted a ventilated, large-scale fire test to characterize the initiation and spread of fire along the upper and lower surfaces of a conveyor belt airway. Both temperature gradients and airflow profiles within the gallery were obtained because of various ventilation flow rates. Lowndes et al. (2007) concluded that conducted experimental test program had successfully determined the aerodynamic and thermodynamic characteristics of a full-scale fire gallery. The flame initiation and spread characteristics can also be identified for conveyor belting.

2.1.2. Numerical Simulation. Numerical modeling can also be used to study mine ventilation systems in fire emergency. Numerical models, which are based on a mathematical representation of the physical phenomena involved, are usually highly flexible and economical. They also allow for both large parametric studies and sensitivity analyses. The accuracy of numerical models must be always addressed by comparing the results to experimental findings. Two models can be used to simulate mine fire behavior: the 1D (a network model) model and the 3D (CFD model) model.

2.1.2.1 One-dimensional network model. Mine ventilation system consists of interconnected airways, working places and control devices designed to effectively distribute fresh air and remove harmful gases and dusts from the mines. More specifically, the system is (Vutukuri and Lama, 1986; Rabia, 1988):

- To dilute the concentration of potentially explosive and toxic gases, fumes, and radon generated during mineral production to environmentally safe levels, removing them from the mine;
- To dilute the concentration of the airborne dust to physiologically acceptable levels, removing it from the mine;
- To provide a thermally acceptable environment in which persons can work without undue discomfort or danger of exhaustion from heat, removing heat from the mine as may be necessary.

Careful planning and regular maintenance are necessary so that this system will be able to function effectively with being compromised in any way. This task is often made more complex by the dynamically changing environment of a mine. Additional factors also influence the mine ventilation system.

The behavior of air within an individual airway has been discussed in details by Hartman et al., (1997). Ventilation systems in an operating mine generally consist of multiple, interconnected airways (branches) forming either simple or complex networks connected by junctions (or nodes). Ventilation network analysis is concerned with the interactive behavior of airflows within the connected branches of a complete and integrated network. In a given network, however, theoretically, an infinite number of combinations of airway resistances, fans, and regulators that will give any desired distribution of flow.

Before the mid 1950's there was no practical means of conducting detailed and quantitative ventilation network analysis for complete mine systems (Maas, 1950). The first viable electrical analogue computers to simulate ventilation networks were produced in the United Kingdom (Scott et al., 1953) followed rapidly in the United States (McElroy, 1954). These analogues employed electrical current passing through rheostats to simulate airflows. Successive adjustment of the resistances of the rheostats enabled the linear Ohm's law for electrical conductors to emulate the square law of ventilation networks.

In the nineteen fifties and early sixties, ventilation simulation programs for mainframe digital computers had begun to appear (McPherson, 1964). These programs proved to be much more versatile, rapid and accurate dominated ventilation planning procedures in major mining countries soon. Throughout the 1970's network programs were developed for large centralized mainframe computers (Greuer, 1973; McPherson, 1993). In the 1980's, the enhanced power and reduced cost of microcomputers led to the evolution of self-contained software packages that allowed very easy interaction between the user and the computer. (McPherson, 1993)

In the last three decades, both a number of computer applications and prototype software packages have been developed that simulate the complex ventilation flows and fires created within a mine system. Most of these systems use derivatives of the Hardy Cross iteration method for balancing closed network systems such that the resulting pressure loss across the entire network equals to zero (Kirchhoff's laws). It is assumed that all the fluid-dynamic quantities are uniform in each airway cross section and pressure gradients are only present in the longitudinal direction. Both heat and mass transfer occur by defining branches between nodes. These branches represent flow paths for the transfer of mass, energy, and momentum between nodes (Floyd and Hunt, 2005).

In 1989, the U.S. Bureau of Mines/Michigan Technological University mine ventilation mainframe program was successfully transferred over to the PC platform (VnetPC) (Ng, 1989). The updated program enabled the ventilation network analysis program to reach a wider audience. As a Microsoft® windows based program, VnetPC™ is designed to aid mine environmental engineers in planning subsurface ventilation layouts.

VnetPC provides both tabular and graphic method of constructing the network geometry, setting the airway resistance, and defining the fan curve. After the simulation is done, this program will produce listings and visual graphics of branch airflow, frictional pressure drops, ventilation cost of each airway, fan operating points and air power losses (Anon., 1996). Unfortunately, the current version of VnetPC (VnetPC Pro) cannot be used to calculate either mine fires, gas flow, or heat distribution.

Ventsim was developed by Chasm Consulting in Queensland, Australia in 1993 and updated to Ventsim Visual in 2011 (Anon., 2011). It is the first ventilation package with a 3D graphics interface. This outstanding property makes it both very simple and intuitive in not only building but also operating a ventilation network model. By navigating the network model in a 3D environment, this tool allows the user to quickly achieve any viewpoint required.

As a mine ventilation package, Ventsim Visual was originally developed to perform network simulations. With additional functions added into the existing program, Ventsim Visual can model the dissipation of smoke, dust, and gas for emergency planning. It can simulate the heat released from the combustion of diesel engines, rock strata, electrically powered mining equipment, and blasting. Ventsim Visual can also calculate the humidity and refrigeration essential in a cooling system designed for deep mining operations. Additionally, Ventsim Visual can assist in both selecting fans and performing “what if” scenarios. Its financial analysis feature can provide users with both the operating and the total cost of either an airway or a network by taking into considering the time-value-of-money (Anon., 2011).

Ventsim Visual can also accept real-time information generated by underground mine ventilation monitoring sensors, undertake network simulations, and interpret both key system data and operational changes. Once the simulation program has updated readings, it can remodel the entire mine system, report the flows in all branches, and compare individual branch readings with expected values (Gillies et al., 2003).

The first significant attempt to include the effect of fire in network system calculation was made in the late 1970s. Greuer (1977) produced a tool able to perform a steady state calculation of networked system, providing temperature, velocity, and pollutant distributions by using a hardy-cross-like method. The program was later modified by Chang et al. (1990) to accommodate dynamic state modeling of the fire. The updated version of this program enhanced the capability on the transient-state modeling problem.

The resulting program, MFIRE, could provide useful information for fighting a mine fire and planning fire evacuation routes (Chang et al., 1990). MFIRE allows researchers to simulate the mine ventilation system in its normal steady state condition. It can also simulate the mine ventilation system in its transient state after a mine thermal event or fire begins. Consequently, MFIRE is able to estimate the air quantity and pressure distributions in the steady state condition, as well as output information about the propagation of time dependent air temperature and fire gas concentration in the mine.

MFIRE was used to deal with a complex tunnel network for calculating the distribution of pollutant concentrations in the tunnel domain (Ferro et al., 1991; Borchiellini et al., 1994; Jacques, 1991). These verified its ability to perform steady state calculations. A series of in-mine experiments was performed to obtain temperature profiles as a function of both time and distance from a fire (Laage and Yang, 1991; Laage and Yang, 1995; Laage et al., 1995). MFIRE was then used to calculate the temperature distribution in airways. The transient state simulating temperature distributions were reasonably predicted to within a few degrees. This model was also used to investigate both the direction and the rate of air flows, temperature distribution, and emergency ventilation responses (Cheng, 2001; Miclea, 1991).

Many researchers have indicated that MFIRE is able to analyze the consequences of a fire in a complex network of underground mines. MFIRE is a powerful tool to use when predicting the gross consequences of mine fires. The output can help to locate fire detection equipment and evaluate the escape route (Lea et al., 1995). The biggest limitation of this program is the inability to identify the smoke rollback phenomena. MFIRE is unavailable at present due to ongoing updating process.

VentGraph was developed by Strata Mechanics Research Institute of Polish Academy of Sciences, Cracow, Poland in 1988. This simulation package is one of the very few systems available for simulating a mine fire (Dziurzynski et al., 1988). It is characterized by its division into several software blocks that fulfill different roles related to both mine fire and ventilation. The mine network can be constructed with the direct linking of a branch symbol and the characteristic parameters of the air flow in this branch.

The calculation results can be displayed during the simulation process (Dziurzynski et al., 1991).

Many validation experiments were conducted using data gathered from an actual coal mine fire. Researchers concluded that Ventgraph can determine the amount of CO generated by a fire (Wala et al., 1995). This program can also be used for the purpose of training mine rescue teams in cases where inert gas generators are considered to fight fires. Decision-making during firefighting can also be supported with this program (Dzuirzynski et al., 1997). This program is used in the Australian mining industry to help miners understand mine fire behavior (Wu et al., 2004). This understanding allows them to better prepare for a fire.

Network models allow for a complete and compact description of the ventilation system. This characteristic has two consequences. 1) The boundary conditions, such as the ambient conditions at the portals, can be defined with adequate precision. 2) A large number of scenarios, such as during the assessment of safety strategies for complex mines, can be evaluated.

An intrinsic limitation of network models is due to the fact that the flow in each cross-section is assumed homogeneous. The flow is then identified by a unique set of values for pressure, velocity, temperature, smoke concentration, and more. This peculiar assumption makes network models unsuitable for simulating the fluid behavior in regions characterized by either high temperatures or velocity gradients. Regions characterized by high temperature gradients are typically encountered close to the fire, where well-defined smoke stratification is found (Riess et al., 2000).

Another limitation of network model is that the network is solved using an iterative technique specially developed to solve hydraulic problems (i.e., the Hardy-Cross method). To achieve both the computational simplicity and the rapidity of the model, this method neglects fluid momentum. Pressure gradients were considered as the basic driving forces within the network. A customization of pressure drop coefficients was set up to avoid the solving of additional partial differential momentum equations.

2.1.2.2 Three-dimensional CFD model. Field models have also been used to study fire development in underground mines. These models divide the computational domain into a large number (in the order of thousands) of control volumes, solving the conservation equations (i.e., mass, energy, and momentum) inside each. Doing so allows for a more detailed solution when compared to a network model. A field model can be appropriate for more complex geometries and fluid field because the three dimensions are considered. While field models provide very detailed solutions, they require detailed input information. This input usually requires more computing resources to correctly model the fire. This process can create a costly time delay in obtaining a solution. A network model usually provides a solution more quickly.

The most fundamental equations used to solve fluid motion in a field model are the Navier-Stokes (N-S) equations. These equations are partial differential equations asserting the conservation of mass, momentum, and energy. These equations are solved numerically, leading to detailed predictions of velocity and temperature fields, species concentrations, heat fluxes mapping, and so forth. The solution of the complete Navier-Stokes equations together with associated boundary conditions on a high number of control volumes represents a formidable task.

The availability of computational programs for field model provides an opportunity to analyze fluid behavior flexibly. At present, high performance computers have made Computational Fluid Dynamics (CFD) technology acceptable as a cost-effective, predictive design tool for solving a fluid problem. Numerical solutions for fluid motion equations on a digital computer have evolved over the last 40 years. This technology has become a well-established discipline within a number of science and engineering branches.

In the last two decades, applying CFD as a fire safety engineering tool has become widespread. The issue of CFD modeling of fire phenomena is too wide to be treated within a single literature overview. Several books and literature review papers on the subject have been published in the last two decades, and the interested reader can refer to them (Cox, 1995; Cox, 1998; Novozhilov, 2001). CFD was applied in both tunnel and underground mine operations in 1990s (Edwards et al., 1995), and a number of software, such as FDS (Li and Chow, 2003; Hwang and Edwards, 2005; Lee and Ryou, 2006; McGrattan and Hamins, 2006; Lin and Chuah, 2007; Kim et al., 2007; Ingason and Lönnermark, 2005; Cheong et al., 2009; Kashef and Benichou, 2008; Ingason and Lönnermark, 2005; Cheong et al., 2009), Phoenix (Chow, 1998), Flow-3D (Woodburn and Britter, 1996a; Woodburn and Britter, 1996b), CFX (Rusch et al., 2008; Jain et al., 2008), COMPACT-3D (Karki and Patankar, 2000) , CFD-2000 (Edwards et al., 1999; Edwards et al., 2006; Hwang et al., 2001; Friel et al., 2006) and FLUENT, have been adopted as design and assessment tools. In this section, only the archival papers that directly refer to the CFD modeling of both mine ventilation flows and fires with FLUENT will be discussed.

As a well-known CFD tool, the first version of FLUENT was launched in October 1983. It was originally developed by Creare Inc. in New Hampshire, USA. Over the next ten years, FLUENT developed so quickly that it became gradually accepted as a standard CFD tool all over the world (Anon., 2009a).

FLUENT is a general-purpose CFD software package containing physical models for a wide range of applications, including turbulent flow, heat transfer, reacting flows, combustion, and multiphase flows. It provides physical models on unstructured meshes, allowing the user both easier setup and greater accuracy. With a fully interactive interface, this powerful tool makes model building more productive. FLUENT includes plenty of reliable physical models, providing visualized flow characteristics such as temperature, pressure loss, flow distributions and mixing rates.

In FLUENT, each simulation process, no matter how simple or complex, consists of four basic, but important, steps. The first step includes both building and meshing the geometric model of a computational domain (the boundary should also be identified). Next, the physical model, together with input fluid characteristics and boundary conditions, should be chosen and set up. During the third step, both proper algorithms and convergence limitation must be chosen to solve the numerical model. The results are analyzed during the fourth step. Care must be taken while entering the input in each of these steps to ensure quality results.

The first significant contribution using FLUENT on tunnel fire was presented by Fletcher and Kent (1994). Fletcher and Kent (1994) presented a comparison between numerical and experimental data recorded in a 120m long, 13m^2 cross-section tunnel. They used a k-ε turbulence model together with a mixture fraction model for combustion. Radiation heat transfer has been implemented with a discrete transfer radiation model. A pool fire, with an HRR between 2 MW and 2.4 MW, was located in the middle of the tunnel. Three different ventilation velocity scenarios (0.5 m/s, 0.85 m/s and 2 m/s) were analyzed. A qualitatively good match between predicted and recorded temperature was found with an error between 40-100% in the vicinity of the flame and approximately 40% in the far field (Fletcher and Kent, 1994).

A detailed analysis of CFD capabilities was presented by Wu and Bakar (2000). Wu and Bakar (2000) presented a numerical analysis of two fire scenarios (1.4 kW and 28 kW) in a 10.4m long, small-scale tunnel. This model was developed with FLUENT. A standard k-ε model with buoyancy modifications for turbulence and a mixture fraction model for combustion were adopted. Radiation heat transfer was not taken into account. A comparison with experimental data suggests that the CFD model underpredicts the critical velocity by upto 20%. A comparison with detailed velocity field data suggests a qualitative agreement with the experimental data. Typically, however, higher deviations are recorded. Velocity profiles in the back layering region, close to the ceiling, are slightly underpredicted (~12%). Deviations up to 100% are recorded in the velocity profiles located underneath the back layering nose. Temperatures are significantly over-predicted; they do not show any qualitative agreement with the experimental findings, with deviations up to 500% recorded 30 cm downstream from the fire source. Wu and Bakar (2000) asserted that temperature overprediction is, primarily, due to the hypothesis of fast chemistry embedded in the mixture fraction model adopted for combustion.

Both the k-ε and LES turbulence models were adopted by Gao et al. (2004). They used both the same experimental set-up and data adopted by Fletcher and Kent (1994) one decade earlier. In general, the findings from Gao et al. (2004) and Fletcher and Kent (1994) agreed with each other strongly on the plume inclination angle, with errors between 10% and 30%. Overall, flow behavior could be accurately predicted (i.e., the occurrence of back layering). Local temperature fields, however, were over-predicted by up to 250%.

Bari and Naser (2005) addressed the spread of fire effluents within a longitudinally ventilated tunnel 1.6 km in length. The fire, represented by a burning bus, was supposed to grow up to a 44 MW HRR in 10s and to extinguish in 4min. The fire was modeled as a heat source without dedicated combustion model. The numerical model lacked accuracy. The results were not corroborated by experimental measurements. Additionally, no information on the smoke production model was provided.

A 30MW fire scenario, in a real 1.5 km long tunnel, was designed to predict both velocity and temperature field using FLUENT (Ballesteros-Tajadura et al., 2006). Time dependent simulations were conducted to predict smoke spread in the domain. The final results, however, were not validated against experimental data. Furthermore, the adopted mesh density (~162 cells/m) was largely under the minimum required for achieving accurate field predictions. The effect of the ventilation system was taken into account by introducing a pressure difference across the tunnel domain (which was previously computed on the basis of cold flow simulations).

Vauquelin and Wu (2006) used FLUENT to predict the effect of tunnel width on critical velocity. The CFD data was corroborated with small-scale experimental data provided in Wu and Bakar (2000). Turbulence was addressed using a k-ε turbulence model with a buoyancy modification. Combustion was implemented using a mixture fraction model. Vauquelin and Wu (2006) confirmed that the model was able to predict critical velocity with an uncertainty between 5% and 14%. No conclusions on the accuracy of the predicted flow fields were given.

FLUENT has also been used by Jae Seong Roh et al. (2007) to simulate both temperature and flow fields within a 10m long small scale tunnel (~0.14 m^2 cross section). The average fire size was between 2 kW and 13 kW. The numerical model was validated against temperature measurements taken along the tunnel ceiling. The predicted temperature values deviated from the experimental findings up to 20% for a 5 kW fire and 90% for a 13 kW fire.

A hypothetical fire outbreak in the Louis-Hippolyte-Lafontaine tunnel, under a river in the Montreal area, represented the test case for the work done by Abanto et al. (2006). Simulations were conducted with both FLUENT and an in-house CFD code. The fire was modeled as a volumetric heat source. An un-specified combustion model was used for the second run. A k-ε turbulence model was adopted in both cases. Abanto et al. (2006) provided only qualitative results, and most of those are questionable (e.g., temperature higher than 3000 K in certain domain regions). No comparison to experimental data was provided.

Three different ventilation scenarios involving 10MW and 50MW fires were modeled by Galdo Vega et al. (2007). The MTFVTP (Anon., 1995) was adopted as the source of experimental data. The entire computational domain was meshed, including the ventilation devices. The mesh density adopted for the calculation (117 cells/m) was under the minimum requirements for accurate predictions. The fire was modeled as a source of both heat and smoke, while turbulence was addressed using a k-ε turbulence model with buoyancy modifications. Nonetheless, Galdo Vega et al. (2007) showed an overall agreement between numerical predictions and experimental data. This finding confirmed that simplified fire modeling approaches lead to accurate predictions of global ventilation system behavior. However, higher deviations were expected within the fire's vicinity.

Van Maele and Merci (2008) presented a comparison between LES and k-ε turbulence models for critical velocity prediction. The k-ε turbulence model was implemented in FLUENT. Radiation heat transfer was not considered. Combustion was addressed using a mixture fraction model. The LES calculations were performed using the CFD tool, FDS. Wu and Bakar (2000) provided experimental data for a 15m long tunnel (0.0625 m^2 cross section) under a 3 kW and a 30 kW fire scenario. Van Maele and Merci (2008) demonstrated that both modeling approaches can provide accurate predictions of the critical velocity, with deviations between 20% to 38% and 31% to 8% for k-ε and LES turbulence model, respectively. Neither flow nor temperature fields were validated against experimental data.

CFD models of tunnel fires have been shown to predict critical ventilation velocity and back layering distance within an acceptable level of accuracy (deviation smaller than 30%). The overall flow data (i.e., bulk velocity and temperature) were also accurately predicted, with deviations from experimental values typically within 20%. More complex issues, such as flame spread, soot formation, oxygen vitiation, and combustion modeling, are far from being solved.

Due to all of the previously described complexities, any CFD analysis requires two additional steps, verification and validation. They are used to judge both the appropriateness of its use and the level of confidence in its predictions (McGrattan and Miles, 2008). Validation is a process to check the appropriateness of the governing equations as model of the physical phenomena under investigation. Verification is a process to check the correctness of the solution of the governing equations. Typically, validation is made by comparing the model against experimental data.

CFD analysis of a fire phenomenon within underground mines suffers from limitations set by the size of computational domains. The high aspect ratio between longitudinal and transversal length scales leads to very large meshes. The number of grid points escalates with the tunnel length and often becomes impractical for engineering purposes, even within small mines. Colella et al. (2009, 2010, 2011) assessed the mesh requirements for both ventilation devices and fire-induced tunnel flows. Grid independent solutions could be achieved only for mesh densities larger than 4000 cells/m and 2500 cells/m for ventilation and fire induced flows, respectively.

A high computational cost arises when the CFD model must consider either the boundary conditions or the flow characteristics in locations far from the region of interest. This is the case of mine portals, ventilation stations or fans located long distances from the fire source. In these instances, the numerical model covering only the fire zone cannot present accurate results. An accurate solution of the flow movement requires that the numerical model includes all the active ventilation devices and the entire mine layout.

This limitation of high computational cost is why only a limited number of CFD studies directly focus on the performance of mine ventilation systems. In most of the literature reviewed, the computational domain is limited to a small region close to the fire. The ventilation velocity at the domain boundaries is considered to be known (i.e., estimated with crude correlations or determined by cold flow ventilation tests). If a ventilation system must be assessed, 3D CFD approach is impractical because it produces a de-coupling between ventilation system and fire.

2.1.2.3 Multiscale model. Multiscale models were based on the fact that, in the vicinity of a fire, the flow field has a complex 3D behavior with large transversal and longitudinal temperatures and velocity gradients. The flow in these regions is calculated using 3D tools since any other simpler approachs will not be able to characterize these behaviors satisfactorily. However, it was demonstrated during a mine fire that, some distance downstream from these regions, temperature and velocity gradients would vary gradually from turbulent towards laminar with uniform distribution, and flow behavior could be accurately modeled by 1D models.

The multiscale model was first introduced in the mining industry for the fire time by Lea (1994). A 10 MW diesel pool fire was modeled as a distributed heat source in a UK mine. Three computational models were used to study the effect of fire using FLOW3D, and the calculated flowrates for the airway with the fire source were used as boundary input into the network model which was solved as a whole mine in MFIRE. These two codes run alone and were unable to exchange the data every time step. Although the results indicated that multi-dimensional models had demonstrated the potential for simulating the near fire flow, the physical and numerical models of this technique need to be further developed.

Examples of multiscale modeling methods were also found in other applications such as characterization of the flow pattern over high speed trains moving through tunnels (Mossi, 1999), simulation of blood flow in the circulatory system (Formaggia et al., 2001), computation of gas flows in exhaust ducts of internal combustion engines (Motenegro, 2002), naturally fractured oil reservoirs (Geiger et al., 2009), and tunnel ventilation flows and fires (Rey et al., 2009).

2.2. CONTROL METHODS ON MINE FIRES

Fire is a chemical reaction, producing energy in the form of both heat and light (Anon., 1986). The oxidization of a material can occur when sufficient quantities of both oxygen and heat directly affect the material, or fuel. In these three elements, oxygen sustains the combustion, sufficient heat raises the material to its ignition temperature, and fuel provides the combustible material. Theoretically, the removal of any one of these essential elements will result in the fire being extinguished (Arthur, E.C., ed., 2008).

Underground mine fires, as a special kind of fire, occurred in underground environment, and traditionally can be classified into two maim groups: concealed and open (McPherson, 1993). Concealed fires occur in areas with either limited access, such as a gob, or within the coal itself. Because of lack of oxygen, concealed fires are primarily associated with the smouldering of combustible material. The concealed fire is beyond the scope of this research and thus will not be discussed in detail.

Open fires occur in areas of the active ventilation system where oxygen is greater available. As a result, open fires ten to be accompanied by flaming combustion (McPherson, 1993). Open fires usually commence from a single point of ignition. The initial fire is often quite small and, indeed, most fires are extinguished rapidly by prompt local action. Speed is of the essence. An energetic ignition that remains undetected, even for only a few minutes, can develop into a conflagration that becomes difficult or impossible to deal with. Sealing off the district or mine may then become inevitable.

2.2.1. Detection of Mine Fires. Detection of a combustion as early as possible places a significant role on controlling mine fires effectively (Sengupta, 1990). The easiest method for detecting a mine fire is to monitor both combustion components and products, such as oxygen, carbon monoxide, carbon dioxide, heat, and smoke. A mine-wide monitoring system, including fixed point detection equipment, a sensory data transmission system, and a monitoring system at the surface, is used for long-term monitoring. Portable detection equipment is used to provide a continuous indication of combustion products during a shift while handheld units are used by mine personnel for spot checks.

The U.S. Bureau of Mines (USBM) investigated the product-of-combustion (POC) characteristics of combustible materials used in typical coal mining operations (Margaret, 1990). Through a series of experiments, the Bureau evaluated the effectiveness of early warning mine fire detection. They concluded that smoke sensors are more effective than CO sensors for fire detection because smoke sensors's thresholds are reached before that of CO sensors.

The same result was also obtained from research conducted in both the USBM experimental mine (Conti and Litton, 1995) and the Pittsburgh Research Center's Safety Research Coal Mine (SRCM) (Edwards and Friel, 1996; Edwards et al., 1997). The former research was studied to determine the alarm times of smoke and carbon monoxide (CO) sensors as well as a point type heat sensor (PTHS) for coal conveyor belt fires. This data suggests that smoke sensors provide an earlier fire warning than 10 ppm CO sensors provide. Additionally, 10 ppm CO sensors provide an earlier warning than PTHS provides. The latter research conducted a series of liquid fuel fire experiments, determining that smoke detectors can be more effective for mine fire detection than CO detectors.

Morrow and Litton (1992) evaluated the smoke detectors in six different mines. They recommended that no smoke detector should be used unless it has first been approved by MSHA according to performance standards. They also suggested that any smoke detector failing to respond at an optical density less than 0.044 m^{-1} in 100% of the tests fails and thus cannot be approved for use in underground coal mines. To develop sensitivity tests for smoke detectors, Edwars and Morrow (1995) conducted tests in a smoke chamber. These experiments indicated that an average CO concentration of 5 ppm corresponded to an optical density of 0.022 m^{-1} for both smoldering and flaming coal combustion.

The U.S. Bureau of Mines conducted a series of large-scale experiments where small coal fires were used to ignite the conveyor belt at different air velocities (Litton et al., 1991). Temperature, CO, and smoke levels were continuously measured during each test to determine both alarm time and level. They concluded that the sensor alarm levels are related to the sensor space, the entry cross-sectional area, and the entry air velocity.

Conti and Litton (1993) researched various methods for improving the early detection of carbon monoxide levels. After experimenting with the variables of air velocity, sensor spacing, and position, Conti and Litton (1993) concluded that CO sensors near the roof of an entry offer an advantage in detection due to the buoyancy induced stratification of the combustion products of the fire. This effect was true even during the low temperature smouldering stage of a fire prior to full combustion taking place. Although this effect would tail off gradually with an increase in ventilation flow, it still provided significant improvements in early detection.

Effective fire detection depends upon the sensors defined alarm values. Based on the research results in United States range, Code of Federal Regulations established alarm values for fire sensors used in mine (Anon., 2012b). These values include a 5 ppm alert and a 10 ppm alarm value for CO, a 0.022 m^{-1} optical density for smoke, and a 165 °F safe value for temperature.

2.2.2. Firefighting Methods. Originally, the mine operators in the United States were required by law to report to MSHA any unplanned mine fire event either lasting more than 30 minutes or involving an injury. This regulation was modified in 2007 because of its slack requirement. Current regulations require that any unplanned mine fire event either not extinguished within 10 minutes of discovery or involving any injuries needs to be reported. According to MSHA, if miners attempt to fight a fire for more than 10 minutes in an underground environment and are unsuccessful, the fire will likely become uncontrollable (Trevits et al., 2007).

Firefighting method, as one of the most concerned topic in underground mine fire research, is developed for many years. Generally speaking, two attack methods exist for fighting methods. These methods are dependent on the fire's stage. The first method is direct attack. This method is both the most effective and commonly used method for controlling a small-scale mine fire. The second method is the indirect attack method. This method is used to control underground mine fires beyond their incipient stage when the direct method is not possible. The indirect attack method is, primarily, based on sealing off the affected area so the fire will distinguish by oxygen depletion. Due to the scope of this research, only the direct attack method will be reviewed in detail.

When a fire occurs, the first thing is to fight fire with materials or tools at hand immediately. Usually, using water (Coatesworth, 1929), applying rockdust (Howarth and McCaa, 1929), digging out the combustion materials (Morris, 1987), and utilizing portable extinguishers are the most convenient means to fight fire. All these methods, however, are only effective if the fire is still in its incipient stage and the fire zone is safely accessible. Once the fire has developed, the approach to the fire zone from the intake is often limited by the backing of both smoke and hot gases against the ventilation current, by the heat from the strata, and by falls of roof (Eisner and Shepherd, 1953/54; Mitchell, 1962).

One solution for approaching fire zone is to increase the intake airflow velocity and thus reduce the length of the smoke and hot air back layering. Placing a fire-resistant brattice (Figure 2.1) that acts as a radiation screen across the lower half of the roadway was practiced as an effective way to fight back the smoke's tongue **(**Eisner and Shepherd, 1953/54**)**. This method makes firefighters to advance from downstream some distance to the fire, applying extinguishing agents and devices directly to the fire. Although this method can effectively fight a fire at its early stage, it places miners in close proximity to the fire, exposing miners to the deadly hazards of the fire (Morris, 1987). Moreover, if the underground access is blocked from outside personnel, the fire zone is too large for available underground personnel, or the supply of available firefighting materials and devices are limited, it is impossible to access to the fire zone to fight fire directly, thus indirect firefighting method is needed.

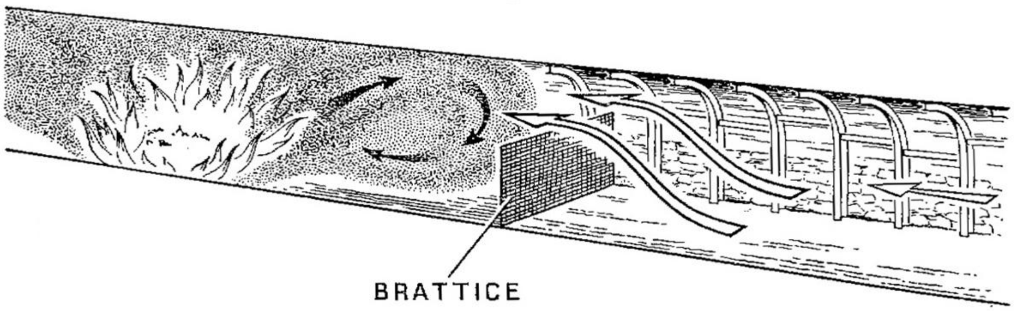

Figure 2.1. Fighting Back the Smoke Tongue with a Brattice (Eisner and Shepherd, 1953/54)

Controlling the ventilation flow of air around a mine is another way to decrease the fire hazards effect on a working face. This control can have a significant impact on saving evacuation time and eradicating fire. Various methods for controlling ventilation include isolating the fire, reversing the mine ventilation, regulating the air flow rates, and short-circuiting airflow (Vutukuri and Lama, 1986). Because making adjustments to the ventilation system can have big influence on whole mine system, more care needs to be put on doing adjustments. The method chosen depends on the type and location of the fire. More than one method is, at times, employed.

Complete isolation of a fire is possible in mines which are divided into special fire sections by building stoppings. This method is, however, not valid in old mine operation. The potential danger area should be managed in the design stage of the mine. In the case of fire, they can be quickly isolated until fire crews arrive (Grekov et al., 1991). Reversal of the main fan is not usually advised as the fan works at a reduced efficiency. Additionally, a significant amount of time can be required for the air flow to reverse. As a result, dangerous gases can be formed and accumulated. Furthermore, reversing the air flow is, in general, only practical if the fire is near the downcast shaft entrance where fumes from a fire would likely spread throughout the entire mine.

Another two methods, regulating the air flow rates and short-circuiting airflow, were considered as more effective way on controlling the mine fire behavior. The ventilation doors and stoppings with regulator can be utilized on the purpose of airflow regulation. When a fire develops, and the fumes make access difficult, these methods might be appropriate to either decrease or prevent any noxious fumes from entering the return airflow. This prevention enables improved firefighting access to the fire itself. It also prevents the smoke from spreading to other areas of the mine workings, aiding in the rescue of personnel (Wala, 1996). Unfortunately, during this procedure, the ventilation flow is reduced in other areas of the mine. This, in turn, has a significant impact on oxygen available to the evacuating works. Air flow reducing also increases the potential for accumulation of explosive gases.

In this research, ventilation control was applied under different scenarios to determine its effectiveness on fire behavior control. Both regulator adjustment and short-circuiting air flow were utilized to get the fire control results with the help of numerical simulation tools.

2.3. INTERACTION BETWEEN MINE FIRE AND VENTILATION

An open fire can cause disturbances in the ventilating airflow. This disturbance can significantly change the characteristics of airflow further within the mine. The sudden increase in temperature associated with an open fire can cause the air to increase in volume significantly. In the underground environment, the only transport pathway for the expanded air is along both directions of the airway. This expansion provides an opposing force to the main airflow, producing a phenomenon known as the choke, or throttle, effect.

Another significant effect due to this sudden expansion of air is known as rollback. The rollback is a phenomenon unique to underground mines. The reduced density causes the mixture of hot air and products of combustion to rise and flow preferentially along the roof of the airway. The pronounced buoyancy effect causes smoke and hot gases to form a layer along the roof. In a level or descentional airway, these smoke and hot gases will back up against the direction of airflow.

2.3.1. The Throttling Effect. The throttling effect results from an increase in the volume of air as it passes through the fire. This increase is a result of both gas expansion and the addition of combustion products, such as fire gases and evaporated water. As a result, the mass flow of air is decreased while the volume flow exiting the airway is increased. This phenomenon produces the throttling effect.

The throttling effect is analogous to increasing the airway resistance (McPherson, 1993). For the purposes of ventilation network analyses based on a standard value of air density, the raised value of this “pseudo resistance” (*Rt’*) can be estimated in terms of the air temperature in the form of

$$R_t' \propto T^2 \tag{2.1}$$

where T is the absolute temperature (K).

Litton et al. (1987) produced an estimate on the increased resistance in terms of the carbon dioxide produced from a fire. According to the studies undertaken in both the US and Japan, the reduction of both air flow and velocity due to the throttle effect can be between 10 and 25% of the flow before the fire began (Litton et al., 1987). At this level, these reductions can create secondary hazards, such as the accumulation of contaminants, inadequate oxygen content, and smoke rollback.

2.3.2. The Buoyancy (Natural Draft) Effect. Miners refer to smoke flowing along the roof, against the ventilating air current, as “smoke rollback” (Mitchell, 1996). A photograph of the buoyancy effect during a small scale tunnel fire is shown in Figure 2.2. In addition to the visual smoke, a rollback with a high temperature also contains high concentrations of both CO and other toxic/explosive gases. These high concentrations create considerable difficulties for firefighters upstream from the fire, particularly if the conflagration has become fuel-rich. According to Edwards et al. (2006), the reversed smoke may also leak through stoppings into adjacent airways, thereby further endangering miners. Tidal flames and local explosions that can occur throughout the rollback pose the most critical danger to firefighter.

Figure 2.2. Photograph of Buoyancy Effect during a Small Scale Tunnel Fire (Wu and Bakar, 2000)

2.3.2.1 Critical velocity. Both experimental and numerical studies have concluded that smoke rollback can be prevented by maintaining a sufficient velocity of airflow to the mine fire. The minimum longitudinal airflow velocity required to prevent the occurrence of rollback is known as the critical velocity.

The exact value of the critical velocity depends, primarily, on the buoyant plume characteristics, including smoke temperature, smoke flow rate, fire source size, tunnel slope, tunnel height, and tunnel width (Atkinson and Wu, 1996; Kennedy et al., 1996; Mitchell, 1996; Edwards and Hwang, 1999; Wu and Bakar, 2000; Edwards et al., 2006; Ko et al., 2010). Three approaches are typically utilized to obtain the value of critical velocity for various tunnels. The easiest technique for predicting the critical velocity is based on semi-empirical equations. These equations basically obtained by Froude number preservation combined with some experimental data. The second approach is based on the dimensionless analysis of HRR. The last one is a rule of thumb to estimate the critical air velocity in a mine entry (Mitchell, 1996).

2.3.2.1.1 **Mitchell's rule of thumb.** Mitchell (1996) presented a simple relationship for estimating the critical velocity of smoke rollback relative to the entry height:

$$V_c = 100\sqrt{H} \tag{2.2}$$

where Vc is the critical velocity of smoke rollback (ft/min) and H is the entry height (ft).

2.3.2.1.2 **Theory based on Froude number.** The Froude number is defined as the ratio of gravity (buoyancy) forces to pressure (inertia) forces:

$$F_r = \frac{Inertia \quad forces}{gravity \quad forces} = \frac{V^2}{gD} \tag{2.3}$$

where g is the gravity, D is the characteristics length scale, and V is the characteristics velocity scale. The equation was rearranged using the density ratio of the smoke to include the stratification effects. Lee et al. (1979) defined the modified Froude number as

$$F_r = \frac{gH(\rho - \rho_f)}{\rho V^2} \tag{2.4}$$

where F_r is the Froude number, g is the acceleration due to gravity, ρ is the average density of upstream, ρ_f is the average density of the fire-site gases, H is the height of tunnel, and V is the velocity of the approaching air.

Lee et al. (1979) stated that, if the Froude Number is kept either at or below a certain critical value, neither smoke nor hot gases will rollback. Essentially, the lower the Froude number is, the weaker the buoyancy forces become. Their scale-model tests in ducts show the critical value of the Froude number is between 4.5 and 6.7. The Froude number may vary with both the size and the condition of the experiment facility.

2.3.2.1.3 **Theory based on HRR.** The relationship between the ventilation velocity and HRR from the fire has also been proposed based on the Froude number (Thomas, 1968; Hinkley, 1970; Heselden, 1976). After substituting an expression correlating the convective part of HRR with the fire induced smoke characteristics (temperature, density, and flow rate), a final correlation was derived as (Kennedy et al., 1996):

$$V_c = k_g K \left(\frac{gH\dot{Q}(1-\lambda)}{\rho c_p A T_f}\right)^{1/3} \tag{2.5}$$

where V_c is the critical velocity, K is an dimensionless empirical constant equal to 0.61, $\dot{Q}$ is the total HRR, λ is the radiative fraction of the HRR, C_p is the air specific heat, A is a cross-sectional area of the tunnel, and T_f is an average temperature of the fire-site gases. T_f can be estimated from the enthalpy conservation equation:

$$T_f = T_0 + \frac{\dot{Q}(1-\lambda)}{\rho_0 V_c c_p A} \tag{2.6}$$

where, T_0 is the ambient temperature. Variable k_g can be calculated from

$$k_g = 1 + 0.037(\alpha)^{0.8} \tag{2.7}$$

where α is the tunnel gradient.

The critical velocity can be determined by solving Equation (2.5), Equation (2.6), and Equation (2.7) simultaneously using iteration. Based on these equations, results from scale model tests indicated that the ventilation velocity, tunnel geometry, and fire intensity are the most essential factors when determining whether or not a smoke rollback occurs along the roof into the fresh air. This correlation, is valid within a limited range of HRR, where the 1/3 law well fits the experimental data. For higher HRR, the correlation fails because it is not able to represent the asymptotic behavior of the critical velocity (Lee et al., 1979).

On the basis of small scale experiments, Oka and Atkinson (1995) suggested that, for high HRR, the critical velocity reaches an asymptotic value. This value is independent from the HRR. A correlation between dimensionless critical velocity and dimensionless HRR proposed by Oka and Atkinson (1995) is presented as

$$V_c^* = \begin{cases} K_v \left(\dfrac{\dot{Q}^*}{0.12} \right)^{1/3} & \dot{Q}^* \le 0.12 \\ K_v f & \dot{Q}^* \rangle 0.12 \end{cases} \tag{2.8}$$

where V_c* and $\dot{Q}$ * are the dimensionless critical velocity and dimensionless HRR, respectively that can be obtained from both Equation (2.9) and (2.10):

$$\dot{Q}^* = \frac{\dot{Q}}{\rho_0 T_0 c_p g^{1/2} H^{5/2}} \tag{2.9}$$

$$V_c^* = \frac{V_c}{\sqrt{gH}} \tag{2.10}$$

The proportionality constant K_v in Equation (2.8) is between 0.22 and 0.38, depending on the burner geometry.

Wu and Bakar (2000) came to a similar conclusion based on results from some small-scale fire tests. They found, however, that the critical dimensionless HRR is determined as 0.20 rather than the 0.12 proposed by Oka and Atkinson (1995). Additionally, the tunnel height H was replaced with the hydraulic tunnel height $\bar{H}$. This hydraulic tunnel height is defined as the ratio of 4 times the cross-sectional area to the tunnel wetted perimeter. The modified correlation is given as

$$V_c^* = \begin{cases} K_v \left(\dfrac{\dot{Q}^*}{0.20} \right)^{1/3} & \dot{Q}^* \le 0.20 \\ K_v f & \dot{Q}^* \rangle 0.20 \end{cases} \tag{2.11}$$

$$\dot{Q}^* = \frac{\dot{Q}}{\rho_0 T_0 c_p g^{1/2} \bar{H}^{5/2}} \tag{2.12}$$

$$V_c^* = \frac{V_c}{\sqrt{g\bar{H}}} \tag{2.13}$$

The proportionality constant K_v in Wu and Bakar's (2000) tests is 0.40, also beyond the range proposed by Oka and Atkinson (1995).

According to Wu and Bakar's (2000) analysis, the difference between the critical dimensionless HRR in Oka and Atkinson's (1995) equations and their equations indicates that the dimensionless critical velocity is related to the dimensions of the experimental facility. The influence of fire intensity on critical velocity is still not certain; it may vary with the test model's geometry.

Five diesel fuel fire experiments were conducted in NIOSH's Pittsburgh Research Laboratory (PRL) Safety Research Coal Mine (SRCM) to determine the critical air velocity for pre-venting smoke rollback (Edwards et al., 2006). These experiments were the first time to test critical velocity in a real size mine entry of 2.06m in height by 2.91m in width. The fire intensity varied from 50kW to 300kW. Experimental results indicate a dependence of the dimensionless critical velocity on the dimensionless HRR to the one third power, expressed as

$$V_c^* = 0.92(\dot{Q}^*)^{0.3} \tag{2.14}$$

The effect of the tunnel slope on the critical velocity was investigated by both Atkinson and Wu (1996) and Ko et al. (2010) in small-scale tests. The former researchers burned propane in small-scale experiments, while the latter researchers burned methanol, acetone and n-heptane as fuel. In both cases, the results showed that the critical velocity increases with the tunnel slope due to the enhanced stack effect:

$$V_{c,\theta} = V_{c,0}(1 + K_\theta \cdot \theta) \tag{2.15}$$

where $V_{c,\theta}$ and $V_{c,0}$ are the critical velocities in an inclined and horizontal tunnel, respectively, and θ is the tunnel slope. Empirical constant K_θ is 0.014 in Atkinson and Wu's (1996) research, and is 0.033 in the research of Ko et al. (2010).

Based on previous studies (supported by experimental measurements), the maximum critical velocity value to be expected in any tunnel fire is between 2.5 m/s and 3.0 m/s. If the airflow velocity is within this range (or eventually larger), the back layering is usually avoided and the smoke is pushed downstream away from the fire region. Although this critical velocity range has been found to be true in most cases, the correlation between influence factors and critical velocity needs to be characterized further.

2.3.2.2 Length of back layering. Back layering can occur for ventilation velocities between 1.0 m/s and 2.5 m/s. The degree, however, depends on the size of the fire source. The length of back layering usually varies between zero and 17 times the tunnel hydraulic diameter (Ingason, 2005). For even lower ventilation velocities (between 0.0 m/s and 1 m/s), the back layering distance can be very large (several hundred meters) and almost uniform in both directions.

Ingason (2005) conducted small scale experiments and proposed an approximated correlation between both back layering distance and tunnel geometry as well as ventilation velocity and the fire HRR:

$$\frac{L_b}{H} \propto \left(\frac{g\dot{Q}}{\rho_0 c_P T_0 V^3 H} \right)^{1/3} \tag{2.16}$$

where L_b is the back layering distance. The proportionality constant, deduced from small-scale experiments, is between 0.6 and 2.2. This correlation was gotten based on the results from small-scale test. Great care must be adopted when predicting the back layering distance for other conditions on the basis of Equation 2.16.

Indeed, this inadaptability was proved in a recent work. Some large-scale experiments were conducted in a 1 km long tunnel (W ~ 10m, H ~ 7m, slope ~ 2%) with fires between 1.8 MW and 3.2 MW. The results indicated that the back layering distance estimated from Equation 2.16 was seriously under-predicted (up to 1 order of magnitude) (Hu et al., 2008).

It is difficult to define with great certainty the extent of smoke reversal for different ventilation velocities. To overcome this problem, Edwards et al. (2006) tried to solve the instability of the smoke reversal by reducing the data with dimensionless variables. An empirical expression about smoke rollback length was expressed as

$$L_b = \left[0.0238 \ln\left(\frac{\dot{Q}}{AV^3 \rho_0} \right) - 0.0479 \right] \frac{c_p (T_f - T_0)}{g} \tag{2.17}$$

As with the critical velocity, the relationship between the smoke rollback length and its influence factors is still unclear. Although the phenomena have been observed for many years, the correlation still remains undefined due to limiting research methods. The development of the research tools has greatly influenced the study of the interaction between a mine fire and ventilation.

3. ANALYSIS OF MINE FIRE MODEL

3.1. INTRODUCTION

The application of 3D in CFD as a fire safety engineering tool has become widespread over the last two decades (Guan and Kwok, 2008). It is the intent of this study to apply 3D calculations in an underground mine designs and planning.

Using 3D CFD simulation techniques enables mining engineers to solve a complete set of partial differential equations, using the conservation of mass, momentum, and energy for ventilation modeling. Results will enable mining engineers estimate, with reasonable accuracy, air velocity and temperature fields, species concentration, heat fluxes mapping, and other relevant ventilation variables of concern. These calculations are performed by following the conservation laws on a high number of control volumes. The control volumes are generated by a numerical discretization of the computational domain.

The numerical solution of the governing equations is limited by the difficulty of resolving the physical model. It will even be more challenging if the model involves the turbulent flow which is typical of an underground environment, especially in the case of a mine fire.

Underground mine fires occur in a confined space. As a result, the full buoyancy effect, throttling effect, and the heat property of surrounding wall conditions must be included as boundary conditions in the numerical model. Difficulty of quantifying these conditions, especially when there is a mine fire, are expected. Further complexity is introduced by the numerical solution of the final set of partial differential equations. The choice of numerical schemes and the accuracy of the grid description will significantly influence the quality of a CFD solution.

Today, computational fluid dynamics (CFD) is a mature tool for predicting not only overall flow behaviors underground but also heat distribution in a confined environment, such as underground airway. More complex issues related to smoke and flame spread, soot formation, oxygen vitiation, and combustion modeling, however, are far from being solved. They will not likely be satisfactorily addressed in the next two or three decades.

Any CFD analysis requires two additional steps: verification and validation (McGrattan and Miles, 2008). Verification is a process that checks the correctness of the solution of the equations' solutions while validation examines the appropriateness of the governing equations for a model under investigation. Typically, validation is made by comparing the results of modeling against experimental data. In this case, the descrepencies that cannot be explained are attributed to both an incorrect hypothesis and errors through over-simplification introduced when building the governing equations.

3.2. FIRE EXPERIMENT

Experimental method is a very important method for studying fire as many specific questions are impossible to answer through theoretical analysis alone. The empirical, or semi-empirical, formulae from an experimental simulation have been commonly applied. Meanwhile, simulation results from the experiment can also be used to verify both the theoretical analysis and the numerical simulation.

3.2.1. The Wombat Mine Introduction. The Missouri S&T Experimental Mine, shown in Figure 3.1, is located approximately one and a half mile from the campus. The mine consists of two parts, the Main Mine and the Wombat Mine. Both are underground dolomite operations used for training purposes. The Main Mine was used in the multiscale model and is discussed in Sections 4, 5, and 7 of this dissertation.

The fire test was conducted in the Wombat Mine. This 32.0m by 23.2m mine is at the east side of the Main Mine, accessed through an entrance at the west side of the mine. The layout of the Wombat Mine is shown in Figure 3.2a. A photograph of both the entrance and an inside view are given in Figure 3.2b. Wombat is ventilated through a 300 CPV centrifugal fan at the east side (See Figure 3.3a); his fan has a 3.68 kW motor produced by LOREN COOK Co.

Located on top of the exhaust shaft and with a 2-hp motor operating at 780 rpm, the fan can provide approximately 11,055 cfm air at 1.2 in W.G. static pressure. The fan curve is presented in Figure 3.3 (b) (Anon., 2010b).

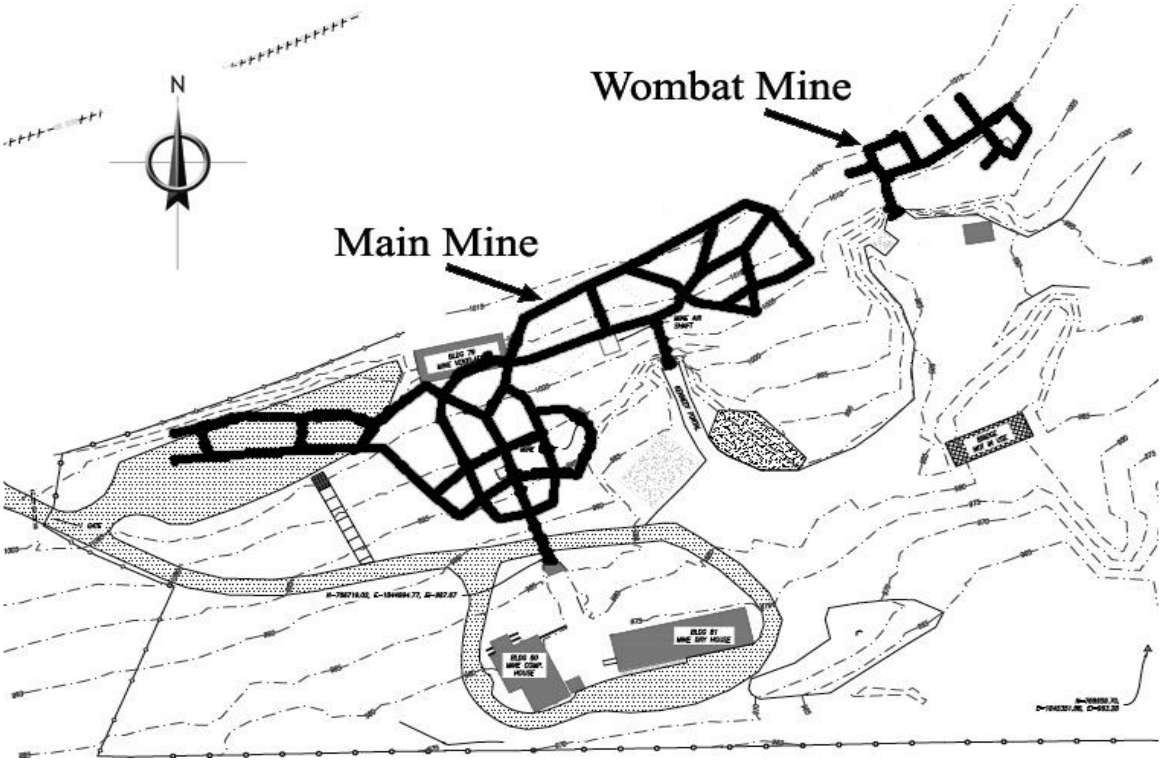

Figure 3.1. Layout of Experiment Mines of Missouri S&T

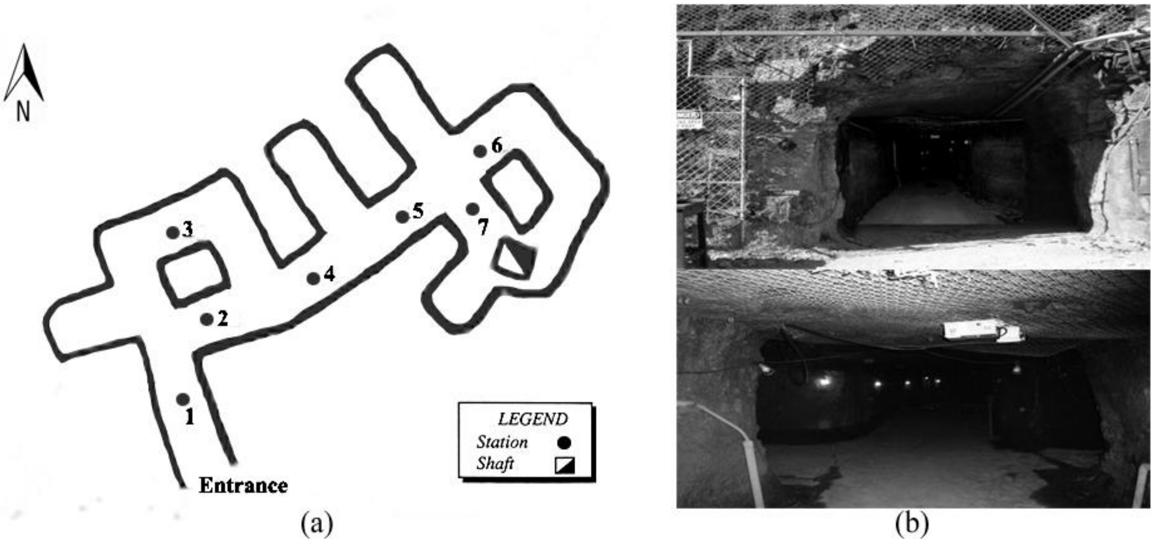

Figure 3.2. Wombat Mine Airways (a) and Photographes (b)

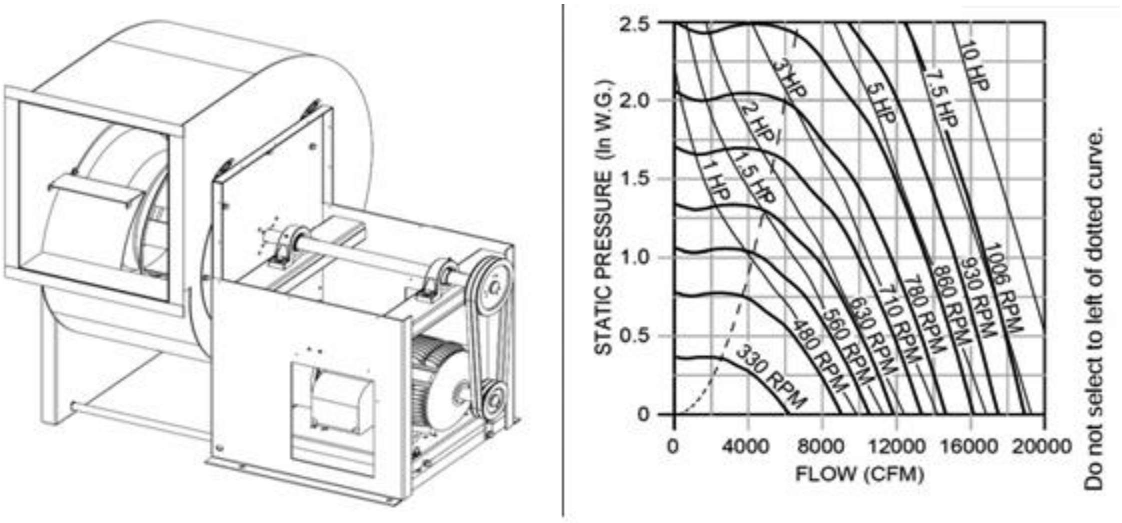

(a) (b)

Figure 3.3. Wombat Mine Exhaust Fan (a) and the Fan Curve (b)

To ventilate the Wombat Mine better, a temporary centrifugal fan was placed in the bulkhead at the center of airway near the entrance. A temporary duct was attached at the end of the discharge of the fan.

The maximum air velocity (V_{max}) was measured at 5.8 m/s at the center of the fan duct. For the Reynolds number exceeding 10,000, the average velocity (V) was assumed to be $0.8 \cdot V_{max}$ (4.64 m/s). Based on the dimension of the duct, the total air quantity provided by the fan was calculated at 0.742 m^3/s. The cross section area at the entrance was 5.42 m^2 (2.63m in width and 2.06m in height). Thus, the calculated average air velocity at the entrance was 0.137 m/s.

3.2.2. Measurement of Parameters. During the test, the fuel mass loss with time was measured, and both temperature and velocity at several designed points were also measured.

The fuel mass loss rate was measured with a digital scale (model FG-60KBM) by A&D Co. The industrial bench scale had a 30 cm × 38 cm stainless platform. A built in RS-232 port was used to transmit weight readings to a computer every second with date and time, saved and stored in CSV format. This scale capability was 150 lb with a ±0.01

lb resolution. The measuring system, including both the scale (a) and the data collecting program (b), are shown in Figure 3.4.

test1-1.csv

	FireTest				
312	10-06-2011	11:54:02	ST	+00001.77	lb
313	10-06-2011	11:54:03	ST	+00001.77	lb
314	10-06-2011	11:54:04	ST	+00001.77	lb
315	10-06-2011	11:54:05	ST	+00001.77	lb
316	10-06-2011	11:54:06	ST	+00001.77	lb
317	10-06-2011	11:54:07	ST	+00001.76	lb
318	10-06-2011	11:54:08	ST	+00001.76	lb
319	10-06-2011	11:54:09	ST	+00001.76	lb
320	10-06-2011	11:54:10	ST	+00001.76	lb
321	10-06-2011	11:54:11	ST	+00001.76	lb
322	10-06-2011	11:54:12	ST	+00001.76	lb
343	10-06-2011	11:54:33	ST	+00001.73	lb

(a) **(b)**

Figure 3.4. Mass Loss Measurement Scale (a) and Data Collecting Program (b)

Temperature were measured using both Rel-Tek's HotBoss*100/TC (0 to 1000 ℃) and HotBoss*100 (0 to 200 ℃) near the fire zone and designated locations away from a fire zone. The photos of thermocouples used in the test are given in Figure 3.5.

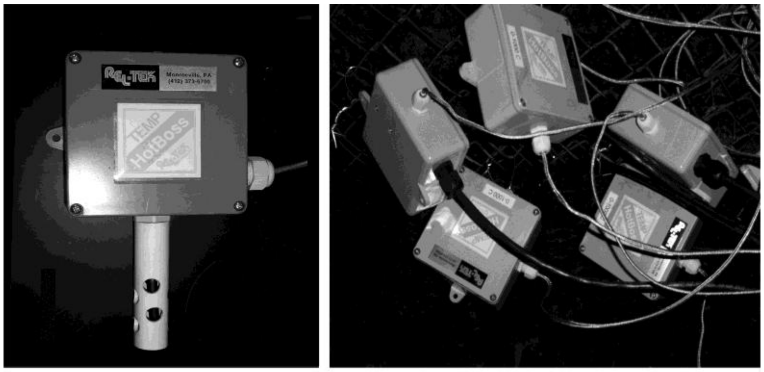

(a) (b)

Figure 3.5. Photos of Thermocouples (a) HotBoss*100/TC and (b) HotBoss*100

The AirBoss*200W also produced by Rel-Tek, was used to measure air velocity during the fire test. This unit is a microprocessor-based, linear air velocity sensor with a range of 0-2000 fpm. It provides dependable outputs for velocities well below 50 fpm, a critical threshold for many life-support applications. The zero fpm set point is verified by completely blocking the air flow. A plastic tube 10 cm in diameter and 30 cm in length provides the airflow with a vector orientation. A photo of AirBoss*200W is given in Figure 3.6.

Figure 3.6. Photo of AirBoss*200W

The sensors were specially designed for this research, and each was calibrated before delivery by the manufacturer. A series of trial tests were conducted in the lab prior to actural testing in the mine to ensure that the wire connection and data collection were set correctly.

3.2.3. Test Scenario Design and Measuring System Arrangement. A round steel pan 23 cm in diameter and 6 cm in depth was used to hold fuel during the fire test. The pan was filled to 5 cm in height. This amount of fuel would sustain a burning fire for approximately 10 minutes. Figure 3.7 is a simple sketch of a fuel pan.

During the fire test, two types of fuels were used: pure kerosene and a mixture of 45% kerosene, 50% diesel and 5% lubricant for comparison in difference in fire behaviors. The influence of the fire source location was also considered; the fuel pan was placed, depending on cases examined, either on the floor or 0.9m from the floor. Conditions both with and without airflow were also considered to represent different ventilation conditions. One, two, or four pans of fuel were ignited to allow for a comparison between fire intensities. A total of 10 cases were performed with each case repeated twice to ensure accuracy. Detailed information on these is listed in Table 3.1. Case 4 (in Table 3.1) was chosen as a basis for describing the simulation process of a numerical model.

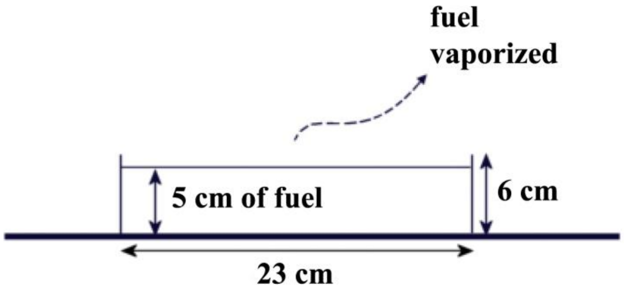

Figure 3.7. Sketch of a Fuel Pan

Table 3.1. Fire Test Cases in the Wombat Mine

Test Cases	Fire Intensity, kW	Fuel Type	Fire Source Location	Air Velocity, m/s
1	one pan	Kerosene	Floor	0
2	one pan	Mixture	Floor	0.25
3	two pans	Mixture	Floor	0.25
4	one pan	Kerosene	Floor	0.25
5	two pans	Kerosene	Floor	0.25
6	one pan	Mixture	0.9m from floor	0.25
7	two pans	Mixture	0.9m from floor	0.25
8	one pan	Kerosene	0.9m from floor	0.25
9	two pans	Kerosene	0.9m from floor	0.25
10	four pans	Mixture	0.9m from floor	0.25

Sensors locations during the fire test are illustrated in Figure 3.8. Stations V1 to V5 represent either the measurement position or the fire source. The fire source was located at V2. Five thermocouples, from T1 to T5, were placed at the same cross section. Two additional thermocouples (T6 and T7) were placed at V3. Two other thermocouples, H1 and H2, were placed at V1 and V4, respectively. Finally, an air velocity sensor (A) was placed at V5.

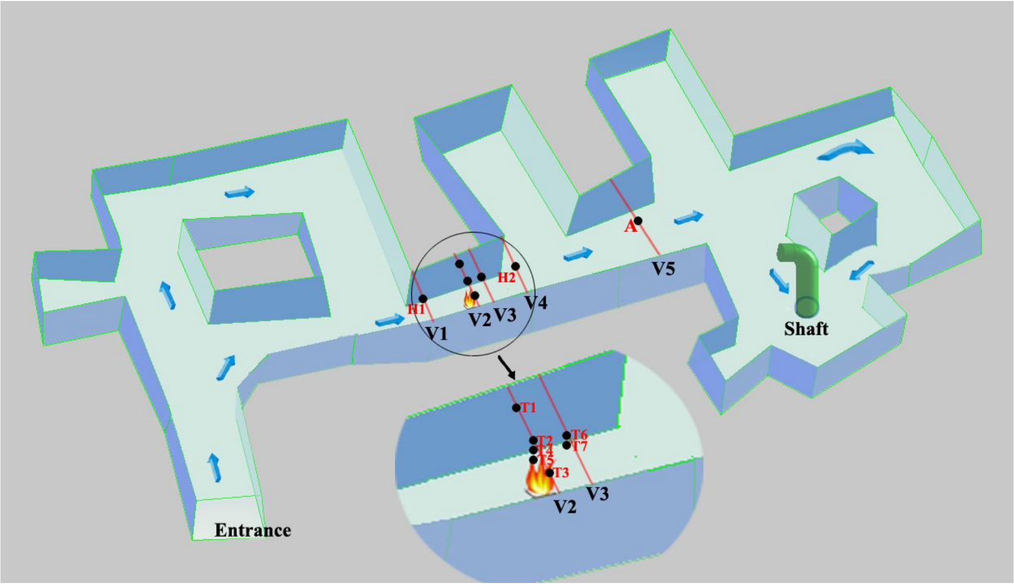

Figure 3.8. Schematic of Showing both Fire Source and Sensors in the Wombat Mine

The location schematic of both fire source and sensors along the Wombat Mine can be found in Figure 3.9. The cross-section from 1-1’ to 5-5’ represents stations V1 to V5, respectively, in Figure 3.8. Rectangle boxes indicate the sensors. The sensors were connected to a computer through I/O boxes DX 4404, DX 8000, and DX-COM. The distances values were in meter (m).

The airway cross-section at the fire source was 1.5m in width and 2.2m in height. The sensor locations at each cross section, for all ten test cases, are shown in Figure 3.10. For test cases 1 through 5, the fire source at cross section 2-2’was located on the floor.

The location of the fire source was lifted 0.9m (not shown in Figure 3.10) away from the floor for test cases 6 through 10.

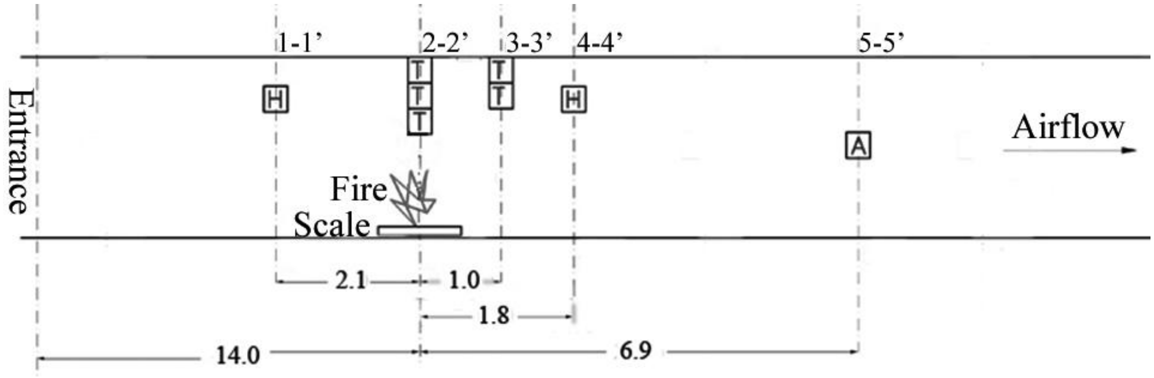

Figure 3.9. Schematic of Showing Locations of both Fire Source and Sensors in the Wombat Mine

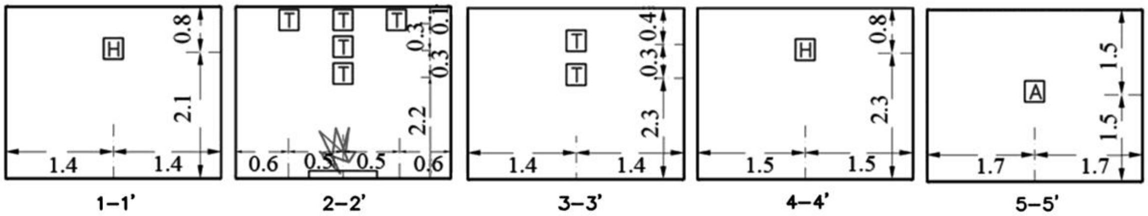

Figure 3.10. Locations of Sensors at Cross Sections in the Wombat Mine

3.2.4. Test Process. As mentioned in Section 3.2.3, a digital scale was used to measure the fuel mass loss rate. The weighing data were transmitted from the scale to a computer approximately five meters away from the scale (where the fire source was placed). The scale was calibrated on-site using a regular 5-lb and 20-lb module before the tests.

Before the mine test began, all sensors mounted at designed positions along the airway according to installation instructions. All connections (both between sensors and the I/O module box as well as between the I/O module box and the computer) were checked with a monitoring program provided by the sensor's manufacturer.

A number of wires and cables were placed near the fire source during the test. To protect them from any possible interference and physical damage, these wires and cables were taped with fire-proof tapes. The transmitters were located in the areas where they remained in required working ambient temperature range (40~85 ℃). The wire joints were sealed with insulating tape.

A ventilation survey was conducted in the Wombat Mine before the fire test. Seven ventilation stations were located with velocity, pressure and dry/wet bulb temperatures measured. All sensors exact locations were also measured.

Once preparations were complete, a trial test was conducted to determine the burn time. Time required for totally exhausting all fire gases was also recorded. The most serious fire scenario was designed for this trial test.

During the test run, one Missouri S&T mine rescue team member with the SCBA (self contained breathing apparatus, produced by Dräger) and the TM*412 multi-gas detector (from Industrial Scientific Co.) was on standby, in case of emergency. Each test was conducted during a 50-minute interval, including 10 minutes for the fire to burn and 40 minutes to remove the fire gases from the mine.

The fire tests were begun on October 6, 2011. After the fire began, no one was allowed to enter the mine; the sensor data was monitored from the outside. Once the sensor reading returned to the initial status, the mine was ready for the next test. After the fire was done, the next test was conducted at, approximately, 40 minutes later. This wait time was necessary for two reasons. 1) The mine needed to be safe enough for researchers to prepare the next test. 2) The heat and fire gases needed to be completely removed from the mine to eliminate any influence on the following test.

The fire tests were completed over a period of two days. A total of ten fire cases were designed for characterizing the fire behavior. Fire intensity, fuel type, fire location, and air velocity were main parameters changed in each case. The detailed information in each case was listed in Table 3.1.

3.3. NUMERICAL MODEL

The 3D CFD technique requires the domain to be subdivided into a number of smaller, non-overlapping subdomains with valume dx dy dz to solve the flow physics within the physical domain. This, subsequently, results in the generation of a mesh (or grid) of cells (elements or control volumes) covering the entire domain. The essential fluid flows that are described in each of these cells are usually solved numerically through fundamental equations governing the fluid dynamics. The set of partial differential equations, known as governing equations, describes the conservation of mass, momentum, and energy. Detailed information on these governing equations can be found in work by Anderson (1995). Discrete values of the flow properties, such as velocity, pressure, temperature, and other transport parameters of interest, are determined subsequently at each of the respective cells.

3.3.1. Physical Model of Mine Fires. Numerous physical models in FLUENT needed to be considered for this study. Each of the models is discussed below.

3.3.1.1 Fluid dynamic models. Because matter can neither be created nor destroyed, mass must always be conserved. This conservation law is pertinent to the derivation of the continuity equation. The partial differential form of the unsteady, three-dimensional mass conservation, or continuity equation, is

$$\frac{\partial \rho}{\partial t} + \frac{\partial (\rho u_i)}{\partial x_i} = 0 \tag{3.1}$$

where ρ is the fluid density and u_i is the velocity in the x_i direction.

The three-dimensional momentum equation for the velocity component u_i can now be written in the following conservation partial differential forms as

$$\frac{\partial (\rho u_i)}{\partial t} + \frac{\partial (\rho u_j u_i)}{\partial x_j} = \frac{\partial}{\partial x_j}[\mu \frac{\partial u_i}{\partial x_j}] + S_{M\,x_i} \tag{3.2}$$

where $S_{M\,x_i}$ is the momentum source term given by

$$S_{M x_i} = -\frac{\partial p}{\partial x_i} + \frac{\partial}{\partial x_j}[\mu \frac{\partial \rho u_j}{\partial x_i}] + \frac{\partial}{\partial x_i}[\lambda(\frac{\partial \rho u_j}{\partial x_j})] + \rho g_{x_i} \qquad (3.3)$$

where p is the pressure and g_{xi} is the accelerator in x, y, and z direction. The proportionality constant of μ is the (first) dynamic viscosity that relates stresses to linear deformation. The proportionality constant of λ is the second viscosity that relates stresses to the volumetric deformation. Currently, not much is known about the second viscosity. Nevertheless, Stokes hypothesis (λ = -2/3 μ) has been found to be a good working approximation for gases.

Drysdale (1986) suggested a fire that clearly corresponds to a buoyancy-driven turbulent diffusion flame. Thus, the dominant body force resulting from buoyancy should be included in the momentum equation. For this research, both accelerators in the x and z (g_{x_1} and g_{x_3}) direction are equal to zero. The gravity acts in the y direction. Hence, the additional source term, due to buoyancy, needs to be incorporated in the y-momentum equation. The source term ($\rho\, g_{x_2}$) was replaced with [$-g_{x_2}$ (ρ-ρ_{ref})], where ρ_{ref} is the reference density and g_{x_2} is equal to 9.8 m/s^2.

Based on the consideration of the first law of thermodynamics, the energy equation can be derived for a combusting fire system. In such a system, the rate of energy change is equal to the net rate of heat addition, plus the heat rate of work done and the rate of heat added or removed by the heat source. In this research, neither the combustion model nor the work was included in the numerical model; only radiation heat from the fire source was considered as an energy source. The conservative partial differential form of the energy equation, in terms of the total enthalpy h, is given by

$$\frac{\partial(\rho h)}{\partial t} + \frac{\partial(\rho u_i h)}{\partial x_i} + \frac{\partial(\rho v h)}{\partial y} + \frac{\partial(\rho w h)}{\partial z} = \frac{\partial}{\partial x_i}[\frac{k}{c_p}\frac{\partial h}{\partial x_i}] + \dot{Q}_s \qquad (3.4)$$

where h is the sensible enthalpy, k is the thermal conductivity, and c_p is the specific heat of the constant pressure. Variable $\dot{Q}_s$ depicts the possibility of either an increase or a decrease in the heat within the fluid element. It can be obtained from the equation

$$\sum \dot{Q} = -(\frac{\partial q_{x_i}}{\partial x_i}) \cdot \Delta V \tag{3.5}$$

where ΔV is the element volume and q_{x_i} is the heat flux (which can be obtained directly from the radiation model calculation).

3.3.1.2 Turbulence model. Both tunnel ventilation and fire-induced flows are characterized by having fluctuating velocity fields. These fluctuations make the fluid velocities, as well as other properties vary in a random, chaotic way. The exact equations describing turbulent motion are already known (the Navier-Stokes equations), despite the complexity of the turbulent flow.

Typically, the description of turbulent flows can be addressed by decomposing the instantaneous fluid velocity *u(t)* into both a steady mean value $\bar{u}$ and a fluctuating component *u'(t)*. This approach, known as Reynolds decomposition, allows a turbulent flow to be characterized in terms of the mean value properties ($\bar{u}, \bar{v}, \bar{w}, \bar{p}, \bar{T}$), together with statistical properties of their fluctuations (*u', v', w', p', T'*) (Versteeg and Malalasekera, 2007). In many engineering applications, knowing the mean values of the flow properties is usually of greater significance than knowing the fluctuating components. For most engineering purposes, the turbulent fluctuations are not necessary to be resolved. The information provided by the time averaged fluid properties are adequate.

Various methods are available for modeling turbulence. In this study, the widely recognized standard *k-ε* turbulence model was used for this purpose. This model is a semi-empirical model based on the transport equations for both the turbulence kinetic energy (*k*) and its dissipation rate (*ε*). The transport equation for *k* (see Eq. 3.6) is derived from the exact equation. The transport equation for *ε* (see Eq. 3.7) is obtained using physical reasoning, as its exact transport equation contains many unknown and unmeasurable terms.

$$\frac{\partial \rho k}{\partial t} + \frac{\partial(\rho k \bar{u}_i)}{\partial x_i} = \frac{\partial}{\partial x_j}[(\mu + \frac{\mu_t}{\sigma_k})\frac{\partial k}{\partial x_j}] + G_k + G_B - \rho\varepsilon \tag{3.6}$$

$$\frac{\partial \rho \varepsilon}{\partial t} + \frac{\partial(\rho \varepsilon \bar{u}_i)}{\partial x_i} = \frac{\partial}{\partial x_j}[(\mu + \frac{\mu_t}{\sigma_\varepsilon})\frac{\partial \varepsilon}{\partial x_j}] + C_{1,\varepsilon}\frac{\varepsilon}{k}[G_k + C_{3,\varepsilon}G_B) - C_{2,\varepsilon}\rho\frac{\varepsilon^2}{k} \tag{3.7}$$

where G_k represents the generation of turbulence kinetic energy due to the mean velocity gradients and G_B is the generation of turbulence kinetic energy due to buoyancy. $C_{1,\varepsilon}$, $C_{2,\varepsilon}$, and $C_{3,\varepsilon}$ are constants; σ_k and σ_ε are the turbulent Prandtl numbers for k and ε, respectively.

Turbulent viscosity (μ_t) can be computed by combining k and ε as follows:

$$\mu_t = \rho C_\mu \frac{k^2}{\varepsilon} \tag{3.8}$$

where C_μ is a constant of the model.

Constants $C_{1,\varepsilon}$, $C_{2,\varepsilon}$, C_μ, σ_k, and σ_ε have been derived through comprehensive data fitting for a wide range of turbulent flows:

$C_{1,\varepsilon} = 1.44$, $C_{2,\varepsilon} = 1.92$, $C_\mu = 0.09$, $\sigma_k = 1.0$ and $\sigma_\varepsilon = 1.3$ (Launder and Spalding, 1974).

The constants $C_{3,\varepsilon}$, which determine how ε is effected by the buoyancy, should be close to “1” for vertical buoyant shear layers; they should be close to “0” for horizontal buoyant shear layers (Van Maele and Merci, 2006). To make possible the use of a single expression for $C_{3,\varepsilon}$, FLUENT uses the following relationship:

$$C_{3,\varepsilon} = \tanh\left(\frac{v}{u}\right) \tag{3.9}$$

where v is the component of the flow velocity parallel to the gravity vector and u is the perpendicular component (Anon., 2009a).

The generation of turbulent kinetic energy due to mean velocity gradients G_k can be computed as

$$G_k = \mu_t S^2 \tag{3.10}$$

where S is the modulus of the mean rate of the strain tensor, defined as

$$S = \sqrt{2 S_{ij} S_{ij}} \tag{3.11}$$

The mean strain rate is given by:

$$S_{ij} = \frac{1}{2}(\frac{\partial u_i}{\partial x_j} + \frac{\partial u_j}{\partial x_i}) \tag{3.12}$$

The generation of turbulence due to buoyancy is computed with

$$G_B = \beta g_i \frac{\mu_t}{\Pr_t} \frac{\partial T}{\partial x_i} \tag{3.13}$$

where g_i is the component of the gravity vector in the i^{th} direction and Pr_t is the turbulent Prandtl number by default, assumed to be equal to 0.85. The coefficient of thermal expansion (β) is the defined

$$\beta = -\frac{1}{\rho}(\frac{\partial \rho}{\partial T})_p \tag{3.14}$$

The subscript p indicates that the pressure is held constant during expansion.

3.3.1.3 Radiation model. Under mine fire conditions, two modes of heat transfer exist: radiation and convection. As the body of the flame is heated up due to energy release from chemical reactions, it will lose some part of the heat by convection and another part by radiation. The former usually persists at low temperatures, between approximately 150 ^{o}C and 200 ^{o}C, while the latter becomes increasingly dominant for temperatures above 400 ^{o}C. Based on literature reviews, the highest temperature of the fire source is between 1000 ^{o}C and 1500 ^{o}C. Thus, in this research, only thermal radiation was included in the numerical model.

The P-1 model is the simplest radiation model. It is based on the expansion of the radiation intensity I into an orthogonal series of spherical harmonics. The differential equation governing the P-1 approximation for determining the distribution of the incident radiation G can be written as:

$$\nabla \cdot (\Gamma \nabla G) - aG + 4an^2 \sigma T^4 = S_G \tag{3.15}$$

where a represents the absorption coefficient, n is the refractive index of the medium, σ is the Stefan-Boltzmann constant, T is the temperature, and S_G is a user-defined radiation source. The parameter Γ can be obtained from

$$\Gamma = \frac{1}{3(a+\sigma_s) - C\sigma_s} \tag{3.16}$$

where σ_s is the scattering coefficient and C is the linear-anisotropic phase function (Anon., 2009a).

If ε_w and T_w are the emissivities and temperature of the boundaries, respectively, then the boundary condition associated with the above equation according to Gautham et al. (2006) is

$$q_w = \frac{\varepsilon_w}{2(2-\varepsilon_w)}(4\sigma T_w^4 - G) \tag{3.17}$$

When modeling gray radiation, the following equation is obtained for both the radiation flux q_r and its divergence ($\nabla \cdot q_r$) if only four terms in the series are used:

$$q_r = -\Gamma \nabla G \tag{3.18}$$

$$-\nabla \cdot q_r = aG - 4an^2\sigma T^4 \tag{3.19}$$

The expression for $-\nabla \cdot q_r$ can be directly substituted into the energy equation to account for heat sources due to radiation.

3.3.2. Geometrical and Meshing Model for the Wombat Mine. A 3D CFD model was used to simulate the interaction between the fire and ventilation flows in the Wombat Mine. The cross section of the Wombat Mine has a rectangular shape. Wombat Mine is flat with little change in elevation at all airway junctions and all airways are assumed to have constant height of 2.9m. A geometrical representation of the Wombat Mine is given in Figure 3.11.

Section One in Figure 3.11 represents the transversal section cross the fire source (section 2-2’ in Figure 3.9), and Section Two is the longitudinal section, along the airway, through the fire source.

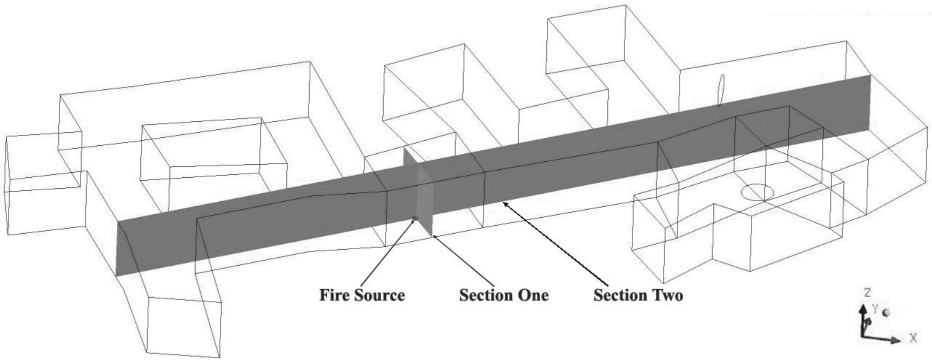

Figure 3.11. Geometrical 3D Model of the Wombat Mine

The computational domain was discretized with a hexahedral mesh arrangement. Test case 4 was adopted and various runs were conducted to assess the mesh requirement. Four different meshes were generated with the resulting solutions compared. The element numbers for the entire Wombat Mine were between 0.9 millions and 3.9 millions. Comparisons of the meshes as well as the corresponding temperature contours at the Section One are presented in Figure 3.12 and Figure 3.13, respectively.

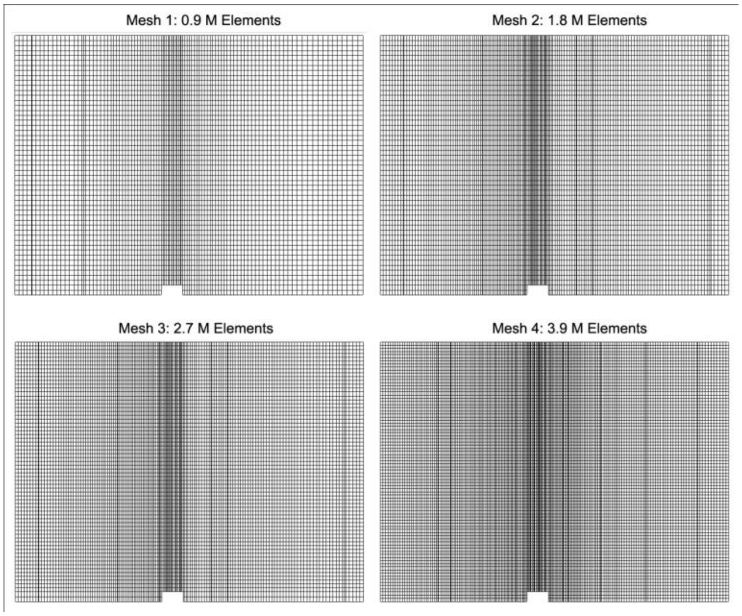

Figure 3.12. Comparison of Mesh 1 to 4 at Section One in the Wombat Mine

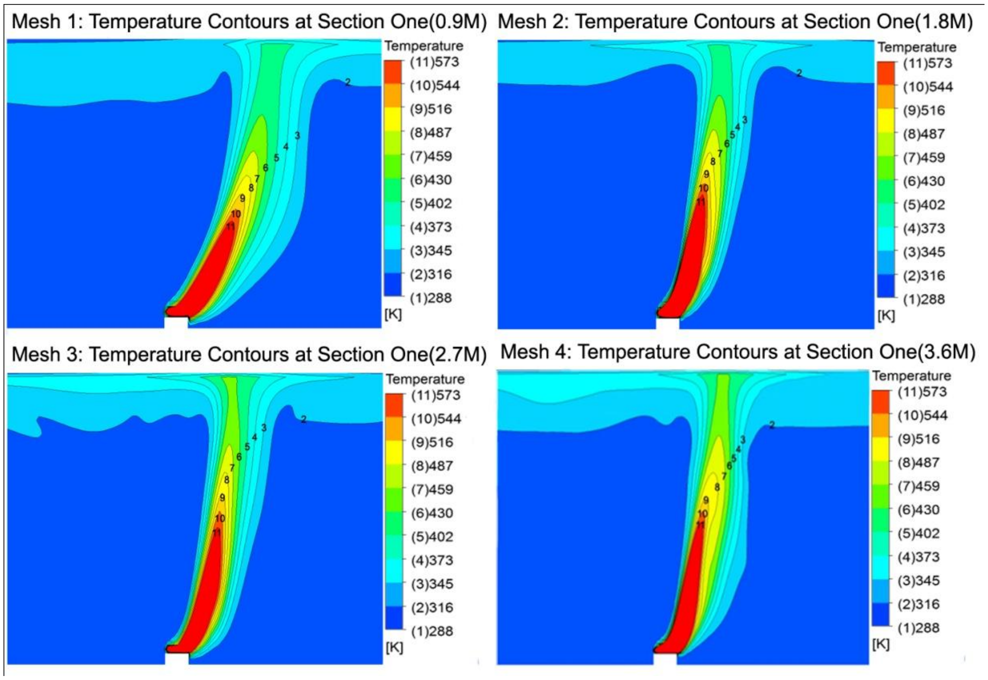

Figure 3.13. Comparison of Temperature Contour for Mesh 1 to 4 at Section One in the Wombat Mine

For the simulation the coarser the mesh (less number of elements the bigger the deviation is from a much finer mesh. For example, a coarser mesh (Mesh 1) at 0.9×10^6 cells results in a 3.15% difference in average temperature at Section One when compared to a finest mesh tested (3.6×10^6 elements). A finer mesh (Mesh 3), however, led to results within 0.18% of the prediction made with the finest mesh. Detailed results of the grid independence study from the Wombat Mine are listed in Table 3.2.

Table 3.2. Grid Independence Study in the Wombat Mine for Case 4

Mesh No.	Element Numbers	Average Temperature, K	Deviation from Mesh 4
1	910037	318.76	3.15%
2	1828178	324.28	1.48%
3	2711180	328.56	0.18%
4	3937655	329.14	-

For best result with a manageable computer time, Mesh 3 (2.7×10^6 elements) was adopted to calculate the numerical model in the Wombat Mine. The final meshed geometry is plotted in Figure 3.14. The skewness of the mesh model is between 3.8×10^{-4} and 0.6 with an average value at 7.4×10^{-2}. This value is much less than 0.6 (the level considered acceptable for an acceptable mesh) (Anon., 2009a).

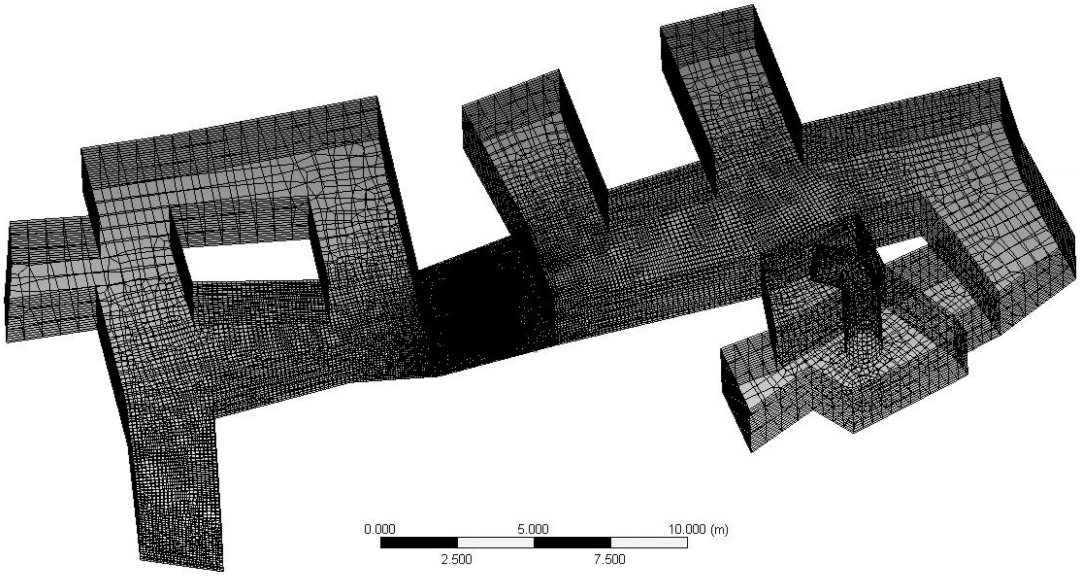

Figure 3.14. Meshed Model of the Wombat Mine

3.3.3. Boundary Conditions. Various boundary conditions were set for the reference case, with each described in details below.

The air flow inlet. As it was the only entrance, the inlet was considered to be a velocity inlet boundary condition, with a constant value at 0.137 m/s. This velocity inlet had a default 10% turbulent intensity and a 2.31m hydraulic diameter. The temperature was set at 288.15 K.

The fuel inlet. The fire has been modeled as a volumetric heat source without using a dedicated combustion model. It has been shown that this simplified approach is the most practical given its low computational cost and ability to reproduce the overall behavior of mine fire induced flows. In the previous reference, the accuracy of the model predictions has been estimated by comparing numerical data against experimental data from a number of enclose fires for both small and large mines.

The fuel inlet was considered as a mass flow inlet with high temperature conditions. The mass flow rate was closely related to the HRR of a fire source. The heat release rate was calculated based on t-square fire model as (Zhou, 2009):

$$\dot{Q}(t)=\begin{cases} a_1(t-t_0)^2 & t_0\langle t\le t_1 \\ \dot{Q}_{\max} & t_1\langle t\le t_2 \\ a_2(t-t_3)^2 & t_2\langle t\le t_3 \end{cases} \tag{3.20}$$

where $\dot{Q}$ is the heat release rate (kW), a_1 is growing factor of growth period (kW/s), a_2 is the decaying factor of decay period (kW/s), $\dot{Q}_{\max}$ is the maximum heat release rate (kW), t is the time (s), t_0 is the time of ignition start (s), t_1 is the start time of steady period (s), t_2 is the end time of steady period and start time of decay period (s), and t_3 is the end time of decay period (s).

Based on the measured results, the fire lasted 600s. At 60s, HRR of fire reached the maximum value, 26.1 kW, and lasted 480s before decaying at 540s. So, the t_0, t_1,t_2 and t_3 were set to 0s, 60s, 540s, and 600s, respectively. The factors a_1 and a_2 can be determined by:

$$a_1=\frac{\dot{Q}_{\max}}{(t_1-t_0)^2} \tag{3.21}$$

$$a_2=\frac{\dot{Q}_{\max}}{(t_2-t_3)^2} \tag{3.22}$$

The calculated results for a_1 and a_2 are the same at 0.00725 kW/s.

The relationship between HRR and the mass loss rate can be given by (Bounagui et al., 2005):

$$\dot{Q}=A_f\dot{m}''\chi\Delta H_c \tag{3.23}$$

where A_f is the horizontal burning area of the fuel (m^2), $\dot{m}''$ is the mass loss rate unit area (kg/(m^{2}s)), χ is the combustion efficiency, and ΔH_c is the complete heat of combustion (MJ/kg).

The heat of combustion of kerosene is 43.2 MJ/kg. The underground mine was reasonably ventilated and a combustion efficiency of 0.85 was used (Edwards et al., 1997). The horizontal burning area of the fuel was 0.0415 m^2. Depending on the amount of heat released into the domain, the mass loss rate, corresponding to the mass flow rate at the fuel inlet boundary, can be calculated.

Since the mass flow rate changed with fire burning time, the fuel inlet boundary condition was set up using a UFD in FLUENT. The mass flow rates at different time period were calculated using equation:

$$\dot{m}''(t) = \begin{cases} t^2 \dfrac{0.017}{60^2} & 0 \langle t \le 60 \\ 0.017 & 60 \langle t \le 540 \\ (600-t)^2 \dfrac{0.017}{60^2} & 540 \langle t \le 600 \\ 0 & t \rangle 600 \end{cases} \tag{3.24}$$

The temperature at the fuel inlet was determined using the following equation (Heskestad, 1995a):

$$T_f = T_a + 9.1\left(\frac{T_a}{g c_p^2 \rho_a^2}\right)^{1/3} Q_c^{2/3} (z - z_0)^{(-5/3)} \tag{3.25}$$

where T_f is temperature at inlet (K), T_a is ambient air temperature (K), g is acceleration of gravity (m/s^2), c_p is specific heat of air (kJ/kg ·K), ρ_a is ambient air density (kg/m^3), and z is the flame height above the fire source (m) which is determined by

$$z = -1.02D + 0.20\dot{Q}_{\max}{}^{2/5} \tag{3.26}$$

The z_0 is a hypothetical virtual origin of the fire (m) which is determined by

$$z_0 = -1.02D + 0.083\dot{Q}_{\max}{}^{2/5} \tag{3.27}$$

where D is fire diameter (m). The Q_c is convective portion of the heat release rate (kW) and determined by

$$Q_c = \chi_c \dot{Q}_{\max} \tag{3.28}$$

where χ_c is convective heat release fraction, 0.7 (Heskestad, 1995b).

In this reference case, a maximum of 26.1 kW HRR was introduced in the computational domain. The calculated flame temperature from Eq. 3.24 was 1450 K which was set as the fuel inlet boundary. This temperature ranges between 1100 K and 1500 K (Lonnemark and Ingason, 2005). The mass flow inlet boundary also considered the radiation thermal condition. As the radiation properties, the internal emissivity was set as 1.

The airflow outlet: Pressure outlet with the possibility of a backflow was used as the airflow outlet boundary. Note that there was no gauge pressure, but with a fan curve provided at the outlet of the shaft. The data for building the fan curve is listed in Table 3.3. Here, *P* represented the static pressure, and *Q* the air quantity.

Table 3.3. Fan Curve for the Wombat Mine Exhaust Fan

	1	2	3	4	5	6	7	8	9	10
P, Pa	62.25	124.50	186.75	249.00	311.25	348.60	373.50	398.40	418.32	435.75
Q, m^3/s	6.608	6.254	5.900	5.487	5.074	4.838	4.484	4.248	4.071	3.776

The outlet had a 10% turbulent intensity, and a 1.22m hydraulic diameter. The ambient temperature was set to 288.15 K.

The wall Boundary Conditions: No-slip conditions have been applied to all velocity components at solid walls. Typically, a zero velocity component in the direction normal to the wall is the appropriate condition for the discretized continuity equation and discretized momentum equation in the direction normal to the wall. At the boundary region, a thin viscous sub-layer is located immediately adjacent to the wall followed by a buffer layer and a turbulent core. To solve a turbulent boundary layer, commonly wall functions are used.

Wall functions are a collection of semi-empirical formulae and functions that interpolate the solution variables at the near-wall cells and the corresponding quantities at the wall. They usually comprise the laws-of-the-wall for mean velocity and temperature and correlations to prescribe near-wall turbulent quantities (k and ε specifically). In this work standard wall functions, based on the work of Lauder and Spalding (1974) have been used. They are:

$$U^* = \frac{1}{\kappa} \ln(Ey^*) \tag{3.29}$$

where,

$$U^* = \frac{U_p C_\mu^{1/4} \kappa_P^{1/2}}{\tau_w / \rho} \tag{3.30}$$

is the dimensionless velocity.

$$y^* = \frac{\rho C_\mu^{1/4} \kappa_P^{1/2} y_P}{\mu} \tag{3.31}$$

is the dimensionless distance from the wall.

Constant k is the Von Karman constant (= 0.4187), E is empirical constant (= 9.793), U_p is the mean fluid velocity at the near-wall node P, y_p is the distance from point P to the wall, k_p is the turbulence kinetic energy at the near-wall node P, and μ is the dynamic viscosity of the fluid, ρ the fluid density.

The log-law is valid as long as the first grid point is located in the fluid region characterized by 30 < y* < 300. FLUENT by default uses the wall functions when y* >11.225; the code uses the laminar stress relationship known as linear law of the wall otherwise.

$$U^* = y^* \tag{3.32}$$

For heat transfer, a wall function approach based on the universal near wall temperature distribution has been used (Launder and Spalding, 1974). For incompressible flow calculation, FLUENT uses the following relationships

$$T^+ = \frac{(T_w - T_P)\rho c_p u_\tau}{q_w} = \mathrm{Pr}_t (u^+ + P) \tag{3.33}$$

where T_w is the wall temperature, ρ the fluid density, c_p the fluid specific heat at constant pressure, q_w the wall heat flux, Pr_t the turbulent Prandtl number (= 0.85 at the wall), and P is a correction function Pee-function, dependent on the ratio between laminar and turbulent Prandtl numbers (Launder and Spalding, 1974). Equation 3.32 is applied as long as y is larger than the non-dimensional sub-layer thickness defined as the intersection distance between the linear and the log-law of the wall. For smaller values of y a linear relationship between T^+ and y^+ is used

$$T^+ = \mathrm{Pr}_t\, y^+ \tag{3.34}$$

where Pr_t is the molecular Prandtl number of the fluid.

Previous relationships are valid for smooth walls where the changeover from laminar to turbulent flows is assumed to take place at $y^+ = 11.63$. For walls that are not smooth, the constant E contained in Equation 3.28 and indirectly in Equation 3.33 is adjusted accordingly. Further details are given in (Anon., 2009a; Schlichting, 1979).

Near wall was treated with standard wall function. The wall materials were considered as the limestone with density at 2810 kg/m^3, specific heat c_p at 910 J/(kg ·k), and thermal conductivity at 1.5 w/(m ·k). The roughness of the rock was set at 0.025m and roughness constant is 0.5. The thermal properties of wall only included the radiation with the internal emissivity 0.96 (Anon., 2012a), the external emissivity 0, and the external radiation temperature 300 K. No heat was generated in wall.

3.4. VALIDATION OF THE REFERENCE CASE

The available experimental data have been used to corroborate the model predictions. Transient simulations were carried out to predict longitudinal velocity and temperature distribution of Case 4 (the base case) using ANSYS FLUENT code. The calculation lasted 600s; there were 20 iterations each second.

3.4.1. Longitudinal Velocity. The longitudinal velocity at cross-section 5-5’ (Figure 3.9) was used as a comparison between the simulation and experiment results. In experiment, the air velocity sensor was placed at point V5, the center of the section 5-5’. The measured velocity value represented the maximum longitudinal velocity value at this section. A factor 0.8 must be adopted to calculate the average longitudinal velocity value (Hartman et al., 1997). The simulation results of the average longitudinal velocity were calculated by dividing volume air quantity with cross section area.

The comparison results for every 60 seconds on the average longitudinal velocity value were listed in Table 3.4. The difference between simulation and experiment result were calculated in Equation 3.35.

Table 3.4. Comparison of Measured and Predicted Average Longitudinal Velocity at Section 5-5’ in the Wombat Mine for Case 4

Time, s	Exp. Velocity, m/s	Sim. Velocity, m/s	Diff., %
0	0.1622	0.1516	6.36
60	0.1595	0.1526	4.33
120	0.1639	0.1535	6.34
180	0.1642	0.1537	6.37
240	0.1716	0.1539	10.30
300	0.1720	0.1542	10.36
360	0.1697	0.1544	9.04
420	0.1683	0.1546	8.15
480	0.1758	0.1547	12.00
540	0.1752	0.1549	11.61
600	0.1748	0.1545	11.64

$$Difference = \frac{Simulation - Experiment}{Experiment} \times 100\% \qquad (3.35)$$

During a 600s period, the average longitudinal velocity from both simulation and experiment results increased gradually with time. When fire starts to burn, hot air expanded to both upstream and downstream direction along the airway. As a result, the air quantity volume increased in the downstream direction, but decreased in the upstream direction. In the experiment, no air velocity sensors were placed in the upstream direction. The comparison results in the downstream direction were matched to each other very well, showing same trends.

The average longitudinal velocity from simulation results went up uniformly with time. The experiment results, however, fluctuated sometimes, believed to be impacted by barometric variations outside. As mentioned in previous sections, the Wombat Mine is a small operation and is immediately affected by the effect of outside weather.

The comparison of average longitudinal velocity between simulation and experiment results were shown in Figure 3.15.

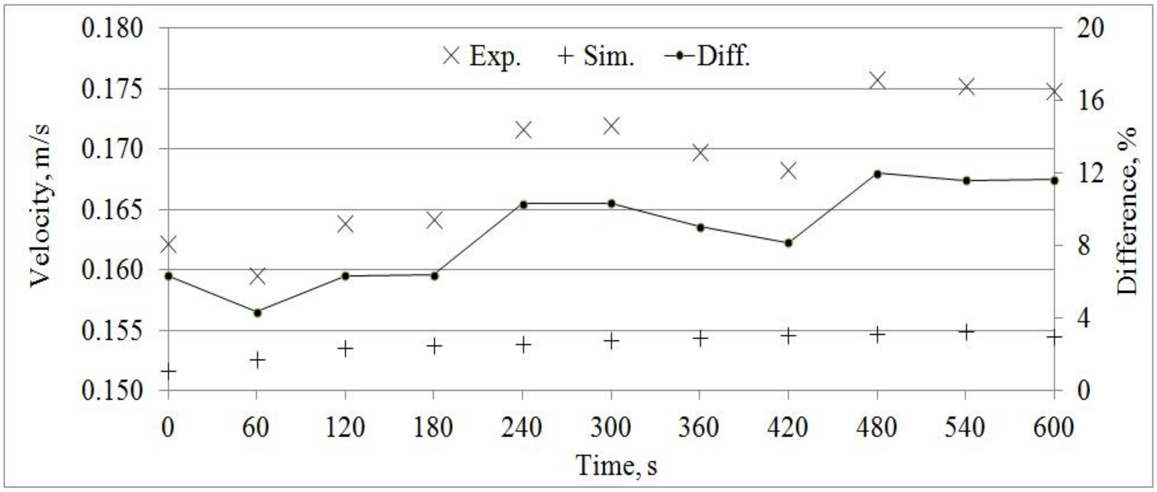

Figure 3.15. Difference between Predicted and Measured Longitudinal Velocity at Section 5-5’ in the Wombat Mine for Case 4

The maximum deviation of 12.0% was found at 480s in the base case. In general, accurate velocity predictions are considered to be acceptable if the average deviation from experimental findings is 17% of less (Colella, 2010). Given the lack of information on velocity measurement in experiment, the accuracy achieved is considered satisfactory and no other attempts to improve the numerical predictions have been performed. However, it is believed that, if more detailed information is available, better predictions are possible.

3.4.2. Temperature. The temperature contours from simulation at Section Two (Figure 3.11) were plotted in Figure 3.16, which shows the temperature distribution from 10s to 540s at different time intervals. Temperature is in Kelvin and the simulation shows temperature variation between 288.15 K and 388.15 K.

Figure 3.16 shows the progression of a fire starting at t = 0s. After fire is started, hot air is slowly being released from the fire source to the surrounding atmosphere. Then, the hot air started to develop and rise to the airway roof on both upstream and downstream direction with the buoyancy effect (t = 50s). With the time passes, the hot air continued to be produced and accumulated under the roof. Consequently, the hot layer became longer and thicker.

Before 60s, the distribution of the hot air was dictated by the airflow. When fuel began to burn, the force due to the heat released was not strong enough at the beginning to flow against the airflow from the inlet direction. As a result, hot air was developed horizontally toward the downstream direction because of the dominant influence of ventilation airflow. As the heat released continue to increase, the tilted angle of the hot air stream decreased and eventually reached the airway roof (t = 40s).

At 60s, the heat release rate reached its peak value, and the fire was fully developed. From this point on, the tilted angle of hot air stream started to increase with time. This is because when more hot air produced and accumulated, the air expansion effect on airflow in both upstream and downstream becomes stronger. When a point of balance is reached, i.e., the forces as a result of the continuingly released the heat equals to the dynamic energy of the ventilation airflow, the hot air tilted toward downstream direction.

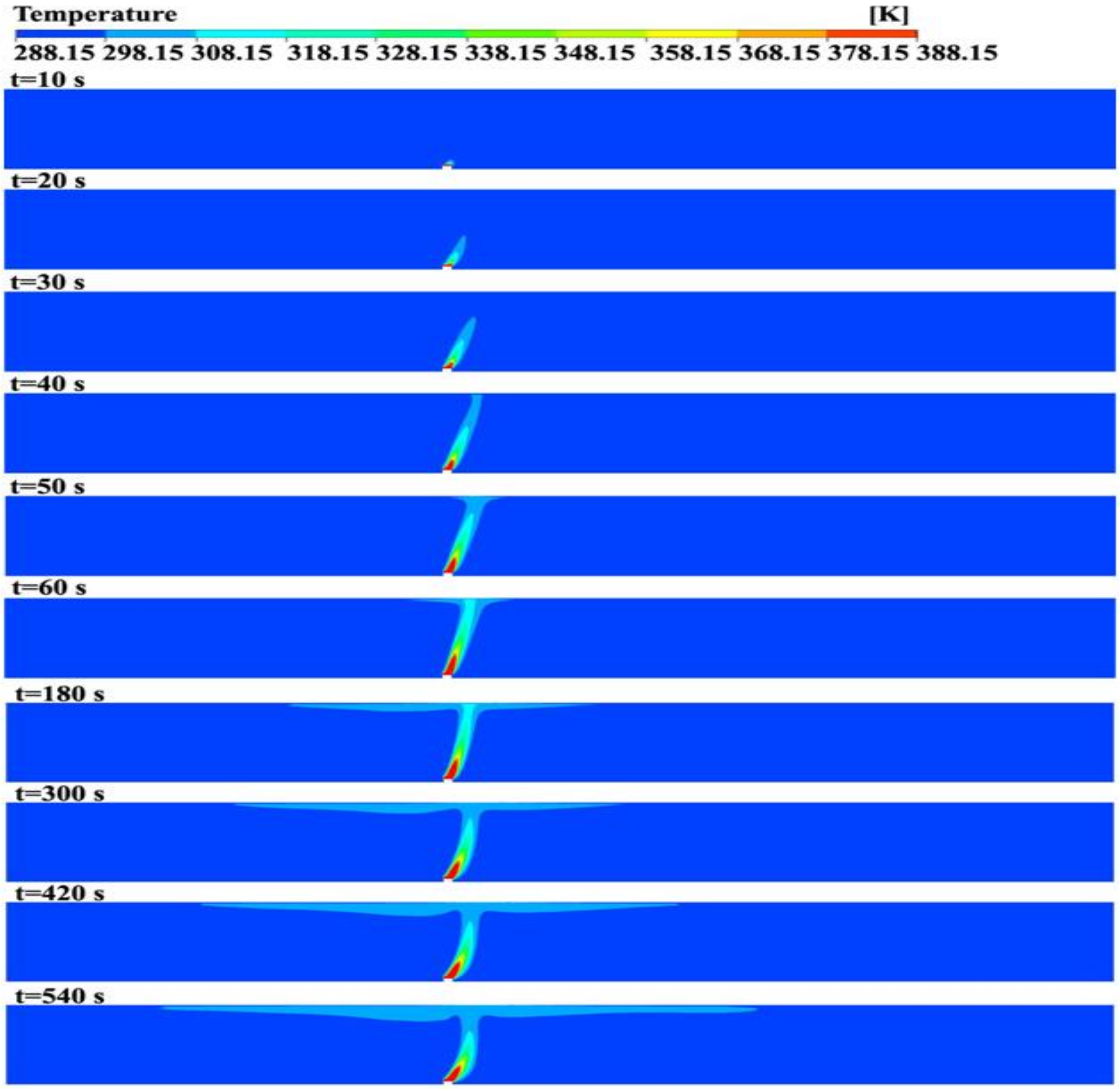

Figure 3.16. Predicted Temperature at Section Two in the Wombat Mine for Case 4 (Ventilating Air Flows from Left to Right)

Based on the simulation, the buoyancy effect as a result of the density variation became strong enough before 60s and gradually weak after 60s. Once the fire is fully developed, the temperature difference as well as the air density between floor and roof decreased. As the air density decreases, together with the increased expansion effect on hot air from upstream direction, resulted in the buoyancy effect start weakening and the flow direction of the hot air will reverse itself. If the air velocity is big enough, the buoyancy effect will be totally disappeared, and the hot air developed horizontally toward to the downstream direction.

The temperature comparison between simulation and experiment results were conducted at 60s, 300s, and 540s. A total of nine points where temperature sensors were located were considered for the purpose of comparison. The temperature difference between the simulation and experiment temperature were calculated using Equation 3.35. The calculated differences were plotted in Figure 3.17 and listed in Table 3.5.

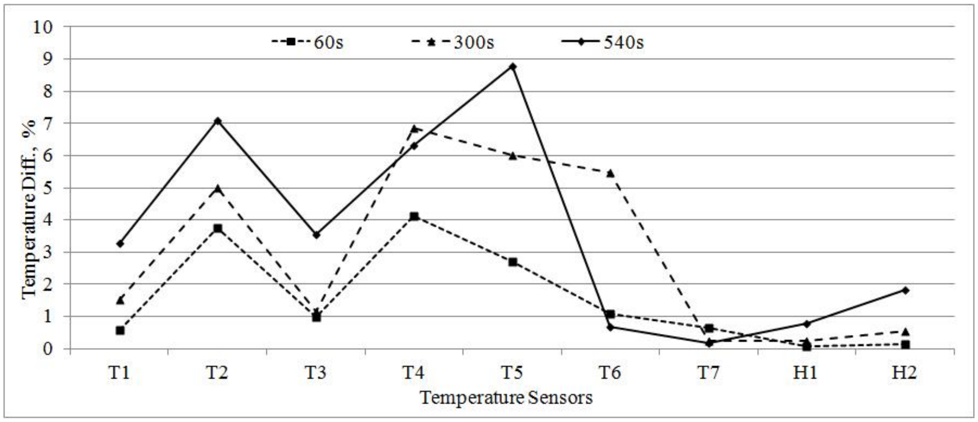

Figure 3.17. Difference between Predicted and Measured Temperature in the Wombat Mine for Case 4

Table 3.5. Comparison of Predicted and Measured Temperature in the Wombat Mine for Case 4

Sensor	60s, K			300s, K			540s, K		
	Sim.	Exp.	Diff., %	Sim.	Exp.	Diff., %	Sim.	Exp.	Diff., %
T1	297.845	296.1	0.59	299.072	303.73	1.53	300.891	311.05	3.27
T2	298.615	310.27	3.76	299.694	315.46	5.00	300.773	323.71	7.09
T3	297.615	294.71	0.99	301.914	305.39	1.14	303.037	314.24	3.57
T4	291.881	304.47	4.13	296.342	318.21	6.87	298.129	318.21	6.31
T5	290.629	298.68	2.70	291.297	309.97	6.02	293.315	321.57	8.79
T6	293.605	290.43	1.09	293.282	310.27	5.48	296.424	294.4	0.69
T7	290.729	288.85	0.65	289.962	290.69	0.25	291.964	292.52	0.19
H1	288.188	288.42	0.08	289.235	289.94	0.24	290.303	292.57	0.77
H2	288.366	288.74	0.13	289.514	291.06	0.53	290.937	296.38	1.84

Based on Table 3.5 and Figure 3.17, it is obvious that at 60s, the biggest temperature difference is 4.13% occurring at T4. At 300s, the difference is 6.87% also at T4, and at 540s, 8.79% at T5. These values are considered acceptable as they are less than the accepted values of between 20% and 30% based on previous publications. No other tests were attempted.

3.5. SENSITIVITY ANALYSIS

The interaction between the mine fire and ventilating airflow was influenced by many factors: fire intensity, air velocity, and fire source location. Sensitivity studies are conducted to review the sensitivity of the impact each factor will have on the accuracy of numerical model.

3.5.1. Fire Intensity. Case 5 in Table 3.1 was calculated to analyze the influence of the fire intensity on the numerical model. The only difference between Case 5 and Case 4 (the base case) was the heat generation rate. The former is twice as much as the latter.

The average longitudinal velocity at section 5-5' (Figure 3.9) was calculated for both simulation and experiment results using the same method as used in the base case. The difference between simulation and experiment results were shown in Figure 3.18.

The average longitudinal velocity from simulation increased uniformly and gradually with time. Some fluctuations occurred sometimes in experiment results due to the weather influence. The maximum difference of 9.32% was found at 540s, which was within the acceptable accurate level of 17% (Colella, 2010).

The temperature comparison between simulation and experiment results were conducted at 60s, 300s, and 540s. A total of nine points at where temperature sensors were located were considered for the purpose of comparison. The differences between the simulation and experiment temperature were plotted in Figure 3.19.

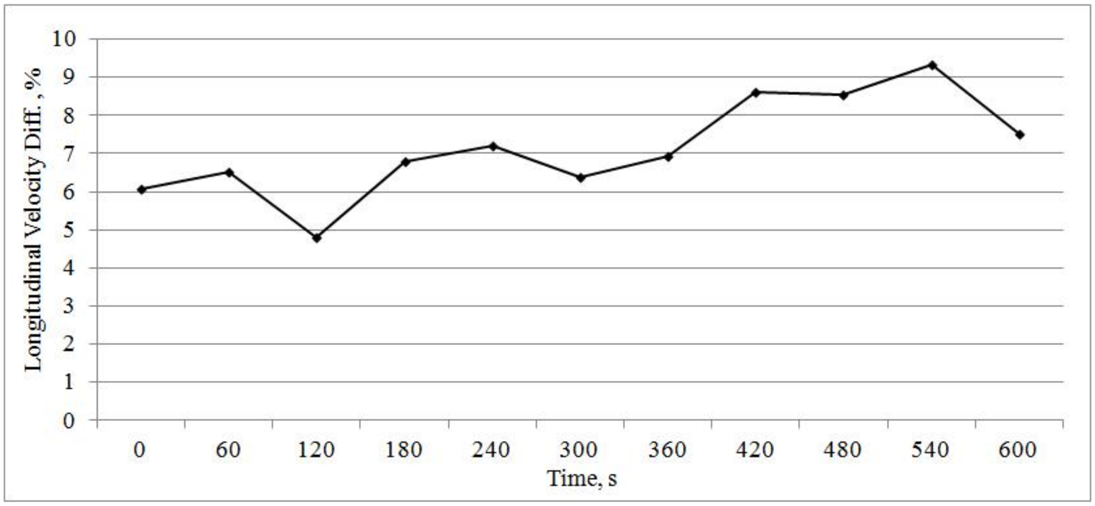

Figure 3.18. Difference between Predicted and Measured Longitudinal Velocity at Section 5-5’ in the Wombat Mine for Case 5

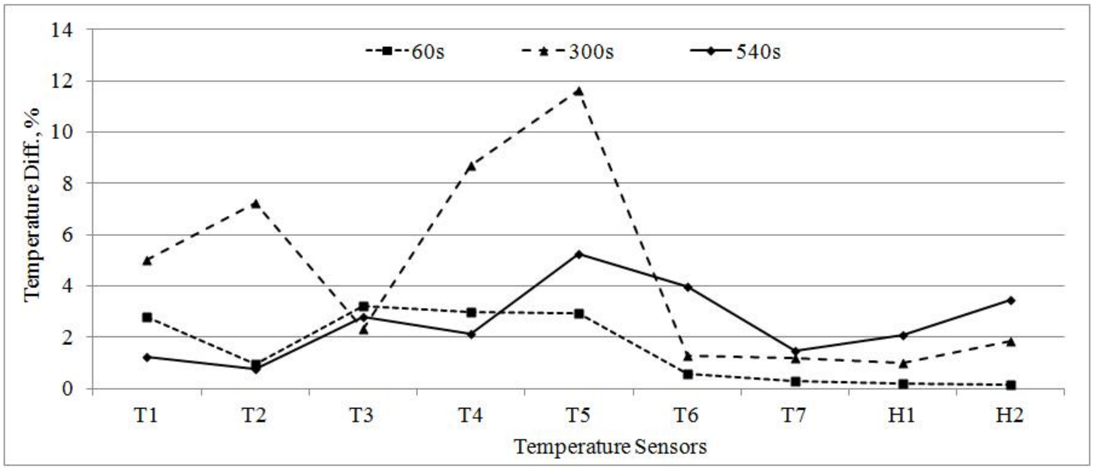

Figure 3.19. Difference between Predicted and Measured Temperature in the Wombat Mine for Case 5

Figure 3.19 shows that it is obvious that at 60s, the biggest temperature difference is 3.00% at T4; at 300s, 11.64% at T5; and at 540s 5.24% also at T5. These differences are within accepted accuracy of between 20% and 30% per previous studies and results are considered satisfactory.

Based on the results on average longitudinal velocity and temperature, they proved that the fire intensity do not have any impact on the accuracy of the numerical model.

3.5.2. Ventilation. Case 1 in Table 3.1 was calculated to analyze the influence of the air velocity on the numerical model result. The only difference between Case 1 and Case 4 (the base case) was the former was without ventilation.

As before, temperature comparison between simulation and experiment results were conducted at 60s, 300s, and 540s and a total of nine points where temperature sensors located were considered for the purpose of comparison. The differences between the simulation and experiment temperature were plotted in Figure 3.20.

Figure 3.20 shows that at 60s, the biggest temperature difference is 0.98% at T1, 2.87% at T5 at 300s, and 4.62% at T5 at 540s. These differences are within accepted accuracy of between 20% and 30% and results are considered satisfactory.

Based on the analysis result on temperature, they proved that the air velocity do not have any impacts on the accuracy of the numerical model.

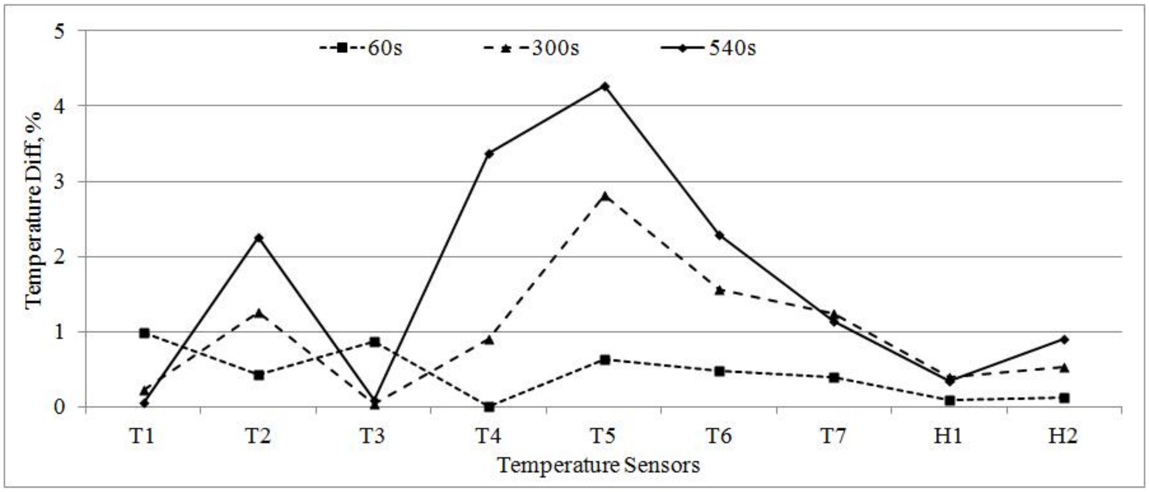

Figure 3.20. Difference between Predicted and Measured Temperature in the Wombat Mine for Case 1

3.5.3. Fire Location. Case 8 in Table 3.1 was calculated to analyze the effect of fire source location on the numerical model result. The only difference between Case 8 and the base case was the fire source raised from floor 0.9m in Case 8.

The average longitudinal velocity at cross section 5-5’ (Figure 3.9) was calculated for both simulation and experiment results using the same method used as in the base case. The difference between simulation and experiment results were shown in Figure 3.21.

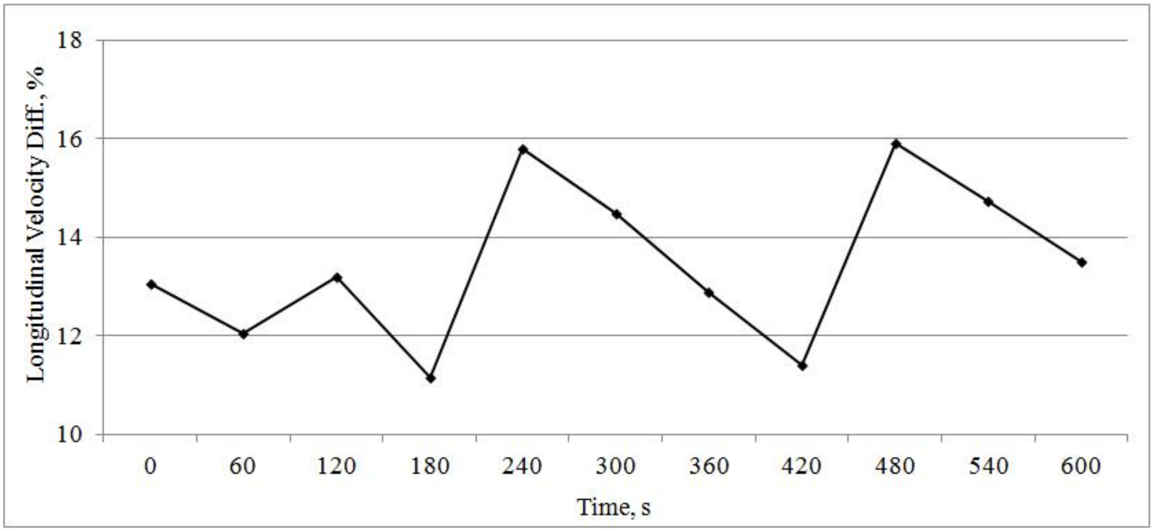

Figure 3.21. Difference between Predicted and Measured Longitudinal Velocity at Section 5-5’ in the Wombat Mine for Case 8

Average longitudinal velocity from simulation increased uniformly and gradually with time. Some fluctuations occurred sometimes in experiment results due to the weather influence. The maximum difference of 15.92% was found at 480s. This discrepancy is likely due to the fact that the fire source was placed on brick piles where airflow can go through, which in modeling, this pile was considered to be solid where airflow can’t penetrate. A more accurate geometric model is recommended to obtain more accurate results. However, this average difference was still within the acceptable accuracy level of 17%.

The temperature comparison between simulation and experiment results were conducted at 60s, 300s, and 540s for all nine points where temperature sensors were located. The differences between the simulation and experiment temperature were plotted in Figure 3.22.

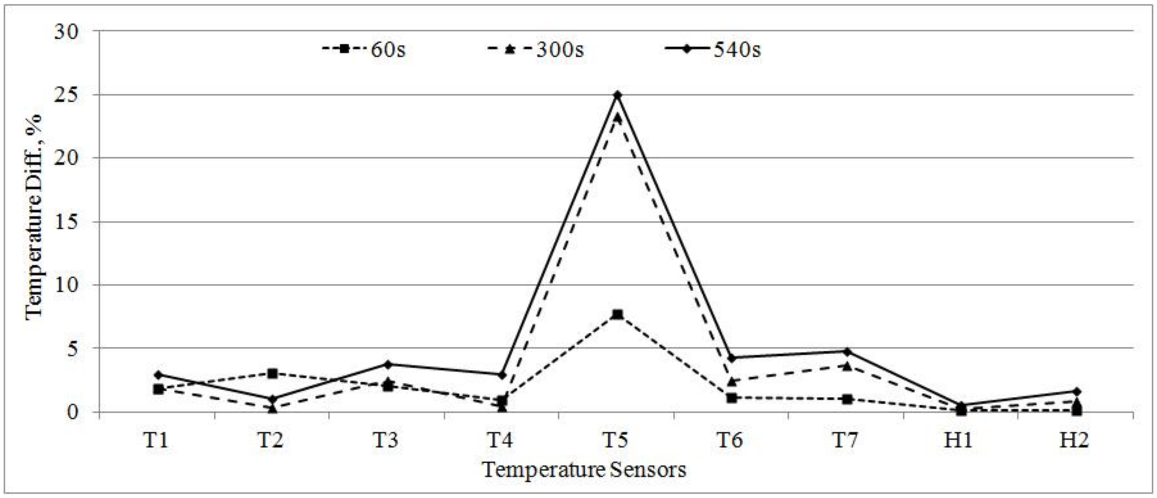

Figure 3.22. Difference between Predicted and Measured Temperature in the Wombat Mine for Case 8

Figure 3.22 shows that differences between experimental and theoretical are uniform throughout the experiment except at T5 for both 300s and 540s. At 60s, the biggest temperature difference is 7.73% at T5, while at 300s is 23.33% at T5, and at 540s is 24.99% at T5. Although these values are still within the accepted accurate values range of between 20% and 30%, there were experimental errors at T5, but readings were ignored without affecting final result. This result concluded that the fire source do not have any impact on the accuracy of the numerical model.

Based on the analysis results on average velocity and temperature, they proved that the fire source location do not have significant impacts on the accuracy of the numerical model.

4. FOUNDATION OF MULTISCALE MODEL

4.1. INTRODUCTION

The interaction between a mine fire and ventilating airflow has been studied using either 1D or 3D methods for many years. Several of these studies have been reviewed and discussed in Section 2. Some calculations provided valuable results with acceptable accuracy, but both methods have certain limitations.

The more popular 1D model has been applied in the mining industry for ventilation simulation as well as fire calculation. Although the approach simplifies the physical model while ignoring many useful information about fire source and boundary conditions, the biggest advantage of using an 1D model is that it can be used to calculate an entire mine ventilation system in less time than the 3D method requires.

The 3D model has been limited only to simulate a mine fire locally. To model a mine fire requires airflow characteristics in and around a fire zone, boundary conditions for the fire, its surroundings, and the fire itself. In these cases, even if only a limited region of the mine has to be investigated, an accurate solution regarding the flow movement requires that the numerical model must include the entire mine layout. For typical mines, this could mean that the area covered by the computational domain would be huge.

Previous studies on ventilation in an airway and fire-induced flows indicated that, in the vicinity of a fire source, the flow field has a complex 3D behavior with large transversal and longitudinal temperature and velocity gradients. The flow in these regions needs to be calculated using 3D tools to aid with calculation (Vauquelin and Wu, 2006; Wu and Bakar, 2000; Karki and Patankar, 2000; Galdo Vega et al., 2007; Van Maele and Merci, 2008; Colella et al., 2009). Any other simpler approach would only lead to inaccurate results.

It has been demonstrated, however, that some distance downstream of these regions, the temperature and velocity gradients in the transversal direction tend to disappear and the flow becomes essentially 1D. In this portion of the domain, the transversal components of the velocity can be up to two orders of magnitude smaller than the longitudinal components. The use of 3D models to simulate the fluid behavior in these areas leads to large increases in the computational requirements but with only marginal improvement in the accuracy of results.

For practical purpose, 3D model should be applied only to model the near fire zone while areas away from fire zone are simulated using a 1D model. This “hybrid” approach, combining 1D and 3D in one task, is referred to as a multiscale approach. Multiscale models allow a significant reduction in the computational time as the more time-consuming portion of the simulation is used only in a limited portion of the domain. It also provides a significant improvement in the accuracy of final results as the flow calculations include the effect of the fire on the entire ventilation system and vice versa.

4.2. DOMAIN DECOMPOSITION METHODS

Multiscale techniques are based on the domain decomposition method which has been developed for discretization techniques (i.e., finite difference, finite volume, and finite elements), mainly in the framework of parallel computing. They allow the original single problem to be reformulated on several computational sub-domains. Eventually, this technique can be applied to solve heterogeneous problems, which are described by a different governing equation, as in this study.

The basic idea is to decompose the global domain into several sub-domains and to eventually solve the resulting problems, characterized by smaller domain size, through parallel computing. Domain decomposition can be performed by adopting two different techniques which generate overlapping and non-overlapping sub-domains. A visual example of a sub-domain decomposition, with and without overlapping, is depicted in Figure 4.1.

Three iterative methods, based on domain decomposition, are described in the literature and they are mainly differentiated by boundary conditions applied at the interfaces and by the presence of overlapping regions (Quarteroni and Valli, 1999). They are:

- Dirichlet-Dirichlet method
- Dirichlet- Neumann method
- Neumann - Neumann method

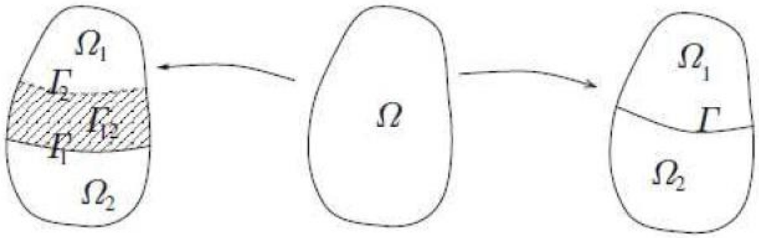

Figure 4.1. Example of Domain Decomposition with and without Overlapping (Quarteroni, 2008)

The Dirichlet-Dirichlet method is applied in the overlapping domain decomposition and uses Dirichlet type boundary conditions applied on Γ_1 and Γ_2 for the sub-domains Ω_1 and Ω_2, respectively.

The Dirichlet-Neumann method is applied in the non-overlapping domain decomposition and uses one Dirichlet-type boundary condition and one Neumann-type boundary condition.

Neumann-Neumann method is applied in the non-overlapping domain decomposition and uses only Neumann-type boundary conditions applied on Γ for the sub-domains Ω_1 and Ω_2, respectively.

A description of the mathematical theory behind domain decomposition methods is not included in this dissertation. The interested reader can refer to Quarteroni and Valli (1999) for details.

The exact structure of the boundary conditions to be applied at the interfaces depends on the differential operator defining the original set of partial differential equations. In the case of the Navier-Stokes equations, only the Dirichlet-Neumann and Dirichlet-Dirichlet methods are used. With S as the Navier-Stokes operator, a Dirichlet-Neumann iterative method must perform the following operating sequence until convergence is achieved (Quarteroni, 2008)

$$a.\begin{cases} S(u_2^{k+1}, p_2^{k+1}) = f in \Omega_2 \\ \mu \dfrac{\partial u_2^{k+1}}{\partial n} - p_2^{k+1} = \mu \dfrac{\partial u_1^k}{\partial n} - p_1^k on \Gamma \\ u_2^{k+1} = \varphi_2 on \Gamma_{2,D} \\ \mu \dfrac{\partial u_2^{k+1}}{\partial n} - p_2^{k+1} = \psi_2 on \Gamma_{2,N} \end{cases} \tag{4.1}$$

$$b.\begin{cases} S(u_1^{k+1}, p_1^{k+1}) = f in \Omega_1 \\ u_1^{k+1} = \alpha u_2^{k+1} + (1-\alpha) u_2^k on \Gamma \\ u_1^{k+1} = \varphi_1 on \Gamma_{1,D} \\ \mu \dfrac{\partial u_1^{k+1}}{\partial n} - p_1^{k+1} = \psi_1 on \Gamma_{1,N} \end{cases} \tag{4.2}$$

where φ_1 and φ_2 are vectorial functions describing the Dirichlet boundary conditions (e.g., prescribed velocities) at the boundary $\Gamma_{1,D}$ and $\Gamma_{2,D}$ of the sub-domains Ω_1 and Ω_2 (refer to Figure 4.2). ψ_1 and ψ_2 are vectorial functions describing the Neumann boundary conditions (e.g., prescribed pressures) at the boundary $\Gamma_{1,N}$ and $\Gamma_{2,N}$ of the sub-domains Ω_1 and Ω_2 (refer to Figure 4.2). Constant k is the multiscale iteration counter, α is a velocity under-relaxation factor required to improve convergence, and n is the normal coordinate.

It is stressed that, when a Dirichlet-Neumann method is adopted, the sub-domains Ω_1 and Ω_2 must be neither overlapped nor gapped. In this research, this method was used to discretize the calculation domain to form the interface of the multiscale model.

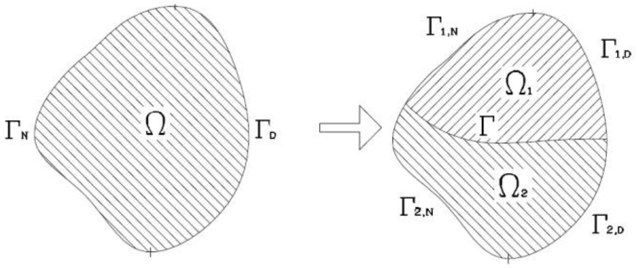

Figure 4.2. Drawings Show the Domain Decomposition for Navier-Stokes Method Using the Dirichlet-Neumann Method (Quarteroni, 2008)

4.3. FORMULATION OF A MULTISCALE PROBLEM

A multiscale model based on domain decomposition techniques has been proven to be adequate for solving heterogeneous problems described by different governing equations (Quarteroni and Valli, 1999). Thus, mine fluid dynamic behavior can be addressed by adopting two different numerical descriptions of the problem using both 1D- and 3D-CFD tools.

The conventional 1D and 3D modeling techniques can be coupled together, with the latter providing the boundary condition for the former, and the solution from the former will then serve as the input for the latter, iteratively. The coupled model is solved on a hybrid computational grid, where 1D elements are linked to 3D ones, generating a continuous domain. The 3D elements are modeled by means of a 3D tool while a conventional 1D model is used for 1D elements. During the solution procedure, 1D and 3D models dynamically exchange information at the 1D-3D interfaces and, thus, run in parallel.

For the sake of simplicity (and only in this section), the mine domain (Ω) is decomposed into two sub-domains Ω_{1D} and Ω_{3D}. Figure 4.3 depicts a schematic of a 1D-3D domain decomposition. The 1D-3D interface Γi is located in $x = i$ in such a way that there is no overlapping or gap between the two sub-domains.

On the left side of Γi, the 1D domain provides average values for pressure $P(i^-)$, temperature $T(i^-)$, velocity $v(i^-)$, and mass flow rate $\dot{m}(i^-)$. Similarly, a set of same quantities can be defined for the right side of Γi but, since the right side of Γi belongs to the 3D domain, integral averaged values must be used:

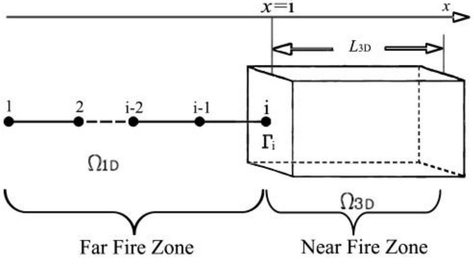

Figure 4.3. Schematic of a 1D-3D Domain Decomposition Example

$$\bar{v}(i^+) = \frac{1}{|\Gamma_i|}\int_{\Gamma_i} v \cdot n dA \tag{4.3}$$

$$\bar{P}(i^+) = \frac{1}{|\Gamma_i|}\int_{\Gamma_i} P dA \tag{4.4}$$

$$\bar{T}(i^+) = \frac{\int_{\Gamma_i} \rho T |v \cdot n| dA}{\int_{\Gamma_i} \rho |v \cdot n| dA} \tag{4.5}$$

$$\dot{m}(i^+) = \int_{\Gamma_i} \rho v \cdot n dA \tag{4.6}$$

where v represents the velocity vector, P the pressure, ρ the density, T the temperature, n the unitary vector normal to the interface Γi.

Following the same approach presented in Formaggia et al. (2001), it is reasonable to assume the continuity of the following quantities at the interface:

Area $A(i^-) = A(i^+)$ (4.7)

Mean pressure $P(i^-) = P(i^+)$ (4.8)

Mean velocity $v(i^-) = v(i^+)$ (4.9)

Mean temperature $T(i^-) = T(i^+)$ (4.10)

Mean mass flow rate $\dot{m}(i^-) = \dot{m}(i^+)$ (4.11)

The solution of the coupled multiscale problem cannot be obtained by means of a standard computing algorithm, but is solved using iterative computing procedures developed in the framework of a domain decomposition method. In this instance, finding a proper coupling technique is essential, as it not only improves accuracy, but also speeds up the calculation process.

4.4. COUPLING TECHNIQUE

4.4.1. Direct Coupling. The solution to the multiscale problem requires the coupling of the 1D and 3D models, which has been obtained by means of a Dirichlet-Neumann method. For the 1D model, the interface velocity can only be prescribed with

Dirichlet boundary conditions. Velocity can be calculated using the mass flow rate defined using Neumann boundary conditions. So, to simplify the simulation process, the mass flow rate (instead of velocity) is used at the 1D-3D interfaces. The Neumann boundary conditions for both temperature and pressure are prescribed at the interfaces.

The iterative algorithm presented here is for a general case in which a 3D model of the near fire zone (Ω_{3D}) is coupled with two 1D models of far fire zones ($\Omega_{1,1D}$ and $\Omega_{2,1D}$) located upstream and downstream, respectively. Two interfaces Γi and Γj are then generated. The algorithm requires a dynamic exchange of information at the interfaces during the computation. A three-stage coupling was adopted for the scope (see Figure 4.4).

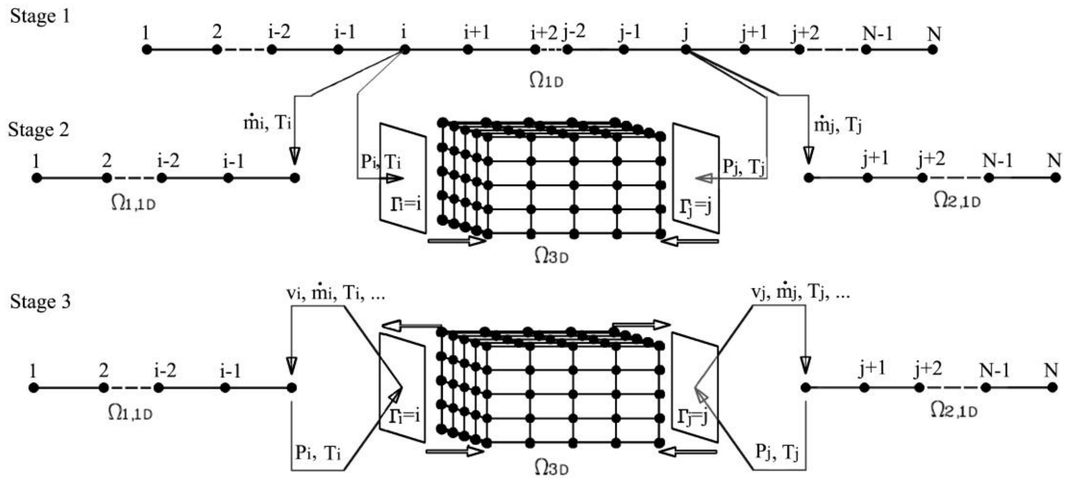

Figure 4.4. Visualization of a Three Stages Coupling Procedure

A full 1D model of the whole system was solved during the first stage. During the second stage, the 1D models ($\Omega_{1,1D}$ and $\Omega_{2,1D}$) and the 3D model (Ω_{3D}) were run in parallel. The initialized boundary values at node *i* for $\Omega_{1,1D}$, at *j* for $\Omega_{2,1D}$, and at Γ_i and Γ_j for Ω_{3D} were provided by the full 1D model run at the first stage. Although these initialized values at the boundaries did not make any change in the final results, it could definitely influence the results at the beginning of the time steps for transient calculation, or prolong the iteration steps for steady calculation. At the third stage, the 1D and 3D models periodically exchanged the boundary conditions at the interface *k-times* until a global multiscale convergence was reached.

The complete sequence of operations conducted during the procedure is described as follows:

STAGE 1

a. Run the full 1D model of the whole system until convergence is reached.

b. Total pressure and temperature values at the nodes corresponding to the interface Γ_i and Γ_j are obtained and stored to be used as boundary conditions of the 3D model Ω_{3D} in the next stage.

c. Mass flow rate and temperature values at the nodes *i* and *j* are obtained and stored to be used as boundary conditions of the 1D model $\Omega_{1,1D}$ and $\Omega_{2,1D}$, respectively, in the next stage.

STAGE 2

a. Run the 1D model $\Omega_{1,1D}$ and $\Omega_{2,1D}$ by using recorded mass flow rate and temperature value at nodes *i* and *j* until a predetermined degree of convergence is reached.

b. Record total pressure and temperature values at nodes *i* and *j* (to be used as boundary conditions for the 3D model Ω_{3D} at the interfaces Γ_i and Γ_j, respectively, in the next stage).

c. Run the 3D model Ω_{3D} by using recorded total pressure and temperature value at the interface Γ_i and Γ_j until a certain degree of convergence is reached.

d. Calculate average mass flow rate and temperature values at the interfaces Γ_i and Γ_j (to be used as boundary conditions for the 1D model $\Omega_{1,1D}$ and $\Omega_{2,1D}$, respectively, in the next stage).

STAGE 3

a. Run the 1D model $\Omega_{1,1D}$ and $\Omega_{2,1D}$ until a predetermined convergence is reached.

b. Run the 3D model Ω_{3D} until a predetermined convergence is reached.

c. Record total pressure and temperature values at nodes *i* and *j* in 1D models $\Omega_{1,1D}$ and $\Omega_{2,1D}$, respectively.

d. Calculate average mass flow rate and temperature values at the interfaces Γ_i and Γ_j in 3D models Ω_{3D}.

e. Exchange the boundary conditions by means of sending boundary values in step c to 3D and values in step d to 1D.

f. Check for global convergence

I. If global convergence is not reached, go back to step a.

II. If global convergence is reached, quit the calculation or proceed to the next time step for a time dependent calculation.

It must be noted that the coupling between grids is physically realized between the pressure nodes of the 1D grid (*i* in Figure 4.3) and the mesh faces lying on the interface Γ_i. Because the prescription for a velocity boundary condition for the 1D sub-domain is performed by using the velocity value of the branch, it cannot be applied directly on the 3D model. A solution for this is to adopt a mass flow rate instead of velocity. Temperature and pressure values can be directly transferred from the 3D to the 1D grid (and vice-versa), since they are naturally defined in nodes.

This coupling approach is called direct coupling. It allows for a significant reduction in the computational time in comparison to a full 3D calculation for the same scenario. However, the timescale of the direct coupling calculations is limited by the computational speed of the 3D portion of the model. This can take from several minutes to up to many hours, depending on the complexity of the scenario.

If one solver exists that is capable of receiving two sets of equations, the coupling problem can be solved at once. Unfortunately, at present, no such tool is available. In most of the cases, there is a different solver for each model. To realize the coupling task, the iterative calculations are necessary with the two solvers continuously exchanging information at boundary interfaces. For this research, the Flowmaster was used for the 1D model, and the FLUENT was usedfor the 3D model.

The actual exchange of information between the 1D and 3D models was made by using a Mesh-based parallel Code Coupling Interface (MpCCI), together with a User-Defined-Memory (UDM). The MpCCI is a tool that can provide a coupling environment for a multi-physical fluid field. The boundary information for each physical model can be dynamically stored in the UDM to be transferred before proceeding to the next time-step calculation for time dependent simulation or the next iteration step for time independent simulation (Anon., 2009a).

4.4.2. Indirect Coupling. The indirect coupling method required 1D and 3D simulations to be run separately. A series of 3D runs are needed for a range of uniform boundary conditions at the interfaces, the results are then used to define the characteristic curves in terms of flow velocities as a function of the total pressure differences across the 3D domain. These curves represent the coupling of the fire behavior with ventilation in the surrounding airways. The 1D model is designed in such a way that it will take into account these curves, coupling them to the rest of the mine. The indirect coupling technique can improve its prediction capabilities by inputting the fire characteristic curves from the 3D model into the 1D model.

Indirect coupling leads to longer set-up times, mainly dedicated to the calculation of the characteristic curves, but then almost instantaneous results are provided for steady state calculation of mine flows and temperatures. This method is mainly used for a steady state simulation. The implementation of indirect coupling techniques for transient calculation is possible, but complicated, since the curves must be eventually updated each time-step to follow the fire growth.

4.5. TOOLS FOR SOLVING A MULTISCALE MODEL

4.5.1. Flowmaster. In this research, Flowmaster was adopted for the ventilation simulation in the Main Mine. It is believed that this is the first time that Flowmaster is used in such an application. Besides the capability of calculating a complex network, the most outstanding feature of Flowmaster is its ability to couple with other programs, such as FLUENT. Fluid properties can be imported and exported through pre-defined boundaries.

4.5.1.1 Introduction. Flowmaster® V7 is an 1D CFD software developed by a UK company of the same name. Over 20 years of development, this software has been leading the way in the field of system simulation related to thermo-hydraulic and thermo-pneumatic piping systems. It has enabled engineers to simulate various fluid systems, including fuel systems for aircrafts, vehicle thermal management systems with air-conditioning, piping systems for shipbuilding organizations, cooling systems for satellites, etc.

As an 1D model, Flowmaster has allowed engineers to model and analyze the fluid mechanics and pipe flow in complex systems based on the CFD technology. Both compressible and incompressible fluid flow systems could be modeled and analyzed. The fluid properties, such as temperature, pressure, volume, and mass flows for each component and every node across the defined system can be calculated under both stationary and transient conditions (i.e., time dependent).

Flowmaster provides a graphical virtual environment where it is possible to design, refine, and test the entire fluid flow system. It is equipped with libraries, including plenty of components for building a numerical model. Each component was defined by a mathematical-physical model which enables the operation method and performance to be adapted to the required situation, e.g., the opening of a valve, fan performance, surface roughness, etc. Individual component parts are connected by the use of nodes to which attributes such as height, temperature, etc. are attached. Each element's results for pressure, temperature, and mass and/or volume flow rates, etc. can be depicted either dynamically in a schematic model or captured in graphic format.

4.5.1.2 Theory. Components in Flowmaster are connected via nodes to form an actual computer model of a flow system. Each selected component represents a mathematical model of a fluid system component. Data tables, curves, and surfaces are used to define the operation and performance of each component. After running the model, possible results are obtained in the components and the connecting nodes for pressure, temperature, volume/mass flow rate, velocity, etc.

The governing equations in Flowmaster are the conservation of mass, momentum, and energy equations whose common format can be found in Equations 3.1, 3.2 and 3.4 in Section 3. These equations stipulate that the same amount of energy, mass, and momentum that goes into a control volume must leave it. Equations 3.1, 3.2 and 3.4 are the Navier-Stokes equations, from which Bernoulli's equation can be derived. This is the relation between pressure, velocity, and elevation, along a streamline (White, 1999).

$$\frac{V^2}{2g} + z + \frac{p}{\rho g} = C \tag{4.12}$$

In the Bernoulli equation, V is the stream velocity (m/s), g is the gravitational acceleration (m/s^2), z is the elevation (m), p is the static pressure (Pa), ρ is the density (kg/m^3), and C is a constant.

For the entire fluid system, all of the components must meet the requirements in the equations below:

Pressure-Flow Equation:

$$p_1 - p_2 = \xi \cdot \frac{\rho}{2} \cdot u^2 \tag{4.13}$$

where p_1 and p_2 are the component pressures at the inlet and outlet, respectively (Pa), ξ is the resistance factor of the component along the fluid direction, ρ is the fluid density (kg/m^3), and u is the flow velocity (m/s).

Mass Equation:

$$Q = A_1 u_1 = A_2 u_2 \tag{4.14}$$

where u_1 and u_2 are the fluid velocities at the inlet and outlet, respectively (m/s), A_1 and A_2 are the areas at the inlet and outlet, respectively (m^2).

Pressure Equation:

$$\Delta p = (p_1 + \frac{\rho \cdot {v_1}^2}{2}) - (p_2 + \frac{\rho \cdot {v_2}^2}{2}) + \rho g (z_1 - z_2) \tag{4.15}$$

where subscript 1 and 2 mean the inlet and outlet of the component, respectively, p is the static pressure (Pa), $\frac{\rho \cdot v^2}{2}$ is the velocity pressure (Pa), and z is the elevation at the position (m).

Heat Equation:

$$T_2 = T_1 + \frac{\dot{Q}}{\dot{m} c_p} \tag{4.16}$$

where T_2 is the temperature at outlet (K), T_1 is the temperature at inlet (K), $\dot{Q}$ is the heat sink or release rate at component (kW), $\dot{m}$ is the mass flow rate of fluid (kg/s), c_p is the specific heat at constant pressure (kJ/(kg ·K)).

In Flowmaster, the solution for a whole model is based on the system of matrix equation. Figure 4.5 shows a simple network analysis where the network includes three two-armed components connected to a common node. It describes how the linear equations for the network are used to construct the matrix to be solved. It will often be the case that the linear equations derived for each component are not explicit functions of mass flow. An iterative solution method is therefore used to solve the matrix.

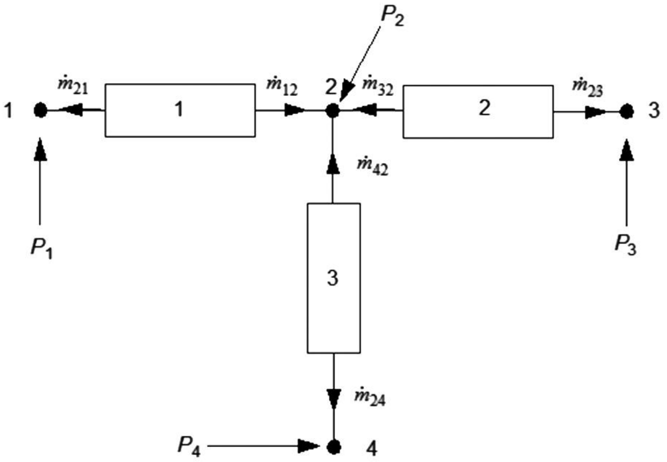

Figure 4.5. Schematic of a Simple Network Using Flowmaster

For the network shown in Figure 4.5, the following linear equations for mass flow can be written:

Component 1

$$\dot{m}_{12} = a^1_{11}P_1 + a^1_{12}P_2 + a^1_{13}$$

$$\dot{m}_{21} = a^1_{21}P_1 + a^1_{22}P_2 + a^1_{23} \tag{4.17}$$

Component 2: $$\dot{m}_{32} = a_{11}^{2}P_{3} + a_{12}^{2}P_{2} + a_{13}^{2}$$

$$\dot{m}_{23} = a_{21}^{2}P_{3} + a_{22}^{2}P_{2} + a_{23}^{2} \tag{4.18}$$

Component 3: $$\dot{m}_{42} = a_{11}^{3}P_{4} + a_{12}^{3}P_{2} + a_{13}^{3}$$

$$\dot{m}_{24} = a_{21}^{3}P_{4} + a_{22}^{3}P_{2} + a_{23}^{3} \tag{4.19}$$

The subscript (*i*, *j*) refers to the row and the column position of the row and column position of the linearization coefficient in the matrix form of the two equations. Based on the flow equation for each component, the mass conservation equation for each node can be constructed as:

Node 1: $$\dot{m}_{21} = a_{21}^{1}P_{1} + a_{22}^{1}P_{2} + a_{23}^{1} \tag{4.20}$$

Node 2: $$\dot{m}_{12} + \dot{m}_{32} + \dot{m}_{42} = a_{11}^{1}P_{1} + (a_{12}^{1} + a_{12}^{2} + a_{12}^{3})P_{2} + a_{11}^{2}P_{3} + a_{11}^{3}P_{4} + a_{13}^{1} + a_{13}^{2} + a_{13}^{3} \tag{4.21}$$

Node 3: $$\dot{m}_{23} = a_{22}^{2}P_{2} + a_{21}^{2}P_{3} + a_{23}^{2} \tag{4.22}$$

Node 4: $$\dot{m}_{24} = a_{22}^{3}P_{2} + a_{21}^{3}P_{4} + a_{23}^{3} \tag{4.23}$$

The solution of the four linear equations requires a matrix expression of the form:

$$\begin{bmatrix} X_{11} & X_{12} & X_{13} & X_{14} \\ X_{21} & X_{22} & X_{23} & X_{24} \\ X_{31} & X_{32} & X_{33} & X_{34} \\ X_{41} & X_{42} & X_{43} & X_{44} \end{bmatrix} \begin{bmatrix} Y_{1} \\ Y_{2} \\ Y_{3} \\ Y_{4} \end{bmatrix} = \begin{bmatrix} Z_{1} \\ Z_{2} \\ Z_{3} \\ Z_{4} \end{bmatrix} \tag{4.24}$$

Substituting mass flow in the equations at each node gives:

$$\begin{bmatrix} a_{21}^{1} & a_{22}^{1} & 0 & 0 \\ a_{11}^{1} & a_{12}^{1} + a_{12}^{2} + a_{12}^{3} & a_{11}^{2} & a_{11}^{3} \\ 0 & a_{22}^{2} & a_{21}^{2} & 0 \\ 0 & a_{22}^{3} & 0 & a_{21}^{3} \end{bmatrix} \begin{bmatrix} P_{1} \\ P_{2} \\ P_{3} \\ P_{4} \end{bmatrix} = \begin{bmatrix} \dot{m}_{21} - a_{23}^{1} \\ \dot{m}_{12} + \dot{m}_{32} + \dot{m}_{42} - a_{13}^{1} - a_{13}^{2} - a_{13}^{3} \\ \dot{m}_{23} - a_{23}^{2} \\ \dot{m}_{24} - a_{23}^{3} \end{bmatrix} \tag{4.25}$$

This is the matrix that Flowmaster solves for mass flow. Clearly, for larger and more complex networks, the hand formulation of the matrix is not practical, this example simply demonstrates how the linearization coefficients derived for the components are used in the network solver. The coefficients in each equation are determined by the corresponding parameters for each component. These are used to calculate the flow into and out of the components as a function of pressure. Flow is then eliminated from the equations using continuity at each node. This leaves a set of equations which that can then be simultaneously solved. The resulting pressures are substituted back into the component equations to calculate new estimates of the flows. Any pressure on components imposes a pressure at their connecting nodes. This iterative process is repeated until convergence is achieved.

4.5.1.3 Components for ventilation model. As a universal fluid flow simulation package, Flowmaster has a unique technique for constructing a network model. Several components in libraries can be used, depending on users' special requirements (Anon., 2007). Components used in this research necessary to build a ventilation network model in the Main Mine are described below.

4.5.1.3.1 Source components. Source components provide boundary conditions of user-defined flow, pressure, or heat. The four sources used in the network model were flow source, pressure source, heat source, and blank end source. A detailed description of each source is described below:

Flow Source: A flow source component supplies a constant flow rate, either to or from the component, irrespective of other conditions. The following equation defines the mass flow to the node:

$$\dot{m}_1 = \rho Q \tag{4.26}$$

The nodal pressure is calculated from the pressure term in the energy equations of one or more of the connecting branches. For a transient ventilation simulation, the flow source has a flow rate variable with time.

Pressure Source: A pressure source applies a constant pressure to the connecting node, irrespective of other conditions. The mass flow rate from the pressure source to the connecting node is determined by the continuity at the node, when all other mass flow rates have been determined by back substitution into an energy equation for the corresponding components.

Heat Flow Source: A heat flow source applies the heat flow rate to the fluid system. The heat flow source models the flow of heat to or from the solid part of a network. It can be constant or can vary with time for transient analysis. In this research, it is used to implement the heat from a fire source to the ventilation network system.

Blank End Source: The blank end acts as a flow source, but with the flow pre-set to zero.

4.5.1.3.2 Pipe component

Rigid Pipe: A rigid pipe component models the frictional pressure drop along a straight pipe assuming linear distribution of the frictional pressure gradient. The model assumes that the pipe has a constant cross-sectional area and a fully developed flow through the pipe.

The friction in the pipe depends on the pipe length, cross sectional dimension, and wall roughness. In the analysis, the following equation describes the pressure drop:

$$P_2 - P_1 = \frac{fL}{d}\frac{\dot{m}_1|\dot{m}_1|}{2A^2\rho} \tag{4.27}$$

where f is the Darcy friction factor, L is the pipe length (m), d the pipe diameter (for a rectangular pipe, this refers to hydraulic diameter) (m), and $\dot{m}_1$ is the mass flow rate at the inlet (kg/s).

The Darcy friction factor f can be determined by (Hartman et al., 1997)

$$f = \frac{K}{0.148} \tag{4.28}$$

where K is the factor calculated from ventilation survey results.

Actually, in turbulent flow, f is not a constant for a given conduit but varies with the Reynolds number. In mine ventilation, the K factor is assumed to be constant for a given airway, regardless of the Reynolds number. This is only an approximation and, on occasion, the error can be sizable (Falkie, 1958). However, for the usual range of the Reynolds number (50,000 to 2 million) encountered in underground mine workings, the error is acceptable in view of the variability of the other factors involved.

4.5.1.3.3 Air side component

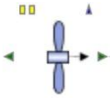

Fan: A fan component is commonly used to model the air flow through the complete cooling pack for steady or transient operating conditions. Its characteristic blowing or exhausting can be defined with a curve to describe the relationship between pressure rise and inlet flow rate.

4.5.1.3.4 Control valve component

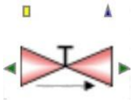

Sluice Valve: a sluice valve component is used to balance the flows in the system. It is simulated by defining a specific loss coefficient vs. position curve. The valve position is specified by ratio (0.0 = closed, 1.0 = fully open). Heat cannot be lost or gained in this component.

The pressure/flow equation used the sluice valve component is:

$$\Delta P = K_v \rho \frac{v^2}{2} \tag{4.29}$$

where ΔP is the total pressure loss (Pa), ρ is the density of fluid (kg/m^3), v is the mean flow velocity (m/s), and K_v is the valve loss coefficient which is dimensionless and dependent on the valve type and position.

The valve position is fixed for a steady state simulation. In transient simulation, the variation of valve loss coefficient with position is specified as a performance curve provided by manufactures. Usually, the curve starts from a minimum opening $\theta_{\min}$ instead of 0 to 1. If the valve opening is greater than zero, but less than $\theta_{\min}$, K_v is extrapolated as follows:

$$K_v = K_{v\theta\min} (\frac{\theta_{\min}}{\theta})^n \tag{4.30}$$

where $K_{v\theta\min}$ is equal to K_v at $\theta_{\min}$, and

$$n = -m(\frac{\theta_{\min}}{K_{v\theta\min}}) \tag{4.31}$$

where

$$m = \frac{dK_v}{d\theta}\Big|_{\theta \min} \qquad (4.32)$$

When the valve is fully closed, the model enforces zero flow, and the above extrapolation is not used.

4.5.1.3.5 Solid component

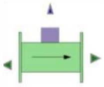

Thermal Bridge: A thermal bridge component is modeled as a discrete loss with a contact area from which heat can flow. The component can be connected directly to two fluid nodes and one solid node to model the heat flow from the heat source to the fluid system.

4.5.1.3.6 Controller components. An outstanding feature of Flowmaster is represented by including a number of controller components which can be connected to other components such as a pipe, valve, etc. They provide a control signal to a component. Having been built in algorithms, the controller enables the component to function in a desired way. In addition to performing automatic functions, the controller can also trigger events to which other components respond to.

Gauge Template: A gauge template component has a single measurement input connection. This may be connected to a node, a component branch, or a component measurement output. The input signal is utilized in a script defined in the gauge template that provided an output signal, which is often used as an input to a controller template. The input and output signals are essentially identical.

Controller Template: A controller template is divided into three blocks: Input Block, Controller Algorithm Block, and Output Block. The Input Block can accept up to five inputs from gauges or other acceptable controllers, and the Controller Algorithm will typically operate on one or more input signals to give an output value; the type of algorithm can be specified with Script. The Output Block is intended to condition the value obtained from the Algorithm Block.

4.5.2. FLUENT. It is a general three-dimensional CFD software package for solving complex fluid problems. The detailed information of its application and theory can be found in Sections 2 and 3. As one of the most powerful CFD tools in the world, it provides user defined functions (UDF) which can meet special requirements of the users.

This special function enables it to couple with other programs. In this research, FLUENT was used for solving the 3D part of the multiscale model.

4.5.3. MpCCI. In this research, MpCCI offered an open coupling interface to allow Flowmaster to co-simulate with FLUENT. Details are as follows:

4.5.3.1 Introduction. MpCCI is a new market segment for Computer Aided Engineering (CAE). It is introduced here to the mining industry for the first time. MpCCI was originally developed in Germany at the Fraunhofer Institute for Algorithms and Scientific Computing (SCAI) back in 2002 and updated to its latest version MpCCI 4.0 in 2007. It offers a variety of new disciplines and solution strategies for providing a code-independent interface for the coupling of different simulation codes. Solving multi-disciplinary problems by using coupled simulation environments is becoming a state-of-the-art technology for the rapidly growing engineering community. The MpCCI interface has been accepted as a standard for such code coupling environments.

Co-simulation permitted the sharing of boundary data between one dimensional and three dimensional models in single or multi-domain systems. Thus, the interaction of the overall fluid system with the 3D effects within a critical part of the network could be simulated.

4.5.3.2 Basic structure. MpCCI enables a direct communication between Flowmaster and FLUENT by providing adapters for each code. The data exchange between two simulation codes requires a “code adapter”, which constitutes a “code plug-in” for data transfer. These code-adapters make use of already existing application programming interfaces (APIs) of the simulation tools. This technique allows an easy installation of MpCCI at the end users site without changing the standard installation of the simulation codes. Since the meshes belonging to different simulation codes are not generally compatible, MpCCI performs an interpolation. In the case of parallel codes, MpCCI keeps track of the distribution of the domains into different processes.

Running a co-simulation with MpCCI requires the following steps (Ludhi, 2006):

Preparation of Model Files: Before starting a co-simulation, both the 1D and the 3D models must be built separately, i.e., a model file must be created for each simulation code and the model files must contain extra information defining the coupling regions.

Definition of the Coupling Process: In addition to the model files, the coupled regions, quantities, and a coupling algorithm must be selected in this step, and other coupling options can be given. This step is completely supported by the MpCCI GUI.

Running the Co-simulation: After starting the MpCCI server, both Flowmaster and FLUENT run in parallel. Each code computes its part of the problem, while MpCCI controls the quantity exchange.

Post-Processing: After the co-simulation, the results can be analyzed with the post-processing tools of each simulation code together with the MpCCI Visualizer.

4.5.4. Coupling Process. An overview of the complete co-simulation process is given in Figure 4.6.

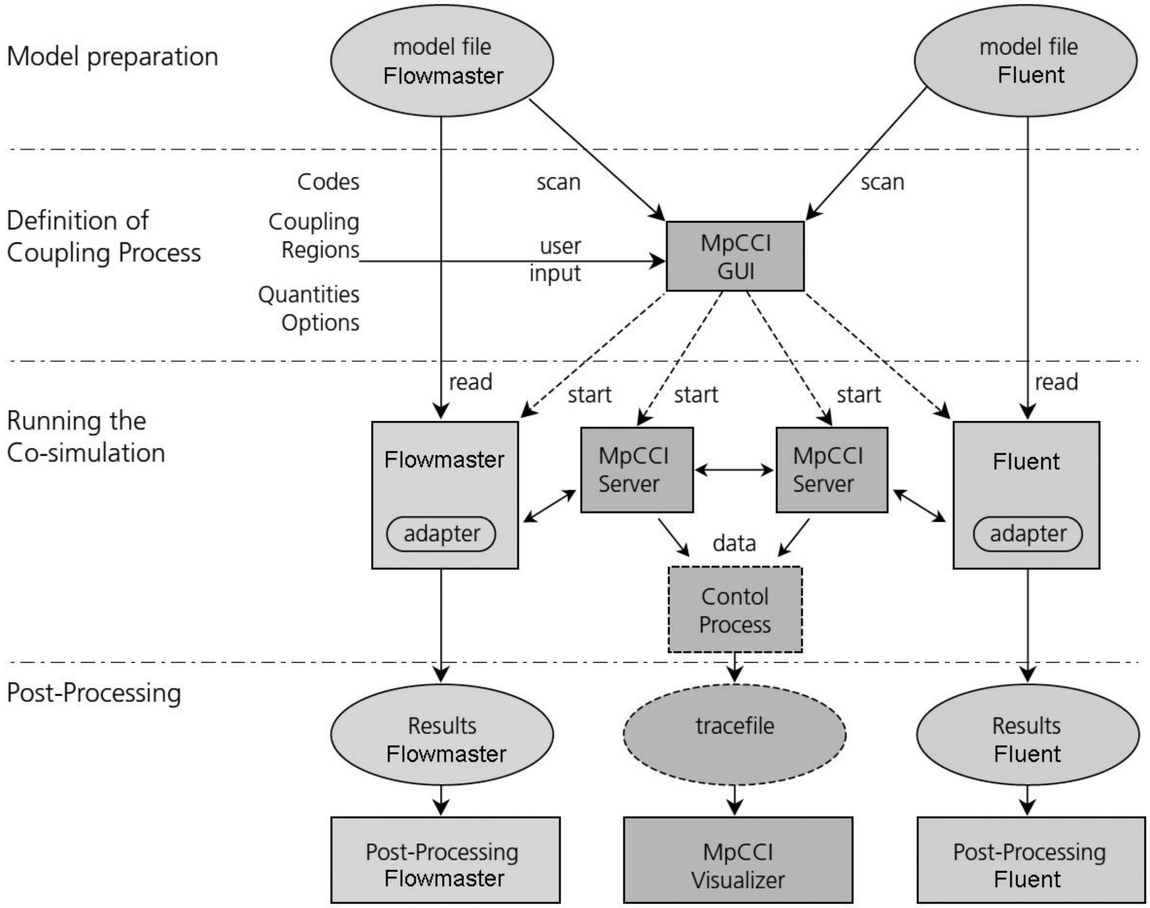

Figure 4.6. Coupling Process for MpCCI (Bayrasy and Kelsall, 2008, edited)

Among these steps, the coupling algorithm is a critical one for determining whether the coupling process is successful or not. MpCCI cannot control the simulation processes of Flowmaster and FLUENT. Therefore, it is important to organize the processes so that, whenever one side sends data, the other side is ready to receive. Also the data is not associated with certain time steps or iterations. During the iteration, which also consists of several time steps in a transient problem, the data will be exchanged several times.

The possible coupling algorithms are mainly determined by the capabilities of the simulation codes and the corresponding code adapters. The code adapters call "send" and/or "receive" functions. These calls can appear at different states of the computation, such as at the beginning of each time step, at the end of each time step, before or after an iteration step, or on direct demand of the user. Most codes only offer exchanges at the beginning or end of a time step, which limits the choice of coupling algorithms.

In this research, Flowmaster and FLUENT were used as coupled simulation codes. Both of them are capable of exchanging data at the beginning of each time step before the iteration. The appropriate coupling algorithms were developed and are depicted in Figure 4.7. This is identified as a transient coupling process. For steady simulation, it is assumed that there is exactly one solution to the coupled problem, which shall be found. The coupling algorithm does not have much influence on the solution in this case. By replacing the time point (shown in Figure 4.7) with an iteration step, the coupling algorithm for steady state simulation can be obtained.

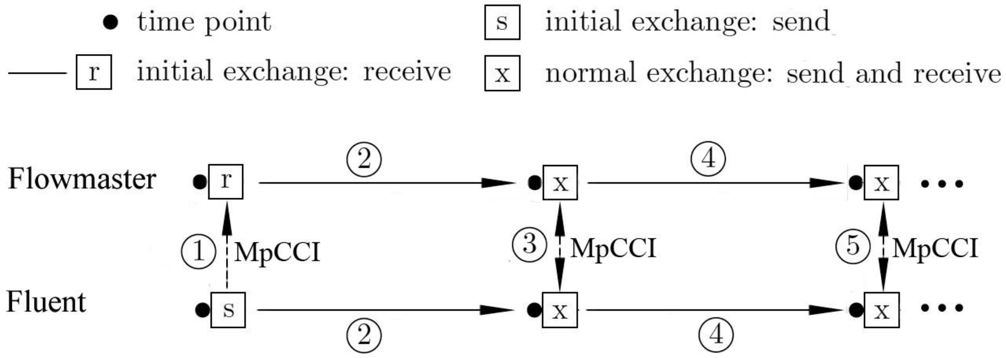

Figure 4.7. Coupling Algorithm for Flowmaster and FLUENT

In Figure 4.7, Flowmaster and FLUENT represent the two coupled codes with the black pots representing the time points from the beginning of the coupling process. The boxes indicate the data exchanges. The first boxes in each code represent the initial data transfer. For both Flowmaster and FLUENT, the boxes are placed at the end of the time points, which means that the codes exchanged data before solution.

The data transfer proceeds from left to right, starting as a sending operation in FLUENT. FLUENT started sending data (1) to Flowmaster. Then, Flowmaster and FLUENT can run in parallel (2). No matter which one finishes computing first, it will wait for the other to finish. Once both runs are complete, data will be exchanged (3) before the next time step. After receiving new boundary data, run (4) can be started and then proceed (5). Thus, each code runs separately and some fluid quantities are exchanged. By using Flowmaster and FLUENT as coupled codes, MpCCI allows the exchange of data that includes the temperature, total pressure, mass flow rate, mass flux, and velocity magnitude.

4.6. CASE STUDY

4.6.1. Problem Description. MpCCI has no limitation on the number of interfaces between 1D and 3D. To describe the coupling process, only two interfaces were included in this study. A simple ventilation network was constructed showing the transient coupling simulation process. A multiscale model was generated by coupling the 1D and the 3D models together. The multiscale model consisted of three airways connected in series, two airways were included in the 1D model with Flowmaster and a third airway in the 3D model with FLUENT. The layout of the multiscale model is shown in Figure 4.8.

Figure 4.8 shows that the left boundary of the 3D model was coupled with Node 2 of the 1D model, while the right boundary of the 3D model was coupled with Node 3 of the 1D model. Two flow source boundaries were placed at Nodes 2 and 3 to represent the interface inlet and outlet, respectively. A constant total pressure of 101,358 Pa and 101,375 Pa were applied at Node 3 and Node 4, respectively in the 1D model. In this example, all of the airways had the same 2.0m × 2.0m cross-section. The two airways modeled in Flowmaster had the same length (12.0m) while the airway modeled in FLUENT had a 6.0m in length.

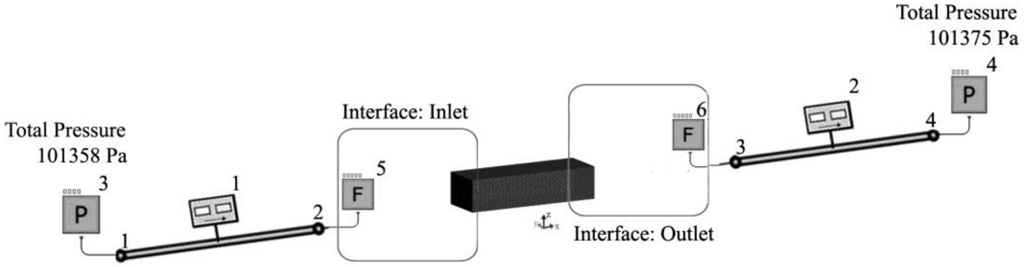

Figure 4.8. Drawing Showing a Multiscale Model

4.6.2. Model Preparation. Before starting a co-simulation, the 3D and the 1D models have to run separately to prepare a model file for each set of simulation code.

Figure 4.9 shows the process of 1D model generation. A simple full 1D network model was constructed first using Solid: Pipe as airway, and Source: Pressure boundary as a force source. To form 1D models for a multiscale model, one airway in the middle was moved out and will be replaced with the 3D model. Thus, two new boundaries were generated, represented by two Source: Flow components.

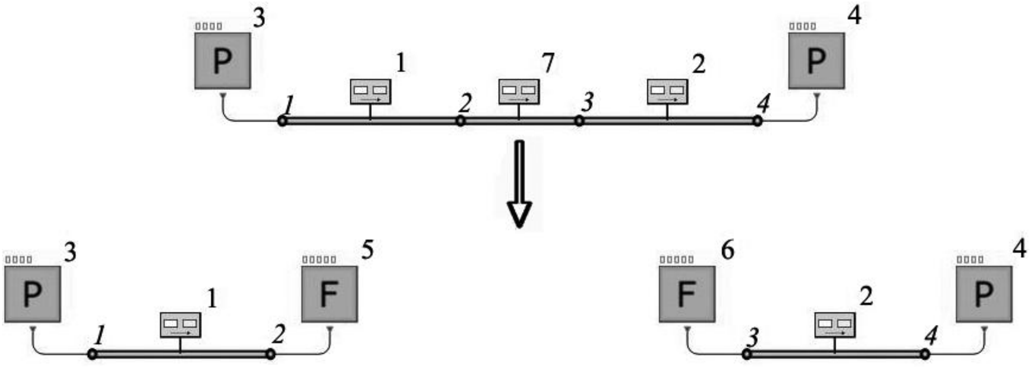

Figure 4.9. Process of Forming 1D Network for a Multiscale Model Example

The geometry and part of boundary information for both 1D models are described in Section 4.6.1. For the two newly generated boundaries, it is necessary to establish initial mass flow rate values. These two flow sources acted as coupling boundaries, communicating with FLUENT by sending total pressure and receiving mass flow rate at each time step. The initial value does not influence the final results, except for increasing the number of iteration steps. Once the 1D network model and co-simulation boundaries setting were ready, a link file had to be created for the coupling process.

The airway that was removed (Figure 4.9) was modeled in 3D. All of the geometric information related to the airway was used to build the 3D model (shown in Figure 4.10). The model contained a definition of two coupling regions: Inlet_Pressure (left) and Outlet_Pressure (right). These boundaries were set to receive total pressure values which were stored in UDM during the coupling process.

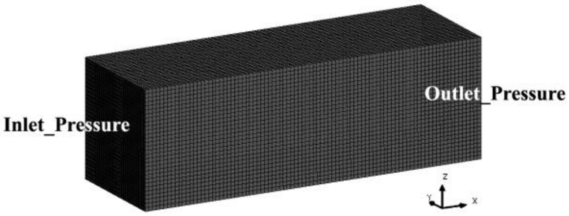

Figure 4.10. Geometric 3D Model for a Multiscale Model Example

The 3D model was solved with FLUENT. A standard turbulent model together with a full buoyancy effect was adopted. Since the ideal gas was used as fluid, the energy option was checked to consider the compressible effect of the fluid and a standard wall function was adopted for the wall boundary condition. To initialize the calculation, a velocity value at the Inlet_Pressure boundary needed to be set. This value was supposed to be generated from the calculation results of a full 1D network model. Here, a 1.0 m/s value was adopted, intended to deviate significantly from the real one to describe the influence of the initial value on the final result. The initial velocity at the inlet was done in 3D to provide the mass flow rate to the 1D model, as an initial value.

4.6.3. Steps of Co-simulation. Running a co-simulation with MpCCI required the following steps, which were completely supported by the GUI function within MpCCI:

Step 1: Models Step (Figure 4.11)

In this first step, the coupled simulation codes, both Flowmaster and FLUENT, and the corresponding input files (e. g., ffft.fmlink and FFFt.cas) were selected. The data file included the models' information, so MpCCI scanned the data files to ensure that everything needed for coupling was included.

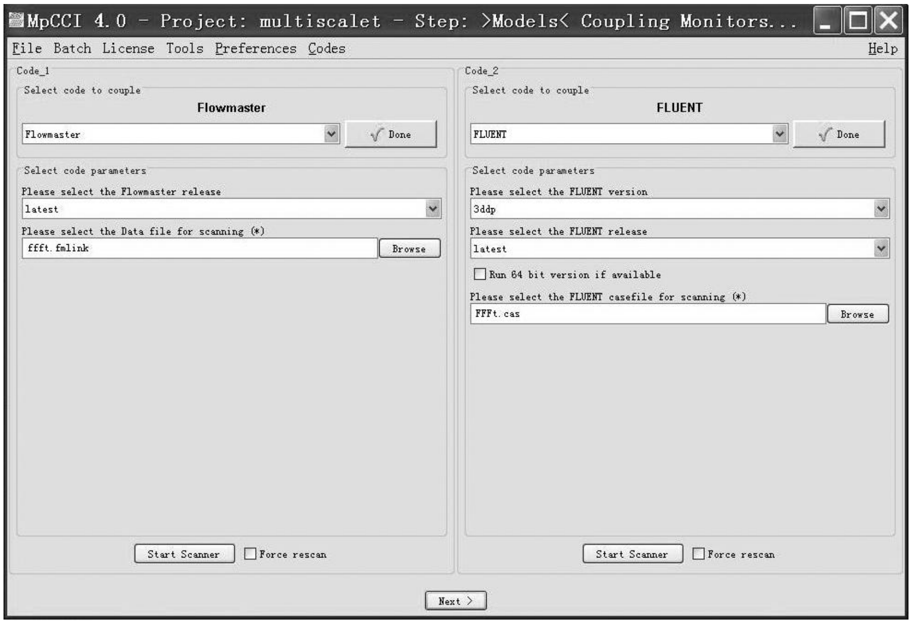

Code_1

Select code to couple: Flowmaster

Flowmaster

Select code parameters

Please select the Flowmaster release: latest

Please select the Data file for scanning (*): ffft.fmlink

☐ Force rescan

Code_2

Select code to couple: FLUENT

FLUENT

Select code parameters

Please select the FLUENT version: 3ddp

Please select the FLUENT release: latest

☐ Run 64 bit version if available

Please select the FLUENT casefile for scanning (*): FFFt.cas

☐ Force rescan

Figure 4.11. Models Step for MpCCI GUI

Step 2: Coupling Step (Figure 4.12)

In this step, the two coupled regions were named Face_1 and Face_2, which referred to the Interface: Inlet and Interface: Outlet in Figure 4.8, respectively. At both Face_1 and Face_2, Flowmaster sent the total pressure value to and received the average mass flow rate value from FLUENT. The total pressure data were stored at UDM0 which corresponded to the udf UDM00_Profile::libmpcci defined in FLUENT.

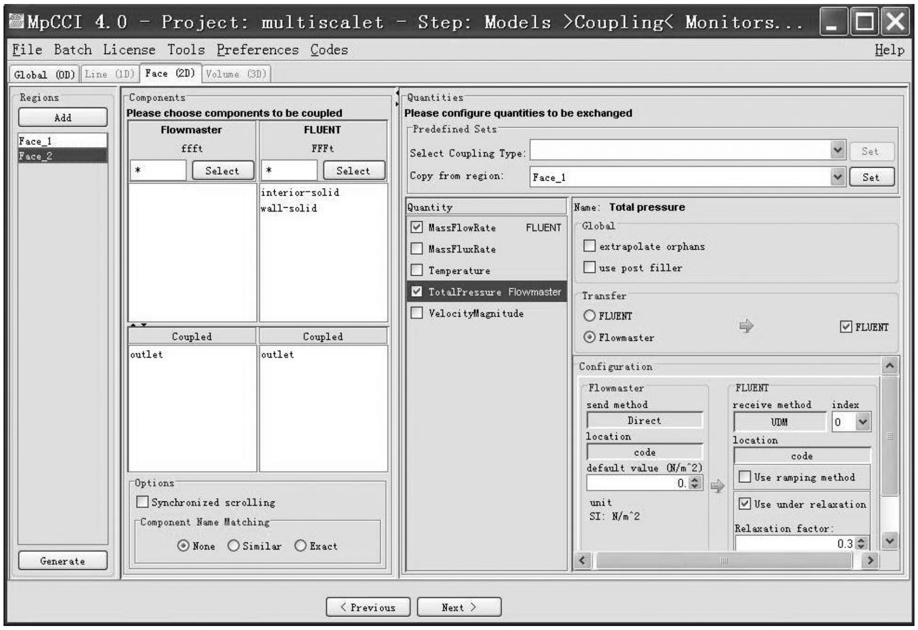

MpCCI 4.0 - Project: multiscalet - Step: Models >Coupling< Monitors...

Regions
Face_1
Face_2

Components
Please choose components to be coupled

Flowmaster
ffft
*
Coupled
outlet

FLUENT
FFFt
*
interior-solid
wall-solid
Coupled
outlet

Options
☐ Synchronized scrolling
Component Name Matching
● None ○ Similar ○ Exact

Quantities
Please configure quantities to be exchanged
Predefined Sets
Select Coupling Type:
Copy from region: Face_1

Quantity
☑ MassFlowRate FLUENT
☐ MassFluxRate
☐ Temperature
☑ TotalPressure Flowmaster
☐ VelocityMagnitude

Name: **Total pressure**
Global
☐ extrapolate orphans
☐ use post filler
Transfer
○ FLUENT
● Flowmaster
☑ FLUENT

Configuration
Flowmaster
send method: Direct
location: code
default value (N/m^2): 0.
unit
SI: N/m^2

FLUENT
receive method: UDM
index: 0
location: code
☐ Use ramping method
☑ Use under relaxation
Relaxation factor: 0.3

Figure 4.12. Coupling Step for MpCCI GUI

Step 3: Monitoring Step (Figure 4.13)

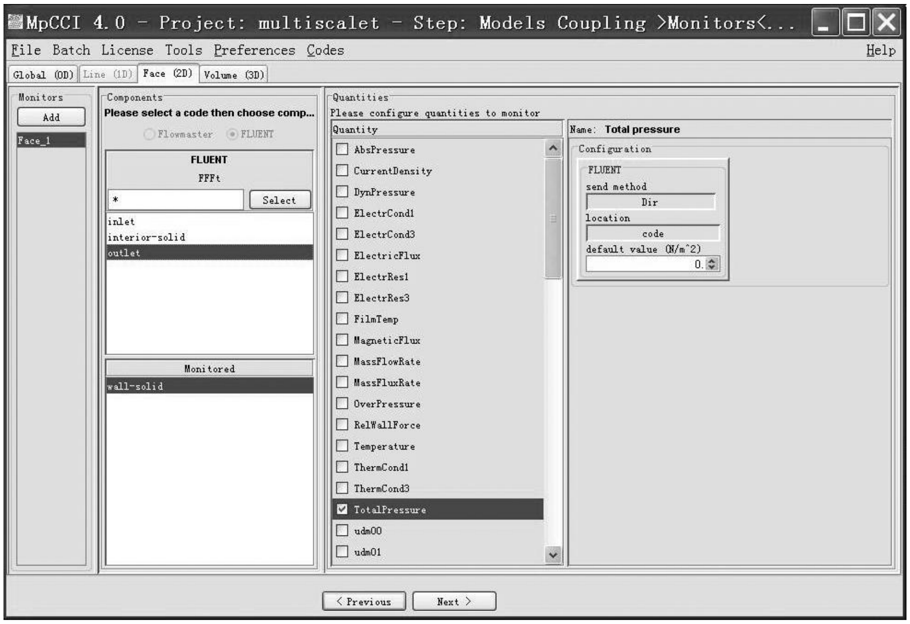

MpCCI 4.0 - Project: multiscalet - Step: Models Coupling >Monitors<...

Monitors
Face_1

Components
Please select a code then choose comp...
○ Flowmaster ● FLUENT

FLUENT
FFFt
*
inlet
interior-solid
outlet
Monitored
wall-solid

Quantities
Please configure quantities to monitor

Quantity
☐ AbsPressure
☐ CurrentDensity
☐ DynPressure
☐ ElectrCond1
☐ ElectrCond3
☐ ElectricFlux
☐ ElectrRes1
☐ ElectrRes3
☐ FilmTemp
☐ MagneticFlux
☐ MassFlowRate
☐ MassFluxRate
☐ OverPressure
☐ RelWallForce
☐ Temperature
☐ ThermCond1
☐ ThermCond3
☑ TotalPressure
☐ udm00
☐ udm01

Name: **Total pressure**
Configuration
FLUENT
send method: Dir
location: code
default value (N/m^2): 0.

Figure 4.13. Monitoring Step for MpCCI GUI

The MpCCI coupling regions may be monitored, and any quantities of interest at the coupling regions were chosen at this step. In this example, the total pressure at the wall in the 3D model and the total pressure and the mass flow rate at the interface in the 1D model were monitored during the coupling process.

Step 4: Edit Step (Figure 4.14)

In the Edit step, the control parameters were grouped into Monitor, Relation Search, and Output sections. The MpCCI GUI provided default values for all of these parameters (which could be modified if necessary).

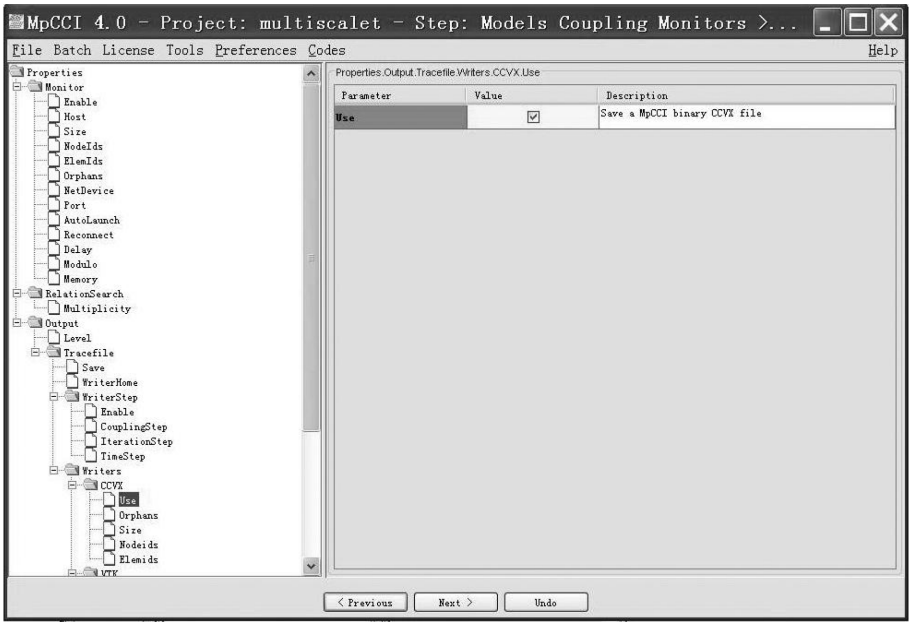

Properties.Output.Tracefile.Writers.CCVX.Use

Parameter	Value	Description
Use	☑	Save a MpCCI binary CCVX file

Figure 4.14. Edit Step for MpCCI GUI

Step 5: Go Step (Figure 4.15)

Before starting the coupled simulation, the start-up of the applications had to be configured. For the MpCCI coupling server, everything was retained as the default value, except for increasing the number of buffers. The coupling algorithm shown in Figure 4.7 was adopted in this example. The initial exchange mode in Flowmaster was set to be "receive" by default; thus, in FLUENT, the initial exchange mode had to be "send". Some other option parameters can be configured if necessary.

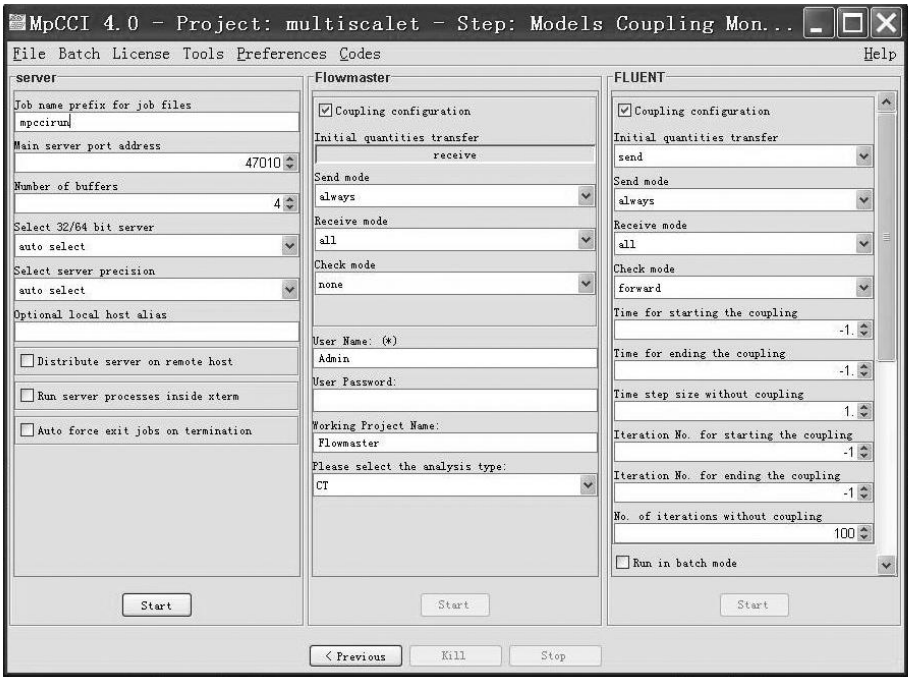

server

Job name prefix for job files: mpccirun
Main server port address: 47010
Number of buffers: 4
Select 32/64 bit server: auto select
Select server precision: auto select
Optional local host alias:
☐ Distribute server on remote host
☐ Run server processes inside xterm
☐ Auto force exit jobs on termination

Flowmaster

☑ Coupling configuration
Initial quantities transfer: receive
Send mode: always
Receive mode: all
Check mode: none
User Name: (*) Admin
User Password:
Working Project Name: Flowmaster
Please select the analysis type: CT

FLUENT

☑ Coupling configuration
Initial quantities transfer: send
Send mode: always
Receive mode: all
Check mode: forward
Time for starting the coupling: -1.
Time for ending the coupling: -1.
Time step size without coupling: 1.
Iteration No. for starting the coupling: -1
Iteration No. for ending the coupling: -1
No. of iterations without coupling: 100
☐ Run in batch mode

Figure 4.15. Go Step for MpCCI GUI

After starting the MpCCI Server, both Flowmaster and FLUENT were started. Each code computed its parts of the problem, while MpCCI controled the quantity exchange. The coupling process stopped when the pre-defined global convergence was reached.

4.6.4. Results Analysis. The transient calculation was set to last 30 seconds, and the mass flow rate distribution was shown in Figure 4.16.

In the 3D model, the absolute value of the mass flow rate increased from zero at the surrounding boundary to maximum value at the airway center. At the Interface: Inlet and Interface: Outlet, the average values of mass flow rate from 3D model were calculated and transferred to 1D model.

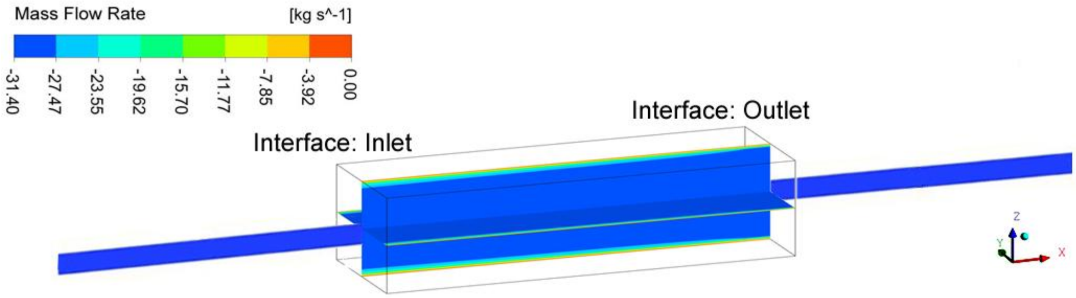

Figure 4.16. Mass Flow Rate Calculated by Multiscale Model (not to scale)

The global convergence check was performed by monitoring the evolution of selected fluid quantities at the 1D-3D interfaces during the *k-iterations*. Figure 4.17 shows the evolution of the total pressure and mass flow rate at the interfaces, and the total pressure at the wall boundary in 3D model was also monitored dynamically.

Flowmaster specifies that when air flows into the component, the mass flow rate is marked as positive, otherwise marked as negative. In Figure 4.17 at each time step, the mass flow rate results at the Interface: Outlet and the Interface: Inlet were shown in the top right and bottom right, respectively. The bottom left figure recorded the total pressure at the Interface: Outlet. The total pressure at the boundaries in the 3D model was recorded in the top left figure.

MpCCI can neither control the calculation process, nor set the convergence level. Each code had to set its own convergence level. The multiscale model was converged only when the calculation results of both codes reached their convergence level. The 1D model runs much fast than the 3D model. The convergence level in the 1D model did not influence the calculation time significantly.

The simulation efficiency was primarily dominated by the 3D model. During each time step in transient simulation, several iterations in 3D model needed to be conducted. The more iterations, the more calculation time was needed, and the more accurate will be the results. Thus, a proper convergence level can provide relatively accurate results with acceptable amount of calculation time to be practical. It is worthy to note that, given the uncertainty in mine ventilation flow behaviors, a lower but acceptable accuracy can be applied to significantly shorten the computing time.

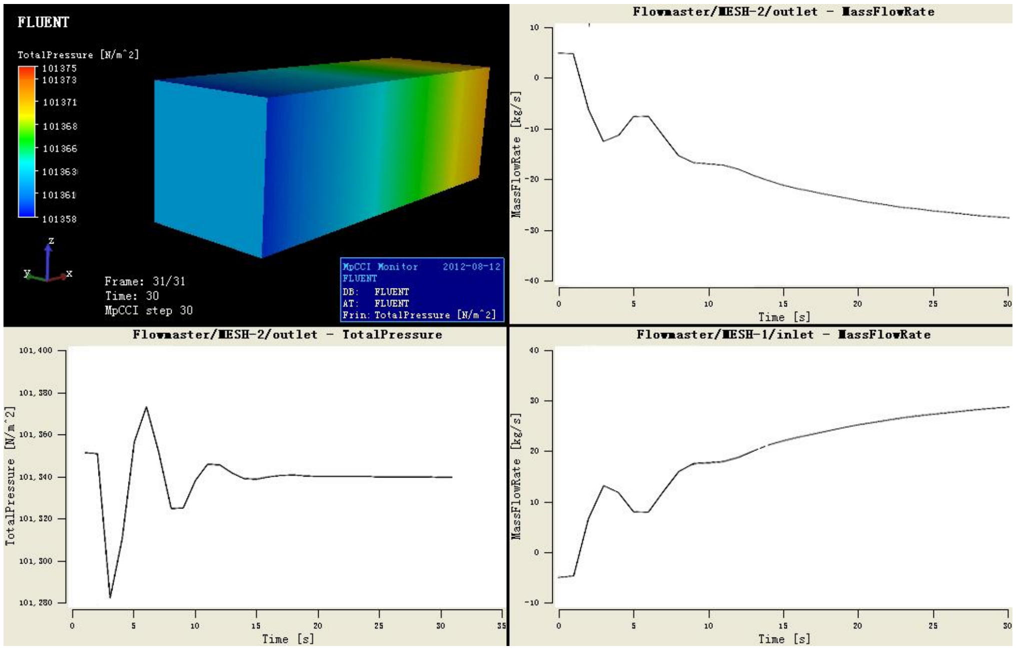

Figure 4.17. Evolution of Total Pressure and Mass Flow Rate at Interfaces in the Multiscale Model Example

Figures 4.18 and 4.19 showed comparisons of transient simulation results of total pressure and mass flow rate at the Inferface: Inlet between the 1D and the multiscale model.

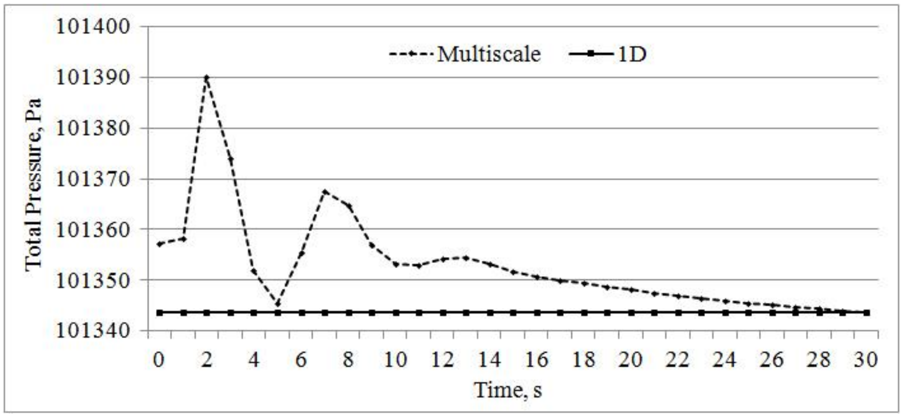

Figure 4.18. Comparison of the Total Pressure for the 1D and Multiscale Model at the Interface: Inlet

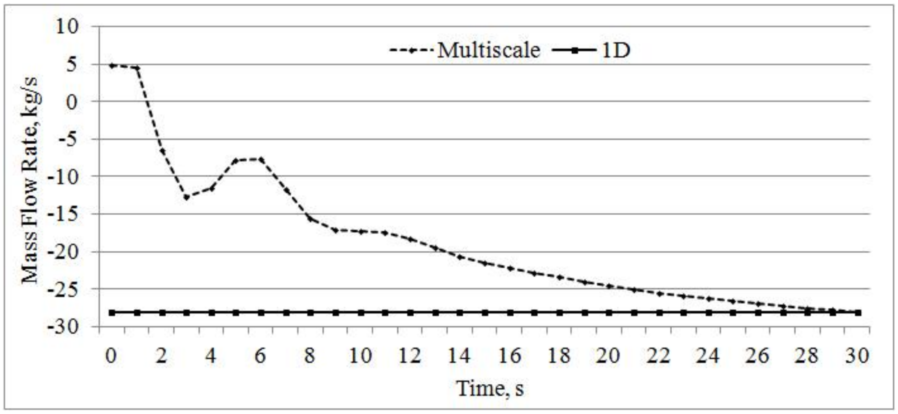

Figure 4.19. Comparison of the Mass Flow Rate for the 1D and Multiscale Model at the Interface: Inlet

For both total pressure and mass flow rate, the simulation results from the multiscale model fluctuated significantly in the first 15s. The consistence of results between multiscale and 1D model did not occur until after about 29 time steps. The reason for the deviation might be the improper initial value applied in the 3D model. Although the improper initialization did not influence the accuracy of the final result, it could present unaccurate results during the first few steps for transient state simulation. For a steady-state simulation, it will definitely increase the computing time to reach the convergence.

To prove the deduction above, another run was tried by applying a different initial value which was more close to the final value to the boundaries in the 3D model. The total pressure and the mass flow rate at the Interface: Inlet from 3D model were compared with 1D model. The comparison results showed they agreed with each other very well. The fluctuation occurred only at the first five time steps.

4.7. ACCURACY ANALYSIS

The global convergence check is performed by monitoring the evolution of any average fluid-dynamic quantity at the 1D-3D interfaces during iterations. In particular, the model checks whether or not the deviation of a certain fluid-dynamic quantity during two sequential multiscale iterations is lower than a fixed tolerance. For example, the maximum deviation allowed was 10^{-6} which was reached after around 30 multiscale iterations in the case study in Section 4.6. It is worth noting that, given the high uncertainty characterizing mine ventilation flow calculations, lower accuracy (i.e. 10^{-3}) can be used that can significantly shorten computing time (~15 multiscale iterations).

The consistency of the boundary conditions is another significant issue from the engineering and co-simulation perspective. This particular affects the communication of pressure between Flowmaster and FLUENT, the former solves for Absolute Total Pressure, while FLUENT solves for gauge pressures. However the pressure is further complicated because at pressure inlets, FLUENT expects gauge total pressures to be specified, while at pressure outlets, gauge static pressures are specified. MpCCI adapter has the ability to take these factors into account. The 3D pressure boundaries are always specified as pressure inlets, and when the flow is truly into the 3D domain, Flowmaster passes the Total Pressure (corrected to Gauge Total Pressure). Otherwise, if the flow is out of the 3D domain Flowmaster passes the Static Pressure (corrected to Gauge Static Pressure.)

The simulation results showed that if both codes show stability and convergence for each sub-problem, this guarantees the existence of a coupled solution. Additional iteration loops at the interface will provide better convergence and stability to the system.

5. ONE-DIMENSIONAL VENTILATION MODEL OF THE MAIN MINE

5.1. INTRODUCTION

The ventilation network calculation was used to determine the airflow and pressure distribution in mine ventilation systems for more than four decades, and with the advance in computer speed and reliability, this has become a routine operation the past two decades. As digital computers became more and more powerful, reliable and readily available, ventilation network calculations have led to considerable improvements in ordinary ventilation planning work.

One of the major developments in the past several decades is the introduction of software package that is capable of modeling a mining fire. Calculation of a mine network involving a fire starts with a normal ventilation simulation, then the simulation of heat and contaminants generation in designated location, followed by modeling and temperatures and concentration distribution accompanying the airflow. At present, all 1D models have to treat fire as the heat source.

5.2. VENTILATON SURVEY

A ventilation survey is an organized procedure of acquiring data that quantifies the distributions of airflow, pressure, and air quality throughout the main flow paths of a ventilation system (McElroy and Kingery, 1957). The main purpose of an accurate underground ventilation survey is to obtain air quantity and pressure gradient along the circuit to determine the value of friction factors for airways. In addition, other measurements such as the airway dimension, wet and dry bulb temperatures, and barometric pressure, are also taken either as an integral part of the survey or separately.

5.2.1. The Main Mine Introduction. A thorough ventilation survey was conducted at the Main Mine, the principal section of the Experimental Mine at Missouri S&T (Figure 3.1). It is an underground room-and-pillar operation covering an area of 115.5m by 71.6m. The Main Mine network consists of 94 branches, including 87 airways, three raises (R1 to R3), two portals (named Wheeler Portal and Kennedy Portal), one shaft, and one fan. The Experimental Mine’s Main Mine is shown in Figure 5.1.

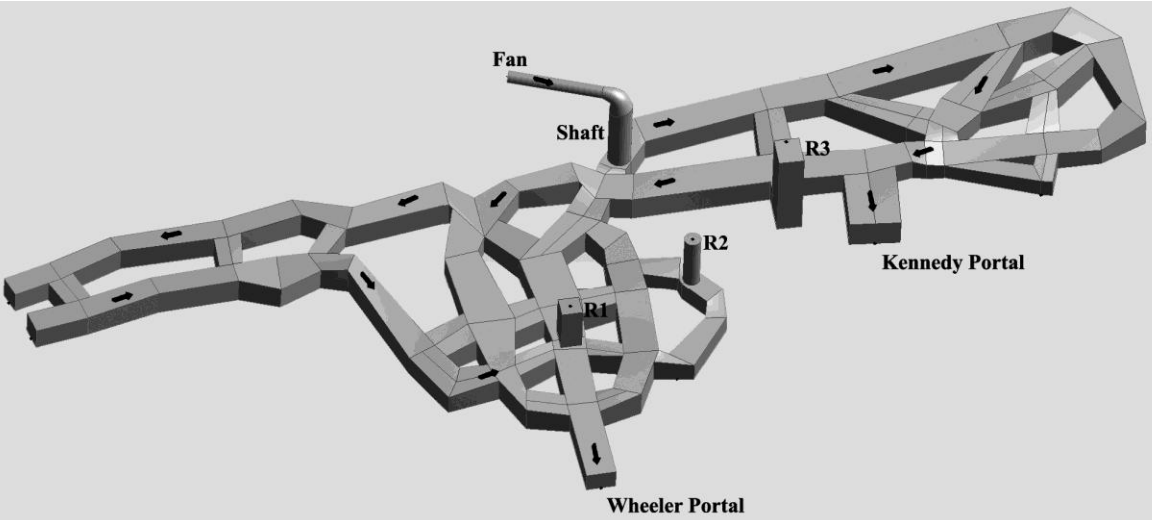

Figure 5.1. Main Mine at the Missouri S&T Experimental Mine

The Main Mine was ventilated using a blowing ventilation system with a 1.2m diameter Joy series 1000 Axial Vane fan (equipped with a 30 kW motor) on top of 1.22m diameter main intake airshaft. The fan provides approximately 25.0 m^3/s (50,000 cfm) of airflow at 500 Pa (2 in.w.g) of static pressure to the underground workings. Figure 5.2 shows the fan installation and fan curve.

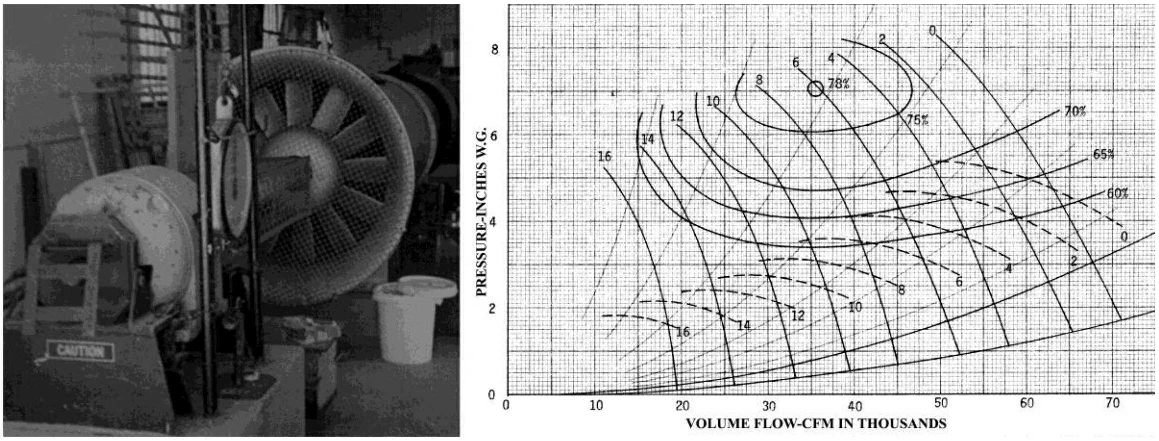

Figure 5.2. The Joy Series 1000 Axial Vane Fan (left) and Fan Curve (right)

5.2.2. Pressure Survey. Two methods have been used in a pressure survey: direct and indirect methods. The former is the trailing hose or gauge- and tube- method pressure drop between the beginning and end of an airway is measured using a rubber hose. It is time-consuming, but more accurate, where mine is small and foot travel is relatively easy. The indirect method uses a barometer or an altimeter to simultaneously measure barometric pressures at a strategical point underground (major intersections, splits, bottom of intake and return airshafts, etc.) and a surface base station, pressure drop for an airway is calculated by computing relative pressure drop against the same surface base station. Air velocities along with cross-sectional area at the same location are used to compute airflow; wet- and dry-bulb temperatures are also necessary for any density corrections. Details of these methods can be found in Hemp (1989). The indirect method was used in the pressure survey of this research because of availability of measuring instrument.

A thorough pressure survey was made at the Main Mine. At the beginning and end of each airway, elevation readings using (type and model numbers) barometers were taken simultanerously. To correct for any density variations, dry/wet bulb temperatures were also measured at these junctions. The differential pressure, ΔP, between two junctions was calculated by subtracting one from the other. A total of 92 airways were identified and measured and corresponding pressure differences were calculated.

5.2.3. Air Quantity Survey. The volume of air passing through a given point in an airway, $Q(m^3/s)$, is determined as the product of the cross-sectional area of the airway, $A(m^2)$, and the mean air velocity, $V(m/s)$:

$$Q = V \cdot A \tag{5.1}$$

Mean velocity at a certain point can be determined by an anemometer traversing the cross-section. Details of the methods used to undertake such measurements are described by numerous authors, including McPherson (1993). In this air quantity survey, a rotating vane anemometer was used to measure the airspeed.

The anemometer was attached to a rod (about 1.5m in length) to minimize body interference during traversing. When the instrument is held in a moving airstream, the airflow exerts a force on the angled vanes, causing them to rotate with an angular velocity that is closely proportional to the airspeed. A gearing mechanism and clutch arrangement couple the vanes to a pointer. The pointer rotates against a circular dial that is calibrated in the meter. At each station, the traverse lasted 60 seconds and was repeated at least once to ensure that the reading deviation was within $\pm 5\%$. All 92 branches were measured and corresponding air quantities calculated.

5.2.4. K Factor Calculation. A ventilation pressure-quantity survey was used to determine the resistance of the mine airways. The principle for resistance calculation is based on the relationship between the pressure and air quantity:

$$R = \frac{\Delta P}{Q^2} \tag{5.2}$$

where R is the airway resistance value (N s^2/m^8). Usually, a more useful indicator, K factor, is adopted to provide a more representative value for evaluating mine airway conditions for the entire mine. This is calculated using the Atkinson Equation:

$$K = \frac{Rn^2 A^3}{OL} \tag{5.3}$$

where A is an airway cross-sectional area (m^2), O is the perimeter (m), L is the airway length (m), and n is the number of airways. Since it is simple network at the Main Mine, n = 1 in all calculations.

In developing a numerical simulation of a mine ventilation field, one of the main purposes for conducting a ventilation survey is to provide the computer with the data needed to construct a network model. Meanwhile, the calculation results from the numerical model should, in turn, be validated by ventilation survey data for checking the accuracy of the numerical model.

5.3. VENTILATION NETWORK MODEL

The Main Mine network was constructed using Flowmaster. The airways were modeled as a Rigid Pipe with boundary conditions defining its physical dimensions and atmospheric characteristics. The blowing fan, airways having stopping, and the dead-end were represented by Fan, Sluice Valve, and Bland End Source, respectively. The surface boundary conditions were established by defining properties of the Pressure Source component. The network model for the Main Mine is shown in Figure 5.3.

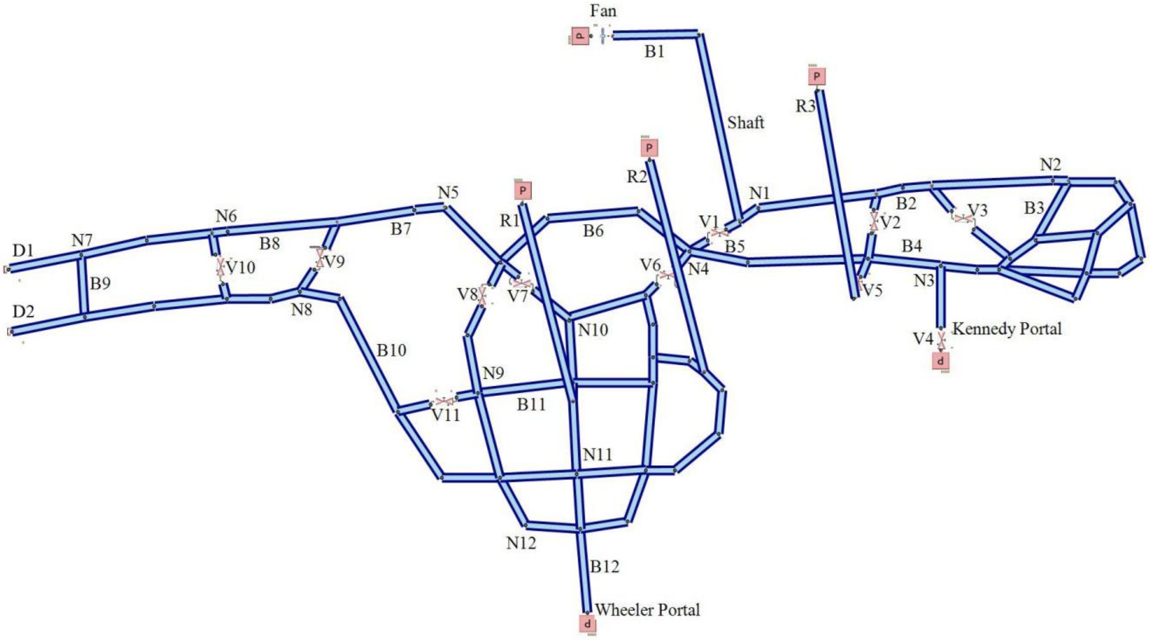

Figure 5.3. The 1D Ventilation Model for the Main Mine

Airways properties, including the geometric dimensions and friction factor, were defined on the basis of ventilation survey data. The fan curve (Figure 5.2) was applied to the fan for modeling the fan component. All pressure source components were considered as atmospheric boundaries connecting to the surface. For the purpose of validation and verification, 12 branches (B1 to B12) and 12 nodes (N1 to N12) were selected for the network model. The airways having stopping were numbered from V1 to V11. Two dead-ends were numbered as D1 and D2.

A steady ventilation simulation was conducted in order to calculate the air quantity and pressure along the Main Mine. Figure 5.4 shows the graphic results of the air quantity determination. The branches are colored in accordance with the different air quantity values identified in the legend (in m^3/s). A air quantity values for branches B1 to B12 are marked in this figure.

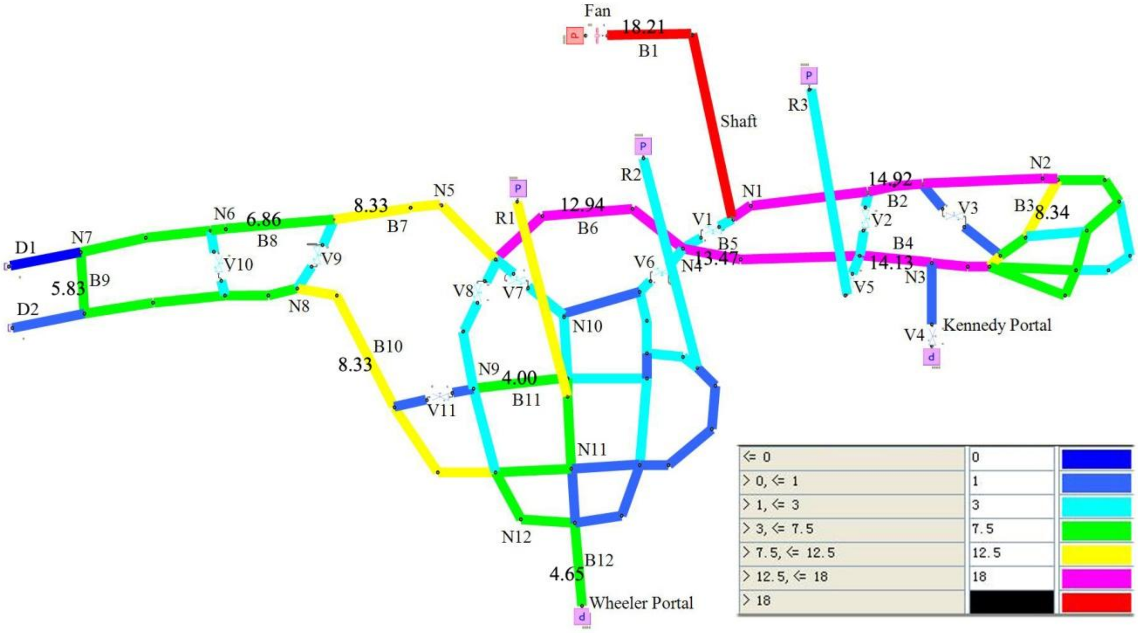

Figure 5.4. Air Quantity Distribution in Steady State in the 1D Model

This is the first time that Flowmaster is used for modeling a mine ventilation network. To ensure its capability of modeling, a verification process is required. In addition to Flowmaster, the same network model was calculated using both Ventsim Visual and VnetPC Pro. A comparison of results of the air quantity at all 12 reference branches obtained by these three tools is plotted in Figure 5.5.

For the purpose of comparison, results from VnetPC Pro are base one. As shown in Figure 5.5, air quantities of all 12 airways calculated by three packages correlate well. The largest discrapancy between Flowmaster and VnetPC Pro was 5.61% difference at branch B3. This margin is acceptable when comparing with the larger 16.27% (at B11) deviation between Ventsim Visual and VnetPC Pro. Analysis of this comparison concluded that the Flowmaster, a new numerical simulation tool introduced to the mining industry for the first time, should also be able to successfully simulate a ventilation system for an underground operation.

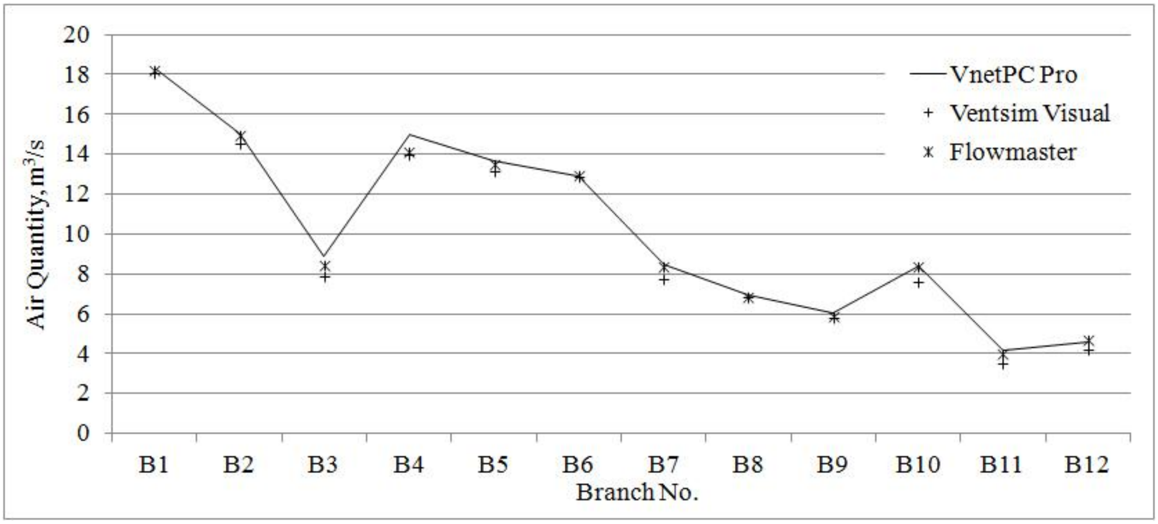

Figure 5.5. Verification of the 1D Ventilation Model Using VnetPC Pro and Ventsim Visual

In addition to verification, validation results were also obtained by comparing the air quantity of numerical predictions and experimental data. Although the Flowmaster can help solve mine ventilation problems, the calculation results should prove to be sufficiently accurate under specific conditions. The air quantities determined by the ventilation survey at 12 reference branches were used to validate the usefulness of the numerical network model. Figure 5.6 shows that results from measurement and prediction matched each other well. The largest relative discrapancy (12.53%) was found at B3. The 1D model predicts the overall flow behavior of a mine ventilation system well.

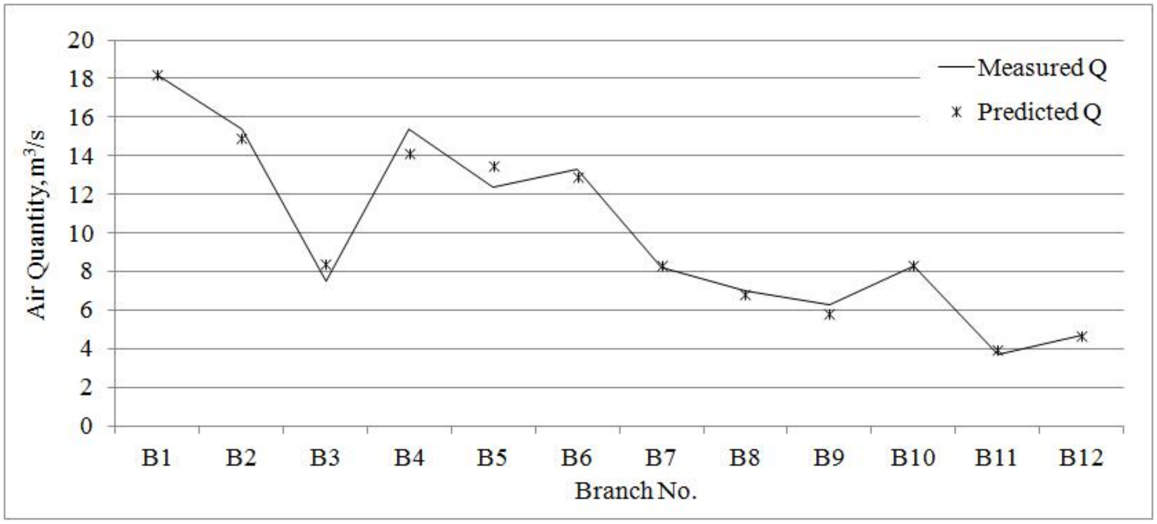

Figure 5.6. Validation of the 1D Ventilation Model

5.4. ONE-DIMENSIONAL HEAT SIMULATION

5.4.1. Case One: 1D Heat Model. A heat model was developed by introducing a heat source to a junction in the ventilation model constructed in the previous section. The heat model has the same ventilation boundary conditions as ventilation model described in Section 5.3. The heat source was represented by the Heat Flow Source component in the Flowmaster. It was placed at branch B7 (where a bobcat was located), 5m away from node N5, in a downstream direction. The heat flowed into the fluid network through a Thermal Bridge component at this chosen point. The network model, with a heat source at B7, is shown in Figure 5.7.

As a main firefighting method, a ventilation control strategy was developed for this case. A fire was assumed to have occurred at B7, producing hot gases. Hot air travelled in a downstream direction causing the temperature at the working place (represented by B9) 40m from the fire source to increase. The regulations for underground mines require that the maximum temperature in which human can safely stay should not exceed 347 K (Anon., 2012b). To meet this requirement, the ventilation system needed to be redesigned. A temporary regulator represented by V12 was used to help realize this goal.

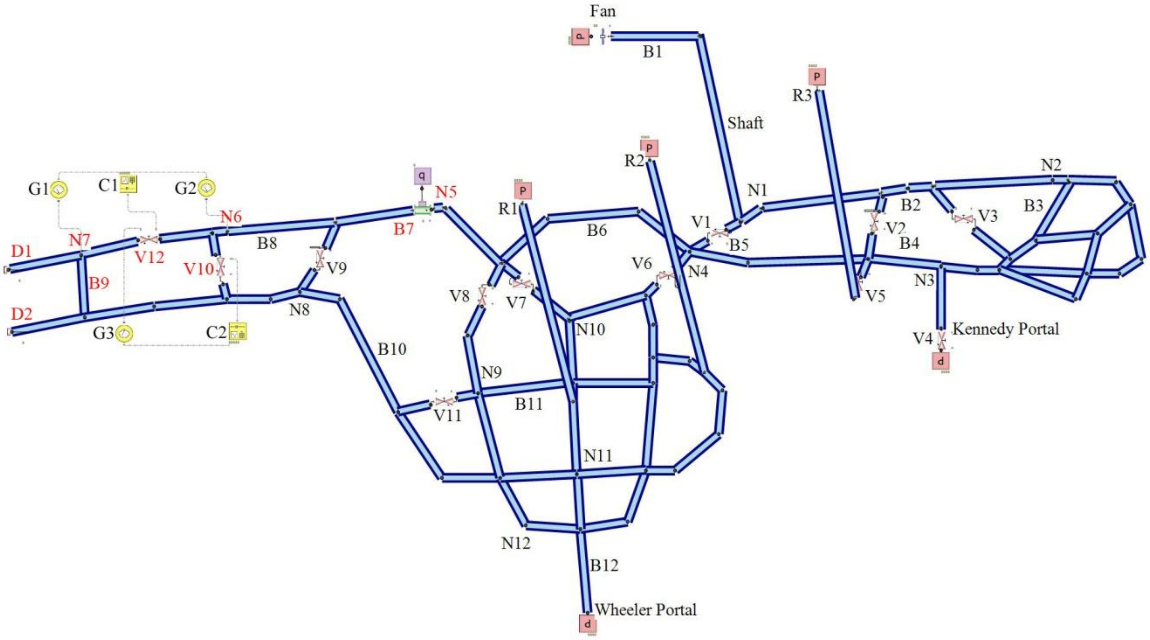

Figure 5.7. The 1D Heat Model in the Main Mine for Case One

In Figure 5.7, some extra components, including a Gauge and Controller template, were used to control the ventilation system in real time. G1 and G2, which were used to monitor the temperatures at N7 and N6, respectively, sent a command to C1, the latter acted accordingly to change V12 status to being either closed or open. G3 was used to monitor the V12 status, sending a command to C2, which controled the status of V10. At any moment, either V10 or V12 is fully open. During the simulation, V10 and V12 changed their status dynamically to ensure that the temperature at B9 was no more than required, say 347 K.

5.4.1.1 Steady heat model. A heat simulation in a steady state was conducted to determine the temperature distribution within the Main Mine. The heat released from the heat source was constant, with an HRR value of 1000 kW. The graphic results for temperature distribution are shown in Figure 5.8. The branches are colored, in accordance with the different temperature values (in K). Only temperature values at reference branches B1 to B12 are displayed.

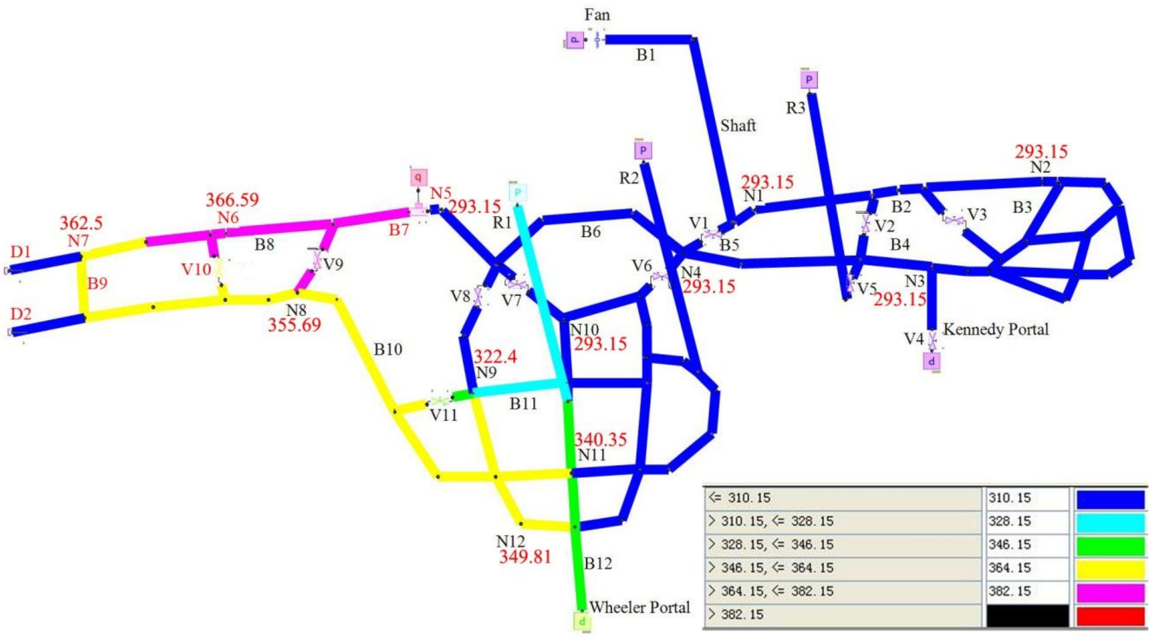

Figure 5.8. Heat Distribution in Steady State in the 1D Model for Case One

Heat was released from the heat source, travelling downstream toward the exit. The closer a location is to the heat source, the higher the temperature it will be at that location. However, an exception was found in the dead-end areas (D1 and D2 in Figure 5.8). The temperature in dead-end did not change very much because no air actually flows into those zones. In an upstream direction, the airways were not affected by the heat source and temperatures remained unchanged, even when the area was next to the heat source. This was because the Flowmaster was not able to calculate the airflow reversal effect within one branch. The air flowing into a branch on one end had to leave the branch on another end. The temperature variation can only be observed in area downstream.

A process to verify that the Flowmaster has the ability to simulate heat was conducted. The same heat model was also calculated using both Ventsim Visual and Ventgraph, both are capable of managing heat. Results of comparisons of temperature at 12 reference nodes, N1 through N12, are plotted in Figure 5.9.

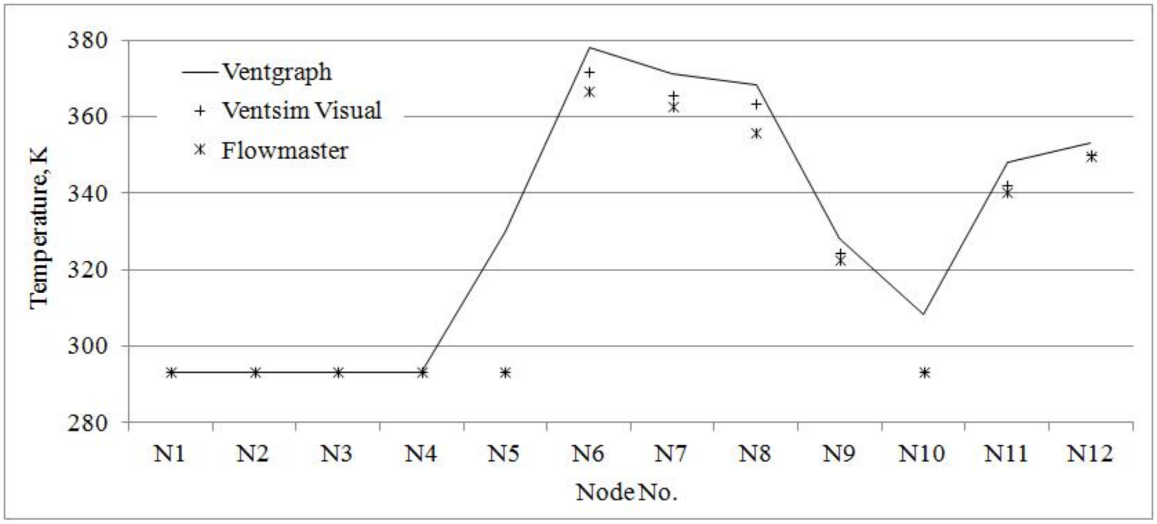

Figure 5.9. Comparison of the 1D Heat Model for Case One

To compare results, temperatures from Ventgraph were used as the reference. At node N5, the temperature results of both Ventsim Visual and Flowmaster did not increase, but there were big differences the temperature calculated by Ventgraph. Because Ventgraph can simulate a reversal effect, the temperatures at some distances upstream increased. Neither the Flowmaster nor the Ventsim Visual can calculate the temperature in areas upstream. The second biggest difference found at N10 was a result from the same reason. For all other 10 nodes, calculated temperature matched very well with each other. The largest deviations were 3.06% and 1.77%, occurred at N6 in the Flowmaster and at N11 in Ventsim Visual, respectively.

5.4.1.2 Transient heat model. The main purpose of this case was to develop a ventilation control strategy in firefighting-planning. To model control activities in real time, a kerosene fire with varied HRR, as shown in Figure 5.10, was applied. As in the steady state simulation, the fire here was represented as a heat source. A transient state simulation was made to calculate the temperature distribution within the Main Mine. The calculation was made in 180 time-steps in which one time step equals to one second.

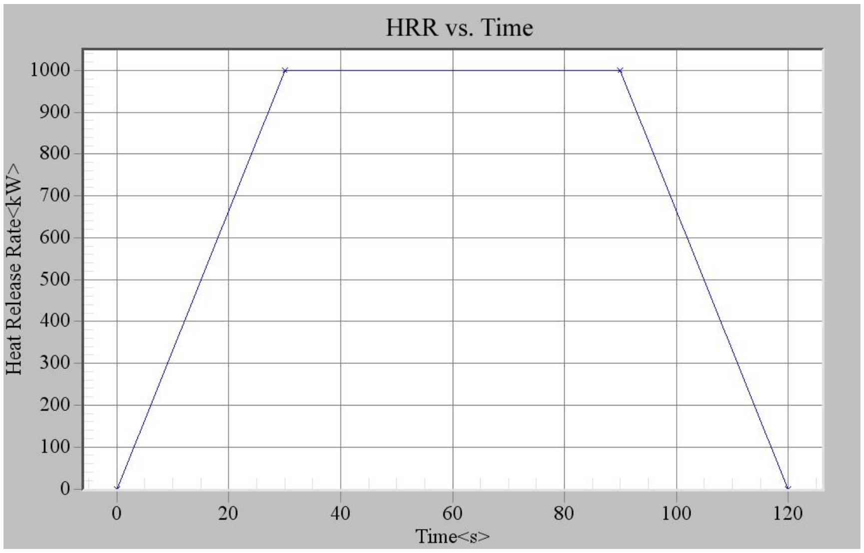

Figure 5.10. Heat Release Rate Curve in the 1D Model for Case One

The heat results at the 30s and 90s are plotted in Figures 5.11 and 5.12, respectively.

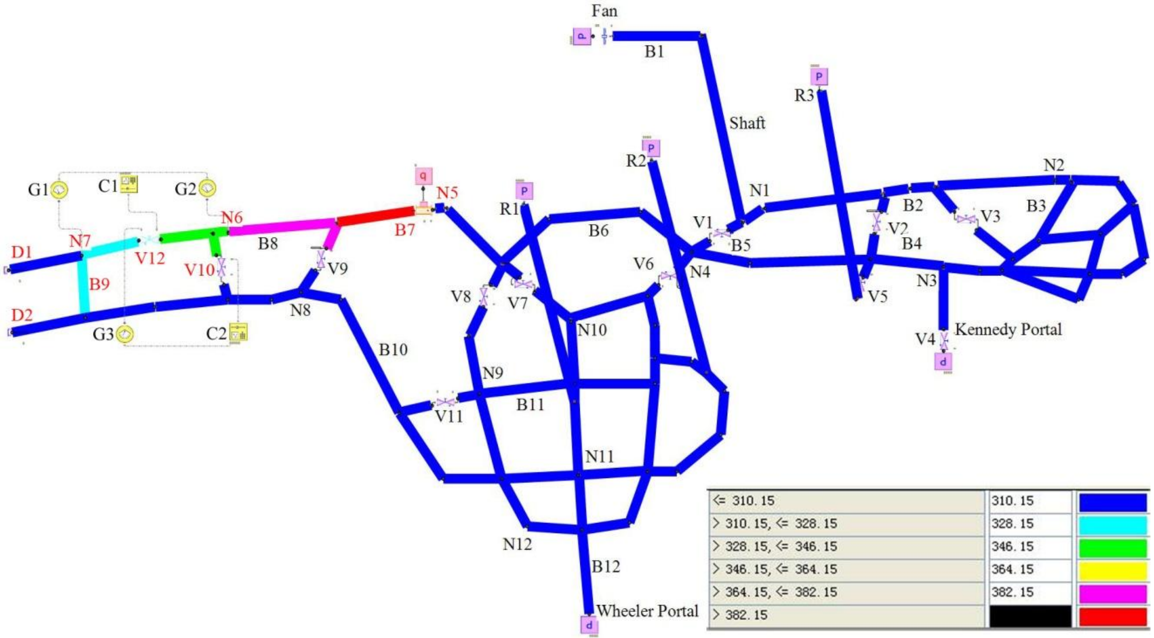

Figure 5.11. Heat Distribution at 30s in the 1D Model for Case One

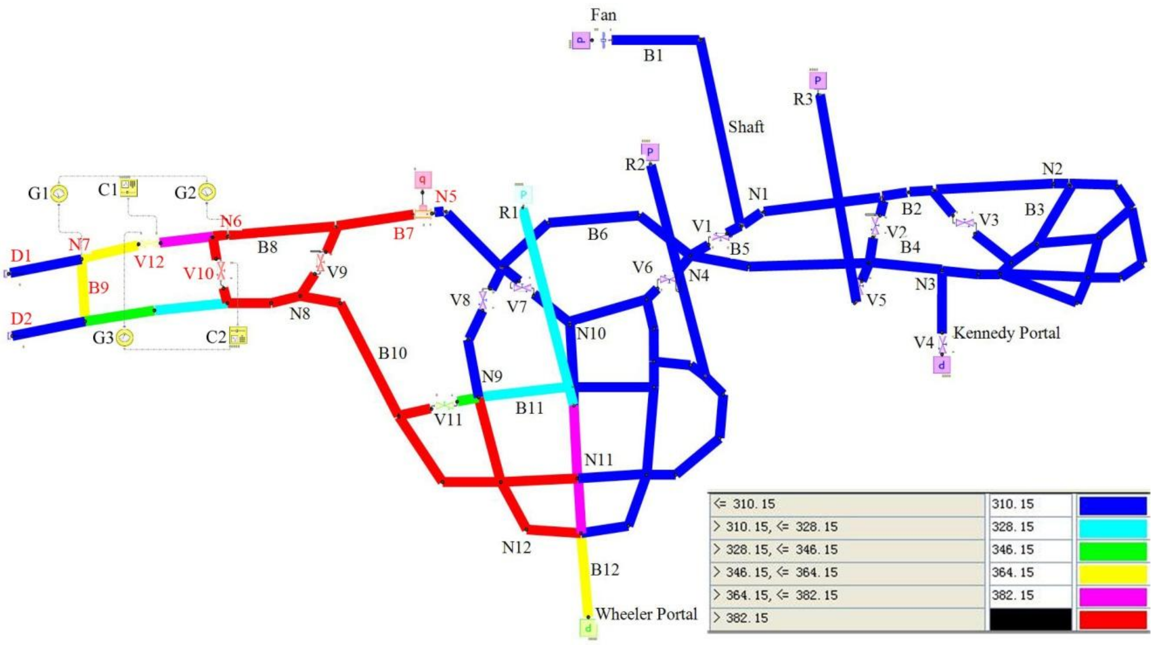

Figure 5.12. Heat Distribution at 90s in the 1D Model for Case One

Branch B9 represents the working place 40m away from the fire source. At 30s, the temperature at B9 was lower than 347 K, meaning that the miners staying in B9 are are safe. Therefore, both V10 (23m from fire) and V12 (33m from fire) retained in their initial status. V12 kept its open ratio at 1 (fully open position). V10 kept its open ratio at 0.05, acting as a stopping to block the air flow. The hot air traveled mainly from N6 to N7 through B9 (Figure 5.11). As time passed, the hot air increased the temperature at B9 until it reached 347 K. This was in 41s.

Temperatures at N7 were monitored by G1, which sent a signal to C1. When C1 received a signal indicating that the temperature at N7 was more than 347 K, it closed V12 to 0 (fully closed position) and blocked the hot air flowing through B9. Simultaneously, V10 was opened to 1 (fully open position) to allow hot air going ghrough. Unblocking V10 helped to prevent hot air from accumulating around the working area. As a result, the temperature at B9 remained at a safe level (Figure 5.12). When the fire was extinguished and the temperature at N6 has decreased, C1 followed the pre-defined command to reinstate the status of V12 to its original position.

Meanwhile, C2 reinstated of V10 to its original position. The regular ventilation condition was reinstated to its original status.

The activities of each Gauge and Controller template were recorded during the simulation. The recorded charts are plotted in Figure 5.13. Chart 1 records the temperature variation with time at N7; Chart 2 and Chart 3 show the regulator status of V12 and V10, respectively; Chart 4 records the temperature variation at N6.

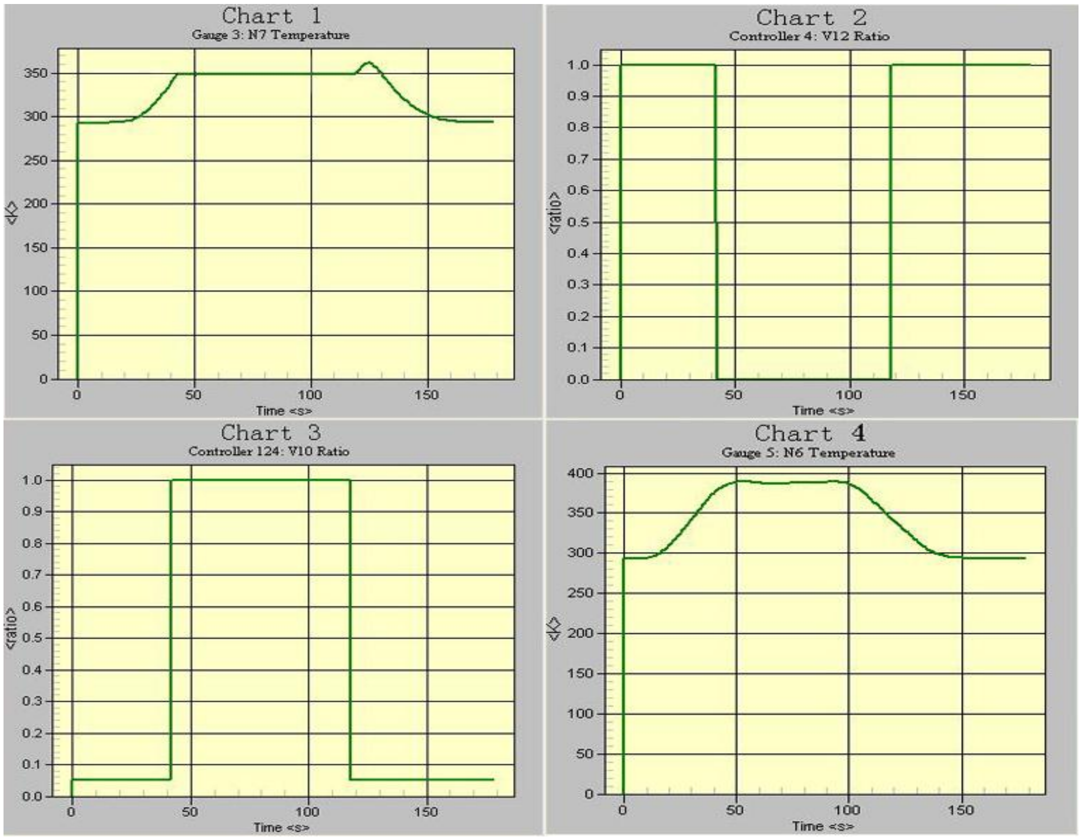

Figure 5.13. History Diagram of Controllers Activity in the 1D Model for Case One

5.4.2. Case Two: 1D Heat Model. Another heat model was developed by adding a heat source to the ventilation network at B2. The heat model has the same ventilation boundary conditions as ventilation model described in Section 5.3. The heat source was placed in the middle of branch B2 and the heat was introduced into the fluid network at B2 through a Thermal Bridge component (Figure 5.14). N1 and N2 represent the interface of the inlet and outlet, respectively, in the multiscale model.

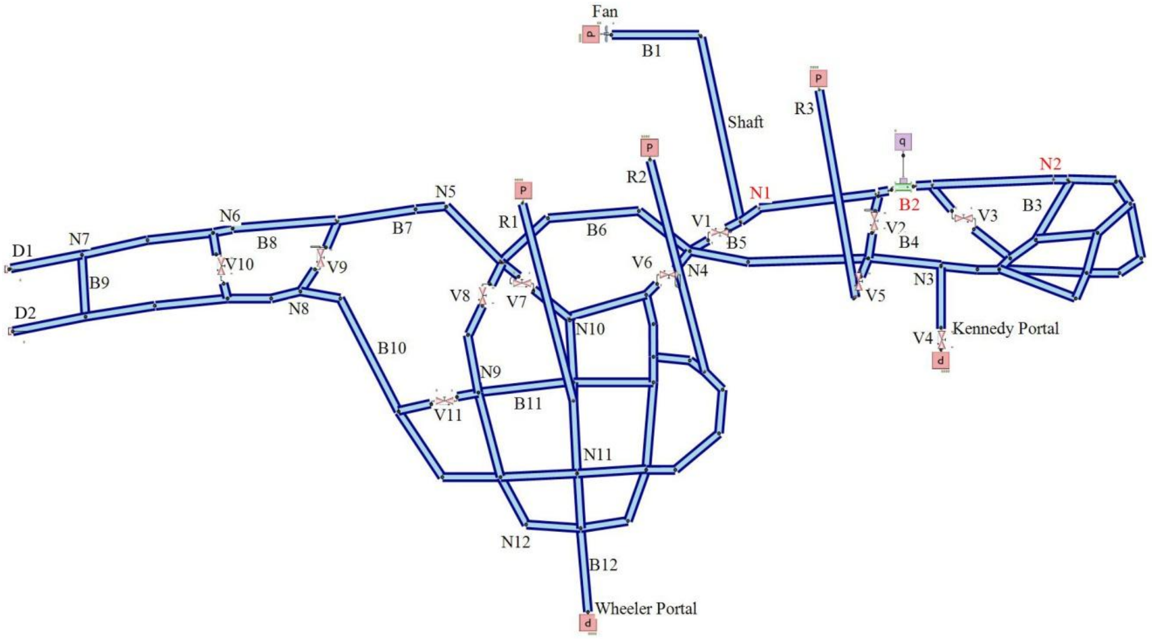

Figure 5.14. The 1D Heat Model in the Main Mine for Case Two

5.4.2.1 Steady heat model. Temperature distribution along throughout the Main Mine in a steady state was calculated. A constant heat of 1000 kW was released from the heat source and the temperature simulation result was shown in Figure 5.15. The branches are colored depending on their different temperature values (in K). Only temperatures at reference branches B1 to B12 are marked with their values.

The heat was released from the heat source (25m from the bottom of the intake airshaft), travelling downstream underground. The closer a location is to the heat source, the higher the temperature it will be at that location. Since the Flowmaster does not have the capability to simulate hot air reversal, temperature variations were not found at airways in the upstream direction or at area where no air move.

A verification process was used again in this case to prove that the Flowmaster has the ability to simulate heat distribution. The same heat distribution was also modeled using both Ventsim Visual and Ventgraph. A comparison of temperatures at 12 reference nodes, N1 through N12, is plotted in Figure 5.16.

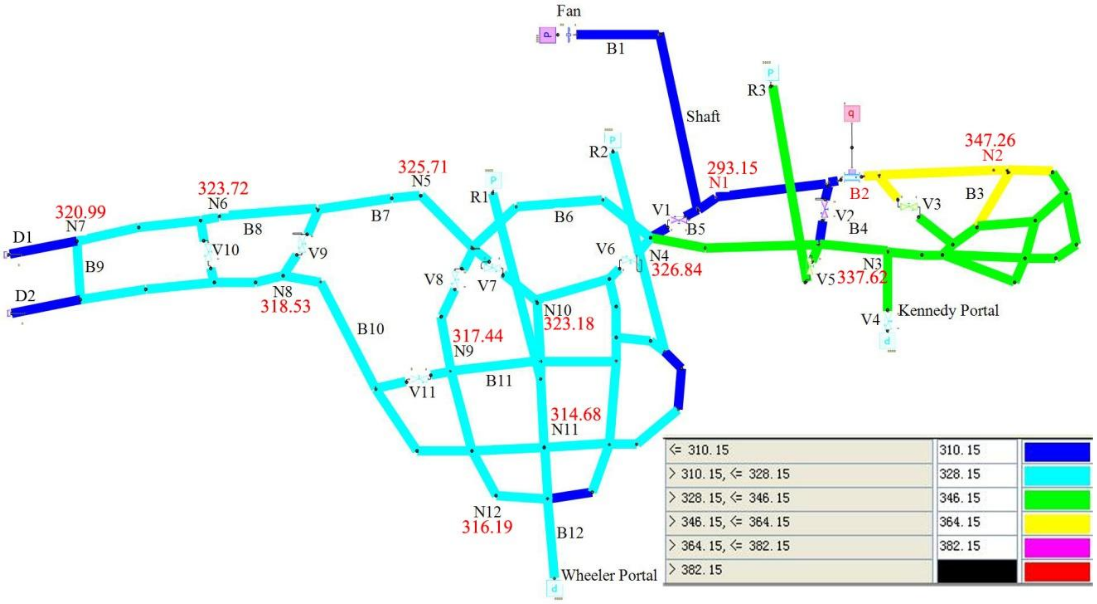

Figure 5.15. Heat Distribution in Steady State in the 1D Model for Case Two

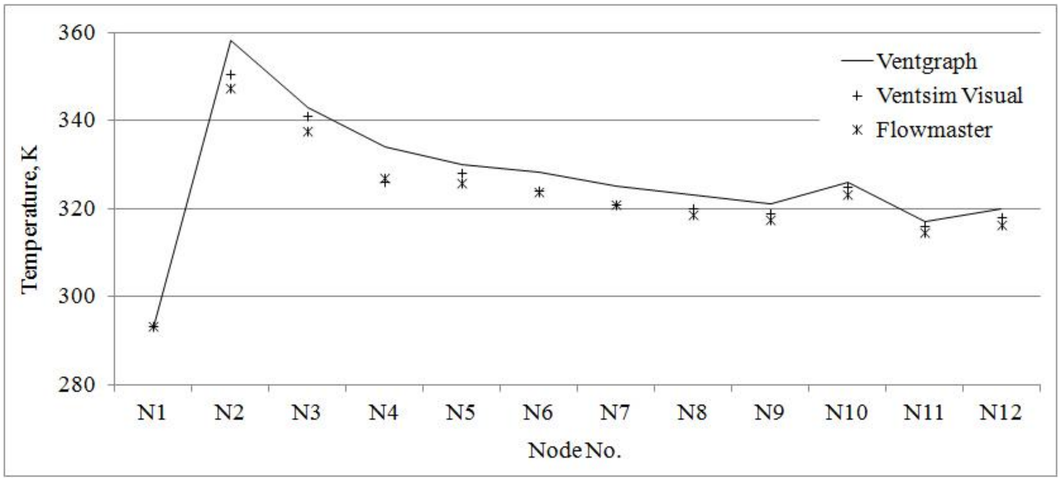

Figure 5.16. Verification of the 1D Heat Model for Case Two

As shown in Figure 5.16, calculated temperatures matched very well with three packages at all 12 nodes, the. For the Flowmaster, the largest deviation was 3.00% at N2. For VentsimVisual, the largest variation was 2.39% at N4.

5.4.2.2 Transient heat model. The main purpose of Case Two was to prepare a 1D model for a multiscale model to study the air reversal effect. The back layering cannot be simulated in a 1D network model. It can, however, provide a 3D model with the boundary conditions for multiscale model simulation. The calculation results, using the multiscale model, were more accurate than when using the 3D model alone. In the 3D model, the length of the back layering was significantly influenced by air velocities at the inlet connected to the 1D model. To simulate the effects of different velocities, varied pressure values were applied to the inlet of branch B1, resulting varied velocities at N1, which represented the inlet interface to the multiscale model. The velocity curve, with time, is shown in Figure 5.17.

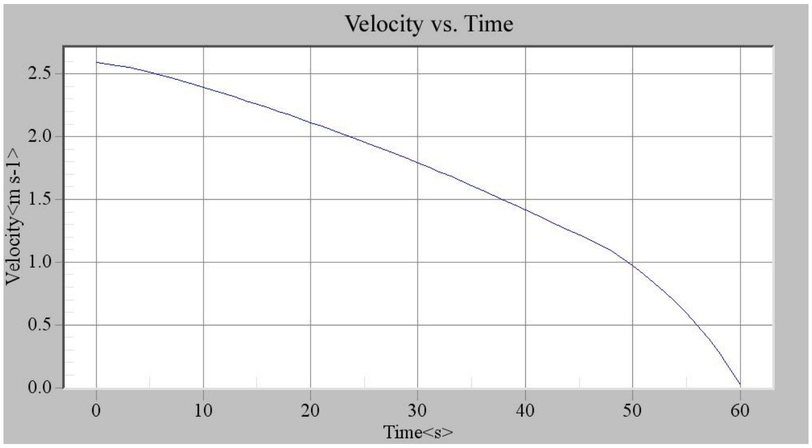

Figure 5.17. Velocity Curve at N1 in the 1D Model for Case Two

The total calculation process lasted 60s. The simulation results at 15s and 60s are plotted in Figure 5.18 and Figure 5.19, respectively.

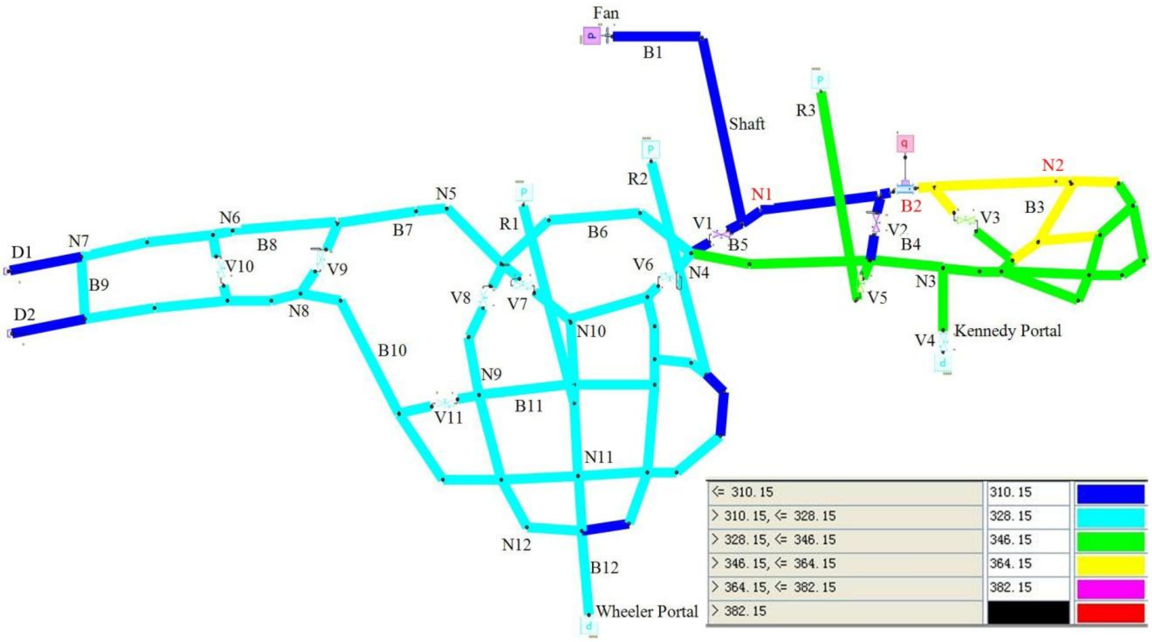

Figure 5.18. Heat Distribution at 15s in the 1D Model for Case Two

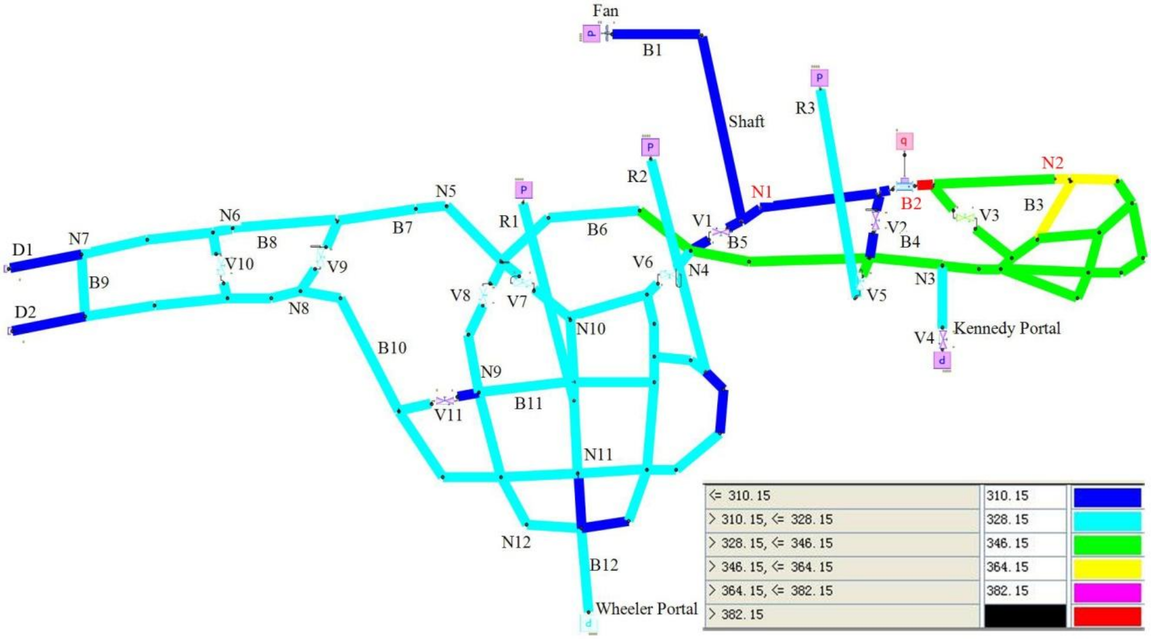

Figure 5.19. Heat Distribution at 60s in the 1D Model for Case Two

Figure 5.18 shows the heat distribution along airways underground at 10s. The heat was released from the heat source and traveled downstream along airways underground. This is expected because the velocity at N1 was strong enough to force the hot air to flow along the airflow direction. As time passed, the velocity continued to decrease, approaching to zero. Temperatures in upstream airways remained unchanged. No sign of back layering was found even at the 60s (Figure 5.19) when air velocity was nearly zero. This is not true in reality. The fact is, as the velocity was reduced to the critical velocity, the back layering started to occur. This result suggests that the Flowmaster alone could not be used to study the airflow reversal effect.

6. THREE-DIMENSIONAL MODEL OF THE MAIN MINE FIRE

6.1. INTRODUCTION

Area near the fire zone presented high temperature and velocity gradients within the mine domain. To obtain accurate information about fluid properties, a 3D model had to be used to solve the fluid field equations near the fire zone. In general, a 3D CFD solver for fire simulation provided detailed flow data, including temperature, velocity magnitude, back layering distance, and so forth. These results helped explain the fire behavior under different conditions, and to provide useful information for firefighting and evacuation process in case of a mine fire.

As a main part of the multiscale model, the 3D model must be accurate by itself. The results from the 3D model significantly determined the final result of the multiscale model. Analysis of meshing quality was a necessary process for ensuring that the results from the 3D model were accurate enough. Additionally, the boundary location of the 3D model played a critical role in obtaining satisfactory results by the multiscale model. Before the coupling process, analysis of the 3D boundary locations was also performed.

Corresponding to the two cases described in Section 5, two 3D models were needed to generate multiscale models, with the first 3D model simulating a steady state condition while the second 3D model a transient state. Both of these were prepared to couple with corresponding 1D model to construct multiscale models described in the next section.

6.2. CASE ONE: 3D FIRE SIMULATION IN STEADY STATE

The 3D CFD technique was used to simulate fire behavior in a steady state, assuming a kerosene fire at branch B7 in the Main Mine (Figure 5.3). The fire was considered a heat source with a constant HRR value of 1MW. Results of the network model in Section 5 provided the 3D model with proper boundary conditions. In this case, the 3D model was designed and prepared to build the multiscale model.

6.2.1. Geometric Model and Boundary Conditions. The fire source was located on the floor of branch B7 as shown in Figure 5.3. To simplify the numerical model, the airway was assumed to have a uniform rectangular cross-section at 2.6m in height and 2.4m in width. A 3D schematic of the calculated domain is presented in Figure 6.1.

The model included three boundaries, Inlet_Air, Inlet_Fire, and Outlet. A blowing fan was located outside of the 3D model blowing air into the model through the Inlet_Air with a value of 1.00634 m/s. The air, together with hot gases released from the Inlet_Fire, travelled out of the airway through the Outlet. Two sections were selected for the purpose of presenting results. Section One crossed the fire source center in a transverse direction, while Section Two along the longitudinal direction.

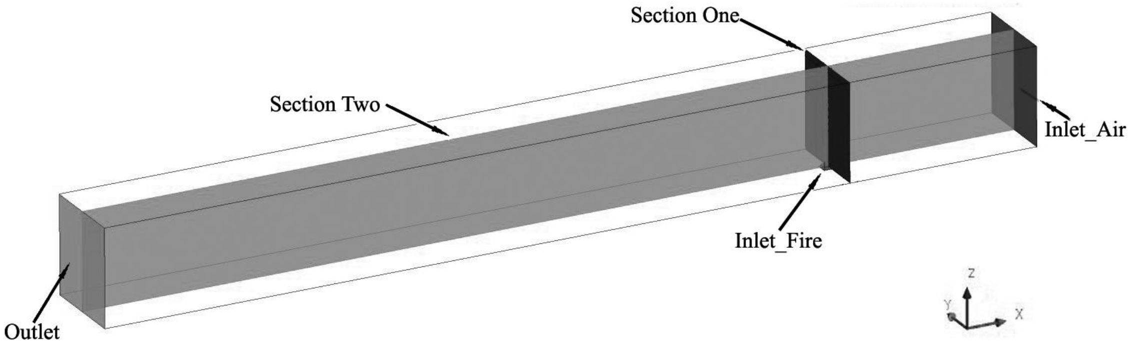

Figure 6.1. Geometric 3D Model in the Main Mine for Case One

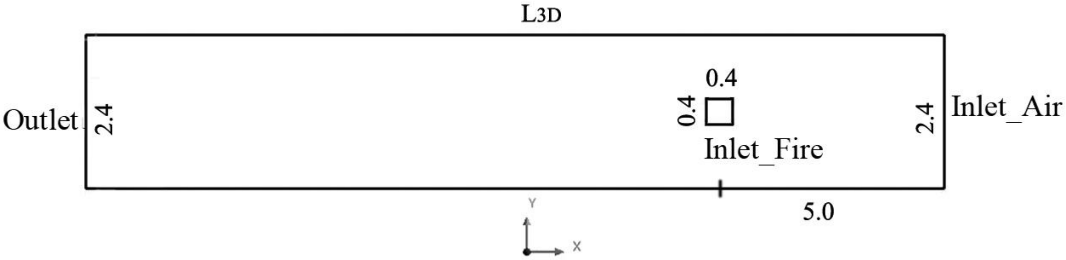

Figure 6.2. Top View of the Geometric Model in the Main Mine for Case One

A 2D schematic top view of the geometric model is shown in Figure 6.2. A fire source, which was placed on the floor in the middle of the airway, was represented by a 0.4m × 0.4m square that was 5m away from the Inlet_Air. The location of the Outlet was determined by L_{3D} which is the length of the model that needed to be determined by analyzing the boundary location. For the purpose of coupling, a uniform flow gradient at the Outlet was required.

6.2.2. Assessment of Mesh Requirement. The computational domain was discretized using hexahedral meshes with refinements close to the fire source. Various 3D models of the entire model were run to assess the mesh requirements. Four different meshes were generated and the resulting solutions compared. The mesh density per meter of airway length ranged from 800 cells/m up to 9200 cells/m. Four examples of the mesh at Section One are shown in Figure 6.3. The wall boundary was meshed with finer cells to meet the standard wall function requirements.

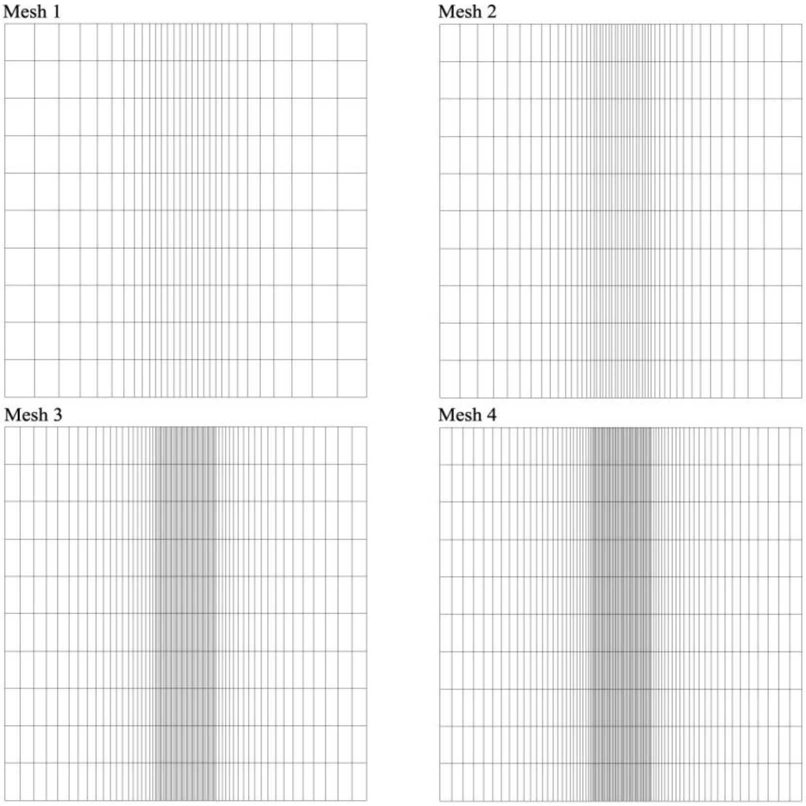

Figure 6.3. Comparison of Four Meshes at Section One in the 3D Model for Case One

Using Mesh 4 (9,200 cells/m) as a reference, the dependence of the computed average velocity as a function of mesh density is shown in Table 6.1 which shows that the solution converges as the mesh becomes finer. For instance, the X-velocity (velocity in longitudinal direction) and temperature computations performed with mesh 3 deviated by 0.19% and 0.36%, respectively, from the prediction performed with the finest mesh, which these increased to 1.15% and 0.64%, respectively, when the number of cells per meter decreased from 6400 to 2400.

Table 6.1. Grid Independence Study in the 3D Model for Case One

	Mesh Density, cells/m	Average Air X-velocity		Average Temperature	
		Value, m/s	Deviation, %	Value, K	Deviation, %
Mesh 1	800	1.1894	2.72	396.83	1.11
Mesh 2	2400	1.1712	1.15	394.96	0.64
Mesh 3	6400	1.1601	0.19	393.86	0.36
Mesh 4	9200	1.1579	--	392.46	--

A comparison of the predicted X-velocity fields and temperatures at Section One is shown in Figure 6.4 and Figure 6.5, respectively. Results show that larger deviations existed in the coarse meshes 1 and 2, while convergence was obtained for the finer 3 and 4 meshes. Based on the results, grid independence was considered reached in mesh 3 and, therefore, all of the following simulations were conducted using this grid. The average skewness for cells in mesh 3 was 1.0×10^{-3}, considered to be at an acceptable level (Anon., 2009a).

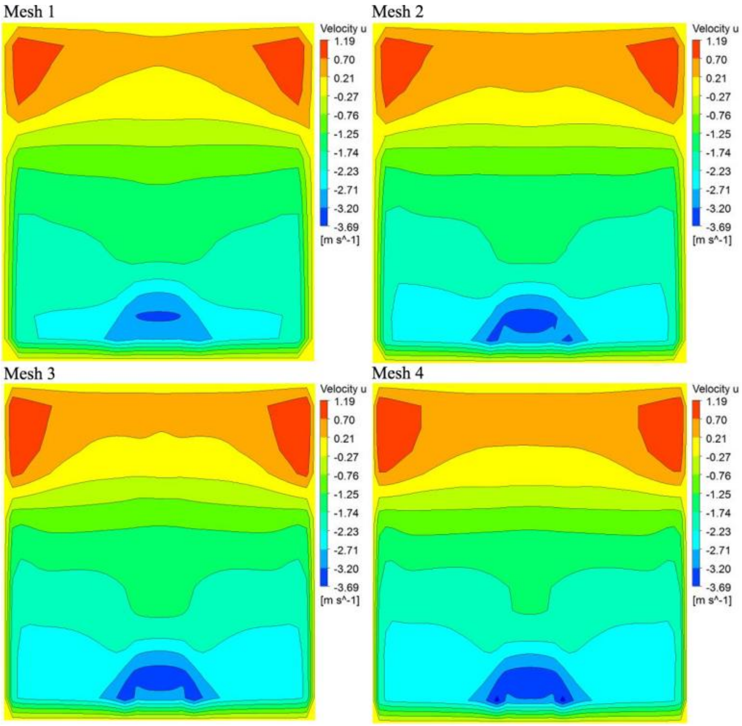

Figure 6.4. Comparison of the X-velocity for Mesh 1 to 4 at Section One in the 3D Model for Case One

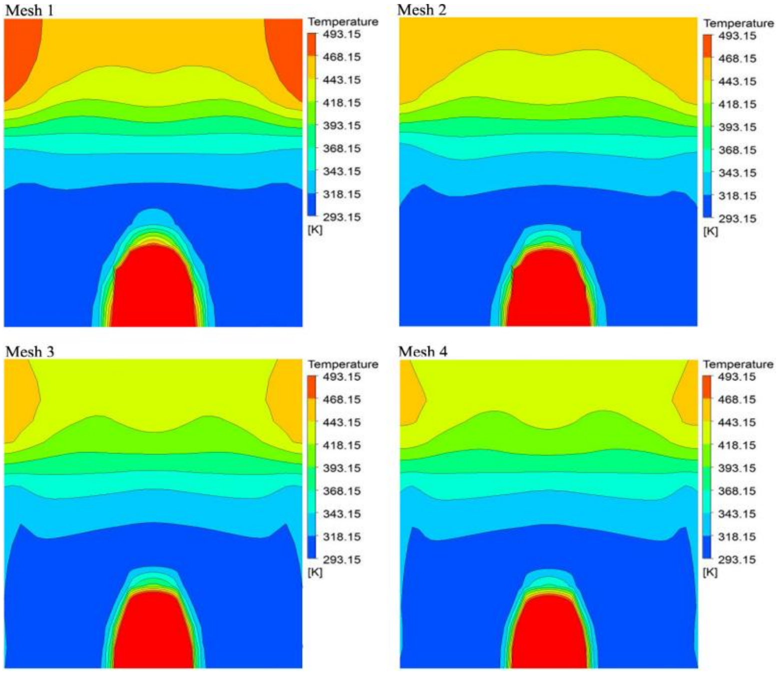

Figure 6.5. Comparison of the Temperature for Mesh 1 to 4 at Section One in the 3D Model for Case One

6.2.3. Effect of the 1D-3D Interface Location. As mentioned before, a critical technique in building a multiscale model is the positioning of 1D-3D interfaces. Indeed, they must be located in a region where the flow is fully developed and is characterized by uniform velocity gradients. Thus, the size of the 3D sub-domain (L_{3D}) plays a crucial role in the accuracy of a global solution. The downstream interface boundary between 1D and 3D domain must be located where the flow evolves in order to be fully developed. Otherwise, the 3D model cannot be used to build a multiscale model because the subsequent coupling would result in errors.

In order to identify the boundary independence limits for scenarios including fire-induced flows, several runs of the 3D model were made for a range of domain sizes. The position of the upstream interface between 1D and 3D domains represented by Inlet_Air was not as critical as the one downstream. Since in the simulated case, the direction of airflow velocity remains unchanged thus the upstream boundary can be moved significantly closer to the fire source. In this case, the Inlet_Air was only 5m from the center of the fire source which cuts back computing time significantly.

The main task was to determine the position of the downstream interface between the 1D and the 3D domains, represented by the Outlet position. In each run, the Outlet was placed progressively farther downstream from the fire, extending the 3D domain length L_{3D} longitudinally (Figure 6.2) and, consequently, reducing the 1D domain length by the same amount.

The dependence of both average temperature and average X-velocity at the outlet boundary of the 3D domain was determined. These values had additional importance as they represented the input of the 1D model to the far field region located downstream from the fire. A total of nine scenarios were run with varied L_{3D} length from 10m to 60m. The results from the model with L_{3D} that equaled to 60m were considered as reference values for each run.

The predicted average temperature and X-velocity, together with corresponding comparison results, are plotted in Figure 6.6 and Figure 6.7, respectively.

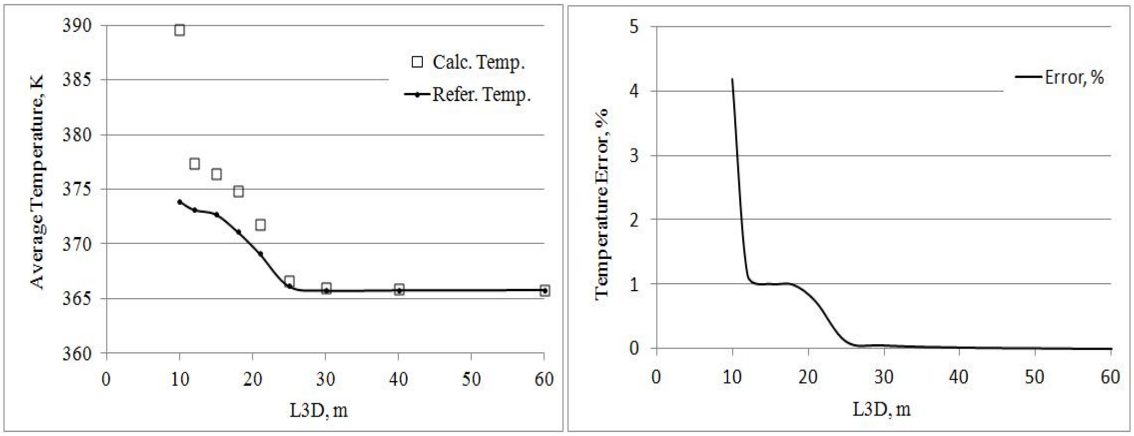

Figure 6.6. Effect of L_{3D} Length on the Average Temperature at Outlet in the 3D Model for Case One

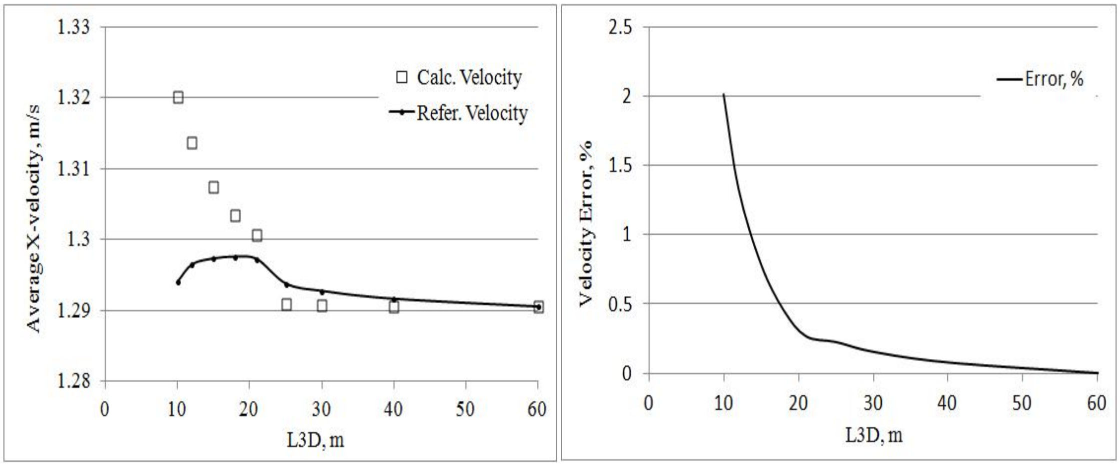

Figure 6.7. Effect of L_{3D} Length on the Average X-velocity at Outlet in the 3D Model for Case One

With L_{3D} as the length of the near fire field, the error caused by an inappropriate interface location can be calculated as

$$Error,\% = 100 \times \frac{\left|V_{calc.} - V_{refer.}\right|}{V_{refer.}} \tag{6.1}$$

where $V_{calc.}$ is the temperature (in K) or X-velocity value (in m/s) at the Outlet calculated for a given value of L_{3D}, and $V_{refer.}$ is the temperature or X-velocity value at the Outlet calculated using a reference scenario.

It was evident that, for 3D domain lengths between 10m and 25m, the deviations in the average temperature and X-velocity from the reference values decreased with an increase in L_{3D}. For 3D domain lengths between 10m and 25m, the deviations in the average temperature from the reference values ranged between 4.19% and 0.11%, respectively; the deviations in the average X-velocity from the reference values ranged between 2.01% and 0.23%, respectively.

For both temperature and X-velocity, the calculated and predicted value matched well when the 3D domain length exceeded 25m with very little variations. For cases where the L_{3D} is at 25m and 60m, the accuracy had only improved by 0.11% for temperature prediction and 0.23% for X-velocity. Therefore, the following calculations were made with the length in the 3D model set at 25m. The downstream 1D-3D interface was located away from the fire source at a distance of approximately ~8 times the airway hydraulic diameter.

Figure 6.8 and Figure 6.9 present the temperature and X-velocity results, respectively at the outlet boundary. It is clear that, for a range of 3D model lengths between 10m and 25m, average temperature and X-velocity fields showed large deviations from the referenced solutions. When the model was larger than 25m, however, the flow field deviation chould be significantly reduced. The pattern of fluid for 3D model lengths of more than 25m tended to have less deviation.

The solution obtained for a 10m long domain had a 4.18% error. The results became boundary independent and provided less than 0.11% error for domain length larger than 25m. Thus, the 3D solution in the vicinity of the fire plume became independent from the boundary location, when the distance between the fire source and the outlet boundary was more than 8 times the hydraulic diameter.

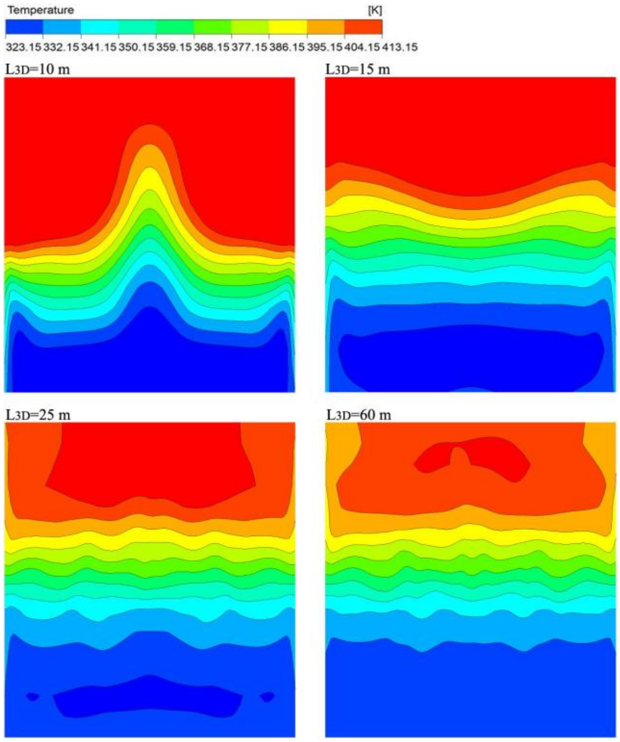

Figure 6.8. Temperature Prediction at Outlet in 3D Model with Different L_{3D} for Case One

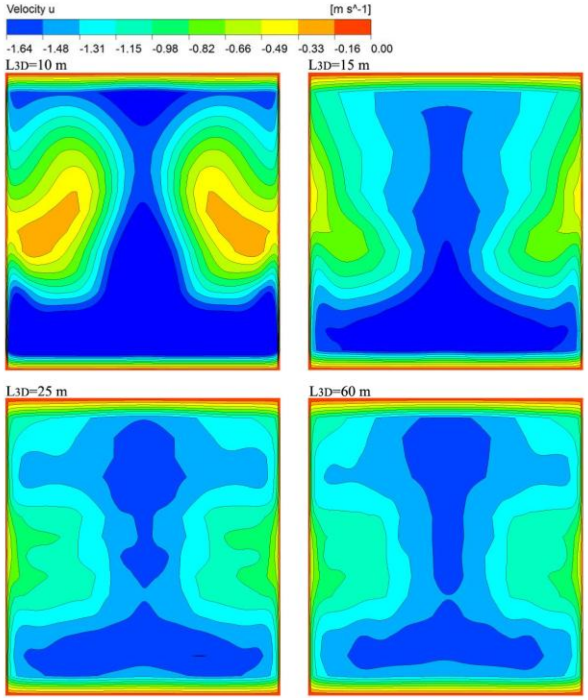

Figure 6.9. X-velocity Prediction at Outlet in 3D Model with Different L_{3D} for Case One

6.2.4. Results. Figure 6.10 presents X-velocity distribution in a steady state for both Section Two in (b) and its outlet (a). In Figure 6.10, the positive direction of X (left to right) was in the oppositive direction of the airflow. A negative velocity value meant that the hot air was flowing along the airflow direction, while a positive velocity value meant that the hot air was flowing against the airflow direction (which predicted the occurrence of back layering).

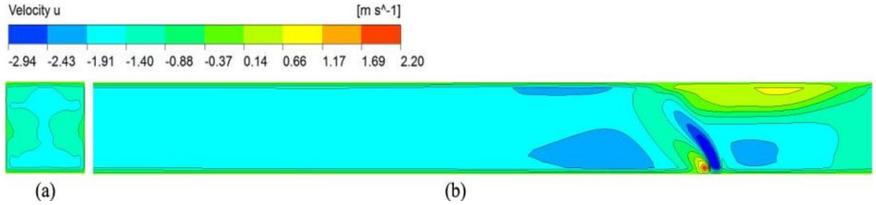

Figure 6.10. X-velocity Prediction at Outlet (a) and Section Two (b) in the 3D Model for Case One

Simulation shows that back layering occurred upstream of the fire zone as the inlet airflow velocity was insufficient to keep a back layering from forming. When the hot air flowed against the airflow to the Inlet_Air, it accumulated along the roof in the upstream direction. Another recirculation area found at the area close to the fire zone downstream, was the result of both the throttling and buoyancy effects. The throttling effect decreased the pressure in the area close to the hot flow downstream, and the buoyancy effect entrained the cold air near those regions and raised it to the roof. This reversed the airflow and resulted in airflow recirculation. Velocity contour at the Outlet developed very well and the average X-velocity at the outlet boundary was 1.2908 m/s.

Figure 6.11 presents temperature distribution in a steady state, and shows the temperature countour at Section Two in (b) and its Outlet (a).

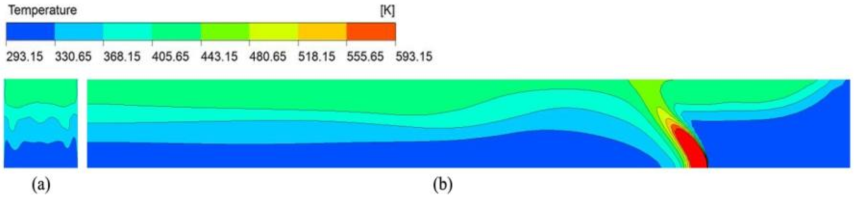

Figure 6.11. Temperature Prediction at Outlet (a) and Section Two (b) in the 3D Model for Case One (Air Flows from Right to Left)

Figure 6.11 also clearly displays the phenomena of a back layering. The hot air rises to the roof because of the buoyancy effect, and the high temperature flow was tilted because of the airflow influence. Hot air flowed against the direction of airflow, accumulating underneath the roof in both upstream and downstream directions. The temperature contour developed very well at the outlet boundary at an average temperature of 366.59 K.

Both the Inlet_Air and the Outlet were connected to the 1D model in the multiscale model simulation. The temperature and mass flow rates were transferred between the 1D and the 3D model at the interfaces. The temperature and mass flow rate values significantly influenced the multiscale model results, especially at the Outlet. The high temperature was distributed in the same direction as the airflow. In Case One, the fire occurred near the working face (B9 in Figure 5.8). Simulation shows that average temperature at the Outlet (366.59 K) exceeded the maximum allowed temperature of 347 K which would put humans at risk. Thus, a method to control ventilation effectively must be taken to eradicate the situation. Detailed information on controlling ventilation in the multiscale model simulation is discussed later.

6.3. CASE TWO: 3D FIRE SIMULATION IN TRANSIENT STATE

The 3D technique was used to simulate fire behavior in a transient state simulation. A kerosene fire was started at branch B2 in the Main Mine (Figure 5.15). The fire was considered as the heat source with a constant HRR value at 1000 kW. The results of the network model in Section 5 provided the 3D model with proper boundary conditions. In this case, the calculated 3D model was designed to build the multiscale model.

6.3.1. Geometric Model and Boundary Conditions. The fire source was located on the floor at branch B2. To simplify the numerical model, the airway had a uniform rectangular cross-section of 2.6m (height) by 2.4m (width). A 3D schematic of the calculated domain is presented in Figure 6.12.

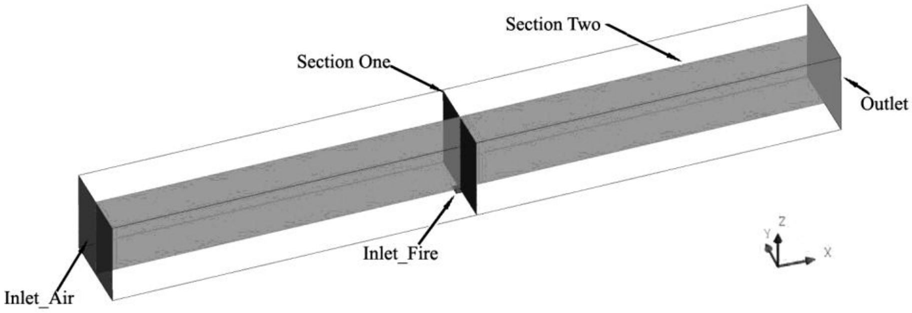

Figure 6.12. Geometric 3D Model in the Main Mine for Case Two

The model included three boundaries, Inlet_Air, Inlet_Fire, and Outlet. A blowing fan was located outside of the 3D model. The fan blew air into the model through the Inlet_Air along Section Two with a linearly varied velocity value with time (from 2.9602 m/s to zero within 60s). The air, together with hot gases released from the Inlet_Fire, travelled out of model through the Outlet. Two sections were generated for the purpose of displaying results. Section One crossed the fire source center in a transverse direction, while Section Two was in the longitudinal direction.

A 2D schematic top view of the geometric model is shown in Figure 6.13. The fire source placed on the floor in the middle of the airway was represented by a 0.4m × 0.4m square half way between Inlet_Air and Outlet. L_{3D} represented the whole length of the entire model that needed to be determined by analyzing the boundary location. For the purpose of coupling, a uniform flow gradient at the Outlet is required.

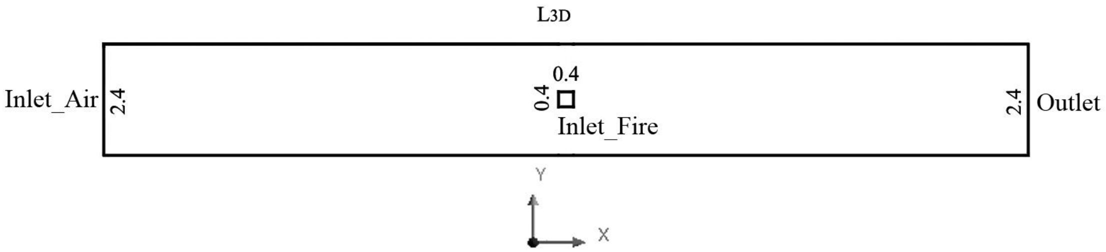

Figure 6.13. Top View of the Geometric Model in the Main Mine for Case Two

6.3.2. Assessment of Mesh Requirement. The computational domain was discretized using quasi structured meshes with refinements close to the fire source. Various 3D models of the entire domain were run to assess the mesh requirements. Four different meshes were generated and the results compared. The mesh density per meter of airway length ranged from 820 cells/m to 9400 cells/m. Four examples of the mesh cross-section along Section Two are presented in Figure 6.14.

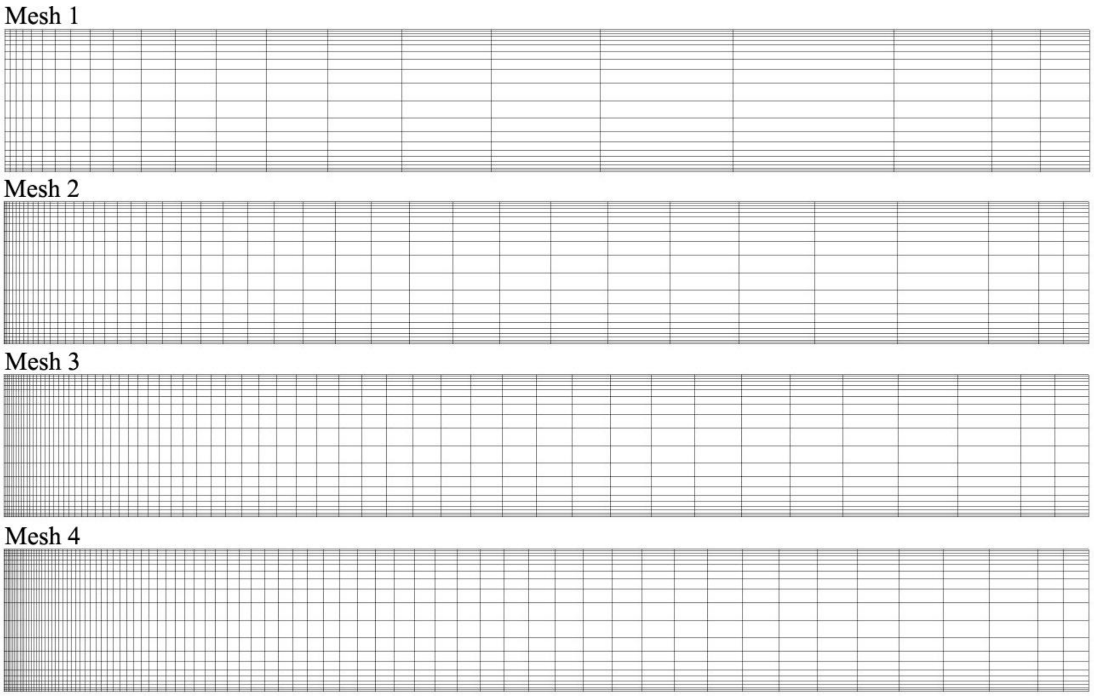

Figure 6.14. Comparison of Four Meshes at Section Two in the 3D Model for Case Two

The dependence of the computed average velocity as a function of the mesh density is presented in Table 6.2. It shows that the solution converges as the mesh becomes finer. For instance, using Mesh 4 as a reference, the X-velocity and temperature computations performed with Mesh 3 deviated by 0.55% and 0.34%, respectively, from the prediction performed with the finest mesh. A comparison of the predicted X-velocity fields and temperature at Section Two is presented in Figure 6.15 and Figure 6.16, respectively.

Table 6.2. Grid Independence Study in the 3D Model for Case Two

	Mesh Density, cells/m	Average Air X-velocity		Average Temperature	
		Value, m/s	Deviation, %	Value, K	Deviation, %
Mesh 1	820	2.8836	9.18	383.98	5.26
Mesh 2	3050	2.7466	3.99	376.37	3.18
Mesh 3	6360	2.6557	0.55	366.03	0.34
Mesh 4	9400	2.6411	--	364.78	--

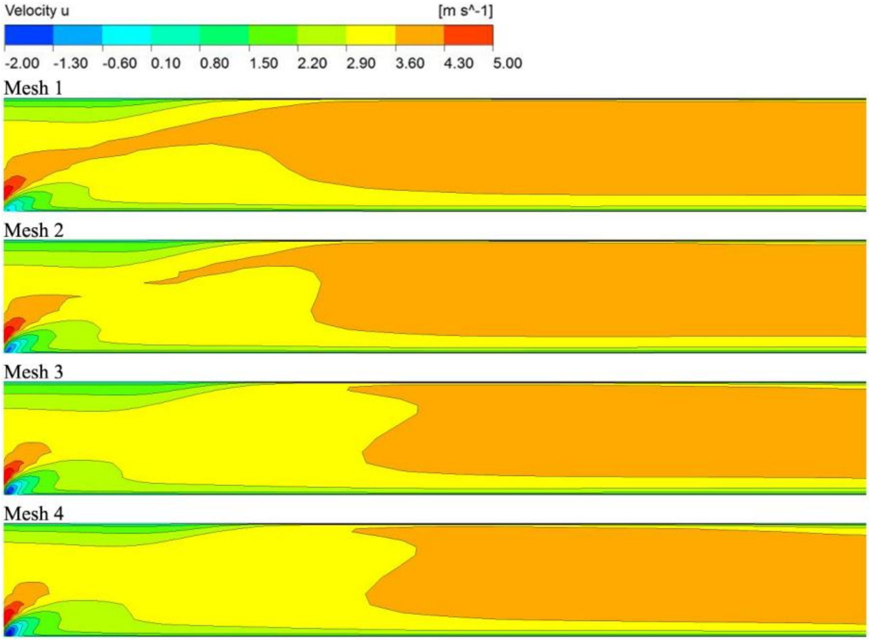

Figure 6.15. Comparison of X-velocity for Mesh 1 to 4 at Section Two in the 3D Model for Case Two

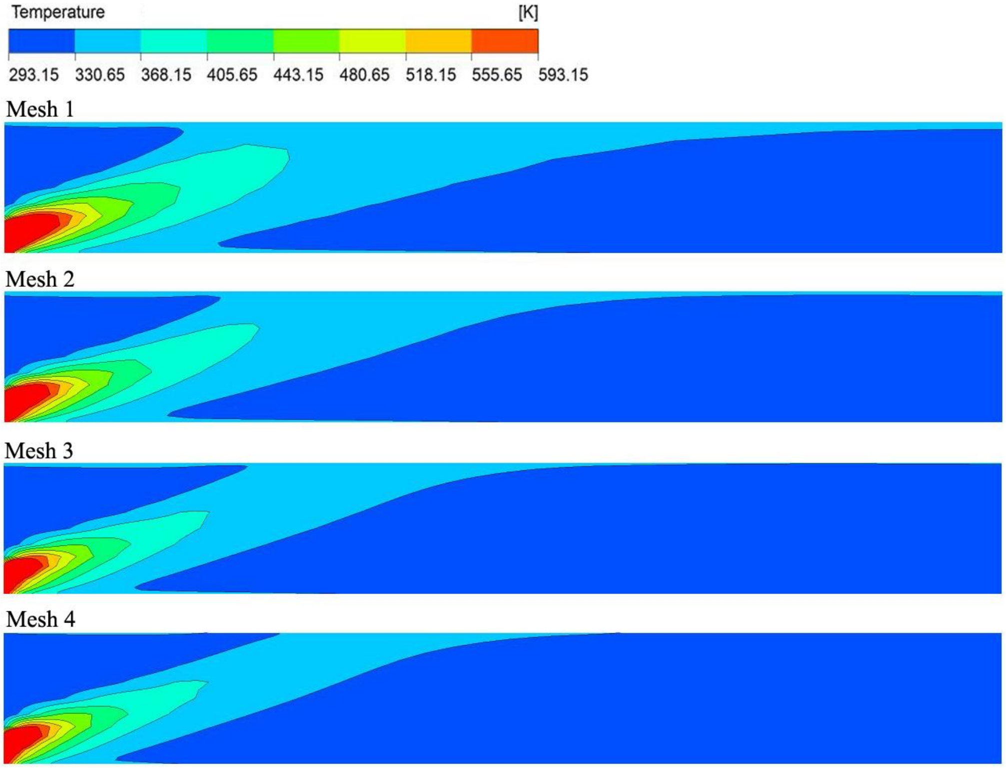

Figure 6.16. Comparison of Temperature for Mesh 1 to 4 at Section Two in the 3D Model for Case Two

As expected from the previous results, the computed solutions showed larger deviations for the coarse meshes 1 and 2, while convergence was obtained for the finer Mesh 3 and 4. Based on the comparison, grid independence was considered reached in mesh 3 and, therefore, all of the following simulations were conducted using this grid. The average skewness for cells in mesh 3 was 6.4×10^{-3}, considered acceptable.

6.3.3. Effect of the 1D-3D Interface Location. As already discussed in previous section, a critical point in the multiscale representation is the positioning of the 1D-3D interfaces. In order to identify the boundary independence limits for cases including fire-induced flows, several runs for the 3D model were conducted for a range of domain sizes. In Case Two, the interface positions between 1D and 3D domains are critical in both directions (upstream and downstream). The length of the back layering in the upstream direction needed to be studied under different scenarios.

In each run, the interface was placed progressively further away from the fire (increasing L_{3D}) in both directions along the longitudinal direction in the 3D domain (Figure 6.13). Consequently, the length in the 1D domain was reduced by the same amount. The fire source was located half way between the upstream and downstream interface.

An analysis was made to clarify the dependence of the average bulk flow quantities in temperature and velocity at both Inlet_Air and Outlet in the 3D domain. These values have an additional importance as they are the input of the 1D model. Since the calculated domain is symmetric in geometry, the analysis at the inlet boundary of the 3D domain is ignored. If the dependence of the flow quantities at the outlet boundary met the requirement, the same is also true for the inlet boundary.

Figure 6.17 and Figure 6.18 represent the average temperatures and X-velocity along the longitudinal direction in the 3D domain, increasing from 10m to 100m, respectively. A total of nine different runs were conducted to identify this distance. Average temperature at the Outlet was recorded, and a 3D model with L_{3D} equaling to 100m was computed and represented the reference values in each run. The errors induced by an inappropriate location of the interfaces were calculated using Equation 6.1.

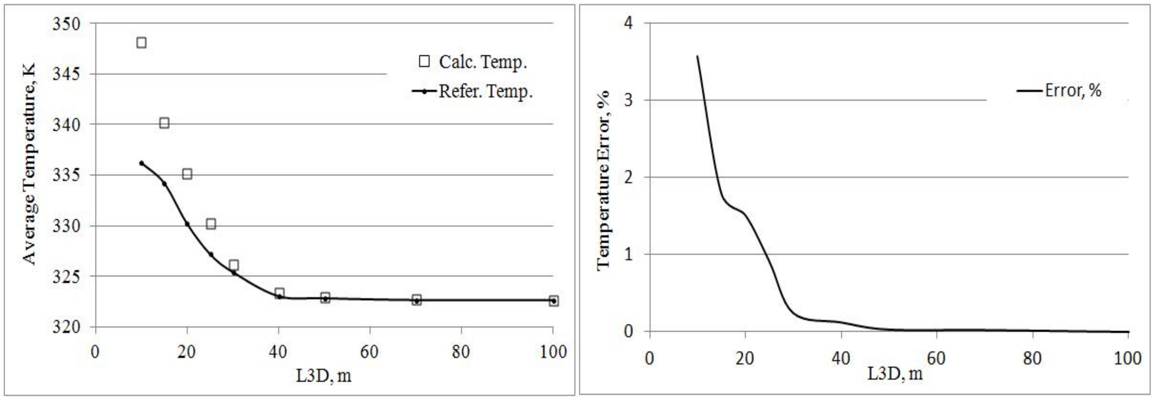

Figure 6.17. Effect of the L_{3D} on the Average Temperature at Outlet in the 3D Model for Case Two

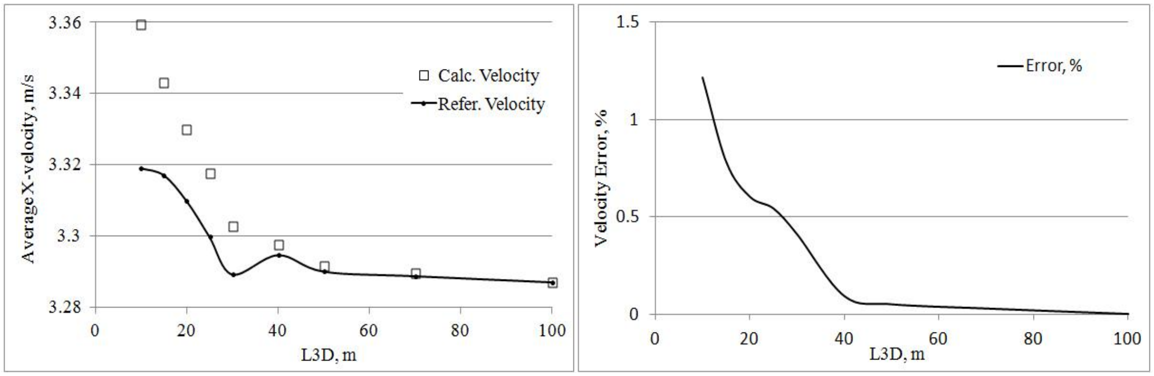

Figure 6.18. Effect of the L_{3D} on the Average X-velocity at Outlet in the 3D Model for Case Two

Results show that for 3D domain lengths between 10m and 40m, the deviations in the temperatures ranged between 3.57% and 0.12%, and the deviations in the X-velocities ranged between 1.22% and 0.09%. No appreciable variations were observed where the 3D domain length exceeded 40m. The accuracy in temperature and X-velocity improved only slightly (from 0.12% and 0.09%, respectively) by increasing L_{3D} from 40m to 100m. Accordingly, the following calculations use 40m as the 3D model length. The downstream 1D-3D interface was then located at a distance from the fire source approximately eight hydraulic diameters of the airway.

6.3.4. Results. After a sensitivity analysis for both meshing quality and location for 1D-3D interfaces, the 3D model was simulated in a transient state for a duration of 60s. Figure 6.19 presents the results of temperature distribution along Section Two at the 15s, 30s, 45s, and 60s, respectively.

Simulation (Figure 6.19) shows that airflow velocity at the Inlet_Air was sufficient to avoid the occurrence of back layering at the beginning. As a result of buoyancy, hot air rises to the roof, and high temperature flow were tilted because of the airflow influence. This situation lasted until the velocity reached the critical velocity of 1.667 m/s at 27s, the reversed hot air started to go across over fire source, resulting in back layering (as shown at 30s, 45s and 60s in Figure 6.19). Consequently, a hot air layer formed along the roof in the upstream direction. The layer continued to accumulate and, as a result, the thickness of the hot air layer increased along the roof. The temperature contour had developed very well at the Outlet. The same phenomena was also found in the X-velocity contour along the same section (Figure 6.20).

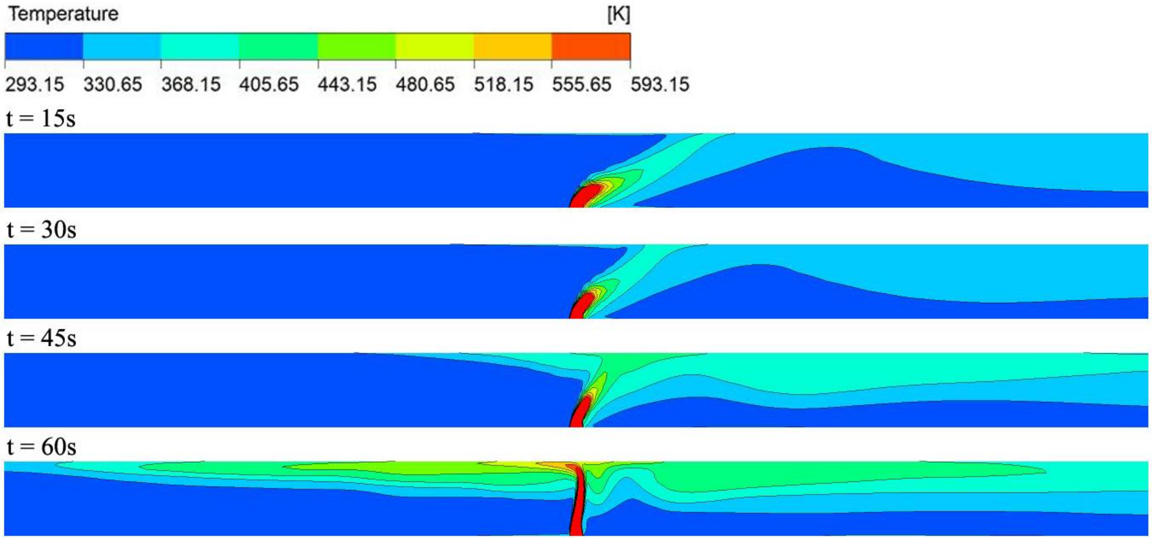

Figure 6.19. Temperature Prediction along Section Two in Transient State in the 3D Model for Case Two (Air Flows from Left to Right)

Figure 6.20 presents only the negative X-velocity distribution along Section Two at 15s, 30s, 45s, and 60s, respectively. The positive direction of X was along the direction of the air flow (from left to right). So, a negative value meant that the hot air flowing against the direction of the airflow, presenting the occurrence of the back layering. At 15s, no back layering occurred. At 30s, back layering was found upstream from the fire zone. The hot air flowed against the direction of the airflow and accumulated under the roof. Another recirculation area downstream close to the fire zone was found. This is a result of a combined throttling and the buoyancy effect. The throttling effect decreased the pressure in the area close to fire zone downstream, while the buoyancy effect entrained the cold air near those regions and rises up to the roof. As a result, recirculation occurred.

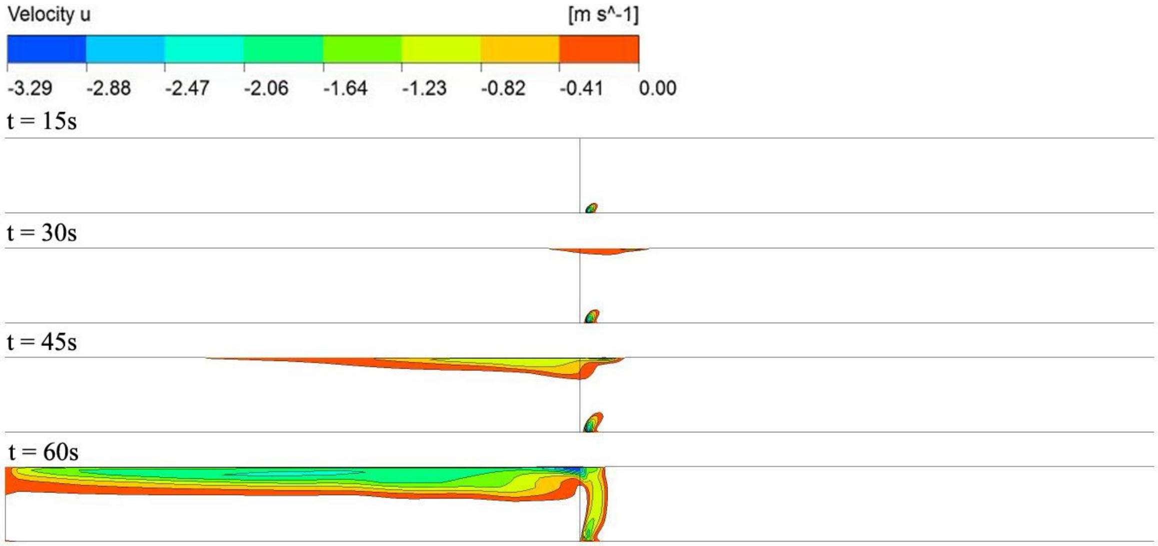

Figure 6.20. Negative X-velocity Prediction in Transient State at Section Two in the 3D Model for Case Two

7. MULTISCALE MODEL OF THE MAIN MINE FIRE

7.1. INTRODUCTION

The multiscale model will be used to describe the behavior of mine ventilation flows under fire conditions. The multiscale applications discussed in this section are designed to include the near fire zone in the 3D sub-domain, while the rest of the tunnel domain is modeled by means of a simple 1D modeling approach. It is clear, in fact, that detailed simulations of the near fire zone cannot be fully accomplished without accounting for the interaction with the remaining part of the mine. In addition to the ventilation flow calculation, further complexity was added by the presence of high temperature and velocity gradients in the plume region. Such high gradient regions, however, did not extend too far downstream from the fire source since they evolved to fully developed flow regions.

A complete analysis of the ventilation system response and its interaction with the fire was a much more complex task. Indeed, when defining the optimum ventilation strategy for a given fire scenario, other significant issues arose. For instance, information of the critical velocity, clearing a certain portion of the mine from smoke, or the temporal evolution of the smoke stratification, was fundamental to the analysis of the circumstances and development of an emergency scenario. Furthermore, such data was fundamental to determining the evolution of hazardous zones in the mine, designing evacuation procedures or determining the correct timing for the activation of fixed firefighting systems.

The aim of this section is to expand the range of applicability by addressing various underground mine fire scenarios. A comprehensive analysis of ventilation controlling strategies and the characterization of critical velocity, as well as back layering effect, made for the Main Mine. The results of multiscale models were compared with the results from both the 1D and the 3D model.

7.2. CASES DESIGN

Computational analysis of mine ventilation flows are primarily focused on assessing the reaction performance of a given ventilation system under emergency conditions. The calculations of the 1D model were used to assess whether the overall ventilation conditions were acceptable for the fire safety strategies. However, they were not suitable for simulating fluid behavior in the regions that were characterized by high temperature or velocity gradients that are typically encountered in the vicinity of a fire source. To deal with such complex flow conditions, the 1D model has to be coupled with 3D model which has the capability of calculating the complex fluid field. In the longitudinally ventilated underground mine, the 1D model also lacked the ability to assessing whether or not the mine ventilation system was able to guarantee a critical ventilation velocity in the fire zone. Such analyses are mainly required for a valid ventilation strategy design, and are also helpful in training courses.

Studies of critical velocity, as well as back layering effect, have attracted researchers' attention for many years. The development of firefighting technology, as well as evacuation strategies, depends on fully understanding the interaction between ventilation flow and fire. Sudy of these issues mainly depends on the experimental method, which is very expensive and only provides very limited data. The primary reason for this is the limitations of the numerical method. At present, the numerical method is not suitable for use for this purpose. The 1D model cannot calculate the back layering, and the 3D model cannot provide accurate results because the boundary conditions not sufficiently accurate without consideration of the entire mine system. The multiscale model can do both, by servering as a powerful tool to study critical velocity, as well as calculating back layering by simulation instead of using an experimental approach.

As a basis for describing the application of the multiscale model in both a practical and a theoretical view, two situations were studied for this research. These two cases involved the Main Mine (shown in Figure 7.1).

In Case One, a fire was supposed to occur at B7. The fire source was closed to the working face, represented by B9 in the downstream direction. To ensure safe conditions at B9, the ventilation control method, that normally plays a key role in mine fire emergencies, was used to control the fire behavior. The ventilation components (e.g., regulators) responsed in accordance with the situation in real time, and the hot air produced by the fire flowed in the required direction.

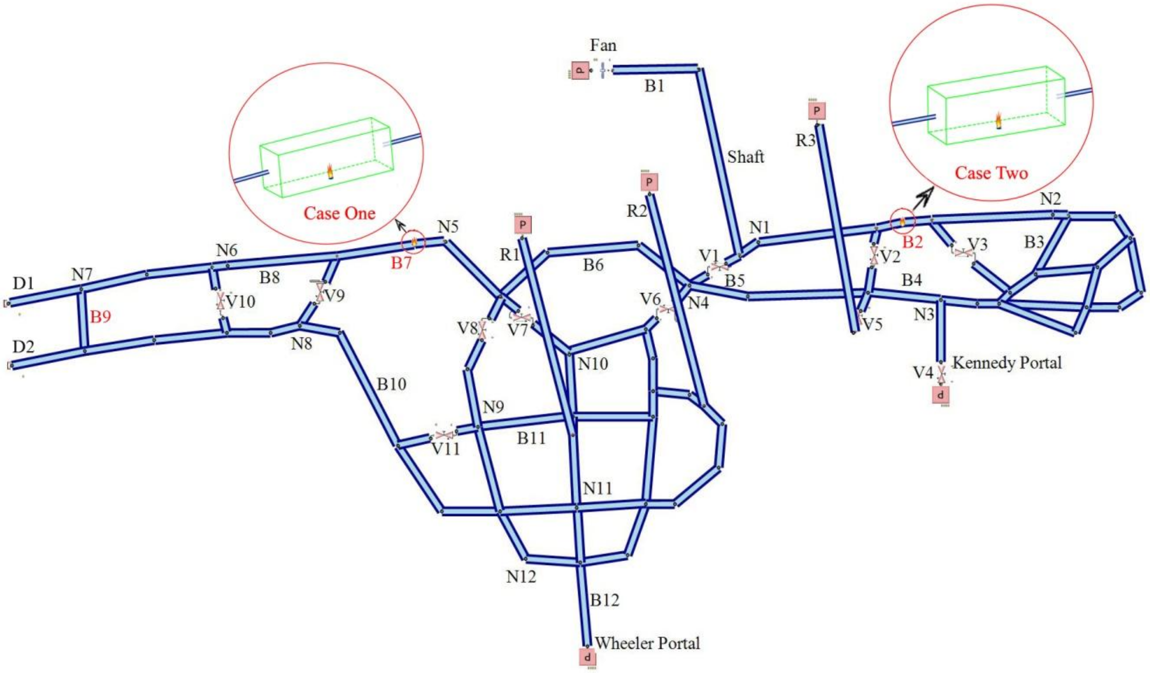

Figure 7.1. Fire Cases in the Main Mine

In Case Two, a fire was supposed to occur at B2. The information obtained from this case was used to analyze the critical velocity, the back layering effect, velocity profile, and temperature distribution. To identify the correlation between back layering distance and air velocity, several different runs were made by changing the fire intensity, and airway dimensions. The simulation results were compared with both the semi-emperial formula and the 3D results.

7.3. CASE ONE: VENTILATION CONTROL STRATEGY

7.3.1. Multiscale Model. The multiscale simulations were conducted using a multiscale model with a direct coupling approach. As already pointed out in the previous sections, this approach allowed the computation of detailed flow and temperature field data in the 3D sub-domain (including the fire), while the rest of the airways be represented by a 1D model. More details on the coupling technique can be found in Section 4. A schematic of the coupling between the 1D model (the far fire zone) and the 3D model (the near fire zone) are depicted in Figure 7.2. The 1D model has the same ventilation boundary conditions as described in Section 5.4.1.

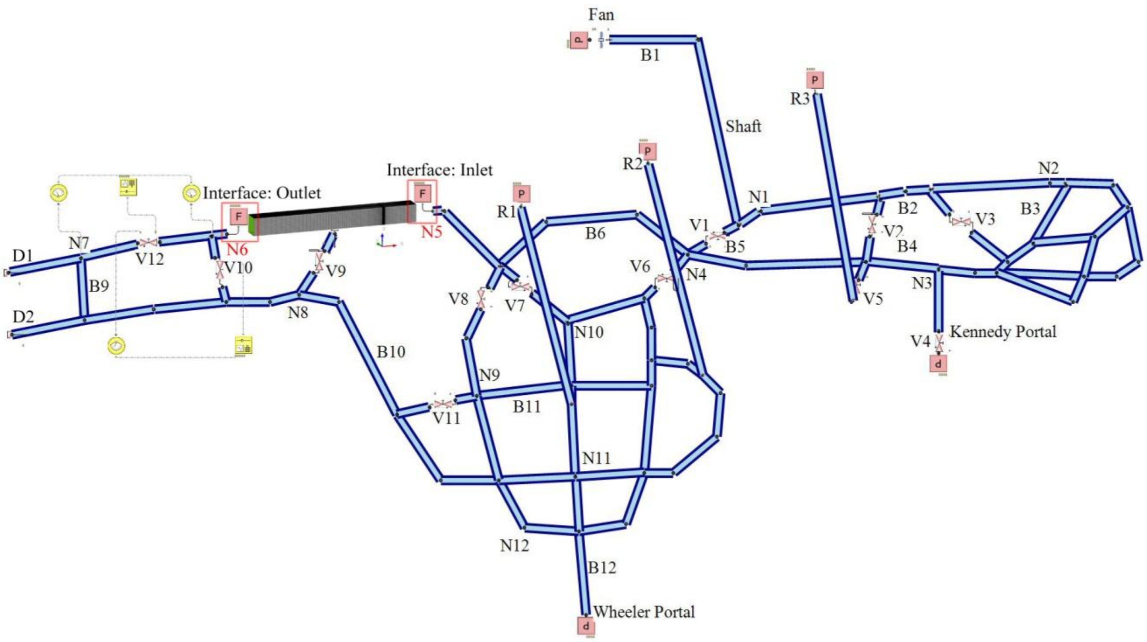

Figure 7.2. Geometric Multiscale Model in the Main Mine for Case One

As already asserted in the previous sections, a critical point of the multiscale representation was the positioning of the 1D-3D interfaces (Γ_i and Γ_j in Figure 4.4). They had to be located in a region where the flow was fully developed. The analysis confirmed that, if a boundary is located at a point more than 8 times of the airway hydraulic diameters away, average and flow field deviations would be significantly reduced, when compared to the reference point from 3D solutions.

The main purpose of this case was to evaluate the performance of the ventilation control strategy for fire prevention through modeling. When a fire occurs, hot gas products and heat will flow downstream towards the exhaust airways then outside, back layering will be formed when the air velocity was less than the critical velocity. This, however, has little impacts on the airflow pattern downstream. To keep the computation time in a reasonable manner, only a small region of the upstream area was included in the 3D model.

It is assumed that the outlet boundary was located 20m (8 times the airway hydraulic diameter) downstream from the fire source. The inlet boundary was 5m away upstream from the fire source. Thus, the total length of the 3D sub-domain is 25m. The whole domain had a uniform dimension of 2.4m in width and 2.6m in height.

A simulation was conducted to simulate the temperature distribution in a transient state along airways in the Main Mine. The calculation was conducted in 180 time steps, each representing one second. The fire source was located between nodes N5 and N6. A fire curve (Figure 5.10) was built for this case. During the first step, the fire grew linearly to 1000 kW within 30s and remained at 1000 kW HRR from 30s to 90s (the second step). During the third step, the fire decayed to zero linearly within 30s. Hot gases were removed from the 3D domain within the next 60s, and continued to travel around the 1D network in the multiscale model.

This case was used to develop a ventilation control strategy underground. Hot gases produced by the fire travelled downstream, causing the temperature at the working place (B9 which is 40m from the fire) to increase. To meet mine safety standard (maximum temperature of 347 K underground in fire emergency) and control measures must be instigated to the existing system. A temporary stopping with a regulator (V12) is needed.

7.3.2. Results. Figure 7.3 to Figure 7.6 show the temperature distribution in the Main Mine at 30s, 44s, 90s, and 106s, respectively after the fire outbreak. In figures, the legend on the bottom right is used for 1D model, while the legend on the top left for 3D model.

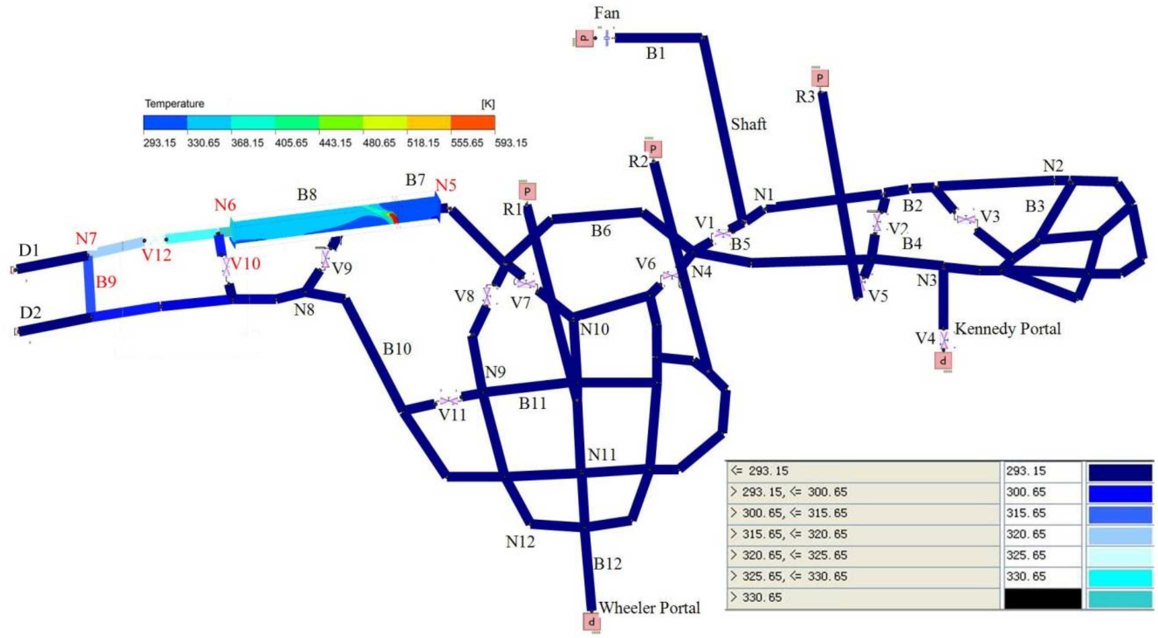

Figure 7.3. Heat Distribution at 30s along Airways in the Multiscale Model for Case One

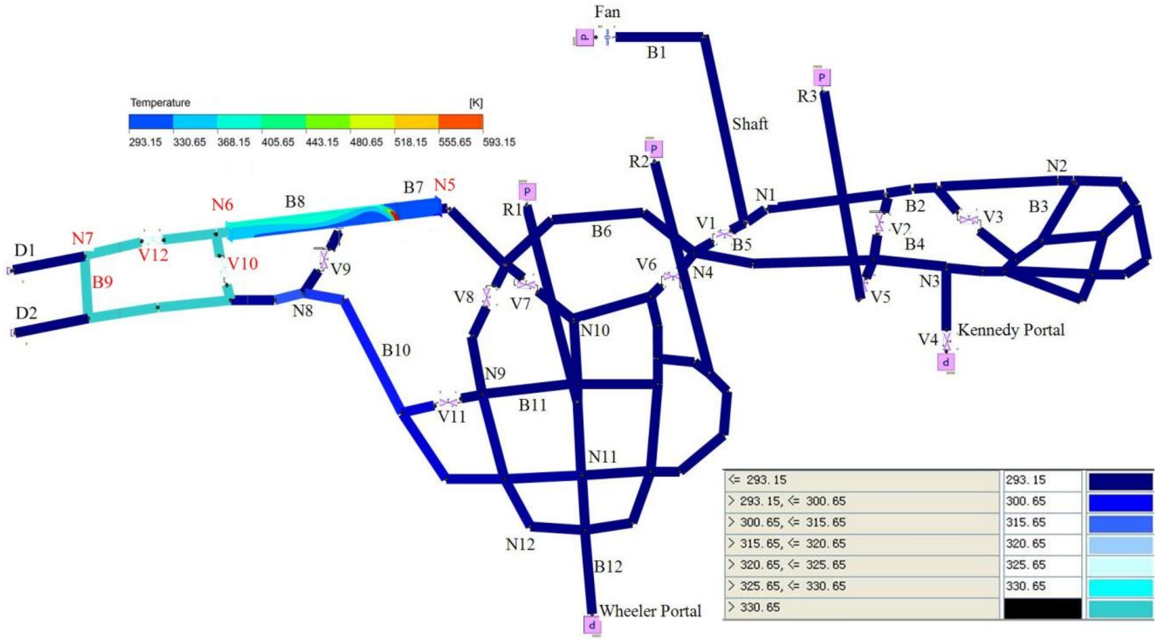

Figure 7.4. Heat Distribution at 44s along Airways in the Multiscale Model for Case One

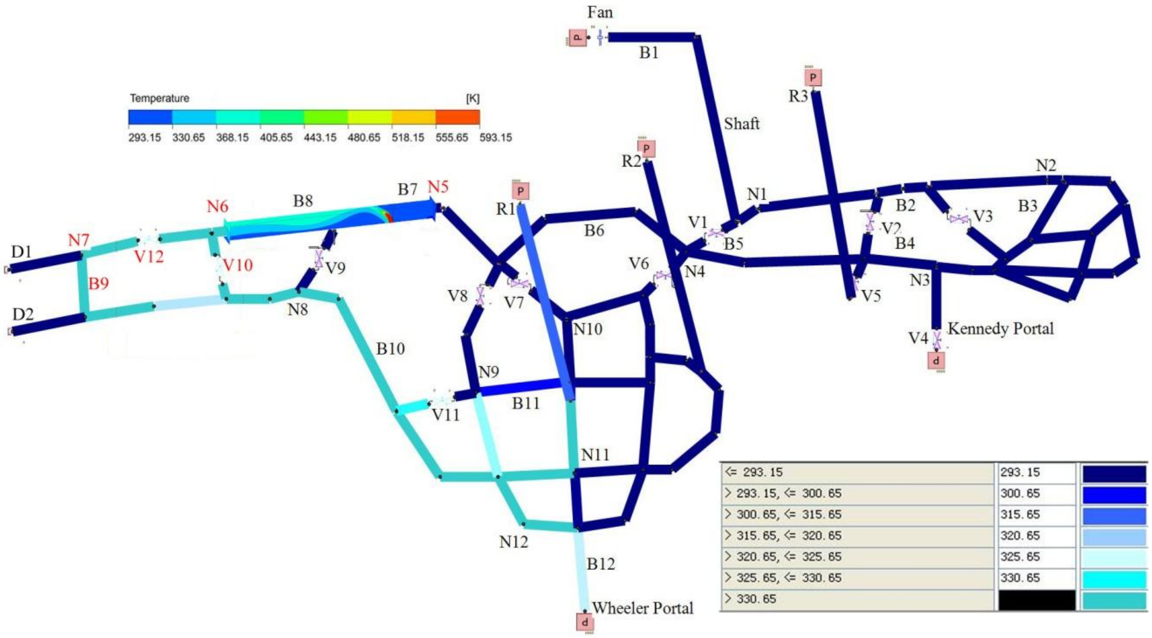

Figure 7.5. Heat Distribution at 90s along Airways in the Multiscale Model for Case One

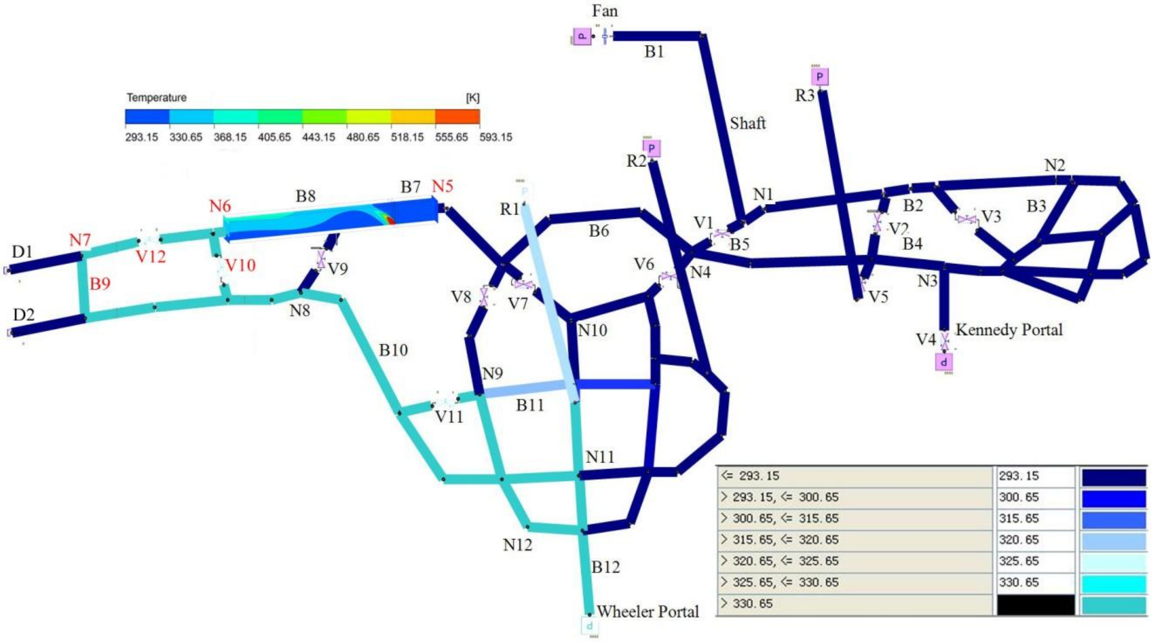

Figure 7.6. Heat Distribution at 106s along Airways in the Multiscale Model for Case One

Heat distribution in and adjacent fire zones for the aforementioned four cased were plotted in 2D schematics as shown in Figure 7.7.

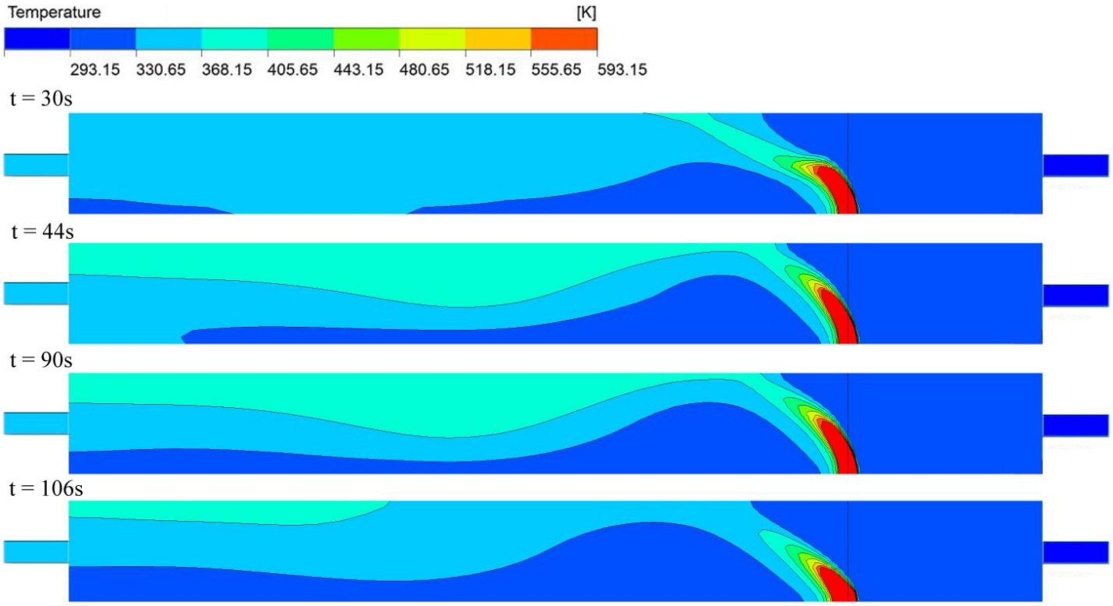

Figure 7.7. Heat Distribution in Transient State at Near Fire Zone in the Multiscale Model for Case One (Air Flows from Right to Left)

Since the network model does not have the capability to treat a reversal effect, impacts of hot gases produced in the fire on upstream airflow was not shown. Temperature distribution was heavily influenced by the direction of the air flow. Since the airflow remains unchanged through the calculation in the multiscale model, temperature distribution in areas upstream also remains unchanged.

Under normal circumstances, heat and combustion products in a fire are expected to be diluted and carried by airflow. No back layering is expected as it poses serious safety hazards to both miners and mine rescue operation. As a result, the working place downstream was placed in a dangerous situation in a fire. Based on the requirement of MSHA (Anon., 2012b), the highest temperature required to keep underground humans safe at the working place was 347 K. Simulation results from calculation in this case are explained below along with a description of how the requirement was met.

At 30s, the fire was fully developed and the heat released by the fire reached its highest intensity (1000 kW). The temperature at the working face (B9) was still less than the safe limit of 347 K. The V10 remained its initial status (set at “0.05”), and temperatue remain unchanged. Hot air travelled downstream through V12 (regulator), B9 (working place), and to other parts of the network.

However, temperature exceeded 347 at 44s. In response to this increasing temperature, of the two devices, V12 was completed closed (set at “0”) while V10 was open (set at “1”). Since V12 is part of the airway, its closing increased the resistance of the airways between N6 and N7, while the opening of V10 decreased the resistance of the airways where it was located. As a result, more air with increased heat was traveling through V10. Since air velocity is nearly zero at B9, the temperature remained at 347 K.

This situation changed at 106s. Because the fire started to decay at 90s, the heat released from the fire decreased accordingly and, consequently, the temperature at N6 was reduced. When the temperature at N6 was less than 347 K, meaning the danger no longer existed. This triggered the re-opening of V12 (set at “1”) and closing of V10 (set at “0.05”) accordingly. All ventilation control devices reinstated to their original position. The heat accumulated at B9 started to flow downstream along the airway and the fire was fully extinguished at 120s. The rest of the calculations were to remove the remining heat from the mine.

Multiscale technique provides a user-defined method on developing firefighting strategy. Its capability of component control in real-time makes it a useful and practical tool for mine safety training. Performance-based planning also benefited from this technique. By using the 3D model to provide an accurate calculation for the area near the fire, and the fire itself, the results are more accurate and can be used for mine emergency training and a better ventilation system design.

To demonstrate the ability of the multiscale mode, comparisons of fluid properties were made at N6 and N7 in both the full 1D and the multiscale model. The prediction results of temperature and longitudinal velocity are presented in Figure 7.8 and Figure 7.9, respectively.

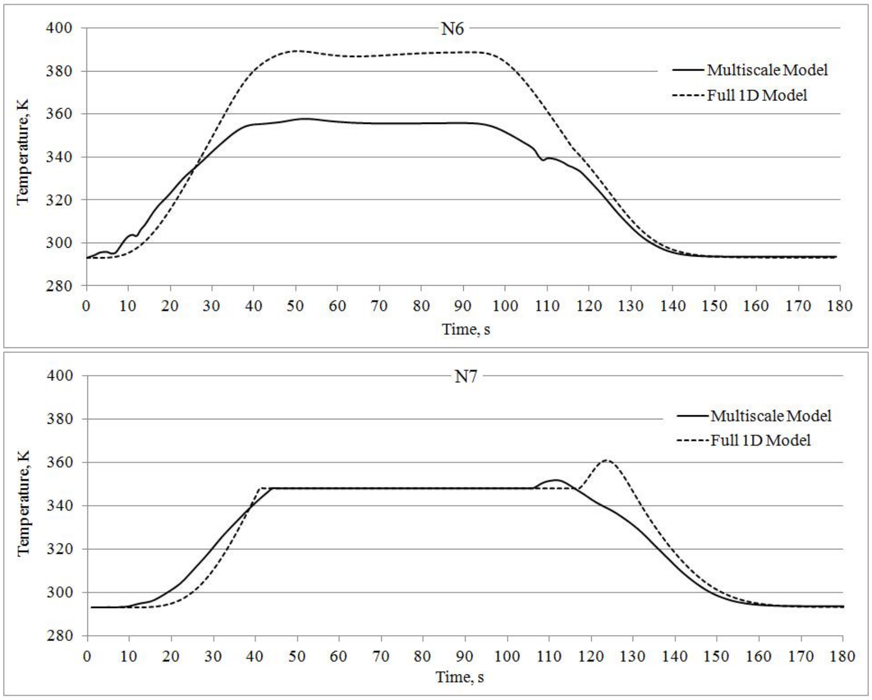

Figure 7.8. Comparison of the Temperature Distribution at both N6 and N7 between the Full 1D and the Multiscale Model for Case One

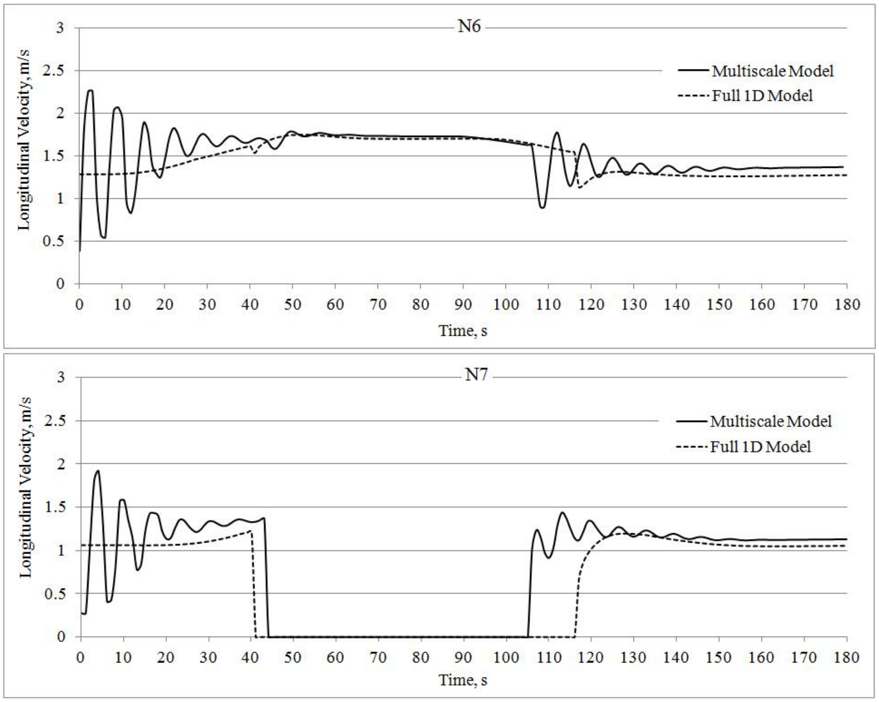

Figure 7.9. Comparison of the Velocity Distribution at both N6 and N7 between the Full 1D and the Multiscale Model for Case One

Node N6 represents the outlet boundary at the interface of the 1D and the 3D model while Node N7 was the inlet of the airway where the working face was located. Since the heat calculated for the 3D domain was released into the rest of the network through N6, the temperature at N6 determined the temperature distribution in the network.

In the full 1D model, regulator V12 was closed at 41s and reopened at 117s, while in the multiscale model, it was closed at 44s and reopened at 106s. The reason for the 3s difference at opening time between the two models is an overestimation of temperature in the 1D model. For the same reason, V12 was reopened 11s later in the full 1D model.

During simulation process, most of the temperature distributions in the full 1D model were higher than that in the multiscale model. The biggest temperature difference between the two models was 33 K, occurred at 95s.

Regulator V12 was fully closed when the temperature at N7 reached 347 K. In the full 1D simulation, regulator V12 was closed when the temperature at N6 reached 380 K, while in the multiscale model, it was 355 K. That means that the multiscale model was more sensitive and reacted more quickly than the full 1D model.

7.4. CASE TWO: CRITICAL VELOCITY AND BACK LAYERING

7.4.1. Multiscale Model. Another multiscale simulation was prepared using the direct coupling approach. As already pointed out in the previous section, this approach allowed the computation of detailed flow and temperature field data in the 3D sub-domain including the fire, while the rest of the tunnel layout was represented by using a 1D model. A schematic of the coupling between the 1D model of the far fire zone and the 3D model of the near fire zone are depicted in Figure 7.10. The 1D model has the same ventilation boundary conditions as described in Section 5.4.2.

A critical point of the multiscale representation was to locate the 1D-3D interfaces. The analysis confirmed that, if a boundary is located at a distance longer than 8 airway hydraulic diameters, the average and flow field deviations would be significantly reduced with a small error, in comparison to a referenced 3D solution.

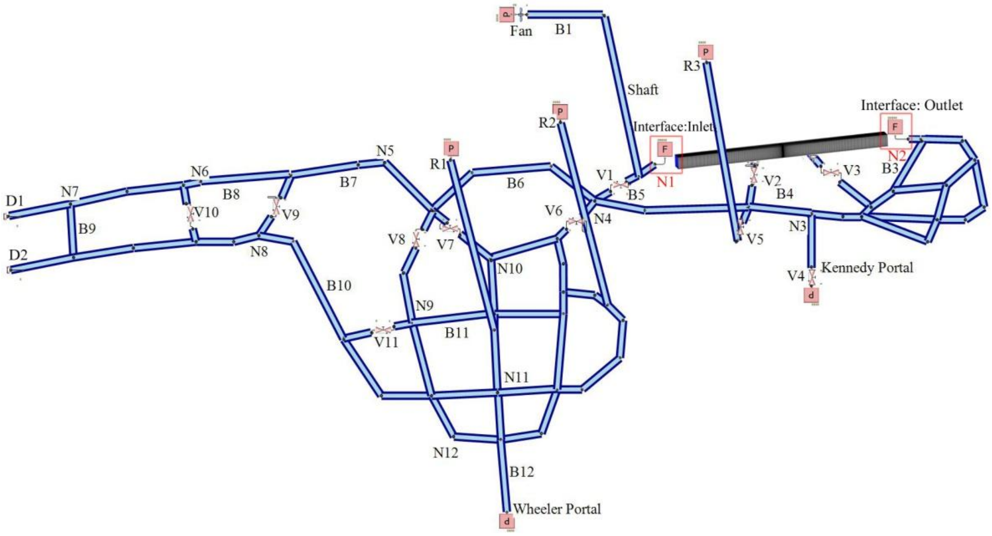

7.10. Geometric Multiscale Model in the Main Mine for Case Two

The main purpose of this case is to study the back layering effect on different boundary conditions. The assumption of a uniform flow at the boundary upstream must be maintained during the entire calculation. The gases will travel against the airflow, during the stage when the velocity is less than the critical velocity. It is essential that all initial back layering is captured within the 3D domain.

Based on this estimation, both the inlet and outlet boundaries were located at a distance of 8 hydraulic diameters (2.495m) of the airway, therefore, the length of the 3D sub-domain was 40m, with the fire located in the middle. The entire 3D sub-domain had a uniform dimension of 2.4m in width and 2.6m in height.

The fire with 1MW HRR was located in the middle of the airway between nodes N1 and N2. The entire simulation lasted 60s. To determine the correlation between the length of back layering and the inlet air velocity, inlet velocity (Figure 5.17) varied with time during the simulation. During the simulation, the boundary information, including the pressure and mass flow rate, were interchanged constantly through the Interface: Inlet and Interface: Outlet. In the 1D model, the boundary was represented with a Flow Component, while in the 3D model, the boundary was a 2D plane.

7.4.2. Results. Figure 7.11 to Figure 7.18 presents the computed temperature and flow fields at 15s, 30s, 45s, and 60s after the fire breaks out.

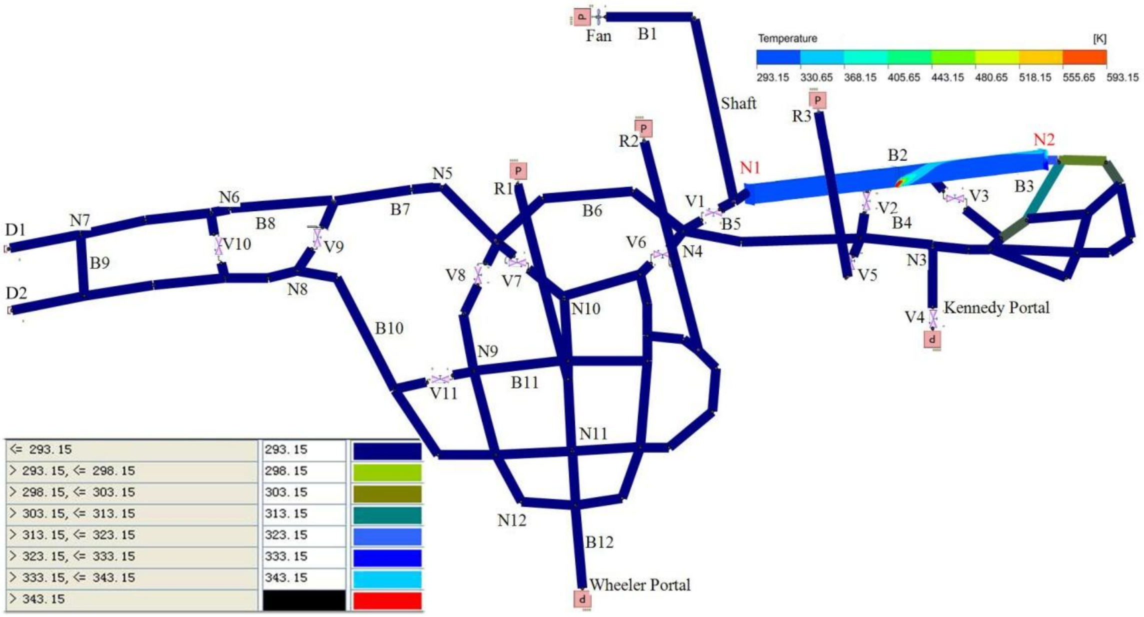

Figure 7.11. Heat Distribution at 15s along Airways in the Multiscale Model for Case Two

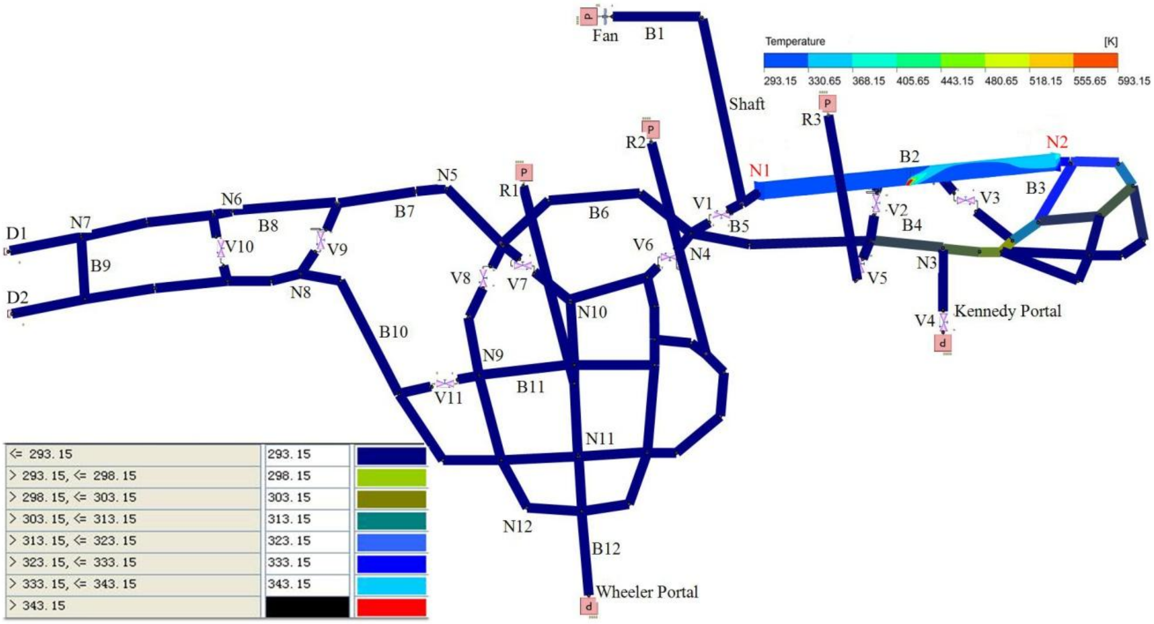

Figure 7.12. Heat Distribution at 30s along Airways in the Multiscale Model for Case Two

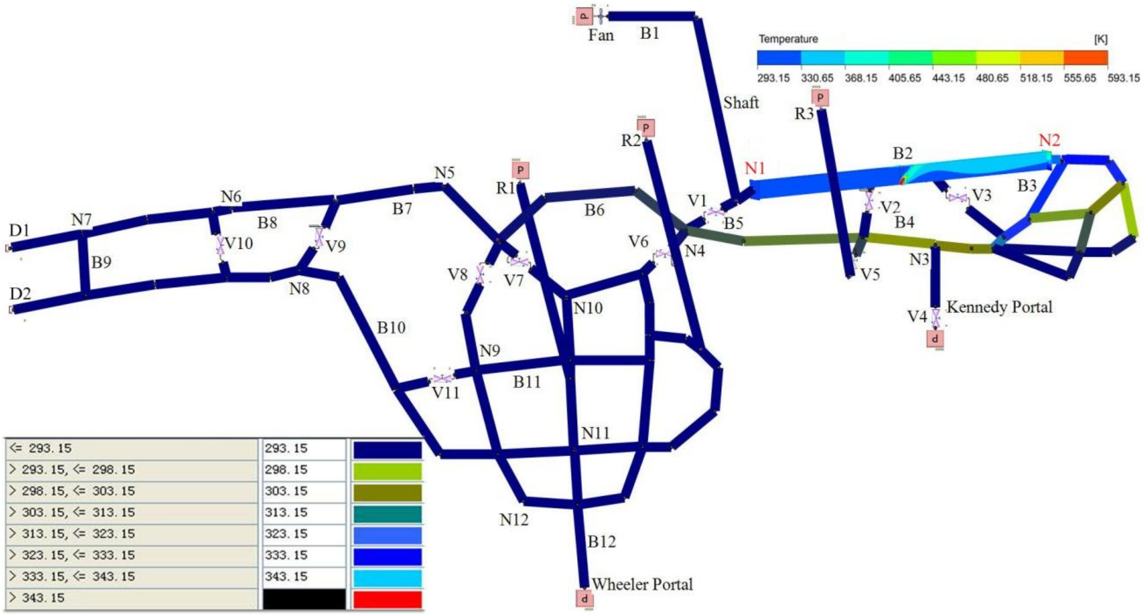

Figure 7.13. Heat Distribution at 45s along Airways in the Multiscale Model for Case Two

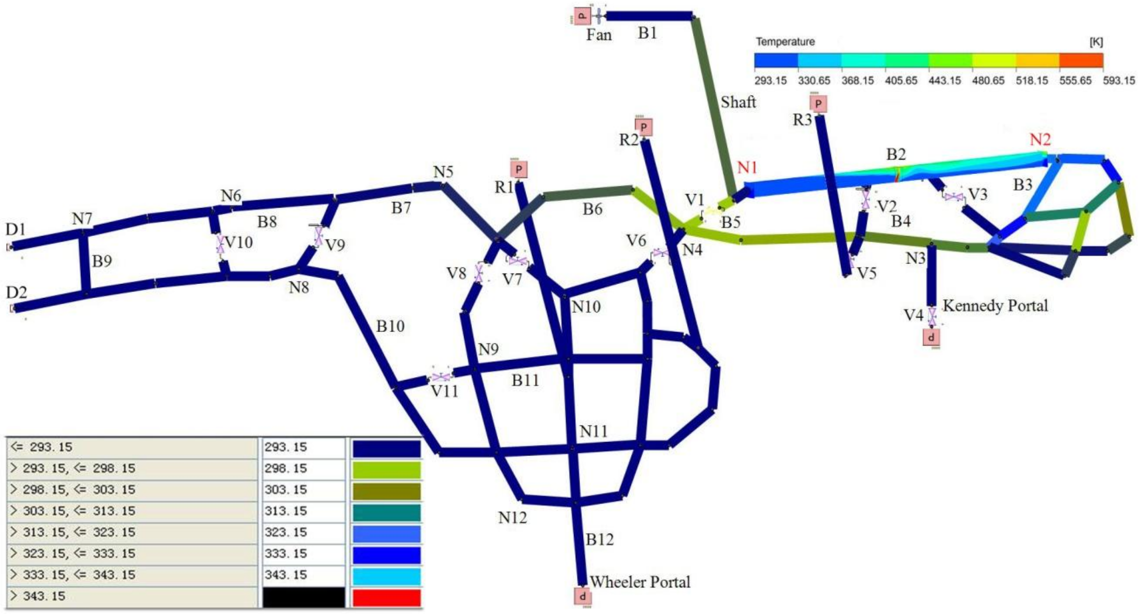

Figure 7.14. Heat Distribution at 60s along Airways in the Multiscale Model for Case Two

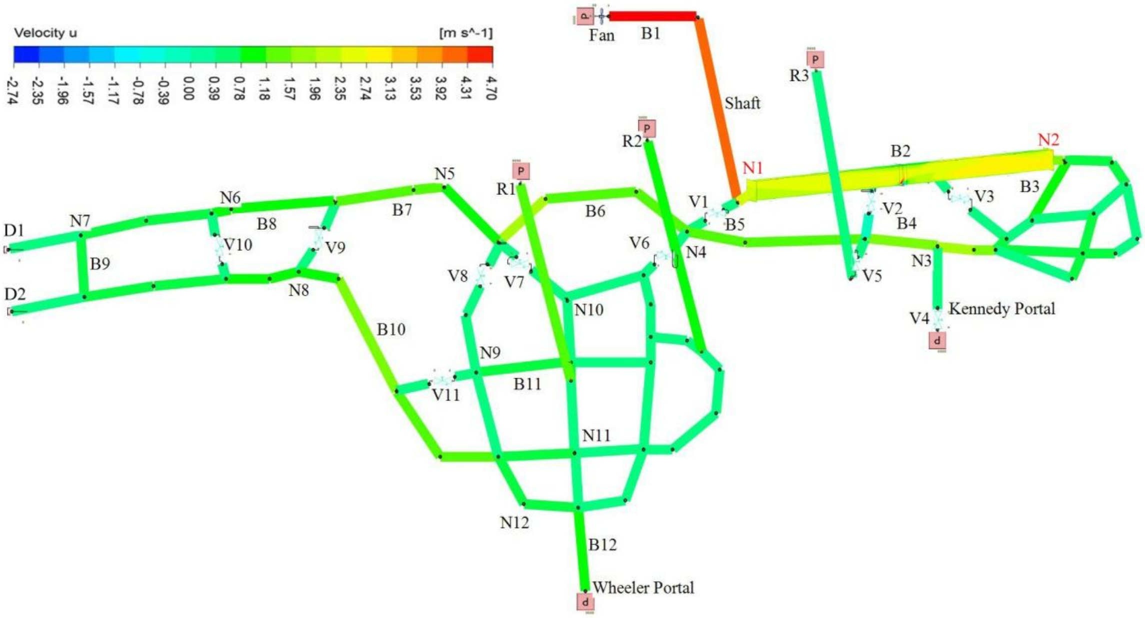

Figure 7.15. Velocity Distribution at 15s along Airways in the Multiscale Model for Case Two

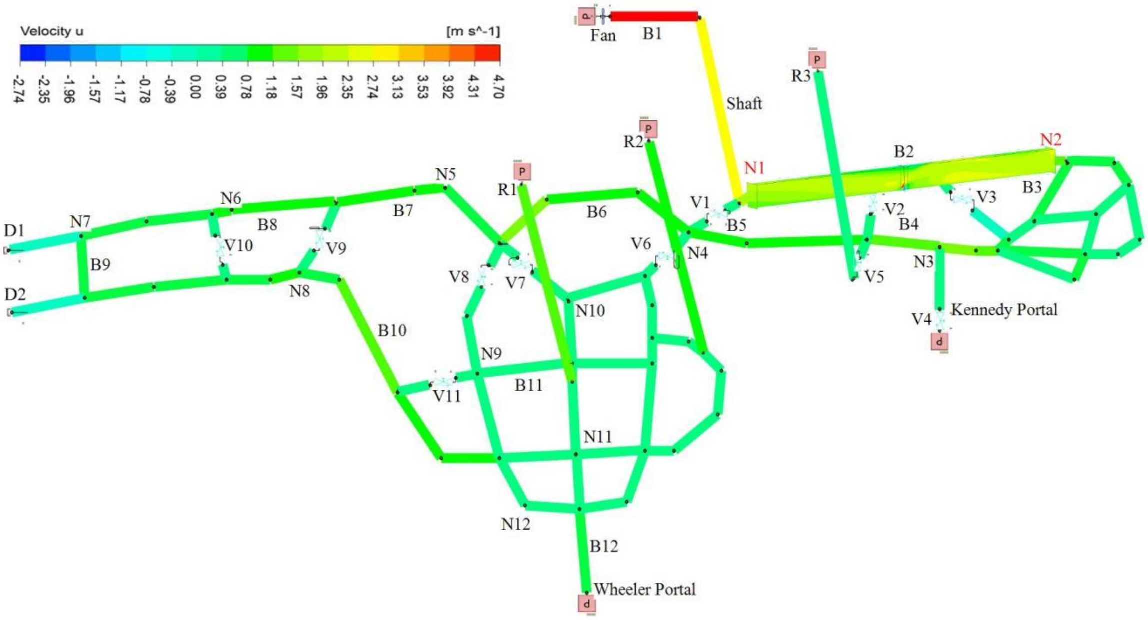

Figure 7.16. Velocity Distribution at 30s along Airways in the Multiscale Model for Case Two

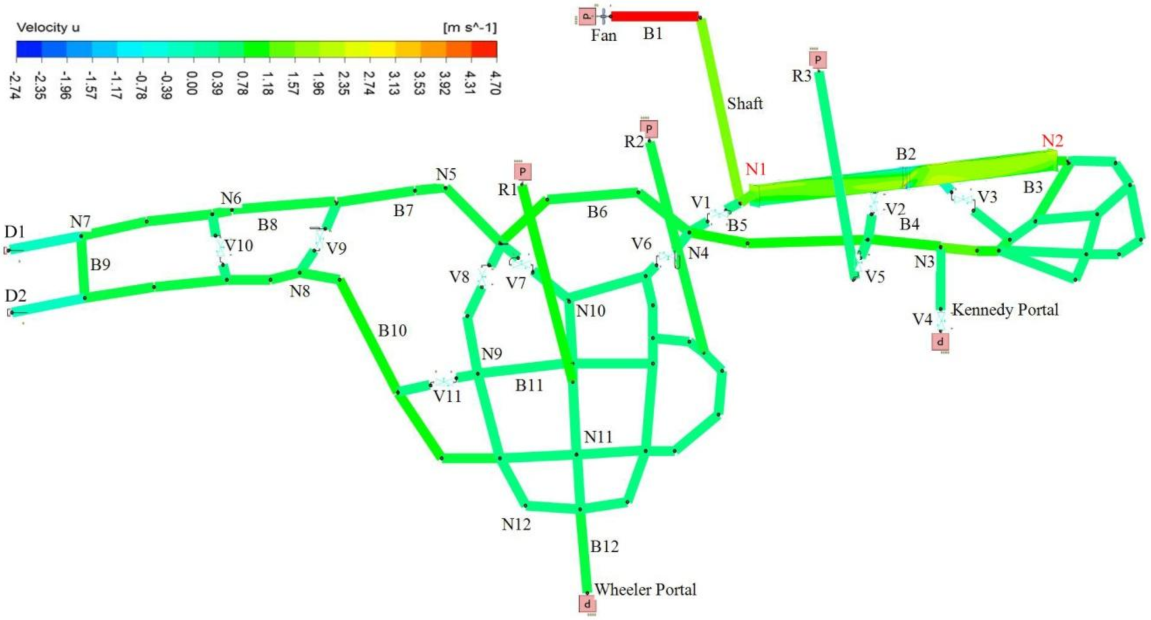

Figure 7.17. Velocity Distribution at 45s along Airways in the Multiscale Model for Case Two

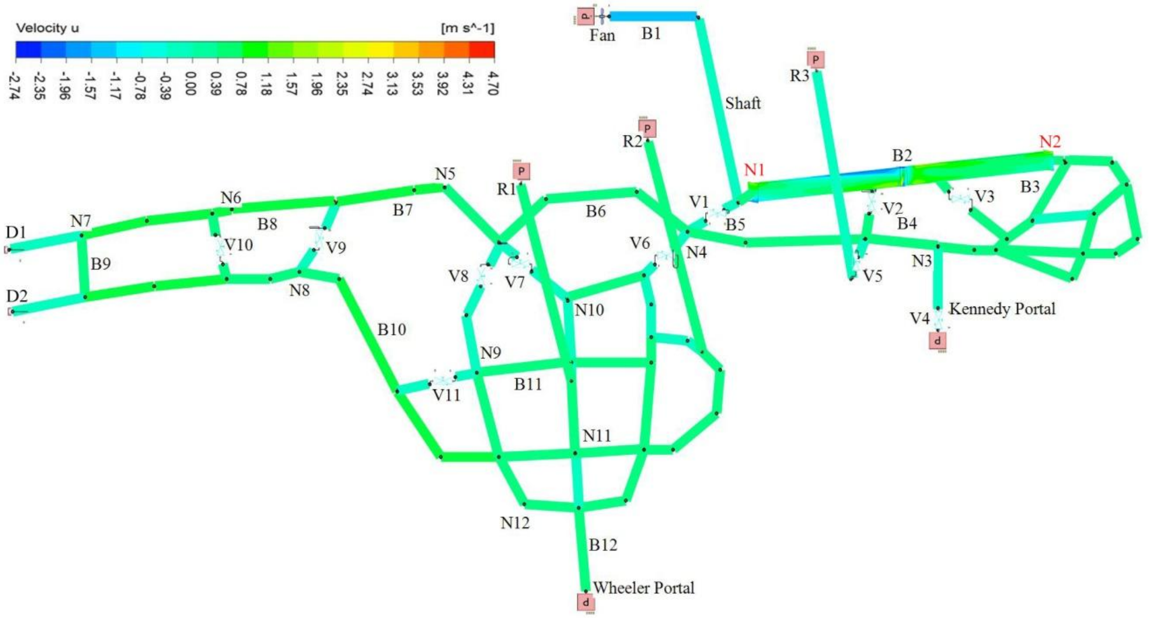

Figure 7.18. Velocity Distribution at 60s along Airways in the Multiscale Model for Case Two

The temperature distributions at the area near the fire zone in 2D are shown in Figure 7.19 at 15s, 30s, 45s, and 60s after the fire breaks out.

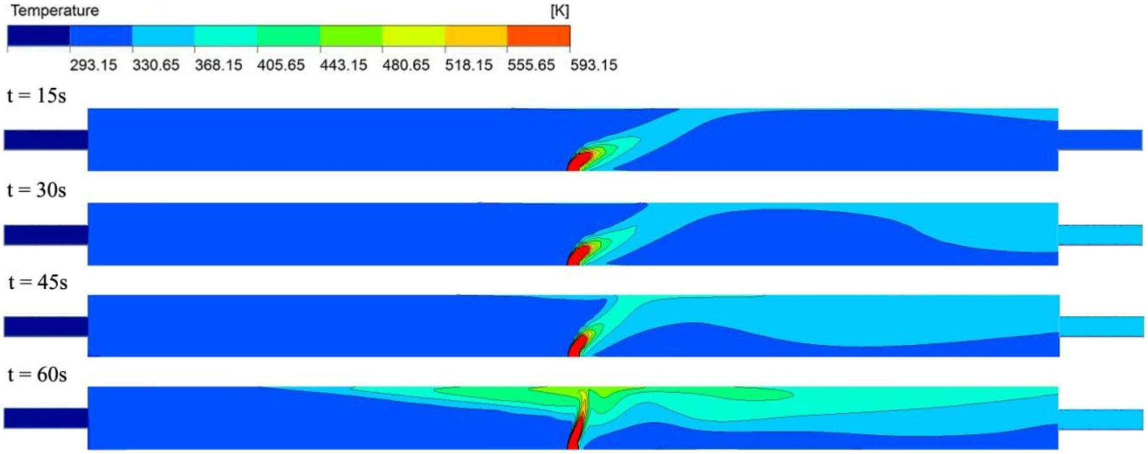

Figure 7.19. Heat Distribution in Transient State at Near Fire Zone in the Multiscale Model for Case Two (Air Flows from Left to Right)

Figures 7.19 shows that at the beginning stage of the fire outbreak, for instance at 15s, the heat released from fire rose to the airway roof and travelled along the airway downstream due to the buoyancy effect. Heat plume from the fire was too weak to against the airflow. As a result, the airflow from the inlet dominated the hot air distribution and made the plume tilted towards the airflow direction.

As time passed, air velocity at the inlet continued to decrease. At 35s, the hot air travels against the airflow and starts to go across the fire source, forming a back layering. The velocity at this moment, 1.601 m/s, is considered as the critical velocity. At 60s, air velocity at the inlet was closed to zero. The temperature distribution trended to be symmetric in both upstream and downstream directions. The length of back layering increased to 16.74m upstream from the fire at 60s.

The negative X-velocity distributions at the area near the fire zone in 2D are shown in Figure 7.20 at 15s, 30s, 45s, and 60s after the fire breaks out. The positive direction of X was along the air flow from left to right. A negative value means that the hot air flew against the airflow, predicting the occurrence of back layering.

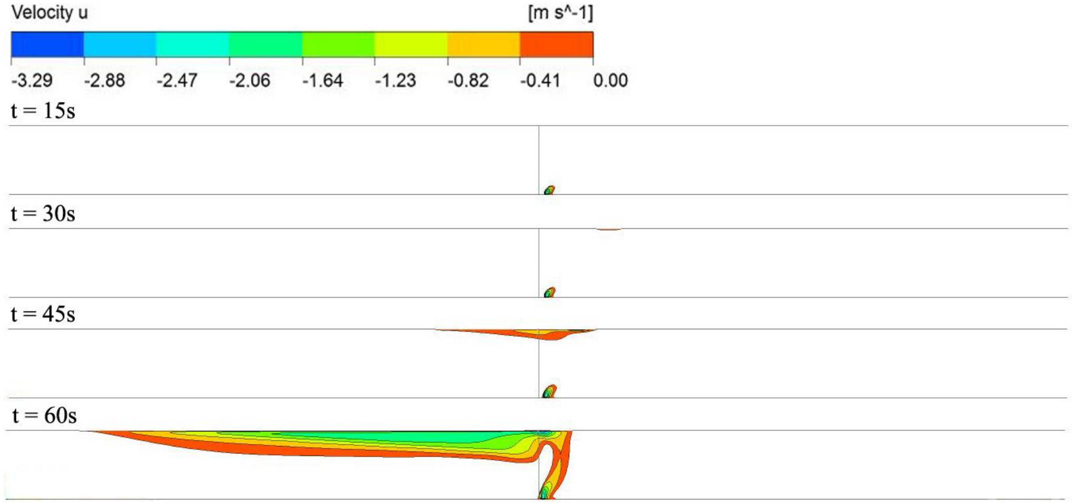

Figure 7.20. Negative X-velocity Distribution in Transient State at Near Fire Zone in the Multiscale Model for Case Two (Air Flows from Left to Right)

Figure 7.20 shows that at both 15s and 30s, no back layering occurred. At 45s and 60s when air velocity at the inlet was less than the critical velocity, back layering formed and the hot air travelled against the airflow. Another recirculation area downstream close to the fire zone was found. This is a result of a combined throttling and the buoyancy effect. The throttling effect decreased the pressure in the area close to fire zone downstream, while the buoyancy effect entrained the cold air near those regions and rises up to the roof. As a result, recirculation occurred.

The critical velocity plays a critical role on planning firefighting strategies. If the velocity at Inlet_Air exceeds the critical velocity, no back layering occures. Otherwise, back layering resulted and extreme care must be exercised to reach the fire zone from the upstream direction. The critical velocity is determined mainly by the airway dimensions and fire intensity. Three popular formulas, including Eq. 2.2, Eq. 2.5, and Eq. 2.11 are currently used to calculate the critical velocity. The solution of Eq. 2.5 referred to the work of Tarada (2010). A total of ten scenarios were designed to examine the impacts of airway width, airway height, hydraulic height, and fire intensity on the critical velcotiy. The critical velocity results from Eq. 2.2, 2.5, 2.11, 3D model, and multiscale model are listed in Table 7.1.

Among these three formulas, Eq. 2.11 was considered to be more accurate than others. A comparison of results from Eq. 2.11, 3D models, and multiscale models is plotted in Figure 7.21.

Table 7.1. Critical Velocity Calculation for Case Two

Scenario	Airway Dimension, m			Fire Intensity, kW	Critical Velocity, m/s				
	W	H	Hydraulic Height $\overline{H}$		Eq. 2.2	Eq. 2.5	Eq. 2.11	3D	Multiscale
1	2.4	2.6	2.495	1000	1.484	1.229	1.519	1.677	1.601
2	2.4	0.65	1.023	1000	0.742	0.960	1.267	2.121	1.329
3	2.4	1.3	1.686	1000	1.049	1.121	1.626	1.529	1.536
4	0.6	2.6	0.975	1000	1.484	1.703	1.236	1.283	1.281
5	1.2	2.6	1.486	1000	1.484	1.465	1.526	1.283	1.486
6	1.2	5.2	1.95	1000	2.098	1.580	1.649	1.480	1.638
7	4.8	1.3	2.046	1000	1.049	0.951	1.623	1.727	1.649
8	2.4	2.6	2.495	2000	1.484	1.465	1.913	2.023	1.925
9	2.4	2.6	2.495	500	1.484	1.012	1.205	1.480	1.493
10	2.4	2.6	2.495	250	1.484	0.823	0.957	1.628	1.216

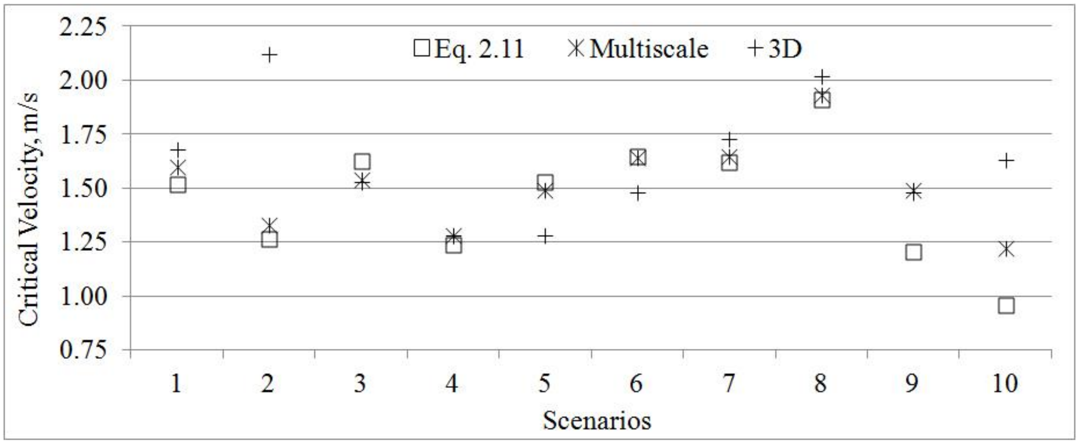

Figure 7.21. Comparison of the Critical Velocity in Different Scenarios for Case Two

Figure 7.21 shows that the critical velocities calculated with Eq. 2.11 matched the results from the multiscale model much better than those from the 3D model. The biggest deviation in the multiscale model and 3D model from Eq. 2.11 is 27.52% and 70.37%, respectively occurred in scenario 10. This indicated that the multiscale model provided better results than 3D model in predicting the critical velocity.

Once back layering occurred, the length of the layering was also critical for firefighting activity. The length of back layering was influenced mainly by air velocity, together with airway dimensions and fire intensity. In the past, the relationship between the layering length and velocity was determined by large-scale or small-scale experiments. In this research, a series of numerical models were run to describe this relationship in a simulative view. A total of ten scenarios, including the reference, were calculated.

The instability of hot air reversal made it difficult to define the extent of the reversal certainly with different ventilation velocities. One thing, however, is certain that the length of back layering varied inversely with the air velocity at inlet, regardless of other factors. Therefore, in this research, a series of logarithmic regression analyses were applied to the ten scenarios. In each scenario, the fire intensity and airway dimension remained unchanged. The back layering distance varied only with the air velocity.

Variable L_b represented the length of back layering, and V represented the air velocity. Based on literature review, the correlation between L_b and V, that was developed for this research, indicated a simple relationship

$$L_b = -A1\ln(V) + B1 \tag{7.1}$$

where $A1$ and $B1$ are constants. They are determined by the fire intensity, airway dimension, and atmospheric conditions. This relationship is discussed with the results from both the multiscale model and 3D model.

Additional formula was developed by introducing a proportionality constant $A2$ into Eq. 2.16. It is in the form as

$$L_b = A2\left(\frac{g\dot{Q}H^2}{\rho_0 c_P T_0}\right)^{1/3}\frac{1}{V} \tag{7.2}$$

Based on Eq. 2.17, a relationship of the length of back layering and velocity was derived as

$$L_b = -0.0714\frac{c_p(T_f - T_0)}{g}\ln(V) - (0.0238\ln(\frac{A\rho_0}{\dot{Q}}) + 0.0479)\frac{c_p(T_f - T_0)}{g} \tag{7.3}$$

In Eq. 7.2 and 7.3, the constant ρ_0 is the average density of the air (1.224 kg/m^3), c_p is the air specific heat (1.0 kJ/(kg K)), g is the acceleration due to gravity (9.8 m/s^2), and T_0 is the ambient temperature (293.15 K). Variable T_f is an average temperature of the fire-site gases that can be calculated using Eq. 2.6. Other factors, including $\dot{Q}$ the total HRR, A the cross sectional area of airway, and H the height of the airway, vary according to different scenarios. This information can be found in Table 7.1.

A logarithmic regressions study was conducted for each scenario to discover the relationship between the length of back layering, L_b, and air velocities, V. The constants, *A1* and *B1* in Eq. 7.1, were determined using logarithmic regression. To determine the constant *A2* in Eq. 7.2, the curve fitting with the least-squares method was used. Results of regression analysis and curve fitting are plotted in Figure 7.22 through Figure 7.31, and listed in Table 7.2.

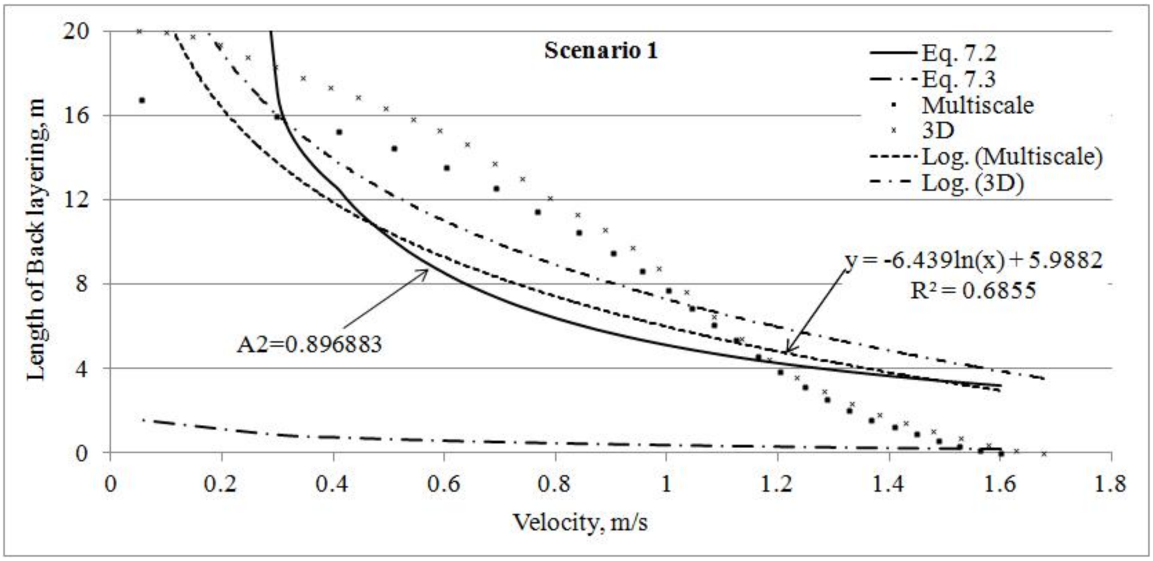

Figure 7.22. Relationship between the Length of Back Layering and Velocity in the Scenario 1 for Case Two

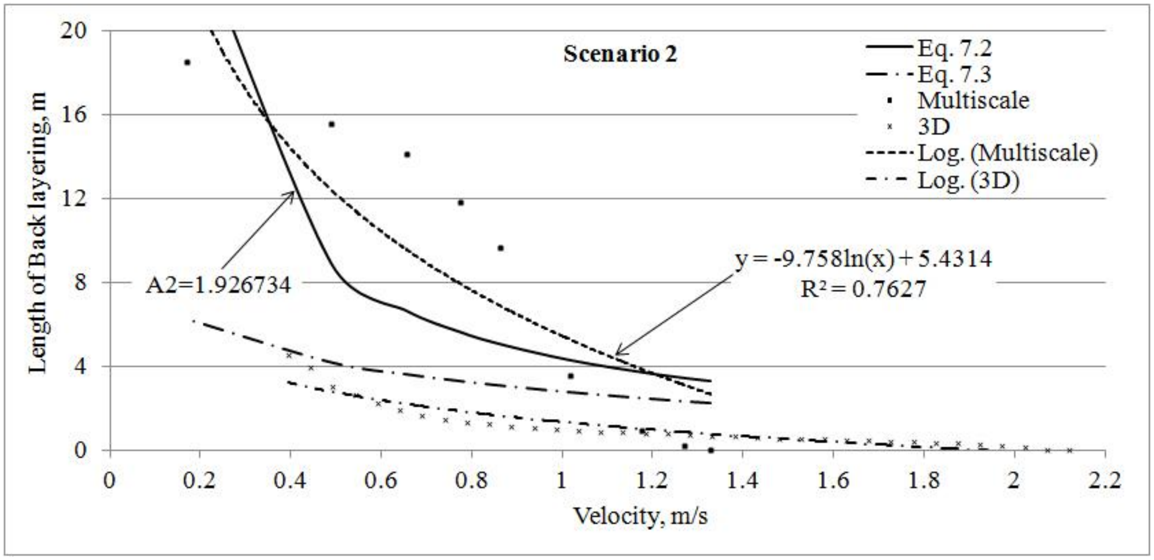

Figure 7.23. Relationship between the Length of Back Layering and Velocity in the Scenario 2 for Case Two

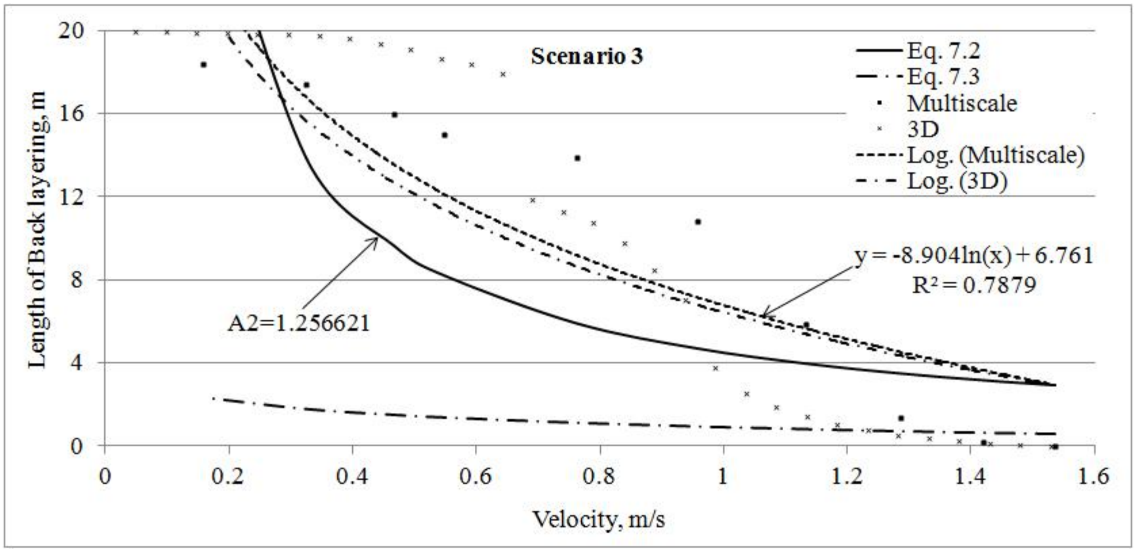

Figure 7.24. Relationship between the Length of Back Layering and Velocity in the Scenario 3 for Case Two

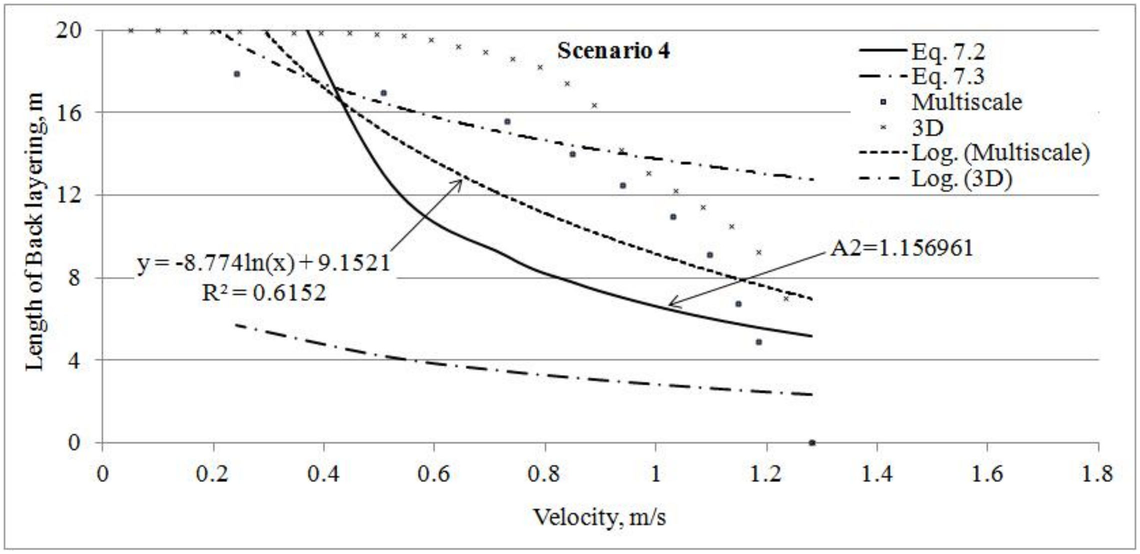

Figure 7.25. Relationship between the Length of Back Layering and Velocity in the Scenario 4 for Case Two

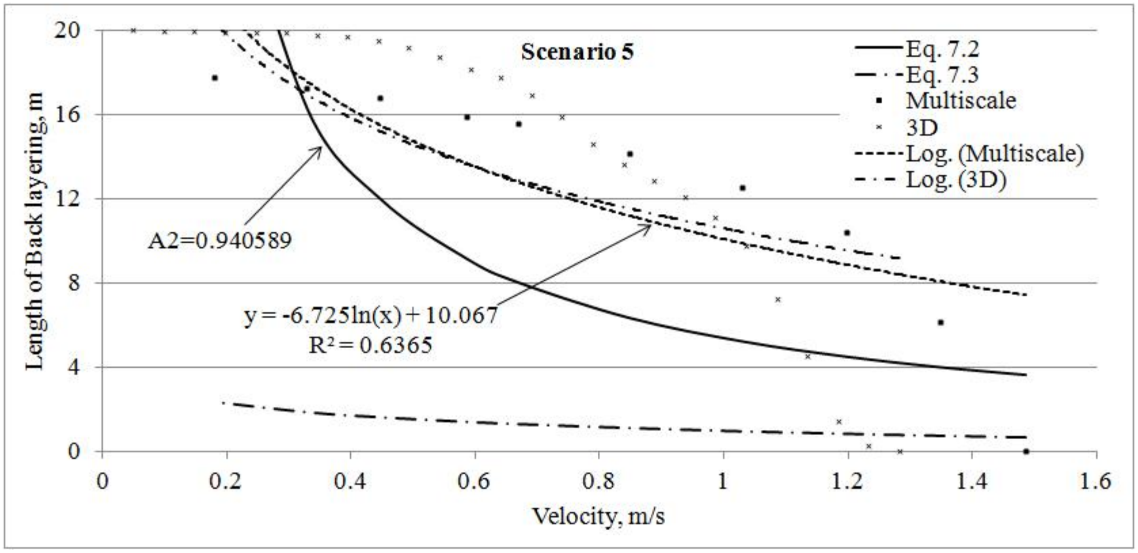

Figure 7.26. Relationship between the Length of Back Layering and Velocity in the Scenario 5 for Case Two

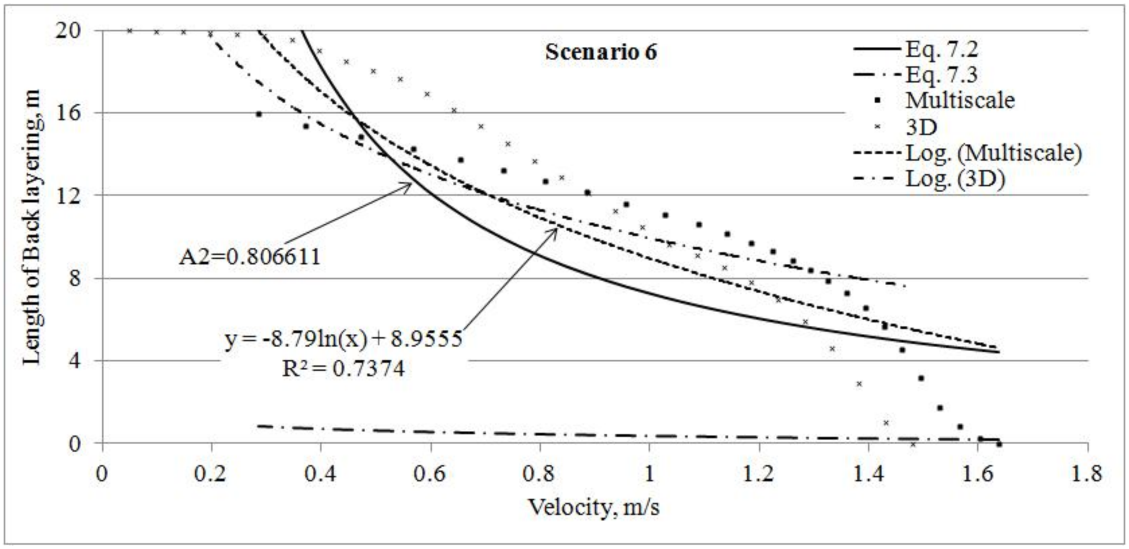

Figure 7.27. Relationship between the Length of Back Layering and Velocity in the Scenario 6 for Case Two

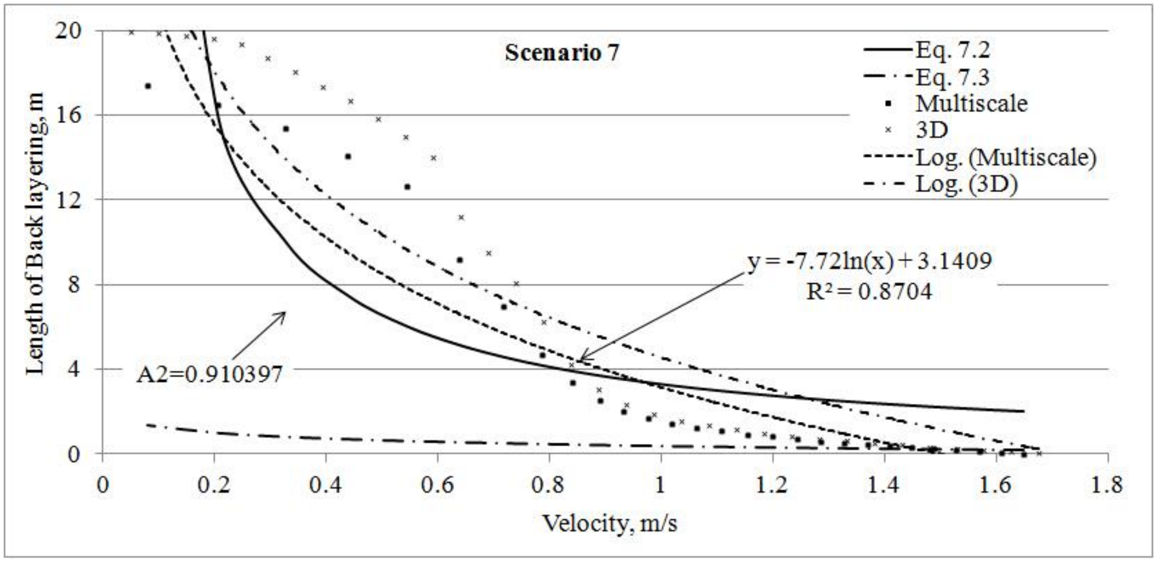

Figure 7.28. Relationship between the Length of Back Layering and Velocity in the Scenario 7 for Case Two

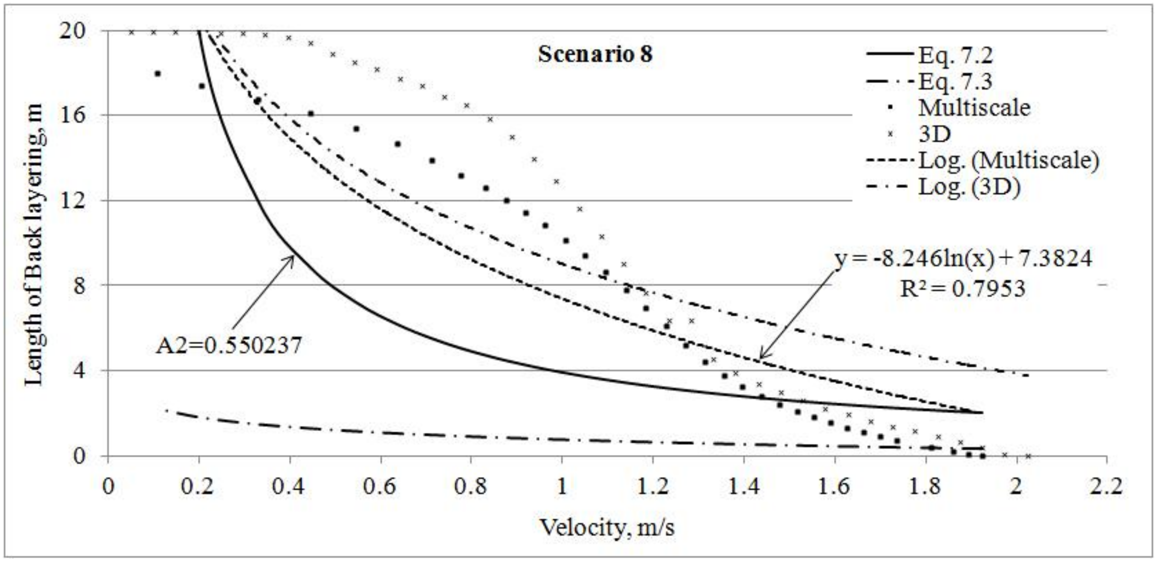

Figure 7.29. Relationship between the Length of Back Layering and Velocity in the Scenario 8 for Case Two

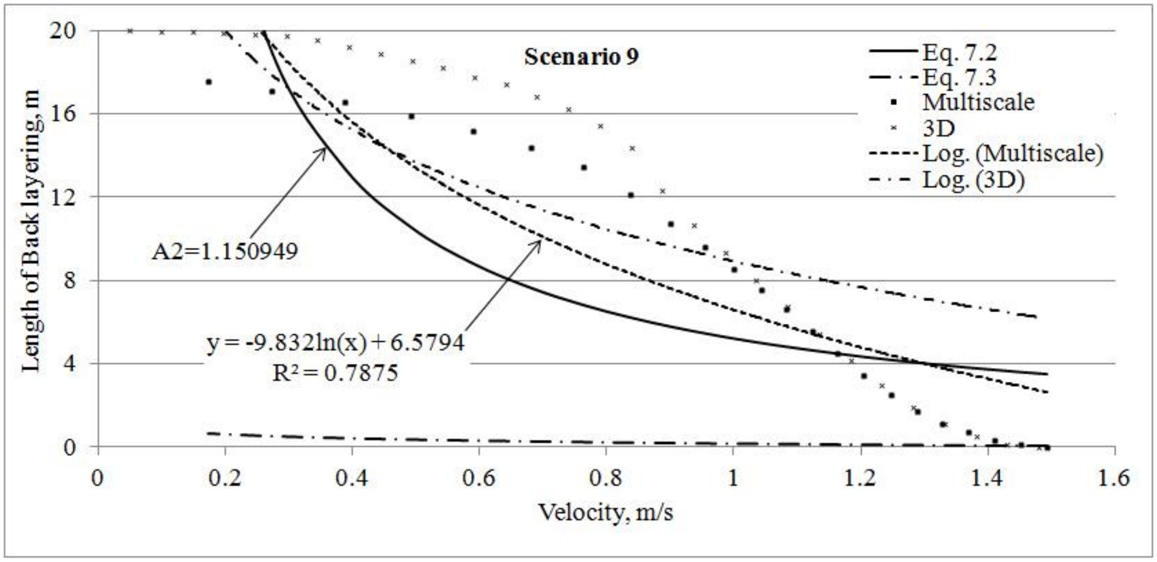

Figure 7.30. Relationship between the Length of Back Layering and Velocity in the Scenario 9 for Case Two

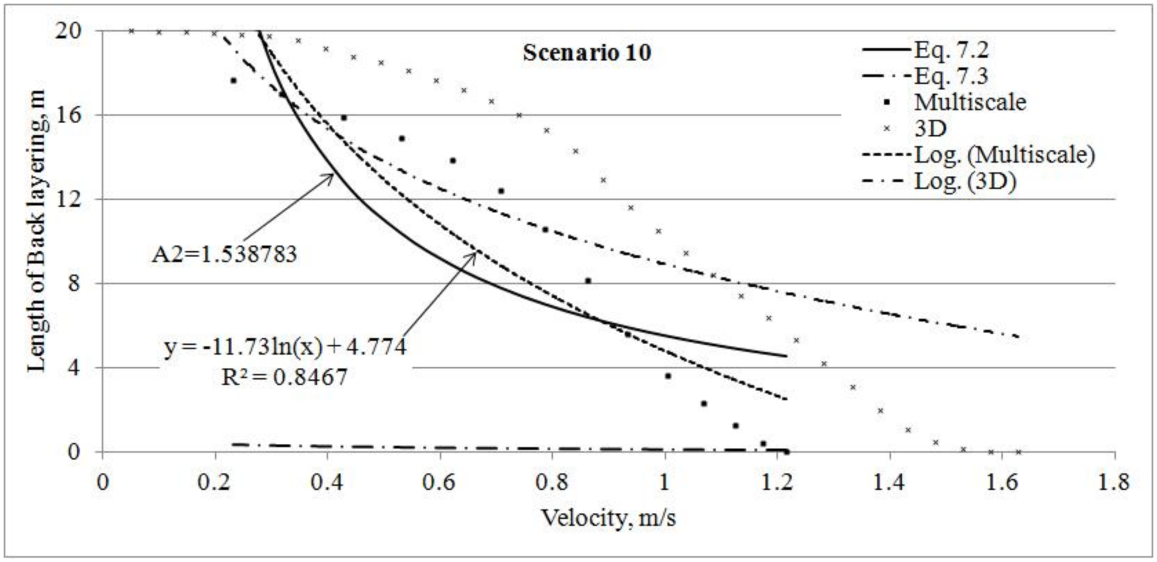

Figure 7.31. Relationship between the Length of Back Layering and Velocity in the Scenario 10 for Case Two

Table 7.2. Relationship between the Length of Back Layering and Velocity

Scenario	Multiscale Model			3D			Eq. 7.2
	A1	*B1*	R^2	*A1*	*B1*	R^2	*A2*
1	6.439	5.9882	0.6855	7.254	7.2939	0.7766	0.8969
2	9.758	5.4314	0.7627	2.026	1.3353	0.8676	1.9267
3	8.904	6.761	0.7879	8.221	6.415	0.6908	1.2566
4	8.774	9.1521	0.6152	3.966	13.755	0.4121	1.1570
5	6.725	10.067	0.6365	5.732	10.573	0.5218	0.9406
6	8.79	8.9555	0.7374	6.02	9.9354	0.6735	0.8066
7	7.72	3.1409	0.8704	8.382	4.5517	0.8212	0.9104
8	8.246	7.3824	0.7953	7.46	9.0222	0.7068	0.5502
9	9.832	6.5794	0.7875	6.875	8.9182	0.6196	1.1510
10	11.73	4.774	0.8467	7.02	8.8895	0.6604	1.5388

Since Eq. 7.3 provided results with big deviations from those of the multiscale model, no further analysis was made using that equation.

Logarithm regressions were conducted with predicted data from both the multiscale and 3D models. The constant *A1* and *B1* in Eq. 7.1 are shown in Table 7.2 for each scenario. The degree of the regression line for approximating the predicted data points were determined by the R^2 coefficient. An R^2 of 1.0 indicates that the regression line perfectly fits the data. For both the multiscale model and 3D models, most R^2 values are located in a range of 0.6 to 0.8.

The proportionality constant, *A2* in Eq. 7.2 (deduced from these ten multiscale model simulations), was almost within the recommended range of 0.6 and 2.2 (Ingason, H., 2005). For scenarios 8, 1, 9, and 10, it was obvious that the *A2* varied inversely with fire intensity. Scenarios 1 to 7 had the same fire intensity, but with different airway dimensions. Comparisons of these seven scenarios revealed that the *A2* varied inversely with the hydraulic diameter of the airway. Because the number of scenarios designed for the mutiscale simulation was not enough, a quantitative analysis of *A2* was not included in this research.

8. CONCLUSION

8.1. SUMMARY

A total of ten fire tests were conducted at the Experimental Mine’s Wombat Mine to determine the temperature and flow distribution in the mine during a mine fire. A total of nine points and one section were selected for measuring temperatures and air velocities. The fuel’s mass loss rate was measured during the test to build a fire curve. These test results showed that the fire behavior in the underground airways was influenced by many factors such as fire intensity, airway dimension, fuel type, fire location, and inlet air velocity.

The 3D numerical models for the Wombat Mine fire were constructed using FLUENT. The three-dimensional Favre-averaged equations for the transport of mass, momentum, and enthalpy with the standard k-e turbulent model were used. An additional source term was incorporated in the z-momentum equation to account for the body force effect on buoyancy. The standard two-equation k-e turbulent model for turbulence also included an additional source term to account for buoyancy effects. The radiant exchange between fluid elements and the mine wall boundaries were simulated through the P1 model. The governing equations were discretized using the finite volume method and solved with the implicit segregated velocity-pressure formulation.

The entire domain was discretized with structural elements. Great care was given to the analysis of meshing requirement. The numerical simulation results were validated with experimental data for temperature and velocity at predetermined points. A level of accuracy with maximum relative deviation of 12% was used in predicting air velocities. For temperature prediction, a total of nine points was used for comparison purposes. During the 600s simulation, the maximum relative deviation was 8.79%, which was smaller than the accepted level of between 20% and 30%. Additional sensitivity analyses for the main parameters that influence fire behavior were conducted, and similar results were obtained. Comparisons of results showed that the 3D model was able to predict the distribution of velocity and temperature in case of an underground mine fire.

The 1D network model of the Missouri S&T Main Mine was built using Flowmaster. The developed 1D model was validated with experimental data from the ventilation survey with acceptable accuracy (maximum relative deviation at 12.53 %) in determining velocity. To ensure the accuracy of calculations regarding mine ventilation, the 1D models were verified using other established and mature simulation tools such as Ventsim Visual, VnetPC Pro, and Ventgraph.

Two cases were conducted using the 1D model for different purpose. Case One uses a kerosene fire with varying HRR to simulate a transient state for determing temperature distribution along airways underground. The ventilation devices were controlled in real time to ensure that temperatures will be in compliance at the working face and a ventilation control strategy in real time was developed successfully in this case. This suggests that the 1D model by Flowmaster can be used as a performance-based fire safety planning tool. The combination of a rich components library and powerful user-defined orders can be useful tools of a comprehensive mine ventilation plan and fire emergency training.

In Case Two, the network involving a constant heat source with varied inlet velocities was simulated also in a transient state. This case was designed to study the critical velocity and back layering effect along an airway during a mine fire. Since the 1D network model lacked the ability to calculate the back layering effect, no reversal phenomena were presented in this case.

The 3D analysis required significant computation resources when simulating either a steady or transient fire underground. It was not practical to deal with fires within the entire mine model because of the excessive amount of time and computing resources required. Two cases were simulated in 1D modeling and their results are used as input for 3D simulations which were constructed based on the same airway where heat source in 1D was located. The validated numerical model in the Wombat Mine was applied to both cases and analysis of meshing requirements in both cases was conducted for both temperature and velocity distribution. These two 3D models were constructed for the multiscale models, to be coupled with 1D models. Significant effort was required to properly determine the interfaces of the 1D-3D model.

In the first case, the distance between the inlet and fire was first set at 5m to reduce the computation time, and the ventilation remain unchanged so there would be no reversal effect during the simulation. To determine the distance between the outlet and the fire source, a total of nine cases were run with a varying L_{3D} of 10m to 60m. The resulting temperature and X-velocity distribution showed that the temperature and flow field developed well after 20m (~8 times the hydraulic diameter of the airway) distance from the fire source. The accuracy improved only 0.11% and 0.23% for the temperature and X-velocity, respectively by increasing L_{3D} from 25m to 60m.

In the second case, considering a different inlet velocity during the simulation with the fire placed in the middle of the 3D model, the distances in both upstream and downstream had the same impact on resulting distribution. To determine a proper L_{3D}, a total of nine different runs were conducted, with L_{3D} varing from 10m to 100m. The predicted temperature and X-velocity distribution showed that the temperature and flow field developed well after 20m (~8 times the hydraulic diameter of the airway) both upstream and downstream from the fire. The accuracy had improved only 0.12% and 0.09% for the temperature and X-velocity, respectively by increasing L_{3D} from 40m to 100m.

The 1D and 3D models prepared previously were coupled with each other for both cases to form the multiscale models. The first case of the technique showed that the technique did have the capability to model the use of ventilation controlling devices in a fire, with the latter case modeling the back layering effect under different ventilation conditions.

Case One showed that the multiscale model can more quickly model the operation of ventilation control devices than a full 1D model can. Both the multiscale and full 1D model show that a safe temperature can be maintained at the working face. The temperatures in the full 1D model, however, were overestimated by up to 33 K comparing to results of the multiscale model, but even so, the response of the regulators in the full 1D model was 3s later than the response time of regulators in the multiscale model.

In Case Two, the critical velocity and back layering effect were modeled in ten different scenarios. Comparison of critical velocities suggested that critical velocities calculated with the multiscale model is up to 62.38% more accurate than the 3D model when compared to results using the semi-empirical formula Eq. 2.11. The scenarios were to reflect the influence of fire intensity and airway dimensions on fire behavior, the multiscale model presented more regularity in the relationship between the critical velocity and the fire intensity (and airway dimension) than the 3D model did.

Simulations were also conducted to determine the relationship between the velocity and the length of back layering. For each scenario, logarithm regressions were conducted with predicted data from both the multiscale and 3D models. A study of the proportional constant in Eq. 7.2 showed that it was varied inversely with fire intensity and the airway hydraulic diameter. No further quantitative analysis was conducted in this research.

8.2. ORIGINAL CONTRIBUTIONS

This research used multiscale modeling techniques by coupling 1D and 3D models together to study the interaction between underground mine ventilation flows and fires. The 1D and 3D models were validated using experimental data from the Missouri S&T Experimental Mine. The developed multiscale models provided both practical (ventilation control in firefighting strategy) and theoretical (critical velocity and back layering effect) analyses.

Flowmaster and FLUENT were adopted for modeling the flow in both 1D and 3D, respectively. As a universal 1D fluid computational tool, this is the first time that Flowmaster was introduced to the mining industry. The related theory is described in detail in this dissertation. MPCCI, provided a coupling interface to couple Flowmaster with FLUENT. A detailed description of the 1D-3D coupling techniques are also presented here.

The computing time required in multiscale modeling techniques can be much reduced when compared to a traditional full 3D simulation. Given this advantage, multiscale techniques can be used to conduct parametric and sensitivity studies, ventilation system planning, and to assess redundancy and performance in regard to different types of fire hazards. The primary engineering value was significantly improved when time-dependent simulations were made since the number of input variables is larger and includes detection time and fire growth curve. Such a broad application of simulations is not possible by traditional 3D approaches.

Another significant advantage is related to the simulation of the entire mine, including the use of ventilation control devices. An accurate solution to the flow movement requires that the numerical model include all the operating ventilation control devices (stoppongs, mine regulators, overcasts, fan, etc.). This allows for an accurate assessment of the fire throttling effect and performance of all ventilation control devices. Although a full 1D model can be used to tackle this task, the accuracy of results is questionable.

An important issue about the use of a multiscale model for mine network with fires relates to an accurate pinpointing of interfaces between the 1D and 3D models. These boundaries must be located in regions where the temperatures or velocity gradients are negligible, and the flow behaves largely as in the 1D simulation. These dictate the size of the 3D domain; this size is case-specific but in general mainly depends on airway geometry.

8.3. FUTURE WORK

Since this is the first time the multiscale model is used to study mine fire and its impact on a ventilation network, several issues will need improvements in the future. Some are directly related to the sub-models adopted for the simulation, while others are related to expand the applications of this new technique.

The sophisticated combustion (e.g. mixture fraction model) models need to be adopted first. A simplified fire representation, like a heat source, cannot accurately simulate CO and smoke distribution, which are just as important as temperature in a firefighting operation.

The resulting information is expected to improve the theories of interaction between mine fires and ventilation. Additionally, this technique could be used to assess the capabilities of a ventilation system to manage fire behavior, planning detection strageties, and plan evacuation strategies.

REFERENCES

Abanto, J., Reggio, M., Barrero, D., and Petro, E., 2006. "Prediction of Fire and Smoke Propagation in an Underwater Tunnel," *Tunneling and Underground Space Technology*, Vol. 22, No. 1, pp. 90–95.

Anderson, J. D., 1995, *Computational Fluid Dynamics: The Basics with Applications*, McGrew-Hill Companies, Inc., 547 pp.

Anon., 1986. "Fire Fighting," *National Coal Board 622.82*, 83 pp.

Anon., 1995. *Memorial Tunnel Fire Ventilation Test Program Comprehensive Test Report*, Bechtel/Parsons Brinkerhoff, Inc., Prepared for Massachusetts Highway Department and Federal Highway Administration.

Anon., 1996. *VnetPC for Windows Version 1.0 Users Manual*, Mine Ventilation Services, 13 pp.

Anon., 2007. *Flowmaster V7-New User Training*, Flowmaster Ltd., 164 pp.

Anon., 2008. *http://www.cdc.gov/niosh /mining/statistics/fatalities.htm.* National Institute for Occupational Safety and Health, Accessed September 2010.

Anon., 2009a. *Ansys FLUENT 12.0*, Ansys, Inc.

Anon., 2009b. "Mining Industry Accident, Injuries, Employment, and Production Statistics and Reports," *http://www.msha.gov/ACCINJ/accinj.htm*. Mine Safety and Health Administration, Accessed December 2011.

Anon., 2010a. *http://www.cdc.gov/niosh /mining/statistics/disall.htm.* National Institute for Occupational Safety and Health, Accessed September 2011.

Anon., 2010b, http://www.lorencook.com/PDFs/Catalogs/CP_Catalog.pdf, Loren Cook Co., Accessed September 2010.

Anon., 2011. *Ventsim Visual^{TM} User Guide*, Chasm Consulting Co., 232 pp.

Anon., 2012a. http://www.thermoworks.com/emissivity_table.html. Accessed Februray, 2012.

Anon., 2012b. *Code of Federal Regulations 30 CFR, Parts §§75.340, 75.344, and 75.351*, Office of the Federal Register, National Archives and Standards Administration, U.S. Government Printing Office, Washington, D.C., September, 2012.

Arthur, E. C., ed., 2008, *Fire Protection Handbook,* 20th ed., National Fire Protection Association®, Quincy, MA, 3450 pp.

Atkinson, G. T., and Wu, Y., 1996. “Smoke Control in Sloping Tunnels,” *Fire Safety Journal*, Vol. 27, No. 4, pp. 335–341.

Ballesteros-Tajadura, R., Santolaria-Morros, C., and Blanco-Marigorta, E., 2006. “Influence of the Slope in the Ventilation Semi-transversal System of an Urban Tunnel,” *Tunneling and Underground Space Technology,* Vol. 21, pp. 21-28.

Bari, S., and Naser, J., 2005. “Simulation of Smoke from a Burning Vehicle and Pollution Levels Caused by Traffic Jam in a Road Tunnel,” *Tunneling and Underground Space Technology*, Vol. 20, pp. 281–290.

Bayrasy, P., and Kelsall, D., 2008. “Coupling of 1D and 3D simulation”, *Proc. 9th MpCCI User Forrum*, Februray 19th and 20th, 2008, Fraunhofer Institute SCAI / Flowmaster Ltd. UK, pp. 106-116.

Borchiellini, R., Ferro, V., and Giaretto, V., 1994. "Transient Thermal Analysis of Main Road Tunnel" *Proc. International Symposium on Aerodynamics and Ventilation of Vehicle Tunnels*, Liverpool UK, July 6-8. pp. 17-31.

Bounagui, A., Bénichou, N., and Kashef, A., 2005. “Heat Release Methods,” *National Research Council Canada, Research Report 186*, NRC-CNRC, 8 pp.

Chang, X., Laage, L. W., and Greuer, R. E., 1990. *A User's Manual for MFIRE: A Computer Simulation Program for Mine Ventilation and Fire Modeling*, United States Bureau of Mines, 175 pp.

Cheong, M. K., Spearpoint, M. J., and Fleischmann, C. M., 2009. “Calibrating an FDS Simulation of Goods-vehicle Fire Growth in a Tunnel Using the Runehamar Experiment,” *Journal of Fire Protection Engineering*, Vol. 19, No. 3, pp. 177-196.

Cheng, L. H., Ueng, T. H., and Liu, C. W., 2001. “Simulation of Ventilation and Fire in the Underground Facilities,” *Fire Safety Journal*, Vol. 36, pp. 597-619.

Chow, W. K., 1998. “On Smoke Control for Tunnels by Longitudinal Ventilation,” *Tunneling and Underground Space Technology*, Vol. 13, No. 3, pp. 271-275.

Coatesworth, D, 1929. “The Prevention of Fires in Mines and Methods of Dealing with Them,” *Transactions of the Institute of Mining Engineers*, Vol. 78, pp. 145-157.

Colella, F., 2010. *Multiscale Modeling of Tunnel Ventilation Flows and Fires*, PhD Dissertation, Politecnico di Torino, May 2010, 195 pp.

Colella, F., Rein, G., Borchiellini, R., Carvel, R., Torero, J. L., and Verda, V., 2009. "Calculation and Design of Tunnel Ventilation Systems using a Two-scale Modeling Approach," *Building and Environment*, Vol. 44, pp. 2357-2367.

Colella, F., Rein, G., Borchiellini, R., and Torero, J. L., 2011. "A Novel Multiscale Methodology for Simulating Tunnel Ventilation Flows during Fires," *Fire Technology*, Vol. 47, pp. 221-253.

Colella, F., Rein, G., Carvel, R., Reszka, P., and Torero, J. L., 2010. "Analysis of the Ventilation Systems in the Dartford Tunnels Using a Multi-scale Modeling Approach," *Tunneling and Underground Space Technology,* Vol. 25, No. 4, pp. 423-432.

Conti, R. S., and Litton, C. D., 1993. "Effects of Stratification on Carbon Monoxide Levels from Mine Fires," *Proc. 6th US Mine Ventilation Symposium*, R. Bhaskar ed., Salt Lake City, June 1993, pp. 489-494.

Conti, R. S., and Litton, C. D., 1995. "A Comparison of Mine Fire Sensors," *Report of Investigations RI 9572,* U.S. Bureau of Mines, Pittsburgh, Pennsylvania, 10 pp.

Cox, G., 1995. "Compartment Fire Modeling," *Combustion Fundamental of Fire,* G. Cox, ed., Academic Press, London, pp. 329-404.

Cox, G., 1998. "Turbulent Closure and the Modeling of Fire using Computational Fluid Dynamics," *Philosophical Transaction of the Royal Society,* Vol. 356, pp. 2835-2854.

DeRosa, M. I., 2004. "Analysis of Mine Fires for All U.S. Underground and Surface Coal Mining Categories: 1990-1999," *NIOSH Information Circular,* No. 9470, 36 pp.

Drysdale, D., 1986. *An Introduction to Fire Dynamics(3rd),* John Wiley and Sons, England, 574 pp.

Dzuirzynski, W., Nawrat, S., Roszkowski, J., Trutwin, W., 1997. "Computer Simulation of Mine Ventilation Disturbed by Fires and the Use of Fire Extinguishers," *Proc. 6th International Mine Ventilation Congress,* USA, pp. 389-393.

Dziurzynski, W., Tracz, J., and Trutwin, W., 1988. "Simulation of Mine Mires," *Proc. 4th International Mine Ventilation Congress*, Brisbane, 3-6 July, 1988, Melbourne, The Australian Institute of Mining and Metalurgy, pp. 357-363.

Dziurzynski, W., Tracz, J., and Trutwin, W., 1992. "Computer Simulation of Transients in Mine Ventilation," *Proc. 5th International Mine Ventilation Congress*, Hemp, E., ed., Marshalltown, South Africa, Johannesburg, pp. 193-200.

Dziurzynski, W., Tracz, J., and Wala, A., 1991. "Graphical Technique for rapid Comparison of Mine Ventilation Network Analyses," *Proc. 5th Mine Ventilation*

Symposium, Wang, Y. J., ed., June 3-5, West Virginia University, Morgantown SME, Littleton-Colorado, pp. 351-355.

Edwards, J. C., Franks, R. A., Friel, G. F., and Yuan, L., 2006. "Experimental and Modeling Investigation of the Effect of Ventilation on Smoke Rollback in a Mine Entry," *Mining Engineering*, April, pp. 53-58.

Edwards, J. C., and Friel, G. F., 1996. "Comparative In-mine Evaluation of Carbon Monoxide and Smoke Detectors," *Report of Investimation 9622*, 11 pp.

Edwards, J. C., Friel, G. F., Franks, R. A., and Opferman, J. J., 1997. "Mine Fire Detection Under Zero Airflow Conditions," *Proc. 6th International Mine Ventilation Congress*, R. V. Ramani, ed., Chapter 52. Society for Mining, Metallurgy, and Exploration, Inc.: Littleton, CO, pp. 331-336.

Edwards, J. C., Friel, G. F., Yuan, L., and Franks, R. A., 2006. "Smoke Reversal Interaction with Diagonal Airway – Its Elusive Character," *SME Transaction*, 2006; Vol. 320, pp.149-156.

Edwards, J. C., and Hwang, C. C., 1999. "CFD Analysis of Mine Fire Smoke Spread and Reverse Flow Conditions," *Proc. 8th U.S. Mine Ventilation Symposium*, J. Tien, ed., University of Missouri-Rolla, Rolla, MO, pp. 417-422.

Edwards, J. C., and Morrow, G. S., 1995. "Evaluation of Smoke Detectors for Mining Use," *RI9586*, 19 pp.

Edwards, J. S., Ren, T. X., and Jozefowicz, R., 1995. "Using Computational Fluid Dynamics (CFD) to Solve Mine Safety and Health Problems," *APCOM XXV*, pp. 41-47.

Egan, M. R., 1990. "Summary of Combustion Products from Mine Materials: Their Relevance to Mine Fire Detection," *Information Circular 9272*, 12 pp.

Eisner, H. S., and Shepherd, W. C. F., 1953/54. "Recent Research in Mine Fires," *Transactions of the Institute of Mining Engineers*, Vol. 113, pp.1057-1084.

Ferro, V., Borchiellini, R., and Giaretto, V., 1991. "Description and Application of a Tunnel Simulation Model," In: *International Symposium on Aerodynamics and Ventilation of Vehicle Tunnels*, London, pp. 487-512.

Fletcher, D. F., and Kent, J. H., 1994. "Numerical Simulations of Smoke Movement from a Pool Fire in a Ventilated Tunnel," *Fire Safety Journal*, Vol. 23, pp. 305-325.

Floyd, J. E., and Hunt, S. P., 2005. "A Network Fire Model for the Simulation of Fire Growth and Smoke Spread in Multiple Compartments with Complex Ventilation," *Journal of Fire Protection Engineering*, Vol. 15, pp. 199-229.

Formaggia, L., Gerbeau, J. F., Nobile, F., and Quarteroni, A., 2001. “On the Coupling of 1D and 3D Navier-Stokes Equations for Flow Problems in Compliant Vessels,” *Comput. Methods Appl. Mech. Engrg.*, Vol. 191, pp. 561-582.

Friel, G. F., Yuan, L., Edwards, J. C., and Franks, R. A., 2006. “Fire-generated Smoke Rollback through Crosscut from Return to Intake – Experimental and CFD Study,” *Proc. 11th U.S./North American Mine Ventilation Symposium,* R. V. Ramani ed., Mutmansky, PA, pp. 483-489.

Galdo Vega, M., Marıa Arguelles Dıaz, K, Fernandez Oro, J.M., Ballesteros Tajadura, R., Santolaria Morros, C., 2008. “Numerical 3D simulation of a Longitudinal Ventilation System: Memorial Tunnel Case,” *Tunneling and Underground Space Technology*, Vol. 23, No. 5, pp. 539-551.

Gao, P. Z., Liu, S. L., Chow, W. K., and Fong, N. K., 2004. “Large Eddy Simulations for Studying Tunnel Smoke Ventilation,” *Tunneling and Underground Space Technology*, Vol. 19, pp. 577–586.

Gates, R. A., Gauna, M., Morley, T. A., O’Donnell, J. R., Smith, G. E., Watkins, T. R., Weaver, C. A., and Zelanko, J. C., 2007. “Report of Investigation Underground Coal Mine Fatal Underground Coal Burst Accidents, August 6 and 16, 2007, Crandall Canyon Mine, Genwal Resources Inc., Huntington, Emery County, Utah, ID No. 42-01715,” Arlington, VA: U. S. Department of Labor, Mine Safety and Health Administration.

Geiger, S., Huangfu, Q., Reid, F., Mattha, S., Coumou, D., Belayneh, M., Fricke, C., and Schimd, K., 2009. “Massively Parallel Sector Scale Discrete Fracture and Matrix Simulations,” *SPE Reservoir Simulation Symposium,* Woodlands, Texas, 2-4 February, Paper 118924.

Gillies, A. D. S., Wu, H. W., Tuffs, N., and Sartor, T., 2003. “Real Time Integrated Mine Ventilation Monitoring,” *Queensland Mining Industry Health and Safety Conference 2003*, Townsville, Queensland, Australia, 3-6 August 2003, pp. 133-140.

Grekov, S. P., Kalyusskij, A. E., and Lagutin, V. I., 1991. “Mathematical Description of Filling Process of Fire Section being Isolated by Inert Gases,” *Fiziko-Teknicheskie Problemy Razrabotki Poleznykh Iskopaemykh*, No.4, pp. 111-115.

Greuer, R. E., 1973. “Influence of Mine Fires on the Ventilation of Underground Mines,” *Contract Report No. S0122095*, U.S. Bureau of Mines, 173 pp.

Greuer, R. E., 1977. “Study of Mine Fires and Mine Ventilation, Part I, Computer Simulations of Mine Ventilation Systems under the Influence of Mine Fires,” *Contract No. S0241032,* Department of the interior bureau of mines, Washington D.C, 78 pp.

Guan, H. Y., and Kwok, K. Y., 2008. *Computational Fluid Dynamics in Fire Engineering Theory, Modeling and Practice,* Elsevier Ltd., 530 pp.

Hartman, H. L., Mutmansky, J. M., Ramani, R. V., and Wang, Y. J., 1997. *Mine Ventilation and Air Conditioning (3rd ed.),* 730 pp.

Hemp, R., 1989. "Thermodynamic Aspects of Mine Airflow, Psychrometry," In: *Environmental Engineering in South African Mines,* J. Burrows, ed.,, pp. 29-48 and pp. 435-463.

Heselden, A. J. M., 1976. "Studies of Fire and Smoke Behavior Relevant to Tunnels," In: *Proc. of the Second international Symposium of Aerodynamics and Ventilation of Vehicle Tunnels,* Cambridge, UK: BHRA Fluid Engineering, pp. 23-35.

Heskestad, G., 1995a. "Fire Plumes, Flame Height, and Air Entrainment," Section 2, Chapter 1, *SFPE Handbook of Fire Protection Engineering(2nd, ed.),* P. J. DiNenno, Editor-in-Chief, National Fire Protection Association, Quincy, Massachusetts, pp. 1-17.

Heskestad, G., 1995b. "Smoke Management in Covered Malls and Atria" Section 4, Chapter 13, *SFPE Handbook of Fire Protection Engineering(2nd, ed.),* P. J. DiNenno, Editor-in-Chief, National Fire Protection Association, Quincy, Massachusetts, pp. 292-310.

Hinkley, P. L., 1970. "The Flow of Hot Gases along an Enclosed Shopping Mall," *Fire Research Note No.807,* Fire Research Station.

Howarth, H. C., and McCaa, G., 1929. "Control of a Small Mine Fire with Rock-dust," *Reports of Investigations,* No. 2914, 3 pp.

Hu, L. H., Huo, R., and Chow, W. K., 2008. "Studies on Buoyancy-driven Back-layering Flow in Tunnel Fires," *Experimental Thermal and Fluid Science,* Vol. 32, pp. 1468–1483.

Hwang, C. C., and Edwards, J. C., 2001. "CFD Modeling of Smoke Reversal," *Proc. International Conference on Engineered Fire Protection Design*, Bethesda, MD USA, Society of Fire Protection Engineers, pp. 376-387.

Hwang, C. C, and Edwards, J. C., 2005. "The Critical Ventilation Velocity in Tunnel Fires—A Computer Simulation," *Fire Safety Journal,* Vol. 40, No. 3, pp. 213-244.

Hwang, C. C., Litton, C. D., Perzak, F. J., and Lazarra, C. P., 1991. "Modeling the Fire-assisted Flame Spread along Conveyor Belt Surfaces," *Proc. 5th US Mine Ventilation Symposium*, Littleton, Colorado, Society for Mining, Metallurgy and Exploration Inc. (SME), pp. 39-44.

Ingason, H., 2005. “Fire Dynamics in Tunnel,” *Chapter 11 in The Handbook of Tunnel Fire Safety*, A. Beard and R. Carvel, ed., Thomas Telford, London, UK, pp. 231-266.

Ingason, H., and Lönnermark, A., 2005. “Heat Release Rates from Heavy Goods Vehicle Trailer Fires in Tunnels,” *Fire Safety Journal*, Vol. 40, No. 7, pp. 646-668.

Ingason, H., Nireus, K., and Werling, P., 1997. “Fire Tests in a Blasted Rock Tunnel,” *Report FOA-R-97-00581-990-SE,* Sweden.

Jacques, E., 1991. “Numerical Simulation of Complex Road Tunnels,” *Proc. Aerodynamics and Ventilation of vehicle tunnels conference*, Elsevier Science Publishers Ltd., England, pp. 467-486.

Jae Seong Roh, J. S., Ryou, H. S., Kim, D. H., Jung, W. S., and Jang, Y. J., 2007. “Critical Velocity and Burning Rate in Pool Fire during Longitudinal Ventilation,” *Tunneling and Underground Space Technology*, Vol. 22, pp. 262-271.

Jain, S., Kumar, S., and Sharma, T. P., 2008. ”Numerical Simulation of Fire in a Tunnel: Comparative Study of CFAST and CFX Predictions,” *Tunneling and Underground Space Technology*, Vol. 23, pp. 160-170.

Karki, K. C., and Patankar, S. V., Rosenbluth, E. M., and Levy, S. S., 2000. “CFD Model for Jet Fan Ventilation Systems,” *Proc. 10th International Symposium on Aerodynamics and Ventilation of Vehicle Tunnels*, Boston, MA, USA, November 1-3, 2000.

Kashef, A., and Benichou, N., 2008. “Investigation of the Performance of Emergency Ventilation Strategies in the Event of Fires in a Road Tunnel – A Case Study,” *Journal of Fire Protection Engineering*, Vol. 18, pp. 165-198.

Kennedy, W. D., Gonzales, J. D., and Sanchez, J. G., 1996. “Derivation and Application of the SES Critical Velocity Equations,” *ASHRAE Transactions: Research*, Vol. 102, No. 2, pp. 40-44.

Kim, E., Woycheese, J. P., and Dembsey, N. A., 2007. “Fire Dynamics Simulator (Version 4.0) Simulation for Tunnel Fire Scenarios with Forced, Transient, Longitudinal Ventilation Flows,” *Fire Technology*, Vol. 44, No. 2, pp. 137-166.

Ko, G. H., Kim, G. R., and Ryou, H. S., 2010. “An Experimental Study on the Effect of Slope on the Critical Velocity in Tunnel Fires,” *Journal of Fire Sciences*, Vol. 28, pp. 27-47.

Kowalski-Trakofler, K. M., Alexander, D. A., Brnich, M. J., and McWilliams, L., 2009. “Underground Coal Mining Disasters and Fatalities – United States, 1900-1906,” In: *MMWR*, Vol. 57, No. 51/52, pp. 1379-1383.

Krishnamoorthy, G., Rawat, R., and Smith, P. J., 2006. "Parallelization of the P-1 Radiation Model," *Numerical Heat Transfer, Part B*, Vol. 49, pp. 1-17.

Laage, L. W., and Yang, H., 1991. "Mine Fire Experiments at the Waldo Mine: Heat Flow," *Proc. 5th US Mine Ventilation Symposium*, Morgantown, WV, Society for Mining, Metallurgy, and Exploration, Inc., June 3-5, 1991, pp. 46-52.

Laage, L. W., and Yang, H., 1995. "Mine Fire Experiments and Simulation with MFIRE," *Proc. 7th US Mine Ventilation Symposium*, Chapter 33, A. M. Wala, ed., Lexington, Kentucky, June 5-7, 1995, pp 213-218.

Launder, B. E., and Spalding, D. B., 1974. "The Numerical Computation of Turbulent Flows," *Comput. Methods Appl. Mech. Engrg*, Vol. 3, No. 2, pp. 269-289.

Lea, C. J., 1994. "Computational Modeling of Mine Fires," *The Mining Engineer*, Vol. 154, No. 394, pp. 17-21.

Lea, C. J., Higgins, M., 1995. "Prediction of Smoke Movement in Mines: Sitting of Fire Detectors and Escape Considerations," In: *26th Int. Conf. of Safety in Mines Research Institutes*, Katowice, Poland, Sept., pp. 123-137.

Lee, C. K., Hwang, C. C., Singer, J. M., and Chaiken, R. F., 1979. "Influence of Passageway Fires on Ventilation Flows," In: *Proc. of 2nd International Mine Ventilation Congre*ss, Reno, Nev., pp. 4-8.

Lee, S. R., and Ryou, H. S., 2006. "A Numerical Study on Smoke Movement in Longitudinal Ventilation Tunnel Fires for Different Aspect Ratio," *Building and Environment*, Vol. 41, pp. 719-725.

Li, J. S. M., and Chow, W. K., 2003. "Numerical Studies on Performance Evaluation of Tunnel Ventilation Safety Systems," *Tunneling and Underground Space Technology*, Vol. 18, pp. 435-452.

Lin, C. J., and Chuah, Y. K., 2007. "A Study on Long Tunnel Smoke Extraction Strategies by Numerical Simulation," *Tunneling and Underground Space Technology*, Vol. 23, No. 289, pp. 522-530.

Litton, C. D., 2009. "Evaluation of Smoke Detectors for Use in Underground Mines," *SME Annual Meeting and Exhibit*, February 22-25, Denver, Colorado, preprint 09-072. Littleton, CO: Society for Mining, Metallurgy, and Exploration, Inc., pp. 1-8.

Litton, C. D., DeRosa, M. I., and Li, J. S., 1987. "Calculating Fire-throttling of Mine Ventilation Airflow," *Report of Investigation: RI 9076*, U.S. Bureau of Mines, 21 pp.

Litton, C. D., Lazzara, C. P., and Perzak, F. J., 1991. “Fire Detection for Conveyor Belt Entries,” *Report of Investigations 9380*, U. S. Department of the Interior Bureau of Mines, 23 pp.

Lonnemark, A. H., and Ingason, H., 2005. “Gas Temperature in Heavy Goods Vehicles Fires in Tunnels,” *Fire Safety Journal*, Vol. 40, pp. 506-527.

Lowndes, I. S., Silvester, S. A., Giddings, D., Pickering, S., Hassan, A., and Lester, E., 2007. “The Computational Modeling of Flame Spread along a Conveyor Belt,” *Fire Safety Journal*, Vol. 42, pp. 51-67.

Ludhi, A., 2006. “1D and 3D Co-Simulation between Flowmaster and CFD Packages,” *The 7th MpCCI User Forum*, Flowmaster Ltd., Februray 21st and 22nd, 2006, pp. 56-65.

Maas, W., 1950. “An Electrical Analogue for Mine Ventilation and Its Application to Ventilation Planning,” *Geologie en Mijnbouw*, 12, April.

McDonald, L. B., and Pomroy, W. H., 1980. “A Statistical Analysis of Coal Mine Fire in the U.S. from 1950 to 1977,” *Information Circular 8830*, U.S. Bureau of Mines, 47 pp.

McElroy, G. W., 1954. “A Network Analyzer for Solving Mine Ventilation Distribution Problems,” *U.S. Bureau of Mines Information Circular 7704*, 13 pp.

McGrattan, K., and Hamins, A., 2006. “Numerical Simulation of the Howard Street Tunnel Fire,” *Fire Technology*, Vol. 42, pp. 273-281.

McGrattan, K., and Miles, S., 2008. “Modeling Enclosure Fires Using Computational Fluid Dynamics,” *Chapter 3-8 in SFPE Handbook of Fire Protection Engineering (4th ed.)*, National Fire Protection Association, Quincy, Massachusetts, US.

McPherson, M. J., 1964. “Mine Ventilation Network Problems (Solution by Digital Computer),” *Colliery Guardian*, Aug. 21, pp. 253-254.

McPherson, M. J., 1993. *Subsurface Ventilation and Environmental Engineering*, Chapman and Hall, 905 pp.

Miclea, P. C., 1991. “Application of 'SES' and 'MFIRE' Computer Simulation Programs for Tunnel Fire Modeling - A Comparative Study,” *Proc. 5th US Mine Ventilation Symposium*, Morgantown, Virginia, June 1991, pp 53-60.

Mitchell, D. W., 1962. “Fighting Mine Fires,” *Transactions of the Society of Mining Engineers*, Vol. 223, No. 2, pp. 218-224.

Mitchell, D. W., 1996. *Mine Fires Prevention, Detection, Fighting (3rd.)*, Intertec Publishing Inc, Chicago, IL, 336 pp.

Morris, R., 1987. “Combating Underground Fires in Coal Mines by Direct Attack Methods,” *Mining Science and Technology*, Vol. 4, pp. 291-305.

Morrow, G. S., and Litton, C. D., 1992. “In-mine Evaluation of Smoke Detector,” *USBM Information Circular 9311*, 13 pp.

Mossi, M., 1999. “Simulation of Benchmark and Industrial Unsteady Compressible Turbulent Fluid Flows,” PhD thesis, Mechanical Engineering Department, EPFL.

Motenegro, G., 2002. “Simulazione 1D-Multi D di Flussi Instazionari e Reagenti in Sistemi di Scarico ed Aspirazione in Motori a Combustione Interna,” PhD thesis, Dipartimento di Energetica, Politecnico di Milano

Nakagawa, Y., Konrai, T., and Kohno M., 1991. “A Laboratory-scale Gallery Fire-test on Rubber Conveyor Belts with Fabric Skeletons,” *Fire and Materials*, Vol. 15, No. 1, pp. 17-26.

Ng, D. L., 1989. “Mine Ventilation Computer Code for Personal Computers,” *Information Circular 9215*, United States Bureau of Mines, 33 pp.

Novozhilov, V., 2001. “Computational Fluid Dynamic Modeling of Compartment Fires,” *Progress in Energy and Combustion Science*, Vol. 27, pp. 611-666.

Oka Y., and Atkinson, G. T., 1995. “Control of Smoke Flow in Tunnel Fires,” *Fire Safety Journal*, Vol. 25, No. 4, pp. 305–327.

Pomroy, W. H., and Carigiet, A. M., 1995. “Analysis of Underground Coal Mine Fire Incidents in the United States from 1978 through 1992,” *Information Circular 9426*, U.S. Bureau of Mines, 25 pp.

Quarteroni, A., 2008. *Modellistica Numerica di Problemi Differenziali*, Springer, Italy, Milano.

Quarteroni, A., and Valli, A., 1999. *Domain Decomposition Methods for Partial Differential Equations*, Oxford Science Publications, Oxford, 360 pp.

Rabia, H., 1988. *Mine Environmental Engineering: Essential Theory with Worked Examples*, Entrac Software, 425 pp.

Rey, B., Mossi, M., Molteni, P., Vos, J., and Deville, M., 2009. “Coupling of CFD Software for the Computation of Unsteady Flows in Tunnel Networks,” In: *13th International Symposium on Aerodynamics and Ventilation of Vehicle Tunnels*, New Brunswick, New Jersey, USA, 13-15 May, 2009.

Riess, I., Bettelini, M., and Brandt, R., 2000. "Sprint – a Design Tool for Fire Ventilation," In: *10th International Symposium on Aerodynamics and Ventilation of Vehicle Tunnels*, Boston, USA, November 2000, pp. 629-637.

Rusch, D., Blum, L., Moser, A., and Roesgen, T., 2008. "Turbulence Model Validation for Fire Simulation by CFD and Experimental Investigation of a Hot Jet in Crossflow," *Fire Safety Journal,* Vol. 43, No. 6, pp. 429-441.

Schlichting, H. 1979. *Boundary Layer Theory (7th ed.),* McGraw-hill, New York, 817 pp.

Sengupta, M., 1990. *Mine Environmental Engineering,* CRC Press, Inc Boca Raton, Florida, 264 pp.

Scott, D. R., Hinsley, F. B., and Hudson, R. F., 1953. "A Calculator for the Solution of Ventilation Network Problems," *Trans. Inst. Mine. Eng.,* Vol. 112, pp. 623-631.

Spirko, K., 1991. "One-dimensional Mathematical Model of Heat and Moisture Transfer between Airway Walls and Mine Air in Deep Mines," *Proc. 5th US Mine Ventilation Symposium*, Littleton, Colorado, Society for Mining, Metallurgy and Exploration Inc. (SME), pp 328-338.

Svenska Gruvföreningen, 1985. *Alternativ till Utrymningsväg från Gruva och annan Underjordsanläggning*, Svenska. Gruvföreningen, Stockholm, Sweden.

Thomas, P. H., 1968. "The Movement of Smoke in Horizontal Passages against an Airflow", *Fire Research Station Note No.723,* Fire Research Station, Borehamwood, England, 6 pp.

Tien, J. C., 1974. *Fire Fighting by Using Inert Gas with Special Reference to the Inert Gas Sources,* M. S. Thesis, Michigan Technological University, Houghton, Michigan, 102 pp.

Trevits, M. A., Smith, A. C., and Brune, J. F., 2007. "Remote Mine Fire Suppression Technology," *Proc. 32nd International Conference of Safety in Mines Research Institutes,* 28-29 September, 2007, Beijing, China, pp. 306-312.

Trevits, M. A., Yuan, L., Smith, A. C., Thimons, E. D., and Goodman, G. V., 2008. "The Status of Mine Fire Research in the United States," *Proc. 21st World Mining Congress,* September 7-11, 2008, Krakow, Poland. Sobczyk E. J. and Kicki J., eds., London: Taylor and Francis Group, pp. 303-308.

Tullis, J. P., 1989. *Hydraulics of Pipelines: Pumps, Valves, Cavitation, Transients,* John Wiley and Sons, New York, 288 pp.

Van Maele, K., and Merci, B., 2006. "Application of Two Buoyancy-modified k-ε Turbulence Models to Different Types of Buoyant Plumes," *Fire Safety Journal*, Vol. 41, pp. 122-134.

Van Maele, K., and Merci, B., 2008. "Application of RANS and LES Field Simulations to Predict the Critical Ventilation Velocity in Longitudinally Ventilated Horizontal Tunnels," *Fire Safety Journal*, Vol. 43, pp. 598–609.

Vauquelin, O., and Wu, Y., 2006. "Influence of Tunnel Width on Longitudinal Smoke Control," *Fire Safety Journal*, Vol. 41, pp. 420–426.

Verakis, H. C., 1985. "Reducing the Fire Hazard of Mine Conveyor Belts," *Proc. 5th US Mine Ventilation Symposium*, Littleton, Colorado, Society for Mining, Metallurgy and Exploration Inc. (SME), pp. 69-73.

Versteeg, H. K., and Malalasekera, W., 2007. *An Introduction to Computational Fluid Dynamics: The Finite Volume Method (2nd ed.)*, Pearson Prentice Hall, Glasgow, 503 pp.

Vutukuri, V. S., and Lama, R. D., 1986. *Environmental Engineering in Mines*, Cambridge University Press, 504 pp.

Wachowicz, J., 1997. "Heat Release Rate in Evaluation of Conveyor Belts in Full-scale Fire Tests," *Fire and Materials*, Vol. 21, pp. 253-257.

Wala, A. M., 1996. "Controlling Ventilation for Safe Escape from Coal Mine Fires," *Mining Engineering*, Vol. 48, No.4, pp. 61-66.

Wala A. M., Dziurzynski, W., Tracz, J., and Wooton, D., 1995. "Validation Study of the Mine Fire Simulation Model," *Proc. 7th US Mine Ventilation Symposium*, Chapter 33, A. M. Wala, ed., Lexington, Kentucky, June 5-7, 1995, pp. 199-206.

Wolski, J. K., 1991. "Mine Fire Real-time Simulator Can Help in Selecting the Best Fire Fighting Strategies," *Proc. 5th US Mine Ventilation Symposium*, Littleton, Colorado, Society for Mining, Metallurgy and Exploration Inc. (SME), pp. 82-87.

Woodburn, P. J., and Britter, R. E., 1996a. "CFD Simulation of Tunnel Fire – part I," Fire Safety Journal, Vol. 26, pp. 35-62.

Woodburn, P. J., and Britter, R. E., 1996b. "CFD Simulation of Tunnel Fire – part II," Fire Safety Journal, Vol. 26, pp. 63-90.

Wu, Y., and Bakar, M. Z. A., 2000. "Control of Smoke Flow in Tunnel Fires Using Longitudinal Ventilation Systems—A Study of the Critical Velocity," *Fire Safety Journal*, Vol. 35, pp. 363-390.

Wu, H. W., Gillies, A. D. S., and Wala, A. M., 2004. “Case Studies from Application of Numerical Simulation Software to Examining the Effects of Fires on Mine Ventilation Systems,” *Proc. 10th US Mine Ventilation Symposium*, R. Ganguli and S. Bandopadhyhy ed., Balkema, The Netherlands, pp. 445-455.

Yuan L., and Litton, C. D., 2007. “Experimental Study of Flame Spread on Conveyor Belts in a Small-scale Tunnel,” *National Institute for Occupational Safety and Health*, Pittsburgh Research Laboratory, 10 pp.

Zhang, X. C., Zhang, Y. T., and Tien, J. C., 2011a. “The Efficiency Study of the Push-pull Ventilation System in Underground Mine,” *Underground Coal Operators' Conference, 10 – 11 February*, pp. 225-230.

Zhang, X. C., Zhang, Y. T., and Tien, J. C., 2011b. “Study on Performance-based Design for Mine Fire Safety System,” *SME Annual Meeting Feb. 27-Mar. 02, Denver, CO*, Preprint 11-094, 4 pp.

Zhang, X. C., Zhang, Y. T., and Tien, J. C., 2011c. “Introduction of Firefighting Methods in U. S. Underground Mines,” *Journal of Xi’an University of Science and Technology,* Vol. 31, No. 6, pp. 672-678.

Zhang, X. C., Zhang, Y. T., Habibi, A., and Tien, J. C., 2012. “Experimental Investigation of the Underground Mine Fire under Different Conditions,” *Proc. 14th U.S./North American Mine Ventilation Symposium*, June 17-20, pp. 385-390.

Zhou, L. H., 2009. *Improvement of the Mine Fire Simulation Program MFIRE*, PhD Dissertation, West Virginia University, Morgantown, WV, 149 pp.

Zhu, M., Xu, Y., and Wu, J., 1991. “Computer Simulation of Spontaneous Combustion in Goaf,” *Proc. 5th US Mine Ventilation Symposium*, Littleton, Colorado, Society for Mining, Metallurgy and Exploration Inc. (SME), pp. 88-93.

VITA

Xichen Zhang was born in Meihekou, Jilin province in China in 1974. He got his Bachelor of Science degree in Geological Engineering from the China University of Mining Technology in July 1997 and the Master of Science degree in Geological Engineering from the China University of Mining and Technology (Beijing) in June 2000. He began his studies at the Missouri S&T in August 2007 and earned the Ph.D. degree in Mining Engineering in December, 2012.

Before joining the Mining Engineering Program at Missouri S&T, he had seven years of industrial and research experience with the China Academic of Building Research, in Beijing, China.